Structural and mutational analysis of transglycosylation by chitinase D from *Serratia proteamaculans*

Thesis submitted for the degree of
DOCTOR OF PHILOSOPHY

by
J. Madhuprakash
(Regd. No. 08LPPH27)

Department of Plant Sciences
School of Life Sciences
University of Hyderabad
Hyderabad – 500 046
INDIA

June, 2014

University of Hyderabad
(A Central University established in 1974 by an act of parliament)
HYDERABAD – 500 046, INDIA

CERTIFICATE

This is to certify that Mr. J. MADHUPRAKASH has carried out the research work embodied in the present thesis under the supervision and guidance of Prof. Appa Rao Podile for a full period prescribed under the Ph.D. ordinances of this University. We recommend his thesis entitled **"Structural and mutational analysis of transglycosylation by chitinase D from *Serratia proteamaculans*"** for submission for the degree of Doctor of Philosophy of the University.

Prof. Appa Rao Podile
(Research Supervisor)

Head,
Department of Plant Sciences.

Dean,
School of Life Sciences.

University of Hyderabad
(A Central University established in 1974 by an act of parliament)
HYDERABAD – 500 046, INDIA

DECLARATION

This is to declare that the work embodied in this thesis entitled **"Structural and mutational analysis of transglycosylation by chitinase D from *Serratia proteamaculans*"** has been carried out by me under the supervision of Prof. Appa Rao Podile and is plagiarism free. This has not been submitted for any degree or diploma in any other University or Institution earlier.

J. Madhuprakash

Prof. Appa Rao Podile
(Research Supervisor)

University of Hyderabad
Department of Plant Sciences
School of Life Sciences

(A Central University established in 1974 by an act of parliament)
HYDERABAD – 500 046, INDIA

CERTIFICATE

This is to certify that Mr. J. MADHUPRAKASH has carried out the research work embodied in the present thesis under the supervision and guidance of Prof. Appa Rao Podile for a full period prescribed under the Ph.D. ordinances of this University. We recommend his thesis entitled **"Structural and mutational analysis of transglycosylation by chitinase D from *Serratia proteamaculans*"** for submission for the degree of Doctor of Philosophy of the University. This work was done in part in the laboratory of Prof. Dr. Bruno Moerschbacher at University of Muenster, Germany in the framework of first International Research Training Group in Molecular and Cellular Glycosciences (IRTG-MCGS). I declare to the best of my knowledge that this work has not been submitted earlier for the award of degree or diploma from any other University or Institution.

Prof. Appa Rao Podile
(Research Supervisor)

ACKNOWLEDGEMENTS

I am immensely grateful to all those individuals who have helped me in making this endeavor possible.

At the outset, I would like to take this opportunity to extend my gratitude to my supervisor Prof. Appa Rao Podile for his unrelenting encouragement and constant support, without whom, this endeavor would not have been possible, not to mention his meticulous supervision throughout my doctoral research.

I thank the former Deans, Prof. M. Ramanadham, Prof. R. P. Sharma, Prof. Aparna Dutta Gupta and the present Dean Prof. A. S. Raghavendra, School of Life Sciences and former Heads, Prof. Appa Rao Podile, Prof. A.R. Reddy and the present Head, Prof Ch. Venkata Ramana, Dept. of Plant Sciences, for their support in all possible ways.

My special thanks to Prof. Dr. Bruno Moerschbacher and Dr. Nour Eddine for their encouragement and guidance during my stay at University of Muenster. Also I would like to thank Dr. Dominique Gillete, Mahatani Chitosan Pvt Ltd, Veraval, Gujarat, for chitinous substrates.

I am grateful to Prof. Lalitha Guru Prasad from School of Chemistry, for her guidance and help in carrying out modelling studies.

I thank Prof. M. J. Swamy from School of Chemistry for allowing me to work in collaboration with his group and teaching me ITC, DSC and Fluorescence techniques. I would like to thank all the students from his group for their friendly atmosphere in the lab.

I sincerely acknowledge Prof. T. P. Singh, Biophysics Department, AIIMS, for his kind help in performing crystallization studies.

I thank my doctoral committee members Prof. Ch. Venkata Ramana and Prof. S. Dayananda for their suggestions during my work.

I thank Dr. K. Gopinath for allowing me to use his lab facilities. I thank Prof. P. Reddanna, Dept of Animal Sciences, for allowing me to use the sonication facility. Thanks are also due to all the faculty members of the School of Life Sciences.

I would like to thank Prof. N. Siva Kumar, coordinator of IRTG-MCGS program, for selecting me as a student of MCGS and also DFG for the research fellowship.

I thank all the research scholars of the School of Life Sciences for their cooperation.

The help and cooperation of the non-teaching staff is highly acknowledged.

I thank CSIR for the research fellowship. I would like to acknowledge the infrastructural support provided by UGC-SAP and DST-FIST and DBT-CREBB to the Dept. of Plant Sciences and School of Life Sciences.

My special thanks to Bobbili, Tanneeru, Triveni, Sanjit Kumar, and Avinash Singh for their valuable suggestions and timely help during my Ph.D.

I wish to thank my seniors Dr. B. Sashidhar, Dr. V. L. Vasudev, Dr. Ch. Neeraja, Dr. Aravind, Dr. Praveen, Dr. Anil Singh, Dr. Debashish Dey, Dr. Swarnalee Dutta, Dr. Purushotham, Dr. Anil, Dr. Uma, Dr. Suma and Dr. Swaroopa for their suggestions and help. I thank all my lab mates, Mr. P.V.S.R.N. Sharma, Mr. Subhanarayan Das, Manjeet, Rambabu, Papa Rao, Bhuvan, Mohan, Rajesh, Sandya, Nirosha, Sravani, Dr. Sadaf and Dr. Anjali for their cooperation and cheerful atmosphere in the lab.

I also thank former members of the lab Suprava, Nandu, Suvarna, Bhavana and Durgeshwar for their friendly nature during the stay.

I would like to thank my friends Kishore, Madhu, Ashok, Anil, Pavan, Shiven, Sujith, Surendra, Gnanesh, Venu, Siva, Leela, Koti, Srinu and Mahesh Kumar (late) for the support.

I thank Narasimha, Devaiah, Sita Ram and Malla Reddy for their assistance in the lab.

Words fail to express my heartfelt gratitude for my parents and my brother, and all my family members to whom I'm forever indebted for their love, endless patience, unconditional support and understanding, without their cooperation I would not have come so far.

Above all, I thank God Almighty for his eternal love and blessings in every moment of my life.

J. Madhuprakash

Dedicated to my
Beloved Parents,
Venny & Friends

CONTENTS

ABBREVIATIONS

AMAC	2-aminoacridone
BLAST	Basic Local Alignment Search Tool
bp	base pair
CAZy	Carbohydrate Active Enzyme
CBM	Carbohydrate Binding Module
CBP	Chitin Binding Protein
ChBD	Chitin Binding Domain
CHOS	Chitin/Chitosan Oligosaccharides
CD	Circular Dichroism
C-terminal	Carboxy terminal
°C	degree centigrade/degree Celsius
DSC	Differential Scanning Calorimetry
DP	Degree of Polymerization
EDTA	Ethylene Diamine Tetra Acetic acid
F_A	Fraction of Acetylation
Fn3	Fibronectin type-3
g	Gram
GH18	Glycosyl Hydrolase 18
GlcN	glucosamine
GlcNAc	*N*-acetyl glucosamine
h	hour (s)
HPLC	High Performance Liquid Chromatography
HPTLC	High Performance Thin Layer Chromatography
ITC	Isothermal Titration Calorimetry
IPTG	Isopropyl β-D-thiogalactoside
kb	kilobase
kDa	kilo Dalton
L	Litre
LB	Luria-Bertani
M	Molar
MALD-TOF-TOF	Matrix Assisted Laser Disruption – Time of Flight
mg	milligram
min	minute
mL	milliliter
mM	millimolar
Mwt	Molecular weight
NCBI	National Centre For Biotechnological Information
N-terminal	amino terminal
OD	Optical Density
PA	Pattern of Acetylation
PAGE	Polyacrylamide Gel Electrophoresis
PCR	Polymerase Chain Reaction

PDB	Protein Data Bank
PKD	Polycystic Kidney Disease
rpm	revolutions per minute
SDS	Sodium Dodecyl Sulphate
SEC	Size Exclusion Chromatography
sec	seconds
TG	Transglycosylation
TIM	Triosephosphate Isomerase
TLC	Thin Layer Chromatography
T_m	Transition temperature
µg	microgram
µM	micromolar
ΔHc	calorimetric enthalpy
ΔHv	van't Hoff enthalpy
ΔG	Gibbs free energy
ΔS	Entropy

LIST OF TABLES

LIST OF FIGURES

Introduction

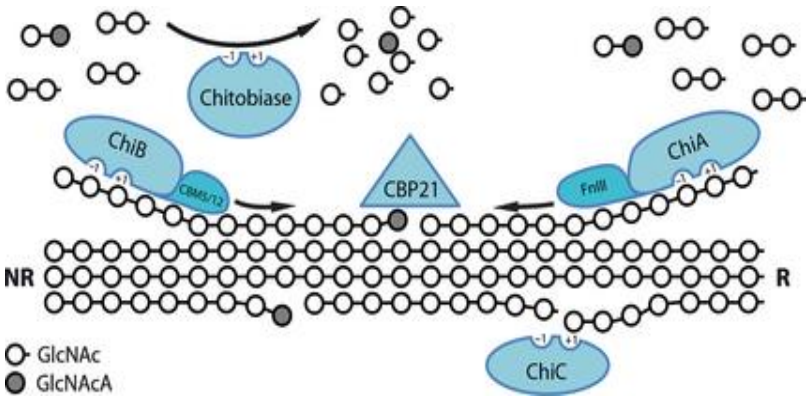

Vaaje-Kolstad et al., 2013.

1.1 Chitin/Chitosan

Chitin is the second most abundant natural polysaccharide consisting of (1→4) linked units of 2-acetamido-2-deoxy-β-D-glucopyranose (GlcNAc, **A**-unit) in a linear form. It is insoluble in water and mainly exists in two crystalline (*α*- and *β*-) forms. The *α*-chitin contains sheets of tightly packed alternating parallel and antiparallel chains (Minke & Blackwell., 1978) and is abundant in the exoskeletons of arthropods, insects, fungi and yeast cell walls. The chains are arranged in parallel orientation in *β*-chitin, which occurs less frequently in nature and is often extracted from squid pens. The insolubility of chitin is a major limitation in eliciting biological activities. One industrial exploitation route for chitin involves its conversion to chitosan, a water soluble copolymer of GlcNAc and 2-amino-2-deoxy-β-D-glucopyranose (GlcN, **D**-unit).

Chitosans are the linear, cationic polysaccharides with random distribution of **A** and **D** units soluble in acidic solutions, and can be prepared by homogeneous de-*N*-acetylation of chitin. The successive sugar units in the chitin/chitosan chain are rotated 180° relative to each other (Fig. 1.1). Thus, the functional and structural unit in these polymers is a disaccharide (Horn *et al*., 2006). The soluble polymeric chitin derivatives *i.e.* chitosans can be described and classified according to the fraction of *N*-acetylated residues (F_A) or degree of *N*-acetylation (DA), the degree of polymerization (DP) or the molecular weight (M_W), the molecular weight distribution (PD, for PolyDispersity), and the pattern of *N*-acetylation (P_A) or sequence (Aam *et al*., 2010). Chitosan exhibits a variety of interesting physicochemical and biological properties. This, in combination with its non-toxicity, biocompatibility and biodegradability, makes chitosan suitable for use in numerous applications in agriculture, cosmetics, water treatment and medicine (Bhatnagar & Sillanpää, 2009; Kim & Rajapakse, 2005). Varied F_A/DA of chitosans affects many of their properties, such as solubility as a function of pH (Vårum *et al*., 1994), binding to lysozyme (Kristiansen *et al*., 1998), susceptibility to degradation by lysozyme (Nordtveit *et al*., 1994), as well as functional properties in drug delivery (Schipper *et al*., 1996) and gene delivery systems (Koping-Hoggard *et al*., 2001).

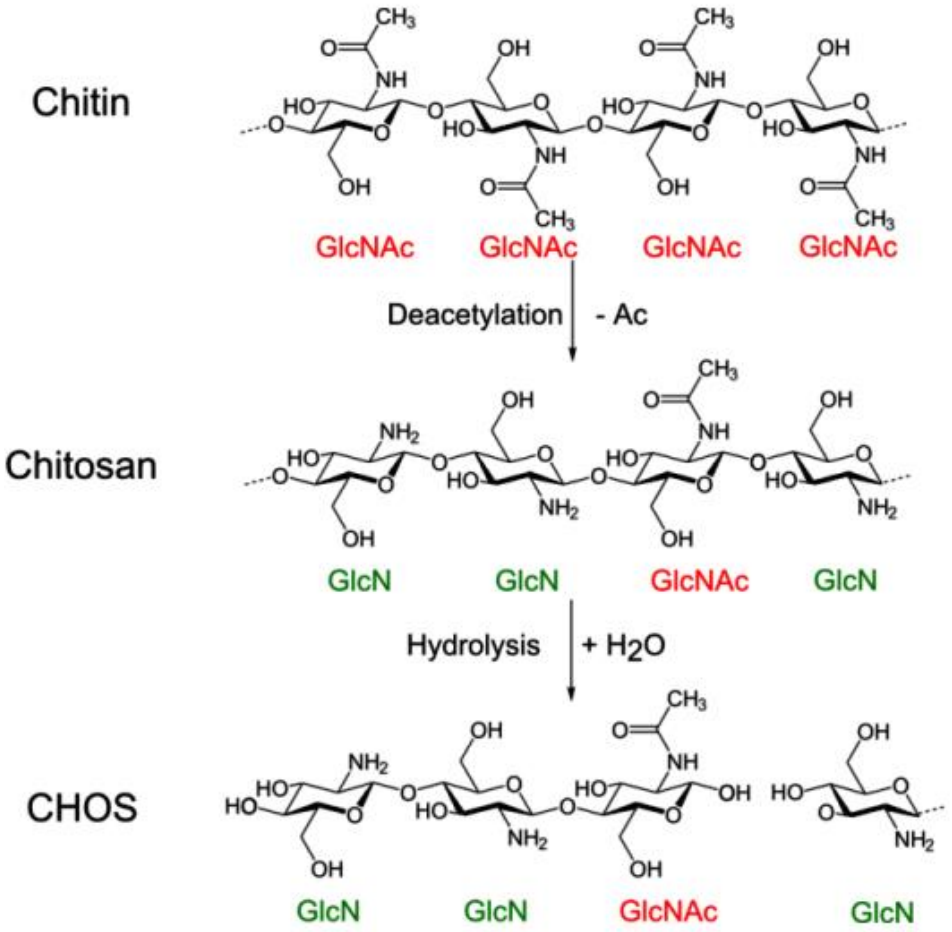

Figure 1.1: Stereochemical visualization of chitin, chitosan and their oligosaccharides (CHOS). Chitosan can be prepared through deacetylation of chitin. CHOS can be obtained by degrading chitin/chitosan either through chemical or enzymatic methods.

1.2 Chitin/Chitosan-Oligosaccharides (CHOS)

CHOS can be produced either by partial depolymerization of chitin/chitosan, or by oligomerization of the basic monosaccharide building blocks *i.e.* GlcNAc and GlcN. The latter strategy has the advantage of yielding highly pure and fully defined CHOS, but it is less preferred because of high costs and low yields. Thus, depolymerization is a more promising strategy even though it typically yields less defined mixtures of CHOS. In general, the available events for depolymerizing chitin/chitosan polymers can be classified into chemical and enzymatic methods.

1.2.1 Chemical Methods for CHOS Production

Chemical methods are routinely used for large scale production of CHOS at the industrial level. The polymeric chitin/chitosan is subjected to partial hydrolysis using concentrated hydrochloric acid followed by column chromatographic fractionation. Chemical hydrolysis mostly gives low DP CHOS up to hexamer, and often results in rather low yields of CHOS and generates high amount of GlcNAc (Uchida *et al*., 1989). Though, solvolysis of chitin in anhydrous hydrogen fluoride results in quantitative yield of CHOS (DP 2–9), it yields low DP oligomers as major end products (Defaye *et al*. 1994). The combination of mild acid degradation and sonolysis under ultrasound irradiation has the potential for the preparation of CHOS with higher DP (Takahashi *et al*., 1995). In a different way, CHOS with larger DP can be produced by partial depolymerization of fully deacetylated chitosan, followed by partial chemical re-*N*-acetylation. Such an approach by Trombotto *et al*. (2008) generated CHOS mixtures with a constant DP ranging from 3 to 10, and varying DAs from 0 to 90%. With this approach of chemical methods of re-*N*-acetylation, oligomers produced will have random PA. So, the longer CHOS prepared using these methods often result in low yields with random PA and require time-consuming purification methods and, hence, are not suitable for large scale production. Moreover, CHOS thus prepared are not ideal for carrying out bioactive studies due to the possible contamination of toxic chemicals. Enzymatic hydrolysis of chitin/chitosan might be a preferred method for the production of bioactive CHOS with non-random PA (Kohlhoff *et al*., 2009).

1.2.2 Enzymatic Methods for CHOS Production

Enzymatic methods may provide an opportunity to produce CHOS with specific DP and PA and, thus, desired bio-activity, to develop an efficient and eco-friendly process. Depending on the usage of different enzymes, the available enzymatic methods were classified into specific and non-specific enzymatic means of chitin/chitosan degradation. The latter mainly employs the usage of lipases (Lee *et al*. 2008), pronase and papain (Vishukumar *et al*. 2005) for CHOS production from chitosans. In a different approach, Coutino Ramirez *et al*. (2006) employed crude enzyme mixtures for CHOS production from crystalline α-chitin and chitosan substrates. The major disadvantage of non-specific enzymatic degradation is production of shorter chain CHOS and as well as low yields because of very poor substrate specificity. Use of purified recombinant enzymes like chitinases and chitosanases, would be a wise idea for obtaining bioactive CHOS with defined chemical composition. A great diversity of chitin and chitosan degrading enzymes exists, including endo- and exo-acting chitinases, endo-chitosanases, and glycosidases, such as GlcNase and GlcNAcase. The specificity of chitin/chitosan-degrading enzymes has been studied by extensive enzymatic degradation of chitin/chitosan polymers, followed by isolation and characterization of the resulting oligomers. Apart from substrate specificity, an important property to be taken care is the processivity shown by chitinases/chitosanases.

When a hydrolytic enzyme is bound to a polymeric substrate, especially an insoluble crystalline material such as cellulose or chitin, it may remain associated with the chain between hydrolytic steps, thus preventing its substrate from re-associating with the insoluble material (Eijsink *et al*., 2008). Processivity may drastically decrease the enzyme efficiency for soluble substrates. The mutant W97A of ChiB from *Serratia marcescens* (*Sm*ChiB), displayed loss of processivity, accompanied by a significant increase in the degradation rate for single polymer chains (Horn *et al*., 2006). Further, chitobiose is the major product of processive chitinases acting on chitin, and low DP CHOS are typically produced from chitosans. Thus, the generation of higher DP CHOS suitable for plant protection and other

biological applications requires the use of a nonprocessive endo-enzyme of known specificity. The choice of the starting substrate material, the enzyme and the processing time affect the outcome of the enzymatic conversion of chitin/chitosan to CHOS (Aam *et al*., 2010; Das *et al*., 2013). The advantage of enzymatic synthesis of CHOS is that there are ample opportunities to manipulate the outcome towards the generation of desired CHOS.

1.2.3 Applications of CHOS

Production of CHOS is of interest not only to agriculture but also to the food and medicine-related biotechnology industries due to their diverse applications. The capacity to produce CHOS on a large scale would allow the use of desired CHOS as a broad-spectrum vaccine against plant diseases (Yin *et al*., 2010; Das *et al*., 2013). Though CHOS display diverse applications, the mechanisms behind for a few of the observed bioactivities are poorly understood. Acidic mammalian chitinase is induced during T_H2 inflammation through an interleukin (IL)-13 dependent mechanism and was heavily over-expressed in human asthmatic tissue (Elias *et al*., 2005; Zhu *et al*., 2004). Thus, the acidic mammalian chitinase was considered as a potential target for asthma therapy. Partially deacetylated CHOS can inhibit family 18 chitinases (Cederkvist *et al*., 2008).

Longer chain CHOS (also called low molecular weight chitosan, LMWC) are considered more effective antifungal agents. LMWC (4.6 kDa, average DP of 23) shows antifungal activity against *Candida krusei* and inhibits spore germination in *Fusarium oxysporum* (Tikhonov *et al*., 2006). Both DP and F_A of the chitosan/CHOS are of great importance for the antifungal potential and LMWC with low F_A so far seems to be the most promising antifungal agents (Eweis *et al*., 2006). The anti-fungal effect of LMWC seems to be caused by its interaction with lipids in the plasma membrane, leading to morphological changes and cell surface disruptions (Palma-Guerrero *et al*., 2009; Park *et al*., 2008). CHOS are known to accelerate wound healing by enhancing the functions of inflammatory and repairing cells (Usami *et al*., 1998). For example, the sub-cutaneous injection of hexameric CHOS enhanced migration of polymorphonuclear cells in dogs (Usami *et al*., 1998). Hexa-

N-acetyl chito hexaose and fully deacetylated CHOS, induce persistent release of IL-8, a potent activator and chemo-attractant of polymorphonuclear cells, from fibroblasts of rats *in vitro* (Mori *et al*., 1997). Köping-Höggård *et al*. (2004) showed that fully deacetylated CHOS (DP 24) formed stable complexes with plasmid DNA, and *in vitro* or *in vivo* experiments proved that these CHOS were effective vectors for delivery of genes.

Furthermore, CHOS have antagonistic effects on tumor-growth in cancer by reducing metastasis (Nam *et al*., 2007) and a beneficial effect of increasing the bone-strength in osteoporosis through promoting the differentiation of mesenchymal stem cells to osteoblasts (Ratanavaraporn *et al*., 2009). CHOS could be used to inhibit family 18 chitinases in *Plasmodium* parasites and thereby preventing malaria (Shahabuddin *et al*., 1993). Several other potential effects of CHOS have been described, including antibacterial (Rhoades *et al*., 2006), immune modulatory effects (Kim *et al*., 2006), and a lowering effect on serum glucose levels in diabetics (Lee *et al*., 2003).

CHOS induced immunity can confer both local and systemic resistance in plants. For example, foliar spray of chitosan on barley triggered localized resistance in the induced leaf against powdery mildew caused by *Blumeria graminis* f. sp. *hordei* (Faoro *et al*., 2008), while chitosan treatments induced systemic resistance in tobacco against tobacco necrosis virus (Iriti *et al*., 2006). Fully acetylated CHOS with degree of polymerization (DP) from 4 to 10 induced peroxidase activity in wheat, although the fully deacetylated CHOS of DP5 and DP7 induced neither peroxidase nor phenylalanine ammonia lyase activities (Vander *et al*., 1998). Oligomers of chitin, but not chitosan, were active elicitors of defense-related lignification in wounded (Barber *et al*., 1989) and intact wheat (*Triticum aestivum* L.) leaves (Moerschbacher *et al*., 1986) and in suspension cultured wheat cells (Gotthardt *et al*., 1992). In view of these diverse applications and difficulties with the chemical methods, enzymatic approach for CHOS production would be an attractive alternative.

1.3 Chitin/Chitosan Depolymerizing Enzymes

Enzymatic depolymerization of chitin and chitosan involves chitinases and chitosanases, respectively. These enzymes are basically referred to as glycosyl hydrolases (GH) as they hydrolyze the glycosidic bonds between the sugars. Carbohydrate-Active enZYmes database (CAZy) provides a continuously updated list of the GH families (Cantarel *et al*., 2009). CAZy classification of GH is based on the amino acid sequence and it provides very useful information since the sequence, structure, and mechanism, are related. Chitinases (EC 3.2.1.14) are one of the glycosyl hydrolases (GH), the best preferred biological tools for chitin degradation and production of CHOS with biological activity. Chitinases usually occur in families GH18 and GH19 and are known to have a unique ability to hydrolyze **A-A** bonds. This property discriminates chitinases from chitosanases. Though chitinases are capable of hydrolyzing soluble chitosan polymers to different extents, they do not hydrolyze **D-D** bonds (Aam *et al*., 2010).

Chitinases hydrolyze chitin polymers and long chain chitooligomers into shorter oligomers and *N*-acetyl glucosamine monomers. Chitinases are found in microorganisms such as bacteria and fungi, plants and animals. Depending upon the source, chitinases have been shown to play various important functional roles in the respective organisms. In the case of bacteria, chitinases degrade chitin for utilizing it as a source of carbon and nitrogen. Fungal chitinases play a key role in hyphal growth and morphogenesis apart from serving nutritional requirement of fungi. Plants produce chitinases to defend themselves from phytopathogenic fungi. Inspite of these diverse functions, chitinases of bacterial origin and a few of plant origin were grouped under family GH18.

1.3.1 Structure & Modular Organization of GH18 Chitinases

The first GH18 chitinase structures were those of chitinase-A from *S. marcescens* (*Sm*ChiA) (Perrakis *et al*., 1994) and of a plant single domain endochitinase called hevamine (Terwisscha van Scheltinga *et al*., 1996). GH18 chitinases exhibit few distinct structural features like the presence of $(\beta/\alpha)_8$ - triose-phosphate isomerase (TIM) barrel fold along with several conserved sequence motifs in the catalytic

domain (Perrakis *et al*., 1994; Terwisscha van Scheltinga *et al*., 1996; van Aalten *et al*., 2000). The most prominent of these motifs is the D*X*D*X*E motif that spans β-strand 4 of the TIM barrel and includes glutamate that acts as the catalytic acid. Another highly conserved residue is a serine, which is part of a less well known but equally diagnostic S*X*GG motif. Many of these important structural features in relation to functional properties were well studied in chitinases from *S. marcescens*. *Sm*ChiA and *Sm*ChiB have deep substrate binding clefts lined with aromatic residues (Fig. 1.2), suggesting that these enzymes are processive exo-acting enzymes (Davies, & Henrissat, 1995). One key feature of the 'deep-cleft' chitinases is the presence of the so-called α+β insertion domain that forms one 'wall' of the substrate binding cleft. This 60–80 residue domain is inserted between strand 7 and helix 7 of the TIM barrel in only few of the GH18 enzymes. The domain may contain extra loops that participate in substrate binding, as is the case in *Sm*ChiB (with a 79-residue α+β domain) but less so in *Sm*ChiA (with a 61-residue α+β domain). *Sm*ChiC lacks the α+β domain and has a much shallower substrate binding cleft lacking most of the aromatic residues seen in *Sm*ChiA and *Sm*ChiB, suggesting that *Sm*ChiC may be a non-processive endo-acting enzyme (Vaaje-Kolstad *et al*., 2013).

1.3.2 Role of Accessory Domains/Proteins with Chitinases

Enzymes have evolved special tactics to ensure efficient degradation of crystalline and inaccessible polymeric chitin substrates. In addition to their catalytic domains, chitinases often have one or multiple carbohydrate-binding modules (CBMs) that are beneficial for enzyme efficiency because they adhere to, and sometimes disrupt the substrate (Zakariassen *et al*., 2009). The substrate binding properties of CBMs in general are well documented (Boraston *et al*., 2004) but exactly how and to what extent CBMs contribute to the efficiency of substrate conversion is not completely clear. So far, well studied potential functions of CBMs include, correct positioning of the catalytic domain on to crystalline substrates and their contributions to processive mode of action, and perhaps even local decrystallization of the substrate (Eijsink *et al*., 2008). The 40–60 residue CBM5 and CBM12 modules often found in chitinases are distantly related and appear as one family in Pfam (PF02839; www.pfam. org).

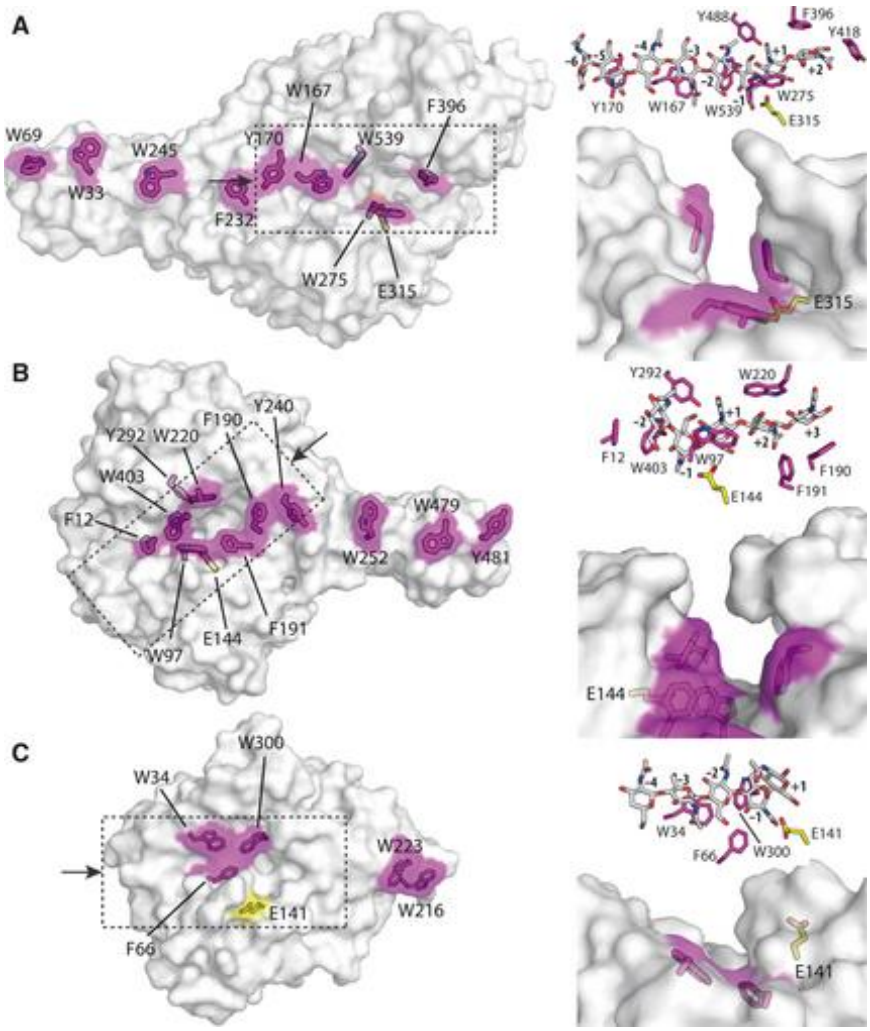

Figure 1.2: Substrate binding clefts of (A) *Sm*ChiA, (B) *Sm*ChiB and (C) *Sm*ChiC. The left figures highlight the aromatic amino acids that interact with the substrate through stacking interactions. The top right of each of the figures (A, B & C) show aromatic amino acids (magenta-colored carbons) in the active site cleft and their interactions with the substrate (grey-colored carbons). Subsites are indicated by numbers. The side chains of the catalytic acids are shown with yellow carbons. The bottom right figures illustrate the depth of the binding clefts. The view is indicated by the arrow in the left figures, where the dashed rectangles indicate the approximate surface areas shown in the bottom right figures. Note that Trp300 in *Sm*ChiC is structurally equivalent to Trp403 in *Sm*ChiB and Trp539 in *Sm*ChiA; this is a fully conserved residue in the −1 subsite (Vaaje-Kolstad *et al*., 2013).

Both are characterized by the presence of conserved exposed tryptophans that interact with the substrate. Several studies have confirmed that the presence of these domains increase substrate affinity as well as the efficiency of chitin hydrolysis, especially for the more crystalline chitin forms (Hashimoto *et al*., 2000; Uni *et al*., 2012). In addition to these well studied CBMs, there are other binding modules like polycystic kidney disease domain (PKD), where their presence is an added advantage for chitinase-mediated crystalline chitin hydrolysis. This domain has a β-sandwich fold, and the sequence "WDFGDG" is highly conserved in the domain. The role of PKD was experimentally proved in case of chitinase A from *Alteromonas* sp. strain O-7 (*Al*ChiA). Mutational studies proved that W30 and W67 in PKD domain of *Al*ChiA play an important role in the efficient hydrolysis of powdered chitin (Orikoshi *et al*., 2005).

Further, chitin-degrading organisms also produce few accessory proteins that disrupt the crystalline chitin substrates and thus increase the efficiency of chitinases. One such protein is the chitin binding protein 21 (CBP21- a CBM33 type protein), which showed a strong affinity to β-chitin (Vaaje-Kolstad *et al*., 2005). CBP21 was an important part of the chitinolytic machinery, secreted in large amounts by *S. marcescens* during chitin degradation as its expression was co-regulated with other chitinases (Uchiyama *et al*., 2003). Initially CBP21 was reported as a non-catalytic protein, which binds to the insoluble crystalline substrate, leading to structural changes in the substrate and increased substrate accessibility for chitinases (Vaaje-Kolstad *et al*., 2005). Later, the same protein CBP21 was reported to catalyze cleavage of glycosidic bonds in the crystalline β-chitin nanowhiskers. The resultant CHOS were identified with a normal sugar at the non-reducing end, and an oxidized sugar, 2-(acetylamino)-2-deoxy-D-gluconic acid (GlcNAcA), at the other end. In the presence of a reductant such as ascorbic acid, CBP21 boosted chitinase efficiency to much higher levels than previously observed (Vaaje-Kolstad *et al*., 2010). Subsequently, similar enzymatic activities have been demonstrated for other members of the CBM33 family, including CBM33s that are active on cellulose (Forsberg *et al*.,

2011). Recently the term lytic polysaccharide monooxygenases (LPMOs) was adapted for CBM33 type proteins.

1.4 GH18 Chitinases-Mode of Catalysis

Hydrolysis of the glycosidic linkage by chitinases is a nucleophilic substitution at the anomeric carbon, and can lead to either retention or inversion of the anomeric configuration (Sinnott, 1990). Both hydrolysis reactions take place through general acid catalysis, and require a pair of carboxylic acids at the enzyme's active site. One carboxylic acid is acting as a proton donor, facilitating leaving group departure, and the other acts as a base (inverting mechanism) or as a nucleophile (retaining mechanism). In both mechanisms, the position of the proton donor is within hydrogen-bonding distance of the glycosidic oxygen. The inverting mechanism (or) single displacement mechanism (Fig. 1.3) is a "one-step" reaction, where the protonation of the glycosidic oxygen occurs simultaneously with a nucleophilic attack on the anomeric carbon by an activated water molecule (Aam *et al*., 2010).

The retaining mechanism, also referred to as the double displacement mechanism (Fig. 1.3) is a two-step reaction, where the first step involves the protonation of the glycosidic oxygen (by the catalytic acid) and a subsequent nucleophilic attack on the anomeric carbon atom by the nucleophile (the second carboxylic acid). This attack leads to breakage of the glycosidic linkage and the formation of a covalent linkage between the anomeric carbon and the catalytic nucleophile (Vocadlo *et al*., 2001). Subsequently, this intermediate is hydrolyzed by a water molecule that approaches the anomeric carbon from a position close to that of the original glycosidic oxygen, leading to retention of the anomeric carbon configuration. Family 18 chitinases use a special variant of the double displacement mechanism, referred to as the substrate-assisted double displacement mechanism. Here, the carbonyl oxygen atom from the *N*-acetyl group of the sugar bound in subsite -1 acts as the nucleophile, leading to formation of an oxazolinium ion intermediate. Because of this involvement of the *N*-acetyl group in catalysis, productive substrate-binding of chitosan and chitosan oligomers to family 18

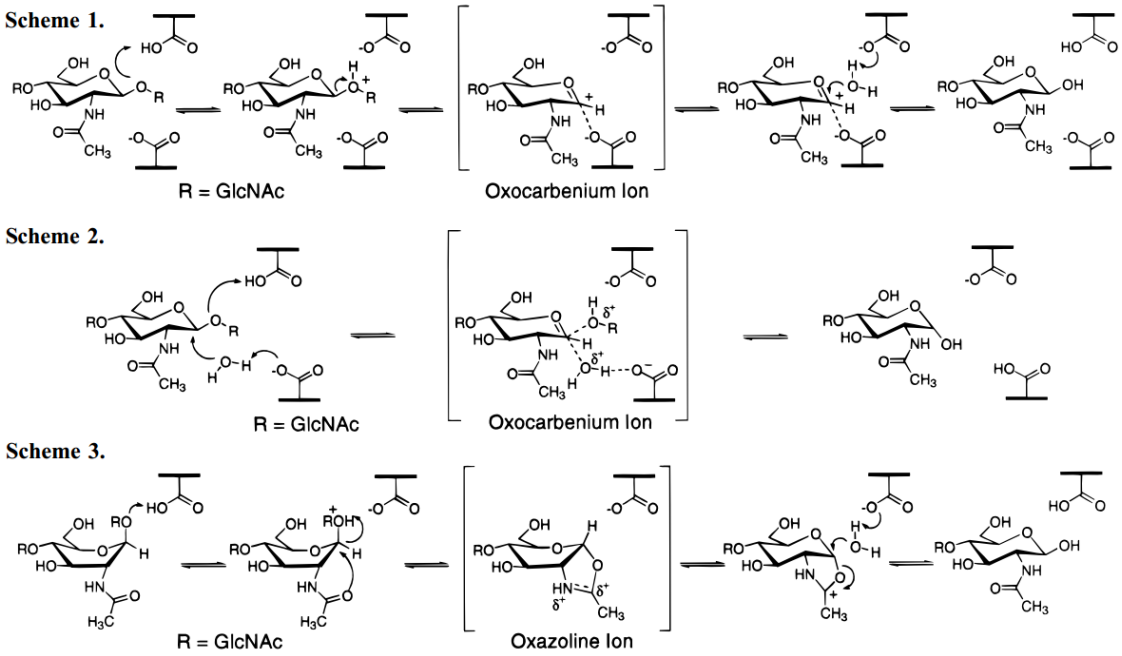

Figure 1.3: Mechanism of chitinase catalysis

Scheme 1. Double displacement hydrolysis mechanism - requires two acidic residues in the active site and leads to retention of the anomeric configuration.

Scheme 2. Single displacement mechanism - requires only one acidic residue in the active site and results in inversion of the anomeric configuration.

Scheme 3. Anchimeric stabilization hydrolysis mechanism of family 18 chitinases - the substrate is distorted to a boat conformation and the oxazoline ion intermediate is stabilized through anchimeric assistance from the neighboring C2′ *N*-acetyl group (Brameld & Goddard, 1998).

chitinases requires that a GlcNAc is bound in the -1 subsite (Tews *et al*., 1997; Brameld & Goddard, 1998).

1.4.1 Transglycosylation

A few of the GHs shows transglycosylation (TG) activity, apart from hydrolysis which involves formation of new glycosidic bond between donor and acceptor saccharides. The regio- and stereo-selective synthesis of glycosidic bond can be achieved through retaining GH showing TG, which follows double displacement reaction (Ly & Withers, 1999). The glycosyl-enzyme intermediate formed during the catalysis is a key step, deciding the direction of reaction towards hydrolysis or TG. Hydrolysis occurs when a water molecule attacks the glycosyl-enzyme intermediate leading to the release of a hydrolyzed sugar. Alternatively, TG occurs when a carbohydrate molecule outcompetes with the water molecule (Fig. 1.4) (Zakariassen *et al*., 2011). Thus, the amino acid residues responsible for acceptor binding seem to be important for TG activity. Since TG is a kinetically controlled reaction, efficient TG requires an enzyme with an active site architecture that disfavors correct positioning of the hydrolytic water molecule and/or favors binding of incoming carbohydrate molecules, through strong interactions in the glycon subsites (Williams & Withers, 2000). Some of the carbohydrate degrading enzymes belonging to different families of GH such as glucanase, amylase, cellulase, xylosidase, levan sucrase, dextran sucrase, etc. have both hydrolytic and TG activities (Cote & Tao, 1990; Kim *et al*., 2000; Muzard *et al*., 2009). GH 18 family chitinases showing TG are known in bacteria (Purushotham & Podile, 2012), fungi (Lu *et al*., 2009), cycads (Taira *et al*., 2010) and plants (Ohnuma *et al*., 2011a). Chitotriosidase from human macrophages synthesized TG products up to DP 6–9 from a DP 5 substrate (Aguilera *et al*., 2003).

TG depends on the substrate concentration, solvent system and even the type of enzyme used, which are often manipulated for CHOS synthesis. This special property of the GH can be exploited for the production of not only longer chain CHOS but also well-defined mixtures of CHOS with new or improved biological activity, by coupling smaller CHOS building blocks to each other or to other

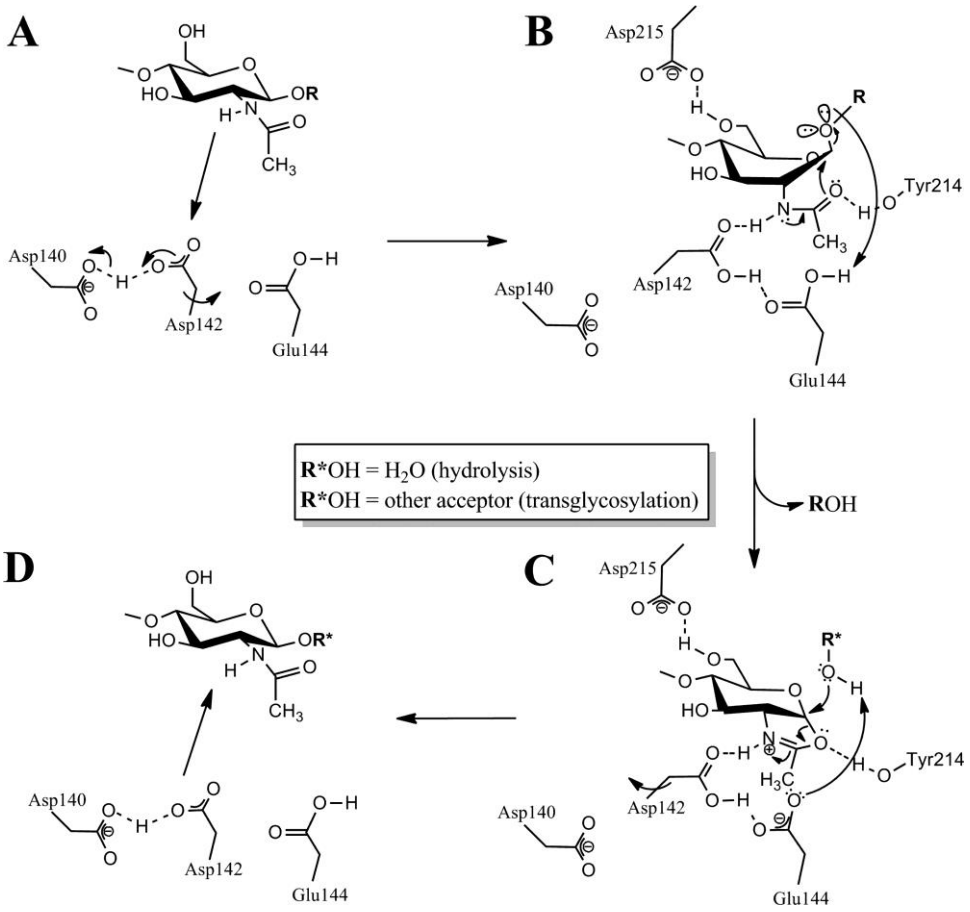

Figure 1.4: Catalytic mechanism of family 18 chitinases exemplified with *Sm*ChiB. (A) Substrate binds the resting enzyme and induces rotation of Asp142 toward Glu144. (B+C) Substrate binding causes distortion of the -1 sugar to a skew-boat conformation (only the -1 sugar is shown); Glu144 functions as a general acid and facilitates leaving group departure by protonating the glycosidic oxygen. Simultaneously, a nucleophilic attack by the acetamido group of the -1 sugar also promotes leaving group departure, leading to the formation of an oxazolinium ion intermediate (C). (C+D) Finally, Glu144 acts as a general base and activates an acceptor molecule that attacks the oxazolinium ion. This results in a hydrolytic or a TG product with retained conformation at the anomeric carbon (D), (Zakariassen *et al*., 2011).

functional groups. Usui *et al*. (1990) synthesized longer chain COS from DP 2 or DP 4 substrates by lysozyme or chitinase-mediated TG reactions, respectively. The addition of ammonium sulphate to the reaction mixture increased the production of CHOS with DP 6 & 7. CHOS were also synthesized in a TG reaction employing lysozyme from hen-egg white with DP 2 produced by a *Vibrio furnissii* chitinase (Yoon, 2005). The main difficulty in using GH with meager inherent TG activity is that the product of the TG reaction is necessarily also a substrate for the same enzyme, which can result in poor yield of longer chain CHOS. To avoid this problem, targeted mutagenesis of chitinases yielding modified enzymes with reduced hydrolytic activity could be employed. The enzyme modifications would need to aim at reducing hydrolytic activity, while increasing binding strength for the glycosyl donor in the glycon subsites.

The TG activity was improved by chemical modification of residues Trp-62 and Asp-101, at -4 and -2 subsites of hen egg white lysozyme (Fukamizo *et al*., 1989) or by mutating a Trp-167 located at subsite -3 of *Sm*ChiA (Aronson *et al*., 2006). The Trp-167 was distantly located from the active site *i.e.*, in the chitin-binding cleft. The mutant *Sm*ChiA had improved TG activity with oligosaccharide substrates as well as *p*-nitrophenyl-di-*N*-acetyl-*β*-D-chitobiose co-incubated with chitotetraose (Aronson *et al*., 2006). The variants of Asp-140/311 and Asp-142/313, analogous residues in *Sm*ChiB and *Sm*ChiA, respectively, showed improved TG activity (Zakariassen *et al*., 2011). Whereas, the aromatic side chains of Phe-166 and Trp-197, in class V chitinase from *Cycas revoluta* (*Cr*Chi-A), located in the acceptor binding site, were showed to control the TG activity (Taira *et al*., 2010) and the introduction of a tryptophan side chain into +1 subsite of family GH-18 (class V) chitinase from *Arabidopsis thaliana* (*At*ChiC) enhanced the TG activity (Umemoto *et al*., 2013). TG reaction, however, generates a mixture of long chain CHOS and may even synthesize large, water insoluble CHOS. To overcome such problems, Martinez *et al*. (2012) evaluated mutations on the catalytic amino acids of two family GH18 chitinases, *Bacillus circulans* WL-12 chitinase A1 (*Bc*ChiA1) and *Trichoderma harzanium* chitinase 42 (*Th*Chit42). These mutated chitinases, where the catalytic machinery was

disrupted enough to abolish hydrolytic activities, but still operational for TG reaction by providing oxazoline activated donor (*i.e.* a transition-state analogue for GH18 chitinase catalysis) for synthesis of desired artificial CHOS, can be considered as novel ‘‘glycosynthases’’.

We have characterized a family 18 TG chitinase D from *Serratia proteamaculans* (*Sp*ChiD) that had a molecular mass of 44.7 kDa, producing TG products like DP7, DP10, DP11-12 and DP11-DP13 from DP3, DP4, DP5 and DP6 substrates, respectively (Fig. 1.5). The *Sp*ChiD displayed TG activity only for 90 min with 2 mM of (DP4) as the substrate, later only hydrolytic products with lower DP were produced (Purushotham & Podile, 2012). The TG products detectable during the initial stages of reaction become substrates for hydrolytic activity of *Sp*ChiD in a prolonged incubation. The TG activity of *Sp*ChiD was dependent on both the length and concentration of the oligomeric substrate and also on the enzyme concentration. The length and amount of accumulated TG products increased with increase in the length of the substrate and its concentration, and decreased with increase in the enzyme concentration. The availability of a TG GH18 chitinase like *Sp*ChiD prompted us to further improve the TG activity and to understand the structural properties for better insights into the mode of TG.

1.4.2 Inhibition of Family 18 Chitinases

Inhibition of family 18 chitinases is emerging as a target for pest and fungal control as well as asthma and inflammatory therapy. To this regard, it is desirable to have access to non-toxic inhibitors that are easy to produce, and have high specificity and efficiency. CHOS that are partially *N*-acetylated have the potential to fulfill these requirements. Family GH18 chitinases follow substrate-assisted catalytic mechanism, where the catalysis has a strong preference for a GlcNAc in the -1 subsite. If the partially deacetylated CHOS bind in such a way that a GlcN ends up in the crucial -1 subsite, they will act as inhibitors. Sugar binding to the -1 subsite leads to an energetically unfavorable distortion (Fukamizo *et al*., 2001) which involves the *N*-acetyl group (Tews *et al*., 1997) and which may amount to an unfavorable ΔG as high as ~8 kcal/mol (Biarnes *et al*., 2007). Though it is not yet substantiated by enough

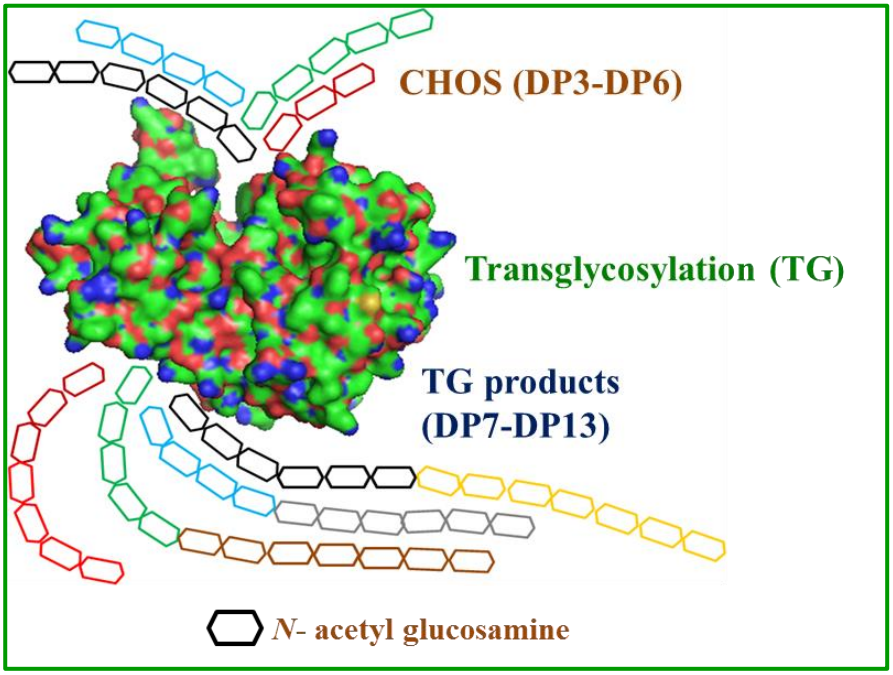

Figure 1.5: Simplified view of the TG displayed by *Sp*ChiD.

experimental data, it is possible that binding of GlcN in the -1 subsite, could be energetically less unfavourable than binding of a GlcNAc. Thus, binding of a GlcN would be non-productive, but perhaps stronger than binding of GlcNAc. This favors the idea of developing partially deacetylated CHOS as inhibitors for family GH18 chitinases (Cederkvist *et al*., 2008).

Most of these inhibitors resemble the structure of oxazolinium-ion intermediates or mimic carbohydrate-protein interactions. The pseudo-trisaccharide allosamidin (Fig. 1.6), which was isolated from the *Streptomyces* sp., is the most effective inhibitor with K_i values at the nM level (Rao *et al*., 2003; Bortone *et al*., 2002; Cederkvist *et al*., 2007; Sakuda *et al*., 1986). The cyclopentapeptides argifin and argadin (Fig. 1.6), which were isolated from the cultured broths of fungal strains *Gliocladium* sp. FTD-0668 and *Clonostachys* sp. FO-7314, respectively (Omura *et al*., 2000; Arai *et al*., 2000), have IC_{50} values in the nM–μM range. Other molecules, such as chitobiose and chitotriose thiazolines (Macdonald *et al*., 2010), xanthine derivatives (Schuttelkopf *et al*., 2006), and CI-4 [cyclo-(l-Arg-d-Pro)] (Houston *et al*., 2002) (Fig. 1.6), exhibit nM-mM level inhibitory activities. Partially deacetylated CHOS, mainly the DP5 molecule with the sequence "**DADAA**", exhibited a very good inhibitory effect with an IC_{50} value of 16 μM against *Sm*ChiB (Cederkvist *et al*., 2008). Chen *et al*., (2014a) reported that fully deacetylated CHOS with DP2-DP7 act as efficient inhibitors against the insect, *Ostrinia furnacalis* chitinase (*Of*ChtI), human chitotriosidase and the bacterial chitinases *Sm*ChiA and *Sm*ChiB with IC_{50} values ranging from 10^1–10^3 μM. The binding strength of the CHOS based inhibitor, an important parameter, which has to be tuned either by increasing the chain length of the CHOS or by coupling additional groups to the reducing end. Unfortunately, complex synthesis and/or limited availability of the starting materials limit the practical application of most of these potent molecules.

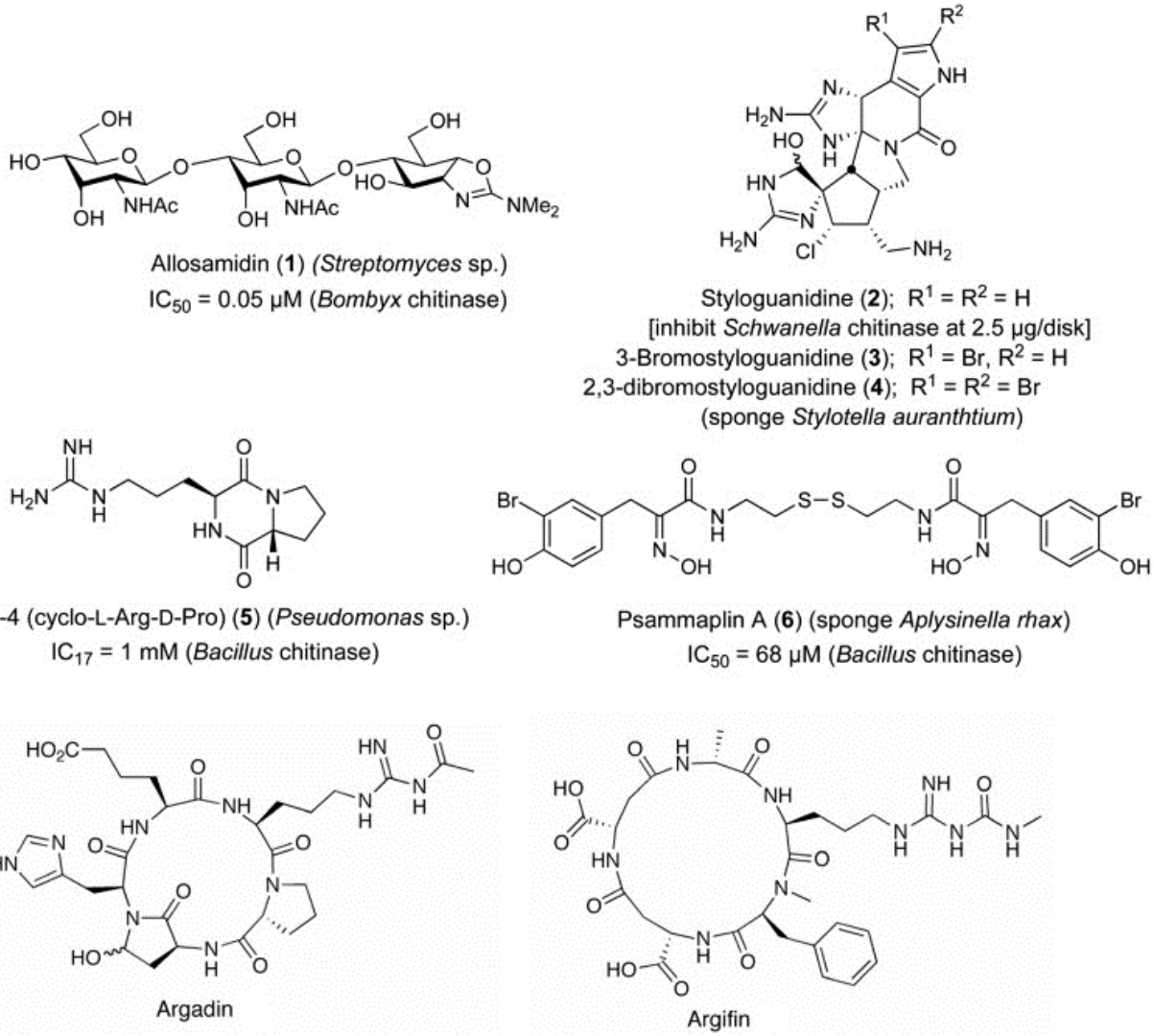

Figure 1.6: Structures of naturally occurring chitinase inhibitors and their inhibitory activities (Omura *et al*., 2000).

1.5 Purpose of this Study

The efficiency of TG by the wild-type enzymes is inevitably limited by enzyme-catalyzed hydrolysis of the product. So, there is a definite need for reducing/curtailing the hydrolytic activity for improving TG activity, to generate longer chain CHOS with immense potential for various biological activities, mainly as plant immune modulators for improved crop health. So, the major focus of this study was to improve the TG activity of *Sp*ChiD both in terms of increasing the quantity of TG products and in extending the duration of TG activity. To address this we have attempted to answer a few questions listed below:

- Which amino acid residues are crucial for TG and hydrolysis of *Sp*ChiD?
- Will the mapping of entry and exit points for CHOS in *Sp*ChiD help in improving TG?
- Will the crystallization of *Sp*ChiD provide insights into the new structural details for better understanding of TG?
- Do the spectroscopic and calorimetric studies help in elucidating the differential binding properties and stability of *Sp*ChiD to CHOS?
- Will the unique enzymatic activities of *Sp*ChiD provide a better option to produce bioactive chitosan oligosaccharides?
- How does the fusion of binding domains can bring changes in the activities of *Sp*ChiD?

Materials & methods

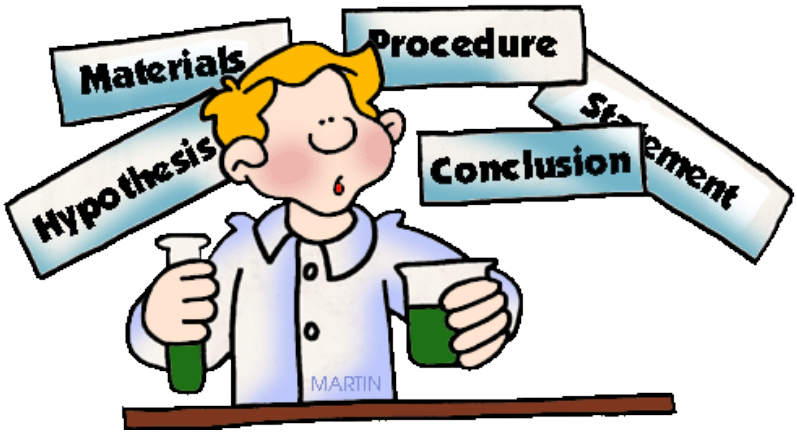

2. 1 Bacterial Strains & Plasmids

The expression vectors pET-22b (+), pET-28a (+) and bacterial strains *Escherichia coli* Rosetta-gami II (DE3) and *E. coli* BL21 (DE3) were purchased from Novagen, Madison, USA for performing cloning and heterologous expression studies, respectively.

2. 2 Biochemicals & Enzymes

2.2.1 Luria Bertani Medium (LB Medium)

LB medium – To 900 mL of water, 10 g tryptone, 10 g NaCl, 5 g yeast extract and 15 g agar was added. The pH was adjusted to 7.2 and the volume was made up to 1 litre.

2.2.2 Chemicals

Isopropyl-β-D-thiogalactoside (IPTG), X-Gal and Agarose were purchased from Sigma-Aldrich (USA). Ampicillin, kanamycin and chloramphenicol were purchased from Calbiochem (Darmstadt, Germany). All other chemicals and routine media components for bacterial culture were of analytical grade and obtained from Merck or HiMedia laboratories (India) unless otherwise stated. The polymeric substrates α-chitin, β-chitin and chitosan substrates were kindly provided by Dr. Dominique Gillete, Mahtani Chitosan Pvt., Ltd. (Veraval, India). Ni-NTA His bind resin was procured from Novagen (Madison, USA) for protein purification. Different DP chitin and chitosan oligosaccharides (DP1-DP6 and a mixture of all these oligosaccharides) were obtained from Seikagaku Corporation (Tokyo, Japan), through Cape Cod (East Falmouth, USA).

2.2.3 Kits & Enzymes

DNeasy Blood & Tissue Kit for genomic DNA isolation, GeneElute HP Plasmid miniprep kit and Gel extraction kit were purchased from Qiagen. Restriction enzymes, T4 DNA ligase and *Taq* and *Pfu* DNA polymerase were obtained from MBI Fermentas (Ontario, Canada). All the kits and enzymes were used as per the manufacturer's instructions.

2. 3 Primers Used for PCR

The primers used in this study for preparing *Sp*ChiD single/double mutants (Table 2.1) and fusion chimeras (Table 2.2) were procured from MWG Biotech Pvt. Ltd. (Bangalore, India).

2. 4 Preparation & Characterization of SpChiD Mutants or Fusion Chimeras

2.4.1 Fold Recognition & Homology Modeling of SpChiD

Fold recognition by FUGUE (Shi *et al*., 2001) was done as described previously by Sashidhar *et al*. (2010). The amino acid sequence of *Sp*ChiD (NCBI_ID: YP_001478954) was obtained from NCBI database (http://www.ncbi.nlm.nih.gov/). A BLAST search of the amino acid sequence against protein databank (PDB) was performed to identify the 3D structures that could share high sequence homology. The 3D coordinates of the basic structure were obtained from the PDB (http://www.rcsb.org/pdb/home/home.do). We built the 3D structure of the *Sp*ChiD protein using the MODELLER (Sali & Blundell, 1993) implemented in Discovery Studio 2.5 (Accelerys Inc, USA). The structure validation of the generated 3D models was performed using Verify_3D (Lüthy *et al*., 1992) and Ramachandran plot (Ramachandran *et al*., 1963).

2.4.2 Selection of Amino Acid Residues for Point Mutations

The amino acid residues that might influence hydrolytic and TG activities of *Sp*ChiD were selected based on the sequence alignment and the crystal structures of the homologous proteins (1E15, 1ITX, 1E9L, 1HKM, 1EDQ and 1D2K). We considered the hydrophobic aromatic residues of chitinases that are mainly involved in catalytic interactions with chitin. Using the 3D model, a few amino acid residues were selected for point mutations based on their probable involvement in hydrolytic and TG activities of *Sp*ChiD.

2.4.3 Generation of SpChiD Mutants

*Sp*ChiD mutants were generated as described by Ke & Madison (1997) (Fig. 2.1) with pET 22b-*Sp*ChiD as template (Purushotham & Podile, 2012). Mutagenic primers were designed and amplification was carried out in two different steps using *Pfu* DNA polymerase. In the first step of PCR, annealing temperature was 52°C and

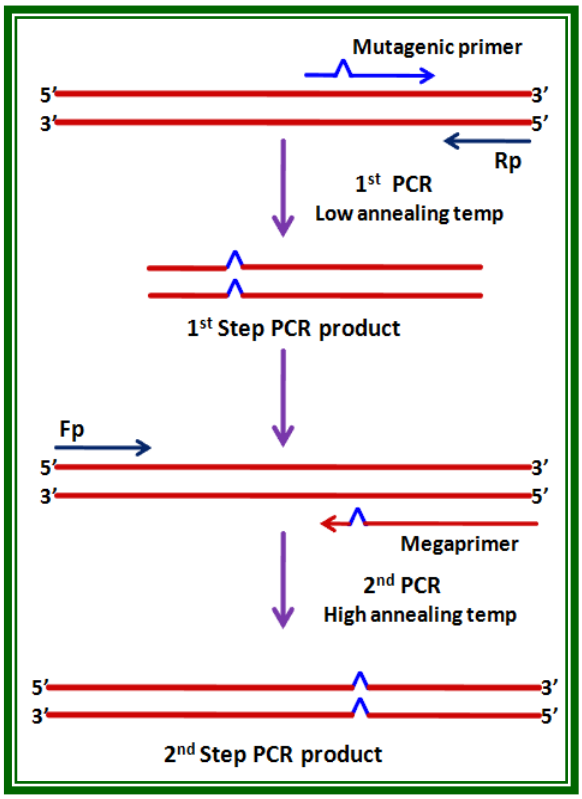

Figure 2.1: Schematic representation of site-directed mutagenesis by single-tube 'Megaprimer' PCR method (Song-Hua & Madison 1997).

Mutant	Mutagenic primer sequence[a]
Y28A	5'–CTT TCC GTC GGT *GCC* TTC AAC GGT GGC–3'
V35G	5'–GGT GGC GGT GAT *GGT* ACC GCC GGT CCT–3'
V35F	5'–GGT GGC GGT GAT *TTC* ACC GCC GGT CCT–3'
T36G	5'–GGC GGT GAT GTT *GGC* GCC GGT CCT GGT–3'
T36F	5'–GGC GGT GAT GTT *TTC* GCC GGT CCT GGT–3'
F58W	5'–AAT TAC TCT *TGG* GGT CTG ATC TAC AAC–3'
S110G	5'–AAA GTC TTG CTG *GGC* GTC GGT GGC TGG–3'
G113S	5'–CTG TCC GTC GGT *AGC* TGG GGC GCT CGC–3'
G113W	5'–CTG TCC GTC GGT *TGG* TGG GGC GCT CGC–3'
W114A	5'–TCC GTC GGT GGC *GCG* GGC GCT CGC GGG–3'
F119A	5'–GGC GCT CGC GGG *GCC* TCA GGC GCA GCC–3'
E153D	5'–GAT CTC GAC TGG *GAT* TAC CCG GTT AAC–3'
E153A	5'–GAT CTC GAC TGG *GCA* TAC CCG GTT AAC–3'
Y154A	5'–CTC GAC TGG GAA *GCC* CCG GTT AAC GGT–3'
W160A	5'–GTT AAC GGT GCC *GCG* GGA CTG GTC GAA–3'
G195W	5'–ACC ATC GCC GTC *TGG* GCC AAC GTG AAA–3'
M220A	5'–ATC AAC CTG *GCG* ACT TAC GAT ATG GCG–3'
Y222A	5'–ATC AAC CTG ATG ACT *GCC* GAT ATG GCG–3'
W241A	5'–GAC TCC AAA CAA *GCG* CCA ACC GTC GCC–3'
R278A	5'–GGT TTC TAT GGC *GCG* GTG CCA AAA CGG–3'
W290A	5' –CCG GGC ATC GAT *GCG* GAC AAG GCG GAT–3'
W395A	5' –GGT GCG ATG TTC *GCG* GAA TAT GGC GCA–3'
Δ30-42 RpO	5'–GTC GAG CTT GTT GAT GAA ATA ACC GAC GGA–3'
Δ30-42 IFp	5'–ATC AAC AAG CTC GAC GTC ACA CAA ATT ACC–3'

Table 2.1: Primers used for site-directed mutagenesis

[a]underlined sequence encodes altered amino acid

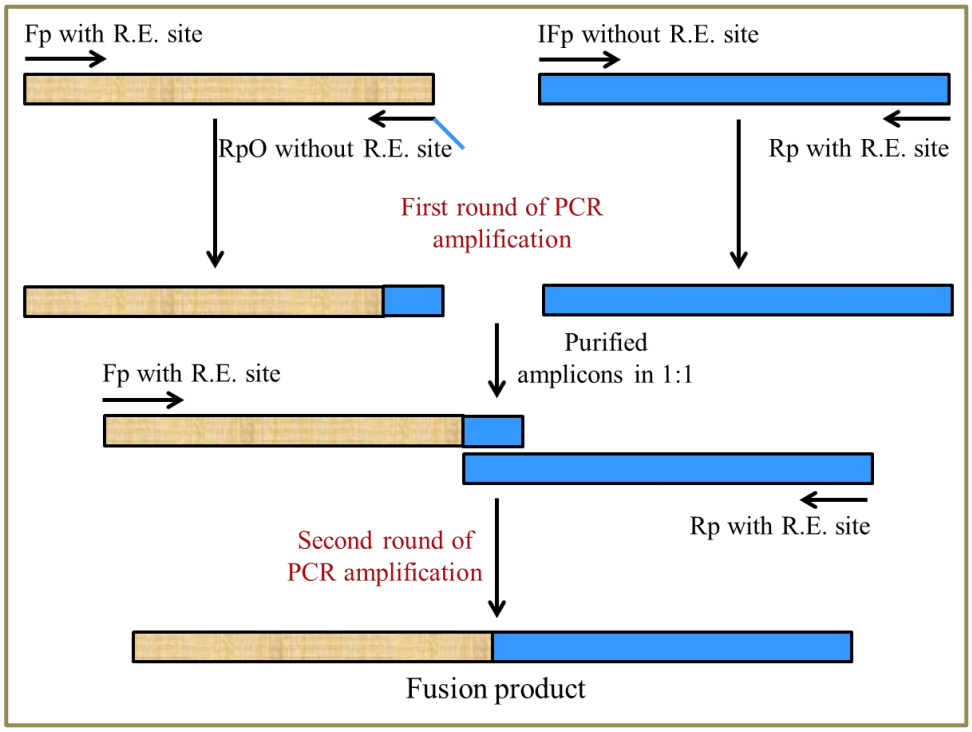

Figure 2.2: **Schematic representation of overlap extension PCR method** used for generation of *Sp*ChiD fusion chimeras.

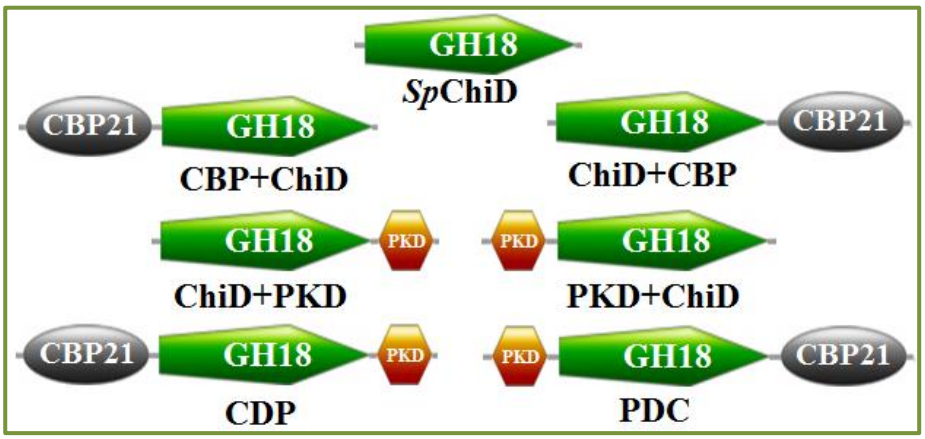

Figure 2.3: **Domain organization of *Sp*ChiD fusion chimeras** generated using overlap extension PCR method. Based on the type of domain fused and its orientation, the chimeras were named accordingly.

S.No	Name of the primer	Primer sequence (5'-3')	Template used for PCR	Name of the gene amplified	Amplicon size (kb)	Primer combination for fusion	Restriction sites	Name of the plasmid
1a.	CBP21 Fp	AAT AAC CAT GGT TCA CGG CTA TGT CGA AAC	pCBP21-pET22b(+)	CBP21 with overhang of ChiD	0.51	CBP21 Fp & Chi D Rp (~1.7kb)	*Nco* I & *Xho* I	CBP+ChiD pET22b(+)
	CBP21RpO	AGC CAT GCC GGC ACC TTT AGT CAA ATT AAC						
1b.	Chi D IFp	GGT GCC GGC ATG GCT CAT GCC GCT TCT TAC	pChiD-pET22b(+)	ChiD without RS at the N-terminus	1.2			
	Chi D Rp	AAT AAC TCG AGC TGT TTC CCG CCG TTA ATC C						
2a.	Chi D Fp	TAA TAC CAT GGG TGC CGG CAT GGC TCA TG	pChiD-pET22b(+)	ChiD with overhang of CBP21	1.2	Chi D Fp & CBP21 Rp (~1.7kb)	*Nco* I & *Xho* I	ChiD+CBP pET22b(+)
	Chi D RpO	TTC GAC ATA GCC GTG CTG TTT CCC GCC GTT						
2b.	CBP21 IFp	CAC GGC TAT GTC GAA ACC CCG GCC AGT CGT	pCBP21-pET22b(+)	CBP21 without RS at the N-terminus	0.51			
	CBP21 Rp	GCA TAC TCG AGT TTA GTC AAA TTA ACG TC						
3a.	PKD Fp	CAA TAA CCA TGG CCG TAC CGG GTA AGC CTA C	pChiA-pET22b(+)	PKD with overhang of ChiD	0.4	PKD Fp & Chi D Rp (~1.6kb)	*Nco* I & *Xho* I	PKD+ChiD pET22b(+)
	PKD RpO	AGC CAT GCC GGC ACC GCC GGA ATC CTG CTT						
3b.	Chi D IFp	GGT GCC GGC ATG GCT CAT GCC GCT TCT TAC	pChiD-pET22b(+)	ChiD without RS at the N-terminus	1.2			
	Chi D Rp	AAT AAC TCG AGC TGT TTC CCG CCG TTA ATC C						
4a.	Chi D Fp	TAA TAC CAT GGG TGC CGG CAT GGC TCA TG	pChiD-pET22b(+)	ChiD with overhang of PKD	1.2	Chi D Fp & PKD Rp (~1.6kb)	*Nco* I & *Xho* I	ChiD+ PKD pET22b(+)
	Chi DARpO	CTT ACC CGG TAC GGC CTG TTT CCC GCC GTT						
4b.	PKD IFp	GCC GTA CCG GGT AAG CCT ACG CTG GCC TGG	pChiA-pET22b(+)	PKD without RS at the N-terminus	0.4			
	PKD Rp	GCA TAC TCG AGG CCG GAA TCC TGC TTA TA						
5a.	PKD Fp	CAA TAA CCA TGG CCG TAC CGG GTA AGC CTA C	PKD+ChiD pET22b(+)	PKD+ChiD with overhang of CBP21	1.6	PKD Fp & CBP21 Rp (~2.1kb)	*Nco* I & *Xho* I	PKD+ChiD+CBP pET22b(+)
	Chi D RpO	TTC GAC ATA GCC GTG CTG TTT CCC GCC GTT						
5b.	CBP21 IFp	CAC GGC TAT GTC GAA ACC CCG GCC AGT CGT	pCBP21-pET22b(+)	CBP21 without RS at the N-terminus	0.51			
	CBP21 Rp	GCA TAC TCG AGT TTA GTC AAA TTA ACG TC						
6a.	CBP21 Fp	AAT AAC CAT GGT TCA CGG CTA TGT CGA AAC	CBP+ChiD pET22b(+)	CBP21+ChiD with overhang of PKD	1.7	CBP21 Fp & PKD Rp (~2.1kb)	*Nco* I & *Xho* I	CBP+ChiD+PKD pET22b(+)
	Chi DARpO	CTT ACC CGG TAC GGC CTG TTT CCC GCC GTT						
6b.	PKD IFp	GCC GTA CCG GGT AAG CCT ACG CTG GCC TGG	pChiA-pET22b(+)	PKD without RS at the N-terminus	0.4			
	PKD Rp	GCA TAC TCG AGG CCG GAA TCC TGC TTA TA						

Table 2.2: Primers used for generation of *Sp*ChiD fusion chimeras

polymerization time was 90 sec. The product from the 1st step PCR was used as mega primer for the 2nd step PCR with annealing temperature of 60°C and polymerization time of 150 sec. Details of the primers used for the generation of *Sp*ChiD mutants were listed (Table 2.1). Agarose gel electrophoresis was performed and the amplicons of desired size (1.2 kb) were gel eluted using Qiagen (Duesseldorf, Germany) gel extraction kit. Both the gel eluted amplicons and expression vector pET-22b(+) were subjected to double-digestion with *Nco* I and *Xho* I at 37°C for 6 h, followed by PCR clean up using Qiagen gel clean up kit. Double-digested amplicons were ligated to *Nco* I and *Xho* I sites of the vector pET-22b (+), at 16°C for 16 h. The inserted mutation was confirmed by automated DNA sequencing.

2.4.4 Generation of SpChiD Fusion Chimeras

Overlap extension/fusion PCR approach was followed for preparing *Sp*ChiD fusion chimeras (Fig. 2.2). Plasmid templates pChiD-pET22b(+), pChiA-pET22b(+) and pCBP21-pET22b(+) with appropriate combinations of primers as listed in the Table 2.2 were used for generating *Sp*ChiD fusion chimeras. Based on the fusion of binding domains to either 'N' or 'C' terminus of the *Sp*ChiD gene, the resulted *Sp*ChiD chimeras were designated as CBP+ChiD, ChiD+CBP, PKD+ChiD, ChiD+PKD, PKD+ChiD+CBP (PDC) and CBP+ChiD+PKD (CDP) (Fig. 2.3). The final amplicons of desired sizes (CBP+ChiD & ChiD+CBP, of 1.7 kb, PKD+ChiD & ChiD+PKD of 1.6 kb, PDC & CDP of 2.1 kb) were double-digested and ligated to *Nco* I & *Xho* I sites of pET-22b (+) expression vector. All the ligation reactions were performed at 16°C for 16 h, using T4 DNA ligase. Ligation mixtures were then transformed individually into the highly efficient competent cells of *E. coli* Rosetta-gami II (DE3) and the selection of positive clones was done on appropriate antibiotic plates. Clones positive for double digestion were further confirmed through sequencing.

2.4.5 Protein Expression, Isolation & Purification

2.4.5.1 Heterologous Expression

E. coli Rosetta-gami II (DE3) cells containing the appropriate *Sp*ChiD mutants (or) fusion chimeras were used for protein over expression studies. Colonies harbouring the desired plasmids were inoculated into the LB medium with ampicillin and

chloramphenicol as the selection antibiotic markers at the working concentrations 100 µg/mL and 25 µg/mL, respectively. Cultures were grown at 37°C for overnight at 200 rpm. The overnight culture was used as starter culture for bulk expression of the desired protein. Glycerol stocks (20%) of all the variants were prepared from the fully gown overnight starter cultures and stored at -80°C. One percent overnight culture was used for bulk expression of proteins and the cultures were grown to an optical density of 0.4-0.6 at 600 nm (OD_{600}), and IPTG was added to a final concentration of 0.5 mM. The cells were further incubated for 16 h at 18°C, followed by harvesting the cultures by centrifugation at 7741×g for 10 min at 4°C.

2.4.5.2 Protein Isolation

Periplasmic fraction (PF) was prepared with little modifications in the protocol as suggested in the pET expression system manual, Novagen. Cells were subjected to an osmotic shock in a two-step procedure for isolating PF. In the first step, the cell pellet was resuspended in 15 ml of ice-cold spheroplast buffer and incubated at 4°C with gentle mixing for 15 min. The PF buffer-1 contains 10 ml of 1 M Tris–HCl, pH 8.0, 20 g sucrose, 200 µL 0.25 M EDTA, pH 8.0, and 200 µL 50 mM PMSF with a final volume adjusted to 100 mL using distilled H_2O. The cells were then harvested by centrifugation at 7741×g, for 8 min at 4°C, and the supernatant was discarded. The pellet was further resuspended in 15 mL of ice-cold filter sterilized PF buffer-2 containing 5 mM $MgSO_4$ and incubated at 4°C for 10 min, followed by centrifugation at 7741×g, for 8 min at 4°C. The supernatant was filtered using 0.2 µm sterile filter and used for purification.

2.4.5.3 Ni-NTA Purification

Before proceeding for purification, the protein in the PF was buffer exchanged against the lysis buffer (50 mM NaH_2PO_4, 300 mM NaCl, 10 mM imidazole with pH 8.0), which was used as equilibration buffer in the further steps of affinity purification. Six mL ethanol suspension of the Ni-NTA agarose was packed into a sterile 10 mL syringe. Column was equilibrated with lysis buffer, followed by PF application onto the column. Flow through was collected and the column was washed with four column volumes of wash buffer (50 mM NaH_2PO_4, 300 mM NaCl, 20 mM imidazole with pH

8.0). Elution of the bound recombinant protein was done in a gradient elution method, where in, elution buffers containing 50 mM, 150 mM and 250 mM imidazole, were used without altering the concentrations of NaH_2PO_4 & NaCl. Two column volumes of the each elution were done to get the purified protein. All the fractions were loaded onto 12% SDS-PAGE to check the purity of protein.

2.4.5.4 SDS-PAGE Analysis

The protein samples were separated by 12% SDS-PAGE on vertical slab gels. The stacking gel contained 4.5% polyacrylamide in 0.125 M Tris-HCl, pH 6.8 and the resolving gel contained 12% polyacrylamide in 0.375 M Tris-HCl, pH 8.8. Electrode buffer contained 0.025 M Tris-HCl, 0.192 M glycine and 0.1% (w/v) SDS of pH 8.5. The samples were boiled at 100°C for 5 min in the sample buffer [1% SDS (w/v) and 12% glycerol (v/v), in 0.063 M Tris-HCl, pH 6.8] and electrophoresis was carried out at 50V in stacking gel and at 100V in resolving gel. The gels were stained in a solution containing 0.5% (w/v) Coomassie brilliant blue G-250, 30% (v/v) methanol and 10% (v/v) glacial acetic acid. Destaining of the gels was done in a solution containing methanol, H_2O and acetic acid in the ratio 45:45:10. Washing was done with destaining solution till the protein bands were visible against a clear background.

2.4.5.5 Preparation of the Protein

Fractions with highest purity were pooled and concentrated using Macrosep Centrifugal Devices (Pall Corporation, USA) with 10 kDa cut-off. Concentrated protein was dialysed against 50 mM sodium phosphate pH 8.0. The purified proteins were quantified using Pierce BCA protein assay kit (Thermo Scientific, USA). Slope from the standard calibration curve constructed as per the instructions given in the kit, using different concentrations of bovine serum albumin (BSA) was for quantifying the protein amount.

2.4.6 Zymogram Analysis

Dot blot assay was performed to detect the activity of purified *Sp*ChiD mutants and fusion chimeras. A composite gel supplemented with 0.1% glycol chitin was prepared. Five µg each of purified chitinase was spotted on to the gel and placed in humid chamber at 37°C for overnight. Followed by staining of the gel was with 0.01%

calcofluor white M2R in 0.5 M Tris-HCl pH 8.8 for 10 min at 4°C. Finally, the brightener solution was removed, and the gel was washed with dH_2O for 30 min at 4°C. Lytic zones were visualized as dark blue spots when the gels were observed under UV transilluminator.

2.4.7 Reducing End Assay

Chitinase activity was measured by a widely used reducing end assay for the quantification of CHOS, called Schales' procedure (Imoto & Yagishita, 1971). All the reactions were performed in 200 µL reaction volumes where an appropriate amount of *Sp*ChiD mutants or fusion chimeras were incubated with colloidal chitin in 50 mM sodium phosphate, pH 8.0 at 37°C, 200 rpm for 1 h. Incubation was followed by centrifugation of the reaction mixture at 13,600×g at 4°C for 15 min. A 40 µL of the clear supernatant containing reducing sugars was mixed with 300 µL of the freshly prepared color reagent (0.5 M sodium carbonate, 0.05% potassium ferricyanide) and boiled for 20 min at 100°C in dark. All the samples were prepared in triplicate and a 200 µL of each sample was taken in 96 well microtiter plate and the OD_{420} was measured using microtiter plate reader (Multiscan, Labsystems, Finland). One unit was defined as the amount of enzyme that liberated 1 µmol of reducing sugar per minute.

2.4.8 Kinetic Analysis

Kinetic parameters for all the *Sp*ChiD mutants or fusion chimeras were obtained by incubating different concentrations of colloidal chitin (0-50 mg/mL) as substrate, with a constant amount of enzyme (38 µg) in 50 mM sodium phosphate, pH 8.0. Proper controls for buffer, enzyme and substrate alone were maintained. All the reactions were carried out at 40°C for 1 h, with constant shaking at 200 rpm. Enzyme activity was measured as per the Schales' procedure described in section 2.4.7. Enzyme activity was defined as the release of one micromole of *N*-acetyl-glucosamine (NAG) per sec under standard experimental conditions. Specific activity was calculated in nkatal/mg of protein. Kinetic values were obtained from three independent sets of data fitting to the Michaelis-Menten equation by nonlinear regression function available in GraphPad Prism software version 5.0 (GraphPad Software Inc., San Diego, CA).

2.4.9 Time Course of Colloidal Chitin Hydrolysis by SpChiD Fusion Chimeras

Time dependent degradation of colloidal chitin by native *Sp*ChiD and its fusion chimeras was performed by incubating 25 mg/mL of colloidal chitin with 38 µg of the respective enzyme in 50 mM sodium phosphate, pH 8.0. Reaction mixtures were incubated at 40°C, 800 rpm in a thermomixer, and a 100 µL of the sample was withdrawn at regular time intervals (30, 60, 90, 120, 150, 180, 210, 360 and 720 min) into sterile 1.5 mL eppendorf tubes and centrifuged at 16,100×g to get the clear supernatant containing soluble CHOS. Enzyme activity was measured as per the Schales' procedure described in section 2.4.7. All assays were performed in triplicate and with proper blanks (buffer + 25 mg/mL colloidal chitin) and controls (buffer alone and buffer + 38 µg of enzyme). Micromoles of the reducing ends released were calculated using the slope from the standard prepared with different concentrations of NAG.

2.4.10 Degradation of 'α' & 'β' Chitin Substrates by SpChiD Fusion Chimeras

The substrate (2.5%, wt/vol) α-chitin (or) β-chitin was used for the degradation studies by *Sp*ChiD and its fusion chimeras. All the reactions were performed at 40°C for 1 h, in 50 mM sodium acetate buffer, pH 5.2 with 1 µM each of *Sp*ChiD or its fusion chimeras. After the incubation the reaction mixtures were spun down at 4,200×g and the clear supernatant was taken for reducing end assay. One unit was defined as the amount of chitinase that liberated 1 µmol of reducing sugar per minute.

2.4.11 High Performance Liquid Chromatography (HPLC)

*Sp*ChiD mutants or fusion chimeras positive for zymogram analysis were considered for HPLC analysis, to check the effects of mutations or domain fusions on the activity of *Sp*ChiD. Two mM DP4 (or) DP2 substrate was incubated with 350 nM of the purified *Sp*ChiD and its variants. Alternatively, 35 nM *Sp*ChiD was incubated with 50 or 100 µM of DP4 to determine the substrate binding with *Sp*ChiD. Reaction was performed in 20 mM sodium acetate buffer, pH 5.6, at 40°C. Fractions were collected up to 6 h, at regular intervals and the reaction was stopped using equal volume of 70% acetonitrile. Reaction mixture (20 µL) from each fraction was injected into HPLC (Shimadzu, Tokyo, Japan) using Hamilton (Hamilton Bonaduz, Switzerland) syringe.

The products were analysed by using SHODEX Amino-P50 4E column (4.6 ID x 250 mm, Showa Denko K.K, USA) through isocratic elution with ACN: H_2O in 70:30 (29). Flow rate of 0.7 ml/min was maintained and eluted CHOS were monitored at 210 nm. Quantification of CHOS was done by comparing peak areas of the products with peak areas obtained from known concentration of the CHOS. Mixture containing equal weight of CHOS ranging from DP1-DP6 was used for standard graph preparation. A linear correlation between peak area and concentration of CHOS in standard samples was established for quantification of reaction products up to DP6. Standard calibration curves for CHOS moieties were constructed separately. These data points yielded a linear curve for each standard sugar with the R^2 values of 0.997–1.0 allowing molar concentration of CHOS to be determined with confidence. The decrease in DP4 concentration was considered for specific activity measurements through a linear regression analysis using OriginPro 8 software.

2.4.12 Product Analysis by MALDI-TOF-MS

The remaining reaction mixtures, after HPLC analysis, were analyzed by MALDI-TOF-MS to determine the mass dependent product identity. Samples for MALDI-TOF-MS analysis were prepared by mixing 1 µL of sample (1 mg/mL substrate) with 1 µL of matrix (10 mg/mL 2,5-dihydroxybenzoic acid (DHB) in 1:1 water/ acetonitrile) on a target plate. Samples were dried under a cold air stream and analyzed with an Autoflex Speed MALDI-TOF mass spectrometer (Bruker Daltonics, Bremen, Germany) equipped with a SmartBeam™ NdYAG-laser (355 nm). The instrument was operated in positive acquisition mode and controlled by the FlexControl 3.0 software package. All spectra were obtained in the reflectron mode with an acceleration voltage of 25 kV, a reflector voltage of 26, and pulsed ion extraction of 40 ns in the positive ion mode. The acquisition range used was from m/z 50 to 4000. The data were collected from averaging 500 laser shots, with the lowest laser energy necessary to obtain sufficient signal to noise ratios. Peak lists were generated from the MS spectra using Bruker FlexAnalysis software (Version 3.0).

2. 5 In silico Analysis of SpChiD & its Mutants

2.5.1 Molecular Dynamic (MD) Simulations

The *Sp*ChiD homology model with DP4 substrate (Madhuprakash *et al*., 2012) was adopted. Point mutations G119S, G119W, W120A and G201W were generated by using "build mutant" module under protein modeling protocol implemented in Discovery Studio 2.5. The *Sp*ChiD and its four variants in complex with DP4 substrate were subjected to MD simulations for 50 nano second (ns) at constant temperature and pressure in a periodic cubic box with an edge length of approximately 1.5 nm. In addition, MD simulations were also performed for the 'apo' form of *Sp*ChiD crystal structure (PDB_ID: 4LGX) which was solved very recently (Madhuprakash *et al*., 2013). We used the AMBER ff99SB force field for the protein. The ligand parameter files with the AMBER ff99SB and GAFF force fields using antechamber (Wang *et al*., 2006) were generated, with ACPYPE script (Sousa da Silva & Vranken, 2012). All the simulations were performed by using GROMACS 4.5.5 software. The protein was solvated in the cubic box using explicit solvent-SPC model water molecules around *Sp*ChiD-DP4 complex structure. The charge of the protein complex was neutralized using three chloride ions. During MD simulations, we initially performed 5000 steps of steepest descent minimization and 1 ns position restrained dynamics to distribute water molecules throughout the system. Finally, we performed MD simulations of the whole system for 50 ns, using 0.002 ps time step. The Particle Mesh Ewald (PME) summation method (Essmann *et al*., 1995) was employed for calculation of electrostatics, with a real space cut-off of 10 Å, PME order of 6 and a relative tolerance between long- and short- range energies of 10^{-6}. Short range interactions were evaluated using a neighbor list of 10 Å updated every 10 steps. The Lennard-Jones (LJ) interactions and the real space electrostatic interactions were truncated at 9 Å. The V-rescale thermostat and Parrinello-Rahman algorithm (Parrinello & Rahman, 1981) were used to maintain temperature and pressure of 1 atm, respectively, whereas, hydrogen bonds were constrained using LINCS algorithm. The last 5 ns of trajectory file obtained from the MD simulations was used for generation of the average structure. The average structure was minimized for 2500

steps of steepest descent minimization and 1000 steps of conjugate gradient method to get energy minimized average structure. From this energy minimized average structure, the interactions between *Sp*ChiD and its mutant complexes were observed. Results were analyzed using Grace for XY plots, VMD and Discovery Studio 2.5 visualizer for trajectory visualizations.

2.5.2 Solvated Interaction Energies

SIE free energy (Bussi *et al*., 2007) is an end-point physics-based, force-field-based scoring function for predicting ligand-binding affinities. This approximation of binding free energy in solution resembles the formalism used in other physics-based binding free energy end-point calculation methods, including Molecular Mechanics-Poisson Boltzmann/ Generalized Born Surface Area (MM-PB (GB)/SA) (Naïm *et al*., 2007) and Linear Interaction Energy (LIE) (Aqvist *et al*., 2002). Binding free energies (ΔG) for the protein–ligand complexes were estimated using the SIETRAJ program. SIETRAJ (http://www.bri.nrc.ca/ccb/pub) is an alternative to the MM-PBSA software provided by the AMBER distribution. It is a set of scripts and executables for carrying out the SIE calculation on molecular dynamics trajectory or a single snapshot of target-ligand complex. This program calculates ΔG for snapshot structures from the MD simulations with a rigid infinite separation of protein and ligand. ΔG is the sum of intermolecular van der Waals (vdW), Coulomb interactions, change in reaction field energy (determined by solving the Poisson–Boltzmann equation) and non-polar solvation energy (proportional to the solvent-accessible surface area). This SIE method was successfully used to calculate the ligand binding studies and each residue contribution in the binding by Tanneeru & Guruprasad (2013) and the similar parameters were considered for the present study. Here, we estimated ΔG by averaging 500 structures from the 50 ns of selected MD snapshots and averaging over the resulting free energies obtained from each snapshot.

2. 6 Structure Determination & Thermodynamic Properties of SpChiD

2.6.1 Crystallization of SpChiD

*Sp*ChiD was crystallized using hanging drop vapor diffusion method in a 24-well plate. Each hanging drop was prepared by mixing 2.5 µl of *Sp*ChiD enzyme solution

(10 mg/ml in 20 mM sodium phosphate buffer, pH 8.0) with equal volume of reservoir solution containing 2M sodium formate and 0.1 M sodium acetate, pH 8.0 and equilibrated against 2 ml of the same reservoir solution. Crystals measuring 0.3 × 0.2 × 0.2 mm^3, which were suitable for X-ray diffraction measurements, were obtained after two weeks.

2.6.2 X-ray Intensity Data Collection

X-ray intensities were collected using a beamline, BM-14 at the European Synchrotron Radiation Facility (ESRF) in Grenoble (France). The beamline was sponsored by the Department of Biotechnology, Ministry of Science and Technology, Government of India, New Delhi. The diffraction intensities were recorded on MAR 300 CCD detector (Rayonix, Evanston, USA). Before mounting in the loop, the crystals were stabilized in a cryoprotecting solution consisting of 25% glycerol and 75% of well solution. The crystals were flash-frozen in a stream of nitrogen at 100K. The data were integrated and scaled with the help of *HKL*-2000 software package (Otwinowski & Minor, 1997).

2.6.3 Structure Determination & Refinement

The structure was determined using molecular replacement method with program MOLREP (Vagin & Teplyakov, 2010) from the CCP4 suite (Winn *et al*., 2011). The co-ordinates of chitinase II from *Klebsiella pneumoniae* (*Kp*ChiII) (PDB code: 3QOK) with which it has a sequence identity of 79% (UniProt-A6T7R3) were used as a search model. The structure was refined with REFMAC 5.5 (Murshudov *et al*., 2011) from the CCP4 suite (Winn *et al*., 2011). The protein chain tracing was carried out by building the model manually with the help of ($2F_o - F_c$) and ($F_o - F_c$) electron density maps. The model buildings were performed using programs O (Jones *et al*., 1991) and Coot (Emsley *et al*., 2004). While examining the electron densities in the Fourier (2Fo – Fc) and difference Fourier (Fo – Fc) maps, the conformations of several segments in the protein were found to be significantly different from that of the model protein (PDB: 3QOK). These were corrected manually and refined. After completing the fitting of the full protein chain into the electron density manually, further cycles of refinement were carried out using the manually improved

coordinates. When the refinement reached the stage of value 0.251 for the R_{cryst} factor, the electron density maps ($2F_o - F_c$) and ($F_o - F_c$) were calculated again and reexamined critically. The positions of 593 water oxygen atoms were determined. These were also included in the subsequent cycles of refinement. Finally, the refinement converged with values of 0.162 and 0.176 for R_{cryst} and R_{free} factors, respectively. The stereochemical quality of the refined model was examined using PROCHECK (Laskowski *et al*., 1993).

2.6.4 Circular Dichroism (CD) Spectroscopy

CD experiments were conducted on Jasco J-810 spectropolarimeter (Jasco International Co., Ltd., Tokyo, Japan), equipped with a Peltier thermostat supplied by the manufacturer. Wavelength scans were performed with 0.06 mg/ml and 0.6 mg/ml samples of *Sp*ChiD for far and near UV regions, respectively. A rectangular 0.7 mL cuvette of 0.2 cm path length was used for all measurements. Experiments were conducted at a scan rate of 20 nm/min with a response time of 4 sec and a slit width of 2 nm. Measurements were made at different temperatures between 30 and 50°C with the help of a Peltier heating system provided with the instrument. A good signal-to-noise ratio was obtained by averaging of 5 consecutive scans collected from 190-260 nm for far UV and 260-350 nm for near UV at 1-nm intervals. Buffer scans were recorded under identical conditions and were subtracted from sample spectra before further analysis.

2.6.5 Differential Scanning Calorimetry (DSC)

All DSC measurements were carried out on a MicroCal VP-DSC apparatus (MicroCal LLC, Northampton, MA, USA). Protein samples were dialyzed against 20 mM potassium phosphate buffer at pH 8.0. The dialysate was used as the reference. Protein samples of 0.5 mg/mL were heated from 10-70°C at a scanning rate of 30°/h and to investigate the effect of ligand binding on the protein thermal unfolding, the mutant E153A of *Sp*ChiD was preincubated for 1 h with 1 mM CHOS with DP2-DP6 before the DSC scans. Sample and reference solutions were properly degassed prior to the DSC experiment in order to eliminate bubbling effects. Reproducibility of baselines was verified by multiple scans, and reversibility of protein unfolding was monitored

by scanning the sample twice. Buffer scans were subtracted from thermograms obtained for *Sp*ChiD and the mutant E153A in the presence or absence of CHOS before proceeding for further analysis. Absolute and excess heat capacities were analyzed using non-two-state fit of the thermogram using the Origin v 7.0 software provided with the instrument.

2.6.6 Fluorescence Spectroscopy

The accessibility of tryptophan residues in the presence and absence of CHOS was studied by acrylamide quenching. The mutant E153A at a concentration of 0.06 mg/mL was pre incubated with 1mM each of DP2-DP6 ligands and titrated with 5 M acrylamide in 20 mM potassium phosphate, pH 8.0 buffer. A control titration with 1mM ligand in 20 mM potassium phosphate, pH 8.0 was performed simultaneously for non-specific changes in relative fluorescence intensity due to ionic-strength variation. Florescence spectra were corrected for buffer subtraction and volume changes before doing further analysis. Florescence intensity was also corrected for inner-filter effect by using the formula

$F = F_{obs}$ antilog $[(A_{ex} + A_{em})/2]$

Where F is the corrected fluorescence intensity and F_{obs} is the background subtracted and normalized fluorescence intensity. A_{ex} and A_{em} are the measured absorbances at the excitation and emission wavelengths. The absorbance of the sample was measured using Shimadzu-3600R UV absorption spectrophotometer. Quenching data were analyzed according to Stern-Volmer equation (Lakowicz, 1999).

$F_O/F = 1 + K_{SV}[Q]$

Where, F_O and F are the fluorescent intensities in the absence and presence of the quencher, respectively. K_{SV} is the Stern-Volmer quenching constant and [Q] is the molar quencher concentration.

2.6.7 Isothermal Titration Calorimetry (ITC)

Calorimetric titrations were performed at 13°C for DP2 and DP3 and at 25°C for DP5 and DP6 CHOS using a MicroCal iTC_{200} System (Microcal, Northampton, MA, USA). Samples of E153A were dialyzed extensively against 20 mM potassium phosphate, pH 8.0 buffer and the last dialysate was used to make solutions of CHOS in order to

minimize heats of dilution during the titrations. All sample solutions were filtered through 0.2 µm filters and thoroughly degassed prior to use. The protein was taken in the ITC cell and titrations were carried out by injecting 2 µL aliquots of each CHOS as ligand. Protein concentration in different titrations was maintained constant as 113 µM and the ligands DP2-6 were maintained at a concentration 2-6 mM. A time interval of 225 s was given between successive injections in order to ensure that equilibrium is attained before the next aliquot is added. During the entire titration the sample in the calorimeter cell was stirred at 260 rpm. Blank titrations were also performed by injecting ligand alone into the buffer solution, which yielded insignificant heats of dilution. The obtained binding isotherms were analyzed by using MicroCal Origin v 7.0 software supplied with the ITC_{200} system. Thermodynamic parameters, *viz*., binding stoichiometry (n), change in enthalpy (ΔH) and association constant (Ka) were obtained by nonlinear least-squares fitting of experimental data using the one set of site binding model. Free energy of binding (ΔG) and change in entropy (ΔS) were deduced from the Ka and ΔH values using the standard thermodynamic equation-

($-RT\ln K\text{a} = \Delta G = \Delta H - T\Delta S$).

2. 7 Elicitor Activity of CHOS Produced by SpChiD or the Mutant W114A

2.7.1 Size Exclusion Chromatography (SEC)

CHOS of large-scale hydrolysates were separated using a SECcurity GPC System (PSS Polymer Standards Service, Mainz) with a refractive index detector (Agilent 1200 series RID®) and a set of 3 HiLoad™ 26/60 Superdex™ 30 prep grade columns. Columns were equilibrated with filtered and degassed elution buffer (150 mM ammonium acetate, pH 4.5) Samples were filter sterilized using 0.22 µm filter and then loaded into a loop with 5 mL capacity. Elution flow rate was maintained at 0.6 mL/min for 22 h.

2.7.2 High Performance Thin Layer Chromatography (HPTLC)

For HPTLC analysis, 20 µL of each aliquot was applied to HPTLC silica gel 60 F_{254} plates Merck, Darmstadt, Germany) with a Camag automatic TLC sampler 4 (Camag, Berlin, Germany). The plate was run in a solvent system comprised butanol/

methanol/ammonia/water in the ratio 5:4:2:1, as a mobile phase. The solvent was evaporated and the products were visualized by spraying the plate with aniline-diphenylamine reagent (400 µL aniline, 400 mg of diphenylamine, 20 mL of acetone, and 3 mL of 85% phosphoric acid) and baking it at 180°C using hot air gun (Black & Decker, Germany) for 3 min. GlcN and GlcNAc monomers (Sigma Aldrich, München, Germany) and CHOS ($(GlcN)_{2–6}$ and $(GlcNAc)_{2–6}$, Seikagaku Corporation, Tokyo, Japan) were used as standards (4 µg of each monomer/oligomer).

2.7.3 Preparation of Elicitors

Chitosans with DA35% and 61% were hydrolyzed using *Sp*ChiD and its mutant W114A. To ensure that the hydrolysates contain desired quantity of longer chain CHOS, time-dependent hydrolysis of chitosan polymers was performed. All the degradation experiments were performed with 1 mg/mL chitosan substrates prepared in 50 mM ammonium acetate pH 5.2 and the reaction mixtures were incubated at 40°C. Fractions collected at regular time intervals were analyzed using HPTLC. For large scale preparation of CHOS, 100 mg of each chitosan polymer was used as the starting substrate. Thus, the prepared hydrolysates were lyophilized overnight, which were then dissolved in sterile MilliQ water to a final concentration of 1 mg/mL for MALDI-TOF-MS analysis and also to test the elicitor activity.

2.7.4 Culture & Maintenance of Rice Cell Suspension System

Suspension cultured rice cells (*Oryza sativa* L.) were kindly provided by Dr. Burkhard Schmidt (University of Aachen, Germany). The cell suspension cultures were grown in MS medium (Murashige & Skoog, 1962) supplemented with sucrose (30 g/l) and 2,4-dichlorophenoxyacetic acid (1 mg/l) and sub-cultured every 7 d in 15 mL medium. The cells were maintained at 26°C in the dark with constant agitation of 120 rpm.

2.7.5 Oxidative Burst Measurements in Rice Cell Suspension Cultures

Hydrogen peroxide (H_2O_2) generation was quantified as an assay for oxidative burst in a medium of rice cells by little modifications in the luminol dependent chemiluminescence method (Warm & Laties, 1982). Prior to experiments, cells were gently separated from the cell culture medium through a sintered glass filter at the third day after sub-culturing. Aliquots of cells (50-60 mg) were transferred to sterile 2

mL eppendorf tubes containing 1 mL of fresh rice cell suspension medium and resuspended on a rotary shaker. Cells were grown at 26°C in the dark with constant agitation of 120 rpm for 4 h. After this preincubation, elicitors to be tested were added and 20 µL of rice cells were aliquoted into sterile microtiter plates at regular time intervals. To this, 50 µL of luminol (0.1 mg/mL) was added and the chemiluminescence was measured using a luminometer (Lumat LB 9501/16, Berthold, Germany). The chemiluminescence can be measured as relative light units (RLU) which is proportional to the amount of H_2O_2 released. The micromolar (µM) H_2O_2 concentration was determined using a standard calibration curve.

2.7.6 TG between Acetylated & Deacetylated CHOS

TG activity of *Sp*ChiD was checked between fully acetylated and fully/partially deacetylated CHOS. Different combinations of substrate like (2 mM DP4 + 2 mM $(GlcN)_3$) or (2 mM DP4 + 2 mM DP2 with pattern **DA**) and/or 2 mM DP4 alone with pattern **DAAA** were incubated with 5 µg of the purified *Sp*ChiD. Fractions were collected at regular time intervals for HPTLC (or) MALDI-TOF-MS analysis. All the reactions were performed in 50 mM sodium acetate pH 5.2 at 40°C.

2. 8 Relatedness of SpChiD with Other Family GH18 Bacterial Chitinases

2.8.1 Multiple Sequence Alignment (MSA)

MSA of *Sp*ChiD (PDB: 4LGX) with other chitinases, *Kp*ChiII (PDB: 3QOK), *Sm*ChiA (PDB: 1CTN) and *Sm*ChiB (PDB: 1E15) was performed. Since, *Sp*ChiD was a single domain protein consisting of only the catalytic TIM barrel domain, the comparison was restricted only to the catalytic domain. Further, another MSA was also performed for *Sp*ChiD with all the single domain GH18 chitinases from the family Enterobacteriaceae and also with few of the well characterized chitinases from *Bacillus thuringiensis*, *B. licheniformis*, *B. circulans*, *S. marcescens*, *Stenotrophomonas maltophilia* and *Flavobacterium johnsoniae*. All the MSA were performed using ClustalW2 (www.ebi.ac.uk/Tools/msa/clustalw2/).

2.8.2 Phylogenetic Analysis

The evolutionary history was inferred by using the maximum likelihood method based on the Jones-Taylor-Thornton (JTT) matrix-based model (Jones *et al*., 1992). The

bootstrap consensus tree inferred from 500 replicates was taken to represent the evolutionary history of the taxa analyzed (Felsenstein, 1985). Branches corresponding to partitions reproduced in less than 50% bootstrap replicates were collapsed. Initial tree(s) for the heuristic search were obtained by applying the Neighbor-Joining method to a matrix of pairwise distances estimated using a JTT model. The analysis involved 131 amino acid sequences of bacterial family GH18 chitinases. List of all abbreviations and the names of enzyme sources were given in Table 2.3. All positions containing gaps and missing data were eliminated. There were a total of 70 positions in the final dataset. Evolutionary analyses were conducted in MEGA6 (Tamura *et al*., 2013).

Abbreviation	Enzyme and source	Accession No.
BcerChiCW	chitinase CW [Bacillus cereus]	AAM48520.2
BtChi a	Bacillus thuringiensis serovar kurstaki str. HD73	AGE76094.1
Pfpu7ChiC	Paenibacillus sp. FPU-7	BAM67139.1
Pfpu7ChiD	Paenibacillus sp. FPU-7	BAM67140.1
PeChi c	chitinase [Paenibacillus elgii]	WP_010499208.1
BsubChi-AF069131	chitinase [Bacillus subtilis]	AAC23715.1
BliTPChi- U71214	chitinase [Bacillus licheniformis]	AAB47847.1
BliChi1-DSM13	[Bacillus licheniformis DSM 13 = ATCC 14580]	AAU21943.2
PehChi80	chitinase Chi80 [Paenibacillus ehimensis]	BAC76694.1
Pfpu7ChiA	[Paenibacillus sp. FPU-7]	BAM67137.1
Pfpu7ChiF	[Paenibacillus sp. FPU-7]	BAM67142.1
BcW12ChiA1-M57601	chitinase A1 [Bacillus circulans]	AAA81528.1
KzChi	chitinase [Kurthia zopfii]	BAA09831.1
CpChiC	[Clostridium paraputrificum]	BAD12045.1
CtChiA	Chitinase [Clostridium thermocellum ATCC 27405]	CAA93150.1
Pfpu7ChiB	[Paenibacillus sp. FPU-7]	BAM67138.1
CpChiA	Chitinase A [Clostridium paraputrificum]	BAA34922.1
BpChiL	chitinase large [Bacillus cf. pumilus SG2]	ABF50676.1
BliChi b-DSM13	putative glycoside hydrolase [Bacillus licheniformis DSM 13 = ATCC 14580]	AAU39297.1
IjChiA	chitinase A [Isoptericola jiangsuensis]	ADD17350.1
VfChidex	chitodextrinase [Vibrio furnissii]	AAC44673.1
PaS9ChiA	chitinase A [Pseudoalteromonas sp. S9]	AAC79665.1
ArthoChiA	chitinase [Arthrobacter sp.]	CAB62382.1
ScChiI	putative chitinase precursor [Streptomyces coelicolor A3(2)]	CAB76866.1
ScChiC	chitinase C [Streptomyces coelicolor A3(2)]	CAB94547.1
SlChiC- D12647	chitinase C [Streptomyces lividans]	BAA02168.1
SpliChi63- M82804	chitinase 63 [Streptomyces plicatus]	AAA26720.1
ScChiD	Chitinase [Streptomyces coelicolor A3(2)]	CAB61662.1
Cellchi63	endo-63 precursor [Cellulomonas sp. GM13]	AAF00931.2
StheChi- D14536	Chitinase precursor [Streptomyces thermoviolaceus]	BAA03404.1
DcChi67	chitinase Chi67 [Doohwaniella chitinasigens]	AAF21468.1
CsChiC	[Chitiniphilus shinanonensis]	BAK53887.1
JlChi	[Janthinobacterium lividum]	AAA83223.1
LeChiA	[Lysobacter enzymogenes]	AAT77163.1
StmChiA	[Stenotrophomonas maltophilia]	CAQ44264.1
StmChiB	[Stenotrophomonas maltophilia]	CAQ46811.1
ScChiE	[Streptomyces coelicolor A3(2)]	CAA16211.1
ArthoChiB	[Arthrobacter sp.]	CAB62499.1
IjChiB	[Isoptericola jiangsuensis]	ADD17351.1
PeChi d	[Paenibacillus elgii]	WP_010502184.1
FjChi d	[Flavobacterium johnsoniae UW101]	ABQ07756.1
PehChi55	[Paenibacillus ehimensis]	BAC76692.1
Pfpu7ChiW	[Paenibacillus sp. FPU-7]	BAM67143.1
RmChi	[Rhodothermus marinus]	AAU11838.1
BcW12ChiC-D89568	[Bacillus circulans]	BAA13974.1

Table 2.3: List of abbreviations and the enzyme sources with accession numbers

Continued…

Abbreviation	Enzyme and source	Accession No.
SlChi	[Serratia liquefaciens ATCC 27592]	YP_008230673.1
SpChiD	[Serratia proteamaculans]	ABV41826.1
SplyChi	[Serratia plymuthica 4Rx13]	YP_008138745.1
SfChi	[Serratia fonticola]	WP_021181207.1
SmWW4Chi	[Serratia marcescens WW4]	AGE18533.1
CrChi	[Citrobacter rodentium ICC168]	YP_003364864.1
CdChi	[Cedecea davisae]	WP_016535963.1
EaChi c	[Enterobacter aerogenes KCTC 2190]	AEG99244.1
KpChi	[Klebsiella pneumoniae subsp. pneumoniae MGH 78578]	YP_001334864.1
KvChi	[Klebsiella variicola CAG:634]	WP_022065505.1
EcChi a- ATCC 13047	[Enterobacter cloacae subsp. cloacae ATCC 13047]	ADF62010.1
EasChi	[Enterobacter asburiae LF7a]	YP_004828221.1
YrChi	[Yokenella regensburgei]	WP_006819576.1
RoChi	[Raoultella ornithinolytica B6]	YP_007873975.1
KoChi	[Klebsiella oxytoca]	WP_004101274.1
CyChi	[Citrobacter youngae]	WP_006684883.1
CfChi	[Citrobacter freundii]	WP_003840873.1
ShfChi	[Shigella flexneri 1235-66]	EIQ80021.1
YeChi2	[Yersinia entomophaga]	ABG33867.1
YeChi1	[Yersinia entomophaga]	ABG33870.1
EaChi a	[Enterobacter aerogenes KCTC 2190]	AEG97068.1
EaChi b	[Enterobacter aerogenes KCTC 2190]	AEG97642.1
CsChiD	[Chitiniphilus shinanonensis]	BAK53888.1
VhpreChiA	[Vibrio harveyi]	AAK11576.1
AcChi1	[Aeromonas caviae]	AAA93130.1
AhChiA	[Aeromonas hydrophila]	AAF70180.1
EcChi b- ATCC 13047	[Enterobacter cloacae subsp. cloacae ATCC 13047]	ADF62328.1
SpChiA	Serratia proteamaculans	ABV39247.1
SmWW4ChiA	[Serratia marcescens WW4]	AGE15954.1
Sm2170ChiA-AB015996	[Serratia marcescens]	BAA31567.1
CpChiB	[Clostridium paraputrificum]	BAA23796.1
SpChiC	Serratia proteamaculans	ABV42574.1
SmWW4ChiB	[Serratia marcescens WW4]	AGE19379.1
Sm2170ChiB-AB015997	[Serratia marcescens]	BAA31568.1
FnChiA	[Francisella novicida]	ABB76136.1
BtChi b	[Bacillus thuringiensis serovar kurstaki str. HD73]	AGE79252.1
PapChiC	[Pseudoalteromonas piscicida]	BAA24795.1
PeChi e	[Paenibacillus elgii]	WP_010502184.1
PeChi g	[Paenibacillus elgii]	WP_010499339.1
PeChi f	[Paenibacillus elgii]	WP_010500806.1
BliChi c-DSM13	[Bacillus licheniformis DSM 13 = ATCC 14580]	AAU40846.1
BliChi a-DSM13	[Bacillus licheniformis DSM 13 = ATCC 14580]	AAU39010.1
BtChi c	[Bacillus thuringiensis serovar kurstaki str. HD73]	AGE79460.1

Table 2.3: List of abbreviations and the enzyme sources with accession numbers

Continued…

Abbreviation	Enzyme and source	Accession No.
FjChiC	[Flavobacterium johnsoniae UW101]	ABQ07559.1
FjChi b	[Flavobacterium johnsoniae UW101]	ABQ07183.1
ScChiM	[Streptomyces coelicolor A3(2)]	CAC16966.1
LpChiA	[Legionella pneumophila str. Lens]	CAH15360.1
PehChi60	[Paenibacillus ehimensis]	BAC76693.1
ScChiL	[Streptomyces coelicolor A3(2)]	CAC10108.1
ScChiK	[Streptomyces coelicolor A3(2)]	CAB44541.1
ArthoChiC	[Arthrobacter sp. TAD20]	CAD43215.1
ScChiH	[Streptomyces coelicolor A3(2)]	CAA15789.1
AeroChi b- BAA09627.1	[Aeromonas sp. 10S-24]	BAA09627.1
CsChiG	[Chitiniphilus shinanonensis]	BAK53891.1
AeroChiII-D31818	[Aeromonas sp. 10S-24]	BAA06605.1
BurChiA	[Burkholderia gladioli]	BAA92251.1
FjChiA	[Flavobacterium johnsoniae UW101]	ABQ07554.1
SmWW4ChiC1	[Serratia marcescens WW4]	AGE16995.1
Sm2170ChiC	[Serratia marcescens]	WP_021504616.1
SpChiB	[Serratia proteamaculans]	ABV40327.1
PaChi	[Pseudomonas aeruginosa PAO1]	AAG05688.1
EfChi	[Enterococcus faecalis V583]	AAO80224.1
MmChi60	[Moritella marina]	CAM88673.1
VhChiA- U81496	[Vibrio harveyi]	AAC46383.1
LlChi	[Lactococcus lactis subsp. lactis Il1403]	AAK06048.1
Pfpu7ChiC	[Paenibacillus sp. FPU-7]	BAM67139.1
NpChi	[Nocardiopsis prasina]	BAC45251.1
ScChiA	[Streptomyces coelicolor A3(2)]	CAB92596.1
SlChiA- D13775	[Streptomyces lividans]	BAA02918.1
ScChiJ	[Streptomyces coelicolor A3(2)]	CAB69724.1
AeroChi c- BAA09628.1	[Aeromonas sp. 10S-24]	BAA09628.1
CvioChiA	[Chromobacterium violaceum ATCC 12472]	AAQ60603.1
VcChiA	[Vibrio cholerae]	AAC72236.1
XAKChiA	[Xanthomonas sp. AK]	BAA36460.1
ScChiB	[Streptomyces coelicolor A3(2)]	CAA20216.1
SlChiB- D84193	[Streptomyces lividans]	BAA25139.1
Soli01- X71080	[Streptomyces olivaceoviridis]	CAA50398.1
AeroChi a- BAA09626.1	[Aeromonas sp. 10S-24]	BAA09626.1
CsChiE	[Chitiniphilus shinanonensis]	BAK53889.1
PeChi b	[Paenibacillus elgii]	WP_010496918.1
BcW12ChiD1- D10594	[Bacillus circulans]	BAA34114.1
PeChi a	[Paenibacillus elgii]	WP_010500590.1
BtChi d	[Bacillus thuringiensis serovar kurstaki str. HD73]	AGE79587.1
BcerExoChi	[Bacillus cereus ATCC 14579]	AAP10651.1
BcerChiCH	[Bacillus cereus]	AAP47142.1
BcerNCTU2	[Bacillus cereus]	ACY39278.1

Table 2.3: List of abbreviations and the enzyme sources with accession numbers

Continued…

Results

3.0 SpChiD - the Unique Chitinase

*Sp*ChiD was a single domain GH18 chitinase comprising 406 amino acid residues, with unique unprecedented catalytic properties. Hydrolytic activity on (CHOS) and colloidal chitin indicated that *Sp*ChiD was an endo-acting processive enzyme, with the unique ability to convert released chitobiose (DP2) to *N*-acetylglucosamine (DP1), the major end product. Apart from these properties *Sp*ChiD showed hyper-TG with DP3-DP6 substrates, generating considerable amounts of long-chain CHOS. *Sp*ChiD was less active on insoluble polymeric chitin substrates due to the absence of accessory domains. In the present study the activities of *Sp*ChiD were thoroughly analyzed using structural and mutational approaches to improve the TG activity of *Sp*ChiD both in terms of increasing the quantity of TG products and in extending the duration of TG activity.

3.1 Site Directed Mutagenesis of SpChiD

3.1.1 Homology Modeling and Selection of Target Sites for Mutagenesis

The NCBI BLAST search of the *Sp*ChiD at PDB identified the crystal structure of putative chitinase II from *Klebsiella pneumoniae* (*Kp*ChiII, PDB_ID: 3QOK). The *Sp*ChiD had 79% of sequence similarity with the template crystal structure. The modelled structure of the *Sp*ChiD (Fig. 3.1) was validated using PROCHECK (99.4% of the residues are in the allowed region) and Verify_3D (94.9% of residues had an average 3D-1D score > 0.2). Thus, the compatibility of *Sp*ChiD 3D model structure with its 1D amino acid sequence was confirmed. The coordinates of chitotetraose (DP4) were built based on the crystal structure of PDB_ID: 1NH6.

To improve the TG activity of *Sp*ChiD, the amino acid residues in the catalytic center, catalytic groove and in the surface exposed region were selected for mutagenesis. In the catalytic center the residues M220, Y222, R278 and Y154 were closer to the catalytic triad D*X*D*X*E (Fig. 3.2 A). We have mutated E153 from the catalytic triad, F119 close to the catalytic triad and a few residues present in the catalytic groove including S110, G113, W114 and F58, where the substrate molecules show major interactions (Fig. 3.2 B). Further, W241 on the surface of the protein,

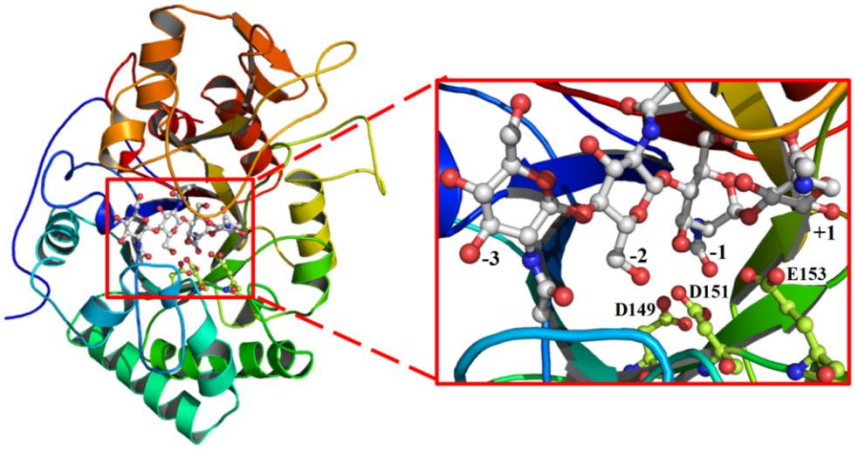

Figure 3.1: **The 3D model of *Sp*ChiD.** Interactions of chitin tetramer with the catalytic residues (D149, D151 and E153) at the active site are highlighted. The side chains of catalytic residues were shown as *sticks* and subsites indicated. Pictures used for representation were made with PyMol (www.pymol.org).

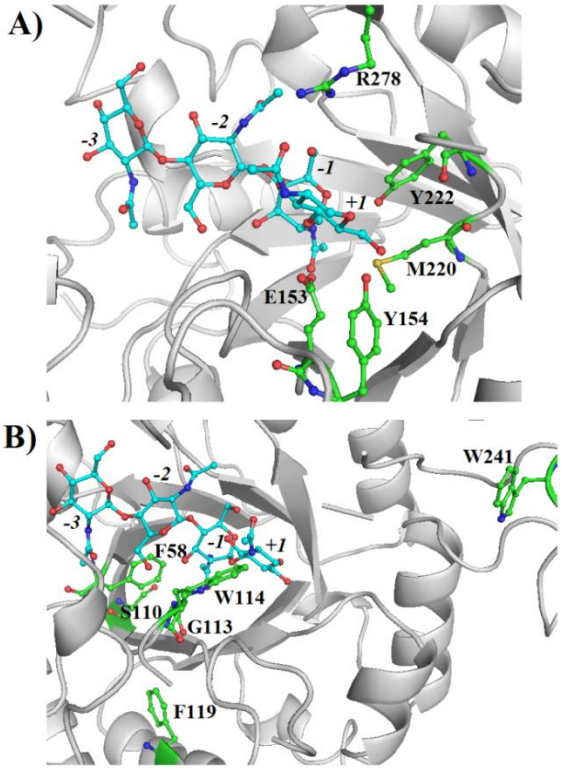

Figure 3.2: **Close view of 3D-model of *Sp*ChiD representing the residues targeted for mutation.** A) The catalytic center (M220, Y222, R278, E153 and Y154). B) The catalytic groove (F58, F119, G113, S110 and W114) and one residue at the solvent accessible region W241. The side chains of residues mutated in this study were shown as *sticks* and subsites indicated. Pictures used for representation were made with PyMol (www.pymol.org). # Residue numbering was changed as per the crystal structure nomenclature.

which is expected to play a role in threading of chitin molecules to the catalytic center, was also selected for point mutation.

3.1.2 Expression, Purification & Dot Blot Assay for SpChiD or the Mutants

E. coli Rosetta-gami II (DE3) cells harbouring the plasmids of *Sp*ChiD and the mutants were used for protein expression. Induced cells were harvested and processed for isolation of PF as described in the section 2.4.5.2. Soluble proteins of *Sp*ChiD and its variants in the PFs were passed through Ni-NTA affinity matrix to obtain pure proteins (details described in the section 2.4.5.3). SDS-PAGE analysis confirmed the purity of collected protein fractions and the mutant protein molecular mass was also around 44.7 kDa (Fig. 3.3 A). The dark blue spots on the in gel assay confirmed the activity of *Sp*ChiD and the mutant proteins that had single/double amino acid substitutions (Fig. 3.3 B).

3.1.3 Hydrolytic & TG Activities of SpChiD

*Sp*ChiD at 35 nM concentration with 50 or 100 µM DP4 substrate produced both DP5 and DP6 TG products (Fig. 3.4 A&B), suggesting that -2 to +2 and -1 to +3 are possible productive binding sites for *Sp*ChiD. This analysis further confirmed that the *Sp*ChiD displays TG even under low enzyme or substrate concentrations. *Sp*ChiD showed a very sharp decrease in the initial concentration of DP4 (2 mM) substrate starting from 5-45 min (1.26% decreased to 0.2%), and complete depletion by the end of 120 min. The TG activity of *Sp*ChiD, although was detectable up to 90 min, the formation of TG products (DP5 and DP6) was relatively high up to 30 min only (DP5 from 1.3% to 6.3%, and DP6 from 1.9% to 4%). Later, the TG activity decreased and completely extinguished after 90 min (DP5 and DP6 were 1.0%, 0.3%, respectively) (Fig. 3.5 A). *Sp*ChiD produced chitobiose (DP2) as the major end product (56.4%) at the end of 120 min, along with the other two degradation products *N*-acetyl glucosamine (DP1) and chitotriose (DP3). The DP1 product (42.4%) was much higher than DP3 product (0.8%) at 120 min.

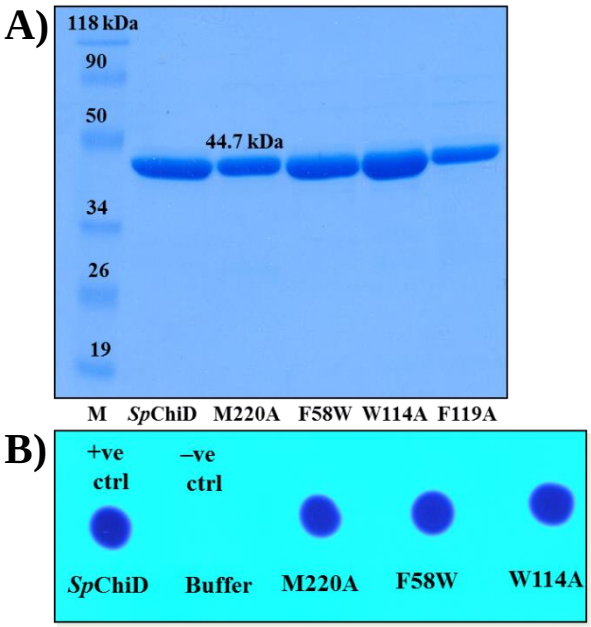

Figure 3.3: **Representative picture showing purification and activity analysis of *Sp*ChiD and the variants.** (A) Recombinant *Sp*ChiD and the variants were (Mwt 44.7 kDa) purified by Ni-NTA agarose affinity chromatography using elution buffer containing 50, 150 and 250 mM imidazole. The sizes of the standards are indicated in kDa. M: Pre-stained protein molecular weight marker. (B) Purified *Sp*ChiD and the variants were spotted (5 µg) on glycol chitin substrate containing polyacrylamide gel and incubated overnight at 37°C in humid chamber. After incubation, the gel was stained with 0.01% Calcofluor white M2R for 10 min at 4°C. The gel was placed on UV transilluminator to visualize lytic zone. *Sp*ChiD was the positive control; buffer as negative control (20 mM sodium acetate, pH 5.6). (Same procedure was followed for all the variants). # Residue numbering was changed as per the crystal structure nomenclature.

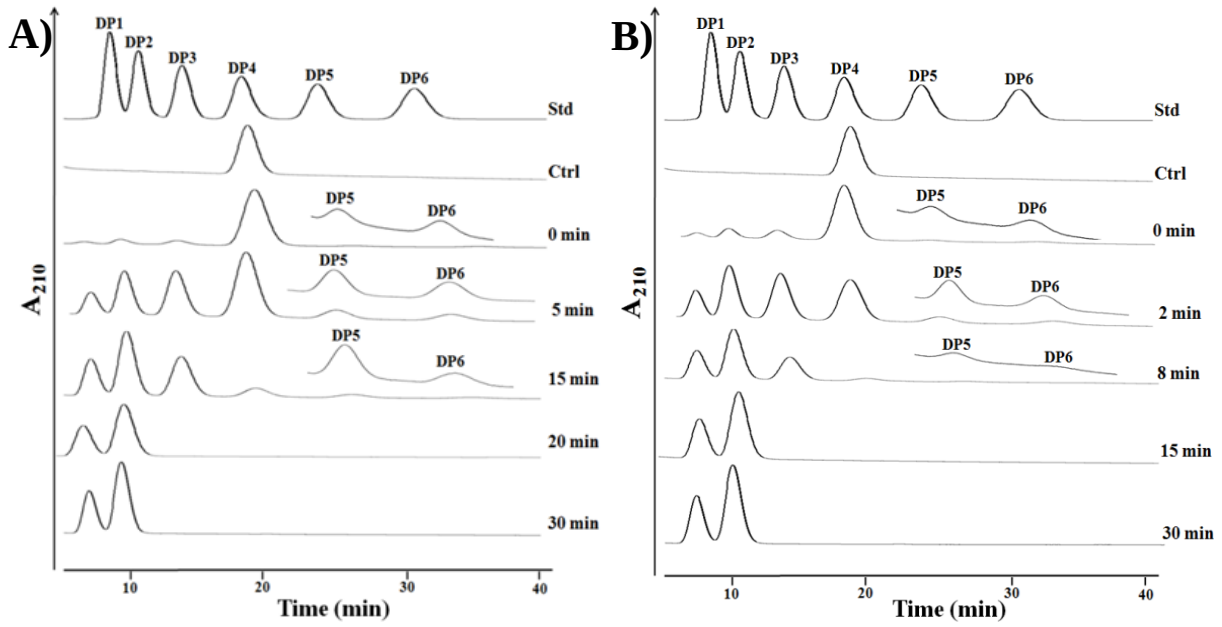

Figure 3.4: **Hydrolytic and TG activities of the *Sp*ChiD with low substrate and enzyme concentrations.** Products were analyzed through isocratic HPLC, with ACN: H_2O in 70:30. Absorbance at 210 nm was recorded. The top most profile in the chromatogram shows a standard mixture of CHOS ranging from DP1-DP6. HPLC chromatogram shows change in the product profile along with DP4 substrate through time. Insets show the magnified view of the low peak area products. Control represents the substrate without the enzyme treatment.
A). Reaction products from 100 µM DP4 and 35 nM *Sp*ChiD.
B). Reaction products from 50 µM DP4 and 35 nM *Sp*ChiD.

3.1.4 Effect of Mutations on Hydrolytic & TG Activities of SpChiD

3.1.4.1 Residues at the Catalytic Center

3.1.4.1.1 Glu153 to Asp Conversion

E153D mutation resulted in significant loss of both hydrolytic and TG activities leaving 92.5% of DP4 substrate at the end of 6 h (Fig. 3.5 B). Only a trace amount of hydrolytic products DP1, DP2 and DP3 were detected even after 6 h. Among the TG products, only DP5 and DP6 were detected (no TG products >DP6), where in the former was detectable at 150th min and the latter at 60th min. The proportion of quantifiable oligomers, DP1 to DP6, generated by E153D mutant was 0.6%, 2.3%, 2.5%, 92.5%, 1.0% and 1.1% at the end of 6 h.

3.1.4.1.2 Tyr154, Met220, Tyr222 & Arg278 to Ala Conversion

Y154A was unique from all other mutants generated, which retained TG activity even when hydrolytic activity increased. The concentration of DP4 substrate and DP3 product followed the same path from 60 min of reaction incubation with almost equal fractions of DP4 and DP3 (0.6% and 0.4%) (Fig. 3.5 C). But, up to 45 min, a gradual reduction in DP4 (7.5%) substrate and simultaneous increase in DP3 (21.0%) product was observed. Reaction mixtures at 150 min showed DP1 (49.7%) and DP2 (49.6%) as the major end products.Y154A was the only mutant which produced nearly equal concentration of DP1 and DP2 products. Y154A also displayed TG activity up to 45 min. At 5 min, the concentration of DP5 and DP6 products was 8.8% and 4.6% that decreased to 3.0% and 0.9% by 45 min, respectively.

The product profile of the mutants M220A and Y222A was similar except that the latter lost chitobiase activity. A gradual decrease in the initial DP4 substrate, through time was detected (Fig. 3.5 D&E) for M220A and Y222A. The relative proportion of the products produced by the mutant M220A was DP1-6.4%, DP2-13.5%, DP3-37.7%, DP5-12.0% and DP6-5.8% by 6 h. No DP1 product was detectable with Y222A, as the chitobiase activity of *Sp*ChiD was abolished. Fraction collected at 6 h showed that DP2 (14.4%), DP3 (40.7%), DP5 (13.6%) and DP6 (6.8%) were produced by Y222A. A rapid increase of DP5 and DP6 products up to

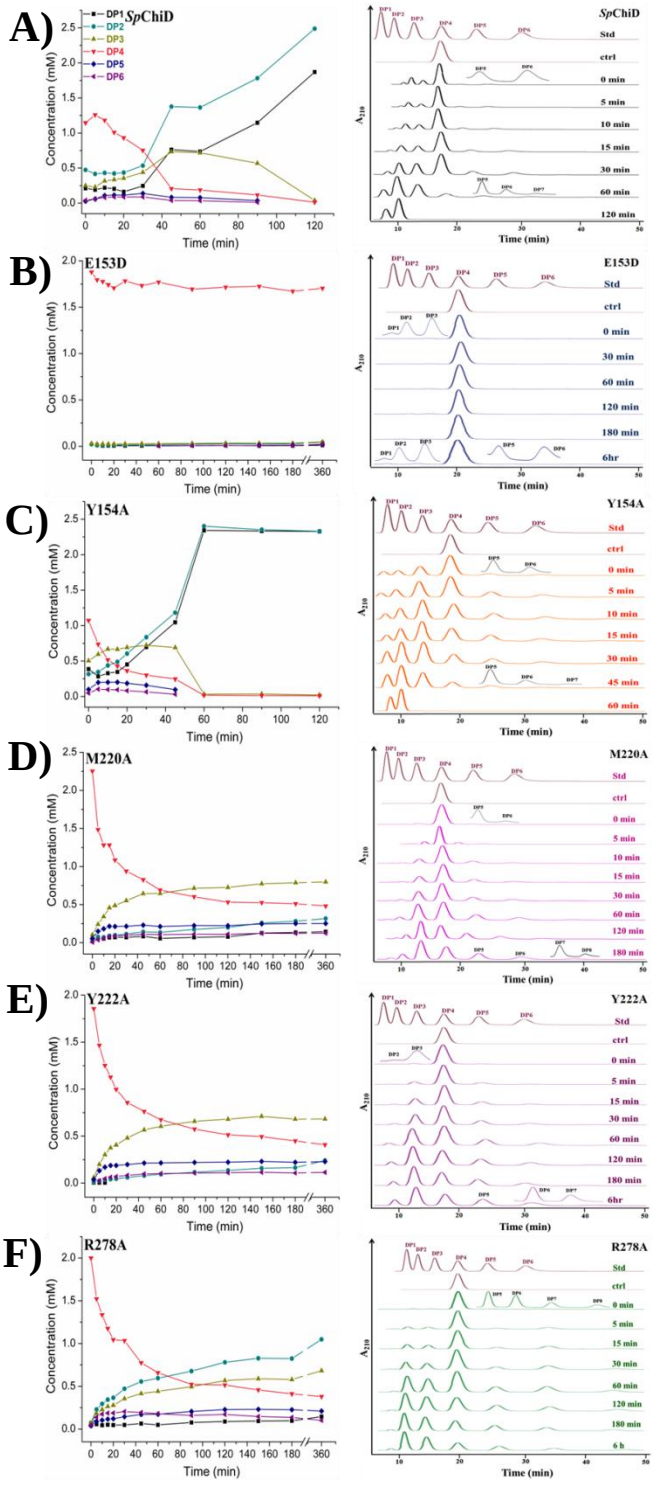

Figure 3.5: **Product profiles of the mutants targeted at the catalytic center.** Left column shows HPLC quantification profiles of *Sp*ChiD (A), catalytic center mutants (B-F), obtained by a linear correlation between peak area and concentration of oligosaccharides in standard. Individual quantification graph represents all the hydrolytic (DP1-DP3) and TG (DP5, DP6) products accumulated during the course of reaction with 2 mM DP4 substrate. Figures in the right column represent the HPLC chromatograms of the respective mutants. The top most profile in each chromatogram shows a standard mixture of CHOS ranging from DP1-DP6. Insets show the magnified view of the low peak area products. Control represents the substrate without the enzyme treatment. # Residue numbering was changed as per the crystal structure nomenclature.

45 min was followed by a state of equilibrium, which continued till the end of 6 h. Both M220A and Y222A produced more of DP5 than DP6 product.

R278A substitution resulted in a gradual decrease of DP4 substrate, generating more of DP5 and DP6 products, although DP2 (40.8%) and DP3 (26.6%) were the major end products (Fig. 3.5 F) at 6 h. The synthesis of DP5 and DP6 products started right from the beginning, but the concentration varied through time. Fraction collected at 30 min showed DP6 (9.0%) > DP5 (6.4%) whereas the fraction at 150th min had DP5 (9.8%) > DP6 (6.2%). Though there was an alteration in the proportion of TG products, both DP5 (8.2%) and DP6 (4.0%), were detectable till the end of 6 h.

3.1.4.2 Residues at the Catalytic Groove

3.1.4.2.1 Phe58 to Trp Conversion & the Double Mutant E153D/F58W

A decrease in the initial concentration of DP4 substrate was detected from 0-5min (62.9% to 48.5%) with F58W (Fig. 3.6 A). There was no decrease in the hydrolytic ability of F58W up to 30 min, but produced more of TG products compared to *Sp*ChiD. There was an increase in quantifiable TG products with 12.9% of DP5 and 6.6% of DP6 after 60 min. Though there was a gradual decrease of TG products, more of DP5 was detectable than DP6 at 6 h. Hydrolytic products DP3 and DP2 remained as the major end products. When F58W was coupled with E153D, the double mutant E153D/F58W regained both hydrolytic and TG activities (Fig. 3.7 A). Fraction collected at the end of 6 h revealed accumulation of 2.2%, 2.1%, 8.0%, 80.1%, 5.9% and 0.8% of oligomers from DP1-DP6 products, respectively. The hydrolysis decreased to a greater extent for E153D/F58W, but produced DP5 product as efficient as *Sp*ChiD at 6 h (Fig. 3.7 B).

3.1.4.2.2 Trp114 to Ala Exchange

The mutation W114A led to a rapid increase in the hydrolysis of DP4 substrate, leaving only 0.5% at 30 min (Fig. 3.6 B). The DP3 product also decreased to 2.4% at 30 min, while the concentration of DP1 and DP2 products was comparable to those produced by *Sp*ChiD. DP2 (56%) was the major end product. Substantial loss of TG

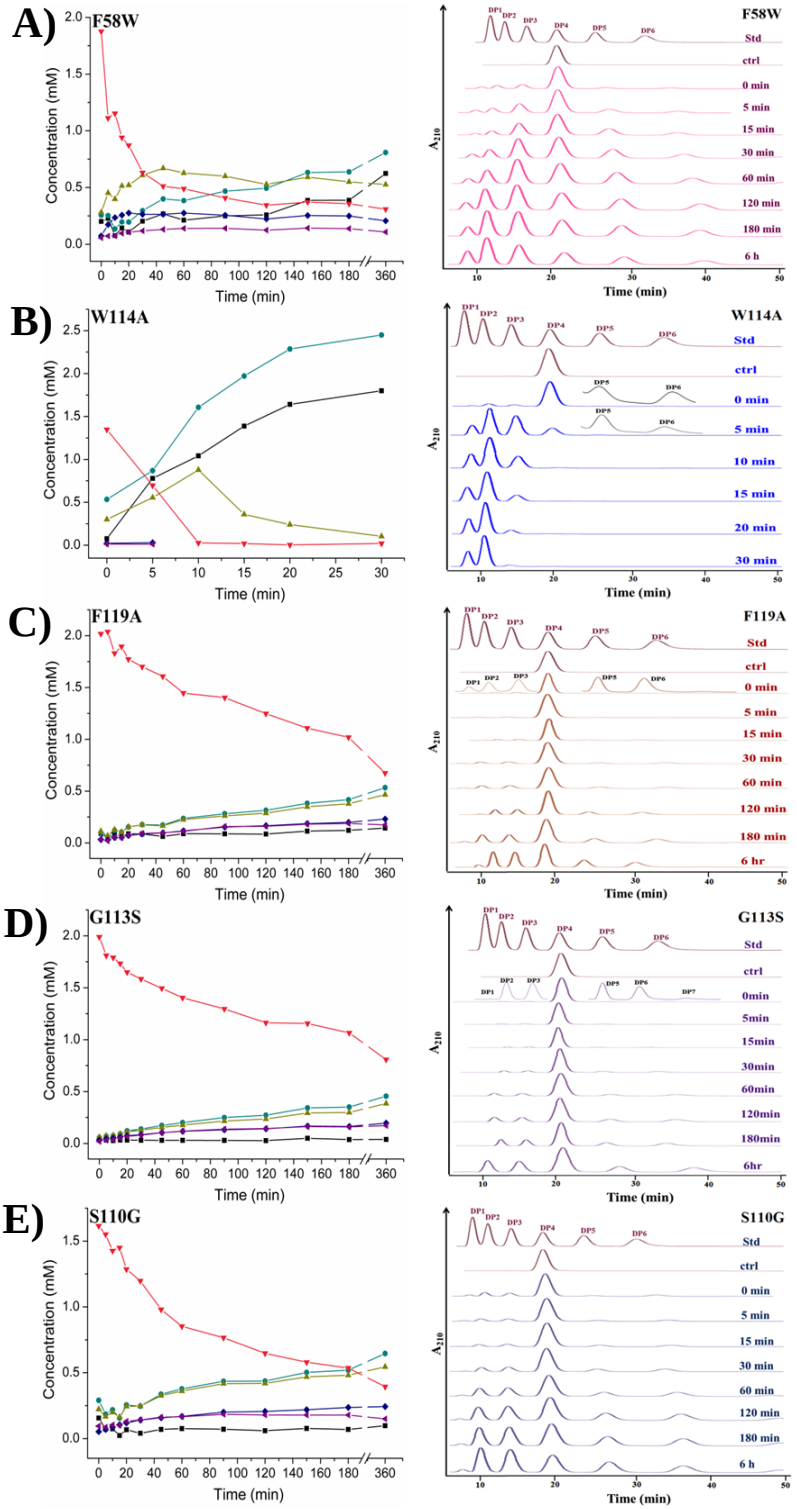

Figure 3.6: **Product profiles of the mutants targeted at the catalytic groove.** Left column shows HPLC quantification profiles of mutants targeted at catalytic groove (A-E), obtained by a linear correlation between peak area and concentration of oligosaccharides in standard. Individual quantification graph represents all the hydrolytic (DP1-DP3) and TG (DP5, DP6) products accumulated during the course of reaction with 2 mM DP4 substrate. Figures in the right column represent the HPLC chromatograms of the respective mutants. The top most profile in each chromatogram shows a standard mixture of CHOS ranging from DP1-DP6. Insets show the magnified view of the low peak area products. Control represents the substrate without the enzyme treatment. # Residue numbering was changed as per the crystal structure nomenclature.

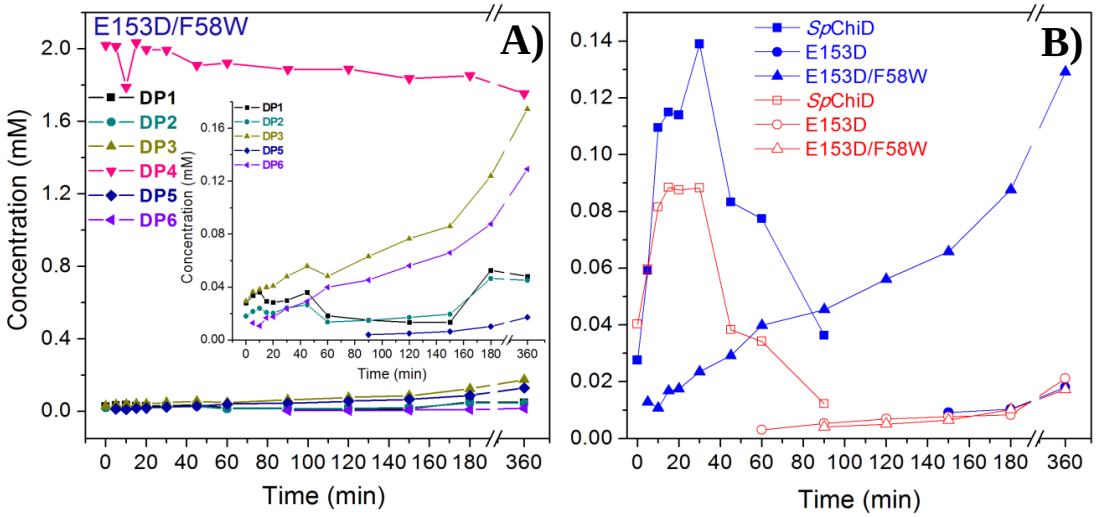

Figure 3.7: **Product profile of the double mutant E153D/F58W.** Profiles were generated by *Sp*ChiD or its variants with 2 mM DP4 substrate in 20 mM sodium acetate buffer pH-5.6 at 40°C. A) Double mutant (E153D/F58W). Inset represents the differences between hydrolytic (DP1-DP3) and TG (DP5, DP6) products generated during the course of reaction. B) Comparison of quantifiable TG products DP5 (blue, filled symbols) and DP6 (red, open symbols) by *Sp*ChiD, E153D, E153D/F58W.

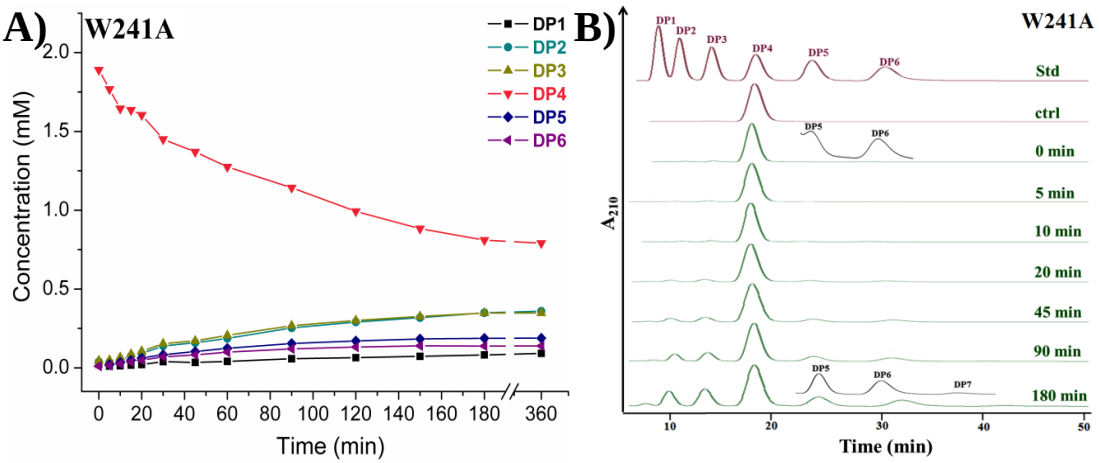

Figure 3.8: **Product profile of the mutant W241A.** HPLC quantification profile (A) and chromatogram (B) of both hydrolytic and TG products analyzed at different time intervals. The reaction mixture contained 2 mM of DP4 substrate, 350 nM of W241A, at pH-5.6, 40°C. The reaction products were analyzed by isocratic HPLC. Products were quantified from respective peak areas of products by using standard calibration curves of CHOS ranging from DP1 to DP6. The top most profile in the chromatogram shows a standard mixture of CHOS ranging from DP1-DP6. Insets show the magnified view of the low peak area products. Control represents the substrate without the enzyme treatment.

Residue numbering was changed as per the crystal structure nomenclature.

activity, with a feeble activity up to 5 min (1.0% of DP5 and 0.5% of DP6), suggested that W114 is an important residue contributing to TG activity of *Sp*ChiD.

3.1.4.2.3 Phe119, Gly113, Ser110 Exchange to Ala, Ser, & Gly, Respectively

The product profiles of F119A, G113S, and S110G showed decreased hydrolytic ability by the three mutants. F119A and G113S produced more or less equal quantities of DP2 with 24.0% and 22.2% and DP3 with 21.0% and 18.7%, respectively as the major end products at 6 h (Fig. 3.6 C &D). These two mutants also produced more of DP5 and DP6 products but, the proportion was less in the early stage and increased gradually through time compared to *Sp*ChiD. Proportion of DP5 and DP6 products produced by F119A at 0^{th} min was 1.3% and 1.5%, respectively, that increased to 10.4% of DP5 and 7.8% of DP6 by the end of 6 h. The product profile of G113S was also similar, where 1.5% of DP5 and 0.9% of DP6 products were detectable at the 0^{th} min, increased up to 9.5% of DP5, and 8.4% of DP6 by the end of 6 h. S110G produced both DP5 and DP6 TG products right from 0^{th} min with 2.2%, 4.1%, respectively (Fig. 3.6 E). The concentration of TG products increased gradually up to 180 min with accumulation of 11.7% of DP5 and 8.8% of DP6 products. Nearly similar quantities of TG products were detectable up to 6 h with accumulation of 11.7% and 7.2% of DP5 and DP6, respectively.

3.1.4.3 Residue at the Solvent Accessible Region (Trp241 to Ala)

Exchange of W241, at the solvent exposed region, to Ala resulted in the reduced hydrolytic ability (Fig. 3.8 A&B). The formation of TG products was slow at the early time points, which increased at later time points and persisted up to 6 h. W241A produced DP2 and DP3 as the major end products. The proportion of DP1 – DP6 products at the end of 6 h of reaction incubation were 4.3%, 18.2%, 18.1%, 42.3%, 9.8% and 7.2%, respectively.

The specific activity and the extent of TG activity for all the mutants were compared with *Sp*ChiD and listed in Table 3.1. The specific activity decreased for mutants E153D/F58W, E153D, F119A, G113S, S110G and W241A and significantly increased for mutants Y154A, F58W, Y222A, R278A, M220A, with a maximum of 8-fold increase for W114A. However, F119A, G113S, S110G, R278A and W241A

Name of the enzyme	Relative % of specific activity	Relative TG activity
*Sp*ChiD	100	+
E153D	49.8	–
Y154A	151.3	+
M220A	204.9	+++
Y222A	168.9	+++
R278A	190.5	+++
W114A	830.6	–
F58W	160.7	+++
G113S	72.8	+++
G113W	11.2	–
G195W	113.6	+++
S110G	74.9	+++
F119A	71.8	+++
W241A	75.8	+++
E153D/F58W	5.7	*

(+) minimal (+++) high (–) nil (*) regained

Table 3.1: Relative specific activity and TG activity of *Sp*ChiD and its mutants towards DP4 substrate.

NOTE: The decrease in DP4 concentration was considered for specific activity measurements through a linear regression analysis using OriginPro 8 software. Efficiency of TG activity for all the mutants from the HPLC quantification data was compared against native *Sp*ChiD.

produced more of DP5 and DP6 compared to DP1. F58W in 60 min (12.9%) and other mutants M220A (12.0%), Y222A (13.6%), F119A (10.4%), and S110G (11.7%) in 6 h produced double the concentration of DP5 compared to *Sp*ChiD (6%) at 30 min (Fig. 3.9 A). Whereas, almost double the concentration of DP6 was generated by G113S (8.4%), F119A (7.8%) and W241A (7.2%) at 6 h compared to *Sp*ChiD which produced only 4% at 30 min (Fig. 3.9 B). The change in proportion of TG products (DP5 and DP6) produced by all the eleven single mutants at the respective time intervals, were quantified and compared against the native *Sp*ChiD (Fig. 3.10 A&B).

3.1.4.4 Activities of the Mutants G113W & G195W Compared Against SpChiD

In an alternative approach to improve the TG of *Sp*ChiD by controlling the movement of CHOS through the active site, we further analyzed residues Gly113 and Gly195 through mutational approach, considering them as probable entry and exit sites, respectively (Fig. 3.11). HPLC chromatogram (Fig. 3.12 A) and the quantification profile (Fig. 3.12 B) of wild type *Sp*ChiD were shown for a closer comparison of hydrolytic and TG activities with the mutants G113W and G195W. Gly113→Trp conversion resulted in a substantial decrease of both hydrolytic and TG activities. A very less quantity of degradation products detected at '0' min with a proportion of 0.4, 0.2 and 0.8% of DP1, DP2 and DP3, respectively. No TG activity was detectable up to 15 min (Fig. 3.12 C). The quantifiable TG products like DP5 and DP6 were detected from 20th min. A marginal increase of hydrolytic (DP1-DP3 with a proportion of 1.0, 0.7, and 1.1%, respectively) and TG (DP5 and DP6 with a proportion of 0.4 and 0.3%) products was observed at 30 min (Fig. 3.12 D). Though there was a considerable decrease in the initial DP4 substrate concentration to 94.4% at 90 min, the increase in proportion of TG products was very less. A similar effect was observed at the end of 6 h with accumulation of quantifiable oligomers from DP1-DP6 in a proportion of 1.1, 1.6, 1.7, 93.6, 0.8 and 1.1%, respectively.

The quantification profile of mutant G195W showed a gradual decrease of DP4 substrate concentration through time (Fig. 3.12 E). The TG products DP5 and DP6 with a proportion of 0.7% and 0.8%, respectively accumulated at '0' min. At 30

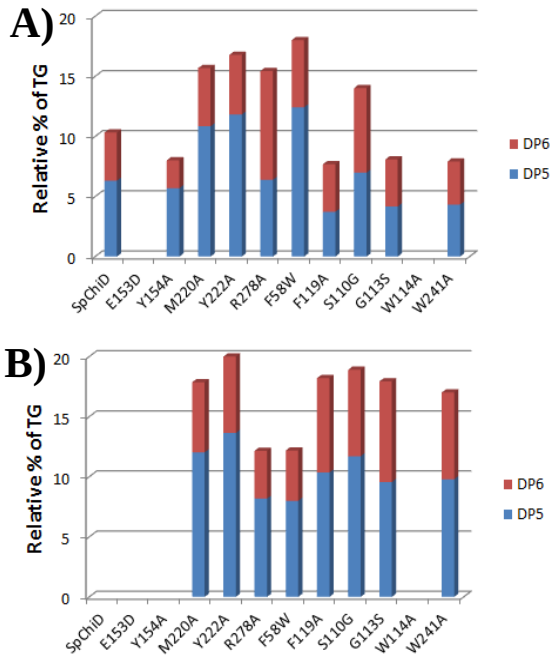

Figure 3.9: **Quantifiable TG products (DP5 and DP6) accumulated by *Sp*ChiD and its mutants.** Reaction mixtures containing 2 mMDP4 and 350 nM of each *Sp*ChiD and its indicated mutants were incubated separately for different time periods from 0 to 360 min at 40 °C. Products were quantified from respective peak areas by using standard calibration curves of CHOS. Comparative profiles show the quantity of DP5 and DP6 TG products produced at 30 min (A) and 6h (B).

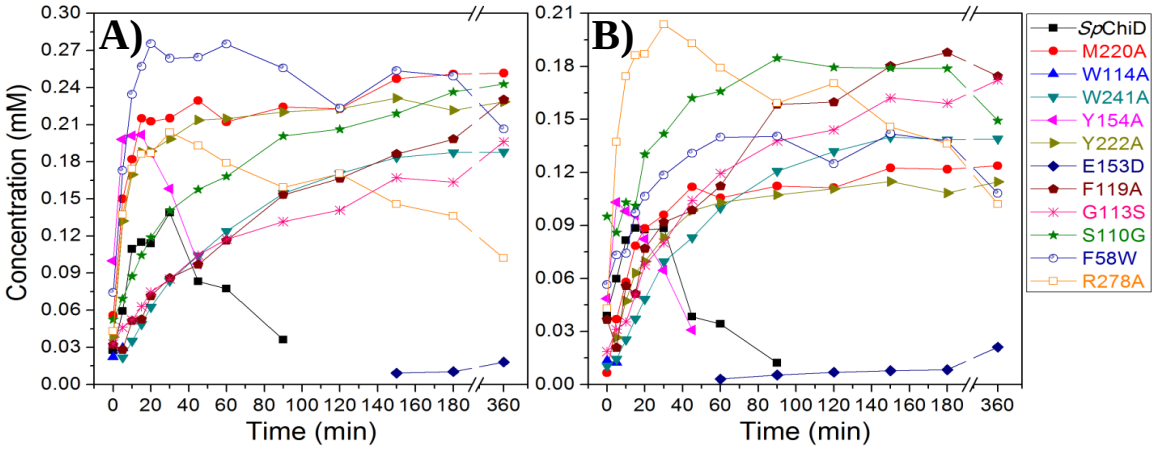

Figure 3.10: **Comparison of quantifiable TG products.** DP5 (A) and DP6 (B) accumulated at different time intervals upon incubation of 2 mMDP4 with *Sp*ChiD and its variants. Reaction was carried up to 6 h, pH 5.6, at 40 °C. Product quantification was done by a linear correlation between peak area and concentration of oligosaccharides in standard samples.

Residue numbering was changed as per the crystal structure nomenclature.

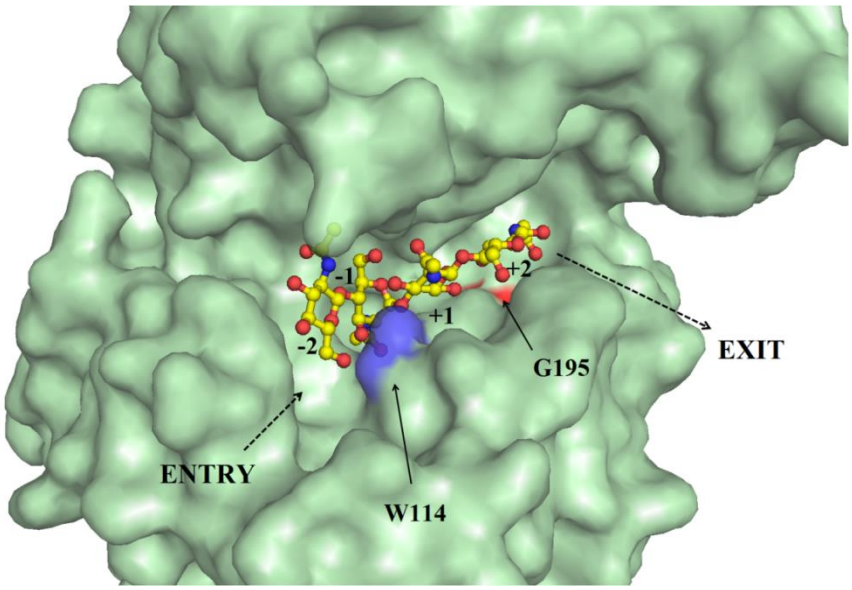

Figure 3.11: **Surface representation of *Sp*ChiD (PDB code: 4LGX)**. The DP4 in the active site represented in the ball and stick (carbon-yellow, nitrogen- blue, oxygen-red). The residues at the probable entry (blue surface-W114) and exit (red surface-G195) sites for the protein *Sp*ChiD were indicated.

Residue numbering was changed as per the crystal structure nomenclature.

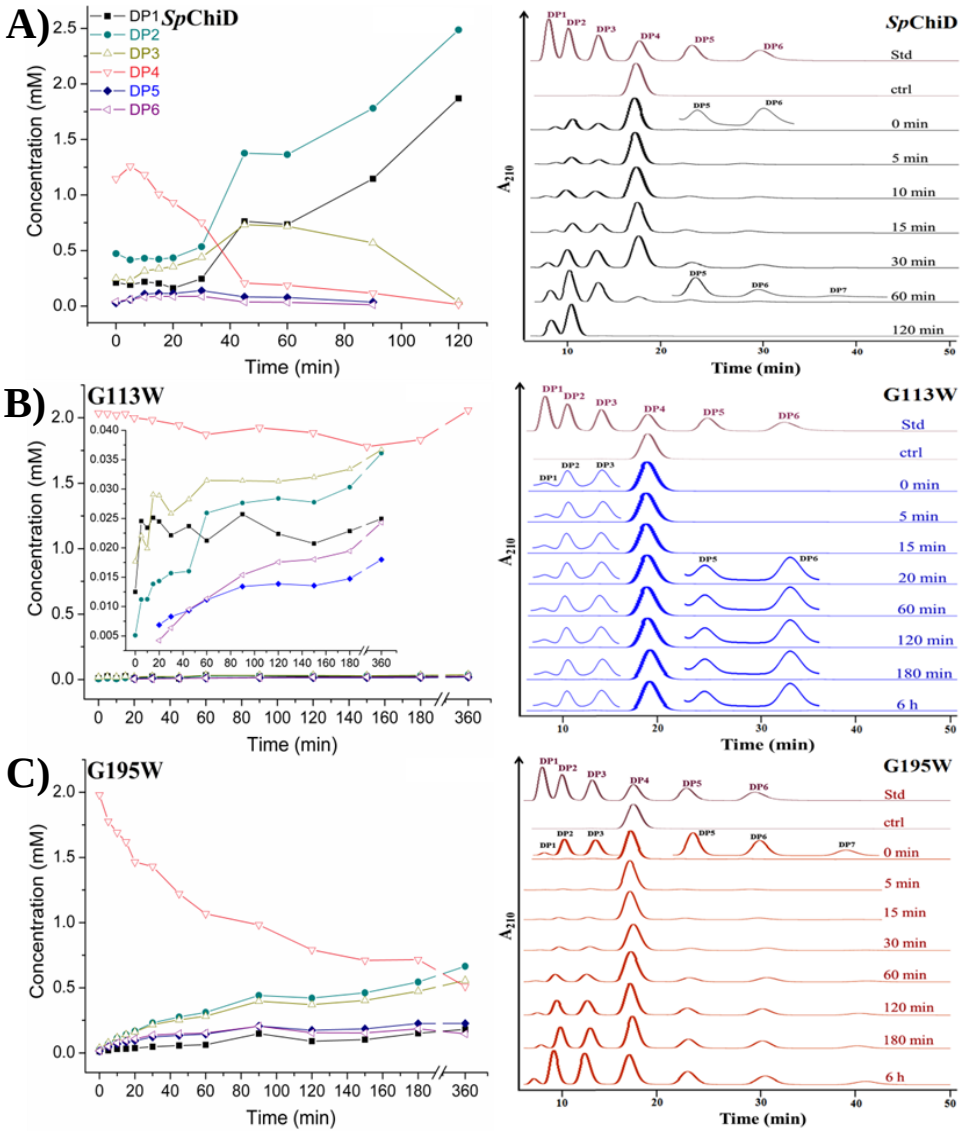

Figure 3.12: **Product profiles of *Sp*ChiD and the mutants G113W and G195W.** Figures on the left column represent HPLC quantification profiles and on the right column are the respective HPLC chromatograms of (A) *Sp*ChiD and the mutants (B) G113W, (C) G195W. In each chromatogram the top most profile shows a standard mixture of CHOS ranging from DP1-DP6. In all the chromatograms insets show the magnified view of the low peak area products present at regular time intervals. Control represents the substrate without the enzyme treatment. Individual quantification graph represents all the hydrolytic (DP1-DP3) and TG (DP5, DP6) products accumulated during the course of reaction. Since the mutant G113W had very less activity, to highlight the reaction products in the quantification profile of G113W, inset showing both hydrolytic and TG products was given for B.

Residue numbering was changed as per the crystal structure nomenclature.

min, the relative percentage of TG products increased to 5.6 (DP5) and 6.3 (DP6). More than half of initial DP4 substrate depleted (41.3%) by 90 min with similar quantities (8.6%) of both the TG products retained. At the end of 6 h the proportion of DP6 decreased to 6.4%, and the DP5 increased to 9.9%. Whereas, the hydrolytic products like DP1-DP3 were present in a proportion of 7.9, 29.1 and 24.3%, respectively, with only 22.3% of DP4 left at the end of 6 h (Fig. 3.12 F). DP2 was the major end product formed with the mutant G195W. The relative percentage of specific activity and TG activity of the mutants G113W and G195W were compared against *Sp*ChiD and its two other variants G113S and W114A (Table 3.1). High resolution mass spectrometry (HRMS) data confirmed the presence of both hydrolytic and TG products for *Sp*ChiD and its mutants G113S, G113W, W114A and G195W (data not shown).

3.2 In silico Analysis of SpChiD & its Mutants

3.2.1 MD Simulations

A multiple sequence alignment of several representative GH18 family proteins showed that the length of proteins is variable. However, the active site of these proteins showed high degree of conservation with few substitutions and occasional deletions/insertions, suggesting that the fold and function of GH18 family proteins is highly conserved. To elucidate the role of amino acid residues interacting with DP4 substrate in the *Sp*ChiD tunnel, we performed five separate 50 ns MD simulations for the *Sp*ChiD and the four individual mutants (W114A, G113S, G113W and G195W) in complex with DP4. The residues showing major interactions with the DP4 substrate in the active site of four *Sp*ChiD mutants were shown in Fig. 3.13 A-D. The residues F58 (−2 subsite); Y325 and W395 (-1 subsite) are positioned at the tunnel entrance side of *Sp*ChiD. The residue W160 is located in the extended loop region of the D*X*D*X*E motif, blocking the tunnel from +1 subsite.

We calculated the root mean square deviation (RMSD) of the homology model complexes and ‘apo’ form of *Sp*ChiD crystal structure (Fig. 3.14 A-E) from the simulations. The root mean square fluctuation (RMSF) plots shown in Fig. 3.15, of all the four mutants were compared with the *Sp*ChiD, which revealed the site-

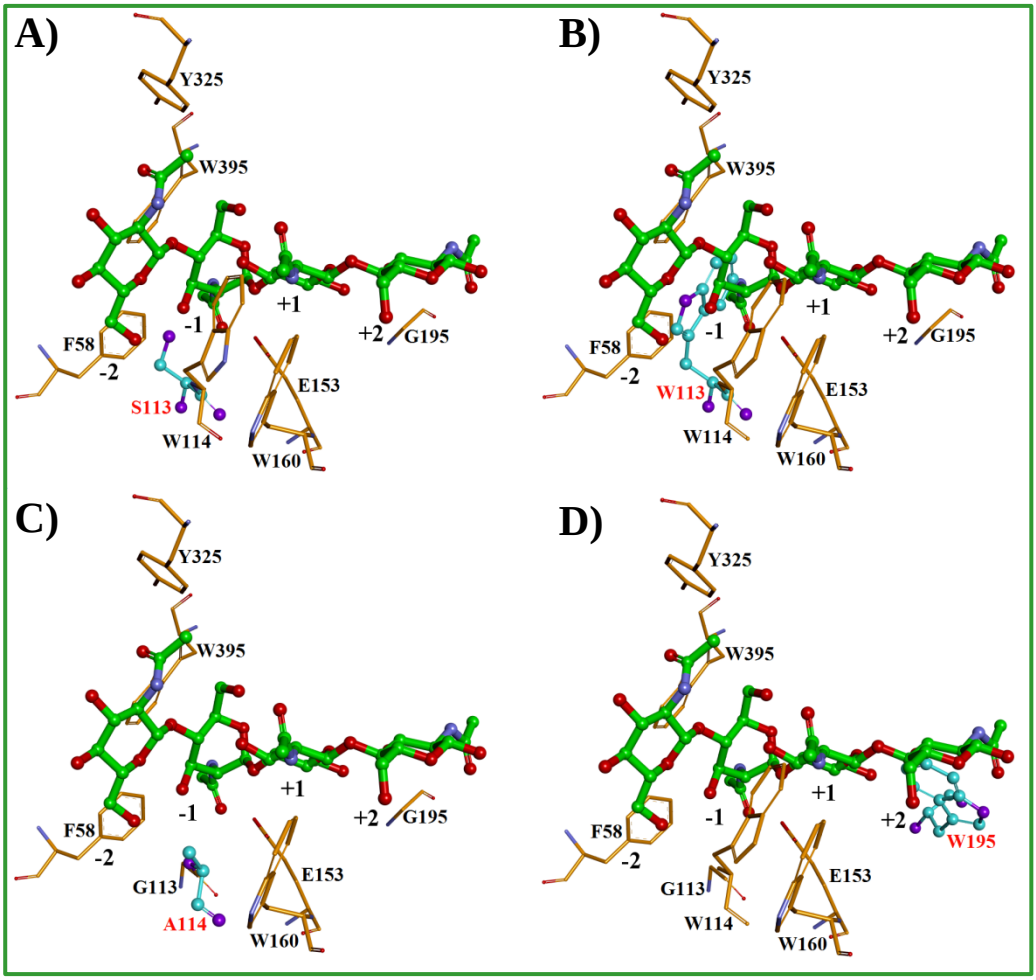

Figure 3.13: **The *Sp*ChiD (PDB code: 4LGX) mutants with DP4 in the active site.** The important active site residue side chains were shown in the stick model. The DP4 represented in ball and sticks model with green-carbons, red-oxygen, blue-nitrogen. The mutants (A) G113S, (B) G113W, (C) W114A, (D) G195W were shown in ball and stick model with cyan-carbons and purple-oxygens, nitrogens.

Residue numbering was changed as per the crystal structure nomenclature.

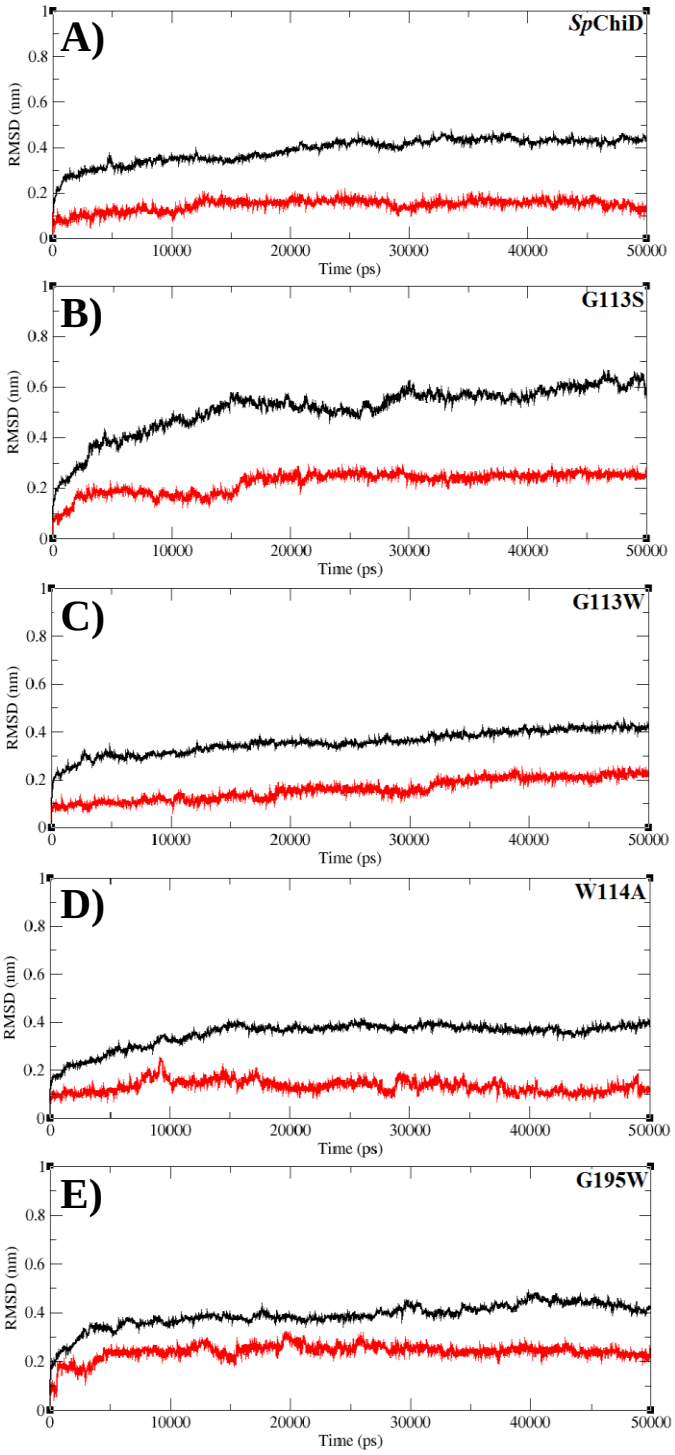

Figure 3.14: **Residue mean square deviation plots**. Obtained from 50000 ps MD simulations of DP4 in complex with A) *Sp*ChiD, B) G113S, C) G113W, D) W114A and E) G195W. The protein represented in black and DP4 represented in red.

Residue numbering was changed as per the crystal structure nomenclature.

specific fluctuations in the protein during the MD simulations. *Sp*ChiD showed greater fluctuations at the residue segment in the chitin path 86-95 that affect the binding of the chitin towards the active site. The extended loop regions (292-300 and 311-325) of the β7 strand of the TIM barrel also showed greater fluctuations. But, these regions were observed far from the chitin binding site. The overall RMSF of the protein was restricted to ~0.08 nm indicating that the protein remained stable. The other loop regions of the protein also displayed minor fluctuations during the simulations.

The mutant G113S also showed increased RMS fluctuations in specific regions compared to *Sp*ChiD (Fig. 3.15 A). The helix region next to the β2 strand of the TIM barrel (71-94) near the active site and the loop region next to the β6 of the TIM barrel (247-251) had greater fluctuations. In addition, the regions 305-310, next to β7, and the region 365-370 between the β10-β11 strands also showed greater fluctuations than *Sp*ChiD. The mutant G113W showed less fluctuations compared to G113S with that of *Sp*ChiD. Further, the region 40-44 between β1-β2 which was in the path of chitin, the region next to β6 (245-251) and the region next to β7 strand (368-369) showed increased fluctuations compared to *Sp*ChiD (Fig. 3.15 B). The other regions displayed minimal differences from *Sp*ChiD.

In comparison with the *Sp*ChiD, W114A mutant (Fig. 3.15 C) exhibited decreased RMS fluctuations in most of the regions. The region 165-170, that corresponds to the extended loop region from the D*X*D*X*E motif, had increased fluctuation than the *Sp*ChiD. The loop region between β10-β11, which is far from the active site, also had increased fluctuations than the *Sp*ChiD. The mutant G195W showed slightly higher fluctuations than the *Sp*ChiD. A broad region corresponding to the segment next to the β2 strand of the TIM barrel (75-94) and the extended loop region (165-170) from the D*X*D*X*E motif showed increased fluctuations (Fig. 3.15 D). The residues in the helix region (311-325), observed next to β7 strand and the region 365−370 between the β10- β11 strands, displayed increased fluctuations.

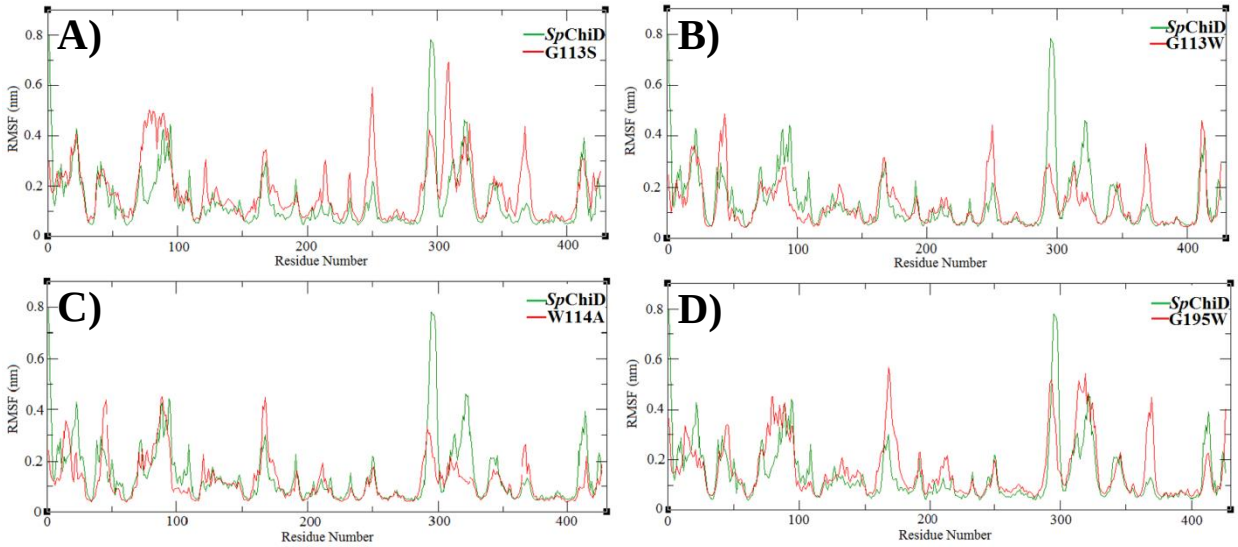

Figure 3.15: **Residue mean square fluctuations plots.** Obtained from 50000 ps MD simulations of the *Sp*ChiD and its four mutants. A) G113S, B) G113W, C) W114A, and D) G195W. *Sp*ChiD represented in green and the mutants were represented in red.

Residue numbering was changed as per the crystal structure nomenclature.

3.2.2 SIE Free Energy Calculations

We have calculated SIE free energies for the *Sp*ChiD and four mutants from the 50 ns of MD simulations. The intermolecular vdW, coulombic energies, the change in surface area and ΔG are shown in the Table 3.2. The *Sp*ChiD with DP4 substrate showed a ΔG of -10.66 kcal/mol indicating good binding of protein-ligand complex. The other four mutants showed less binding in comparison with *Sp*ChiD. The two mutants G113S (-10.32 kcal/mol) and G113W (-10.50 kcal/mol) showed similar binding free energies with DP4. The other two mutant complexes of W114A and G195W had less SIE binding free energies, -9.41kcal/mol and -9.84 kcal/mol, respectively. To understand the importance of the selected residues like Trp114, Gly113 and Gly195 in substrate binding, their contribution in binding free energies was determined both in the native and mutant forms of *Sp*ChiD. The efficient contributions to the binding free energies of DP4 by the selected mutants were listed in the Table 3.3.

The mutant residue Ala114 showed decreased vdW (-0.74 kcal/mol) and coulombic (-0.13 kcal/mol) energies in comparison to Trp114 in the native form of *Sp*ChiD-DP4 complex (vdW = -2.46 kcal/mol, Coulomb = -0.78 kcal/mol). The other two residues in the W114A mutant (in complex with DP4 substrate), Gly113 with decreased energies and Gly195 with slightly increased vdW and coulomb energies were observed compared to native *Sp*ChiD-DP4 complex. For the G113S-DP4 complex, the mutant residue Ser113 showed very less vdW (-0.35 kcal/mol) and coulomb (0.01 kcal/mol) energy contributions in comparison to *Sp*ChiD-DP4 complex (vdW = -1.40 kcal/mol, coulomb = -0.86 kcal/mol). In the mutant complex G113S-DP4, the residue Trp114 showed decreased energy contributions whereas, Gly195 had slightly increased vdW and coulombic energies. For the G113W-DP4 complex, the mutant residue Trp-113 experienced a very high vdW (-4.77 kcal/mol) and coulombic (-1.31 kcal/mol) energies than the *Sp*ChiD-DP4 complex. The other two residues Trp114 and Gly195 displayed decreased vdW and coulombic energy contributions, in comparison to *Sp*ChiD-DP4 complex. In the G195W-DP4 mutant complex, the residue Trp195 showed very high vdW (-3.91 kcal/mol) and coulombic

Name of protein	vdW kcal/mol	Coulomb kcal/mol	RF	ΔG kcal/mol
*Sp*ChiD	-81.32	-34.28	56.88	-10.66
W114A	-64.49	-34.96	50.06	-9.41
G113S	-70.64	-52.03	64.10	-10.32
G113W	-66.41	-70.18	77.63	-10.50
G195W	-60.88	-52.17	58.87	-9.84

Table 3.2: DP4 binding free energies with *Sp*ChiD and its mutants. The SIE binding free energy (ΔG) and its components van der Waal -vdW; Coulomb interaction -Coulomb; Reaction Field -RF.

Name of Protein	Residue Number	vdW (kcal/mol)	Coulomb (kcal/mol)
*Sp*ChiD	Trp114	-2.46	-0.78
	Gly113	-1.40	-0.86
	Gly195	-0.47	-0.25
W114A	Ala114	-0.74	-0.13
	Gly113	-0.65	-0.33
	Gly195	-0.89	-0.28
G113S	Trp114	-0.57	-0.04
	Ser113	-0.35	0.01
	Gly195	-0.69	-0.33
G113W	Trp114	-2.40	-0.58
	Trp113	-4.77	-1.31
	Gly195	-0.74	-0.27
G195W	Trp114	-0.79	-0.04
	Gly113	-0.09	0.21
	Trp195	-3.91	-3.85

Table 3.3: The van der Waals (vdW) and coulombic (coulomb) interaction energy contribution to SIE binding free energy of DP4 with *Sp*ChiD and its mutants from selected binding site residues.

NOTE: SIE free energies for the *Sp*ChiD and four mutants from the 50 ns of MD simulations. SIE free energy is an end-point physics-based, force-field-based scoring function for predicting ligand-binding affinities.

(-3.85 kcal/mol) energies in comparison to *Sp*ChiD-DP4 complex. The two residues Trp114 and Gly113 experienced decreased vdW and coulombic energies compared to the same residues from *Sp*ChiD-DP4 complex.

3.2.3 Hydrogen Bonding

The hydrogen bonding analysis of DP4 substrate in the active site of *Sp*ChiD and the four mutants during 50 ns of MD simulations allowed us to measure the binding efficiency of the ligand. Alteration in the number of hydrogen bonds in the enzyme-substrate complexes revealed the effect of specific mutation on the binding efficiency of substrate. The average number of hydrogen bonds observed for DP4 substrate during the 50 ns of MD simulations with mutants G113S, G113W, G195W, W114A and *Sp*ChiD are 5.8, 9.4, 7.2, 5.6 and 5.6, respectively. The number of hydrogen bonds for *Sp*ChiD and mutant-DP4 complexes is shown in the Fig. 3.16.

3.3 Structure Elucidation of SpChiD

3.3.1 Sequence Comparison

The amino acid sequence of *Sp*ChiD was compared with *Kp*ChiII (PDB: 3QOK), *Sm*ChiA (PDB: 1CTN) and *Sm*ChiB (PDB: 1E15), which were representatives of different types of chitinases belonging to the same GH18 family (Fig. 3.17). As reported in the database UniProt - A8GFD6 (Purushotham & Podile, 2012), the amino acid sequence of *Sp*ChiD consisted of 426 amino acid residues. However, as indicated by N-terminal sequence determination, the first amino acid is Ala1 which corresponds to Ala21 in the data base. In order to compare the sequence of *Sp*ChiD with the sequences of other structures, the sequence numbering in *Sp*ChiD was changed to Ala15 instead of Ala1 and thus the last residue was Gln420 instead of Gln426 (Fig. 3.17). The BLAST algorithm has been used for the alignment of sequences and the relevant aspects were compared. It showed the highest sequence identity of 79% with *Kp*ChiII, (whose structure is not reported so far) while with other chitinases belonging to classes A (*Sm*ChiA) and B (*Sm*ChiB), it showed relatively low sequence identities of 23% and 25%, respectively. The residue methionine at position 89 was modified to sulfone methionine in *Sp*ChiD compared methionine at the corresponding positions in *Kp*ChiII, *Sm*ChiA and *Sm*ChiB. Instead,

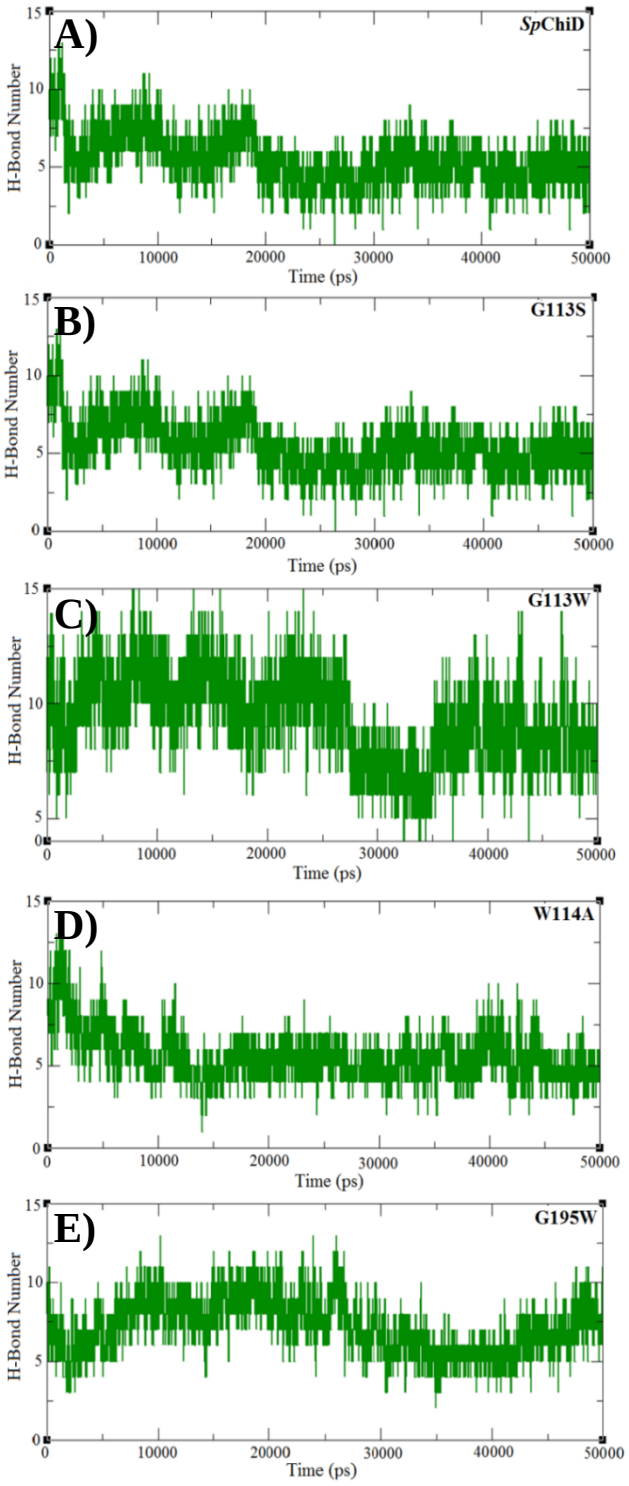

Figure 3.16: **Hydrogen bonding pattern of *Sp*ChiD and its mutants with DP4.** Number of hydrogen bonds (green) formed during the 50000 ps of MD simulations by DP4 with A) *Sp*ChiD, B) G113S, C) G113W, D) W114A, and E) G195W.

Residue numbering was changed as per the crystal structure nomenclature.

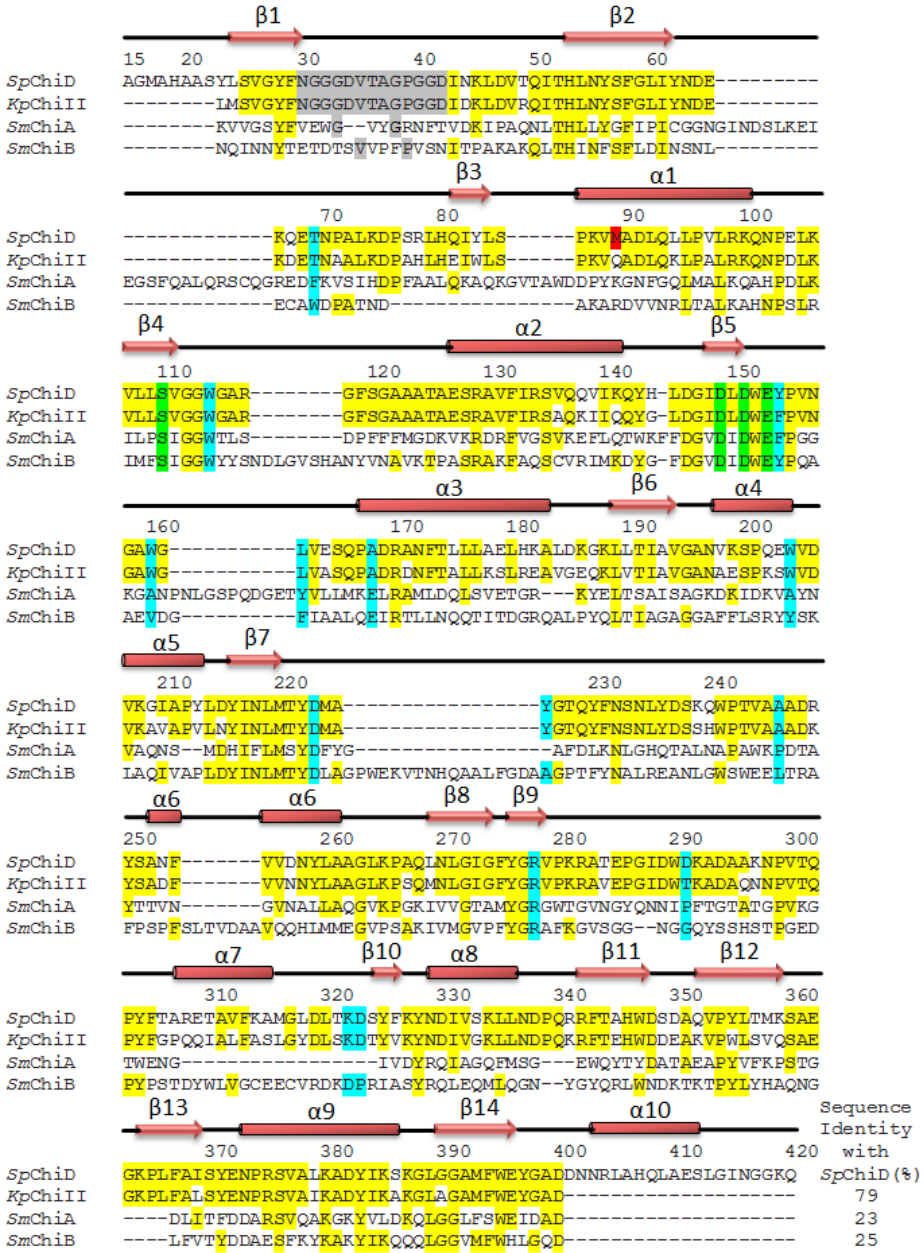

Figure 3.17: **Multiple sequence alignment of chitinases, *Sp*ChiD (PDB: 4LGX), *Kp*ChiII (PDB: 3QOK), *Sm*ChiA (PDB: 1CTN) and *Sm*ChiB (PDB: 1E15).** Since *Sp*ChiD was a single domain protein consisting of only main catalytic TIM barrel domain the comparison was restricted only to the main catalytic TIM barrel domain. The mature protein of *Sp*ChiD consists of residues from Ala15 to Gln420.The identical residues are highlighted in yellow. The residues of loop Asn30 - Asp42 are highlighted in grey. The residue sulfone Met89 (SMet89) shown in red and the catalytic residues in green. The residues of substrate binding cleft were highlighted in cyan. The secondary structure elements such as α-helices and β-strands were also indicated.

these were Gln, Lys and Arg, respectively. The residues that form the substrate binding cleft in *Sp*ChiD are Thr69, Trp114, Trp160, Leu162, Ala169, Ala247, Arg278, Asp291, Lys322 and Asp323 which are highlighted in cyan. The active site residues are highlighted in green. The sequence of the segment, Asn30 - Asp42 (highlighted in grey) which is 100% identical in *Sp*ChiD and *Kp*ChiII but it is completely different in *Sm*ChiA and *Sm*ChiB indicating differences in the structural and functional aspects involving this segment.

3.3.2 Overall Structure of SpChiD

The final model of *Sp*ChiD consisted of 3164 protein atoms from 398 out of a total of 406 amino acid residues in the protein for which the electron density was observed. The details of data processing statistics are given in Table 3.4. The electron density was not observed for three residues Ala15 - Gly16 - Met17 at the N-terminus and five residues, Asn416 - Gly417 - Gly418 - Lys419 - Glu420 at the C-terminus. The positions of 593 water oxygen atoms, one acetate molecule and two glycerol molecules were also determined. The side chains of three residues Ser110, Asp151 and Met220 showed two conformations with equal occupancies (Fig. 3.18 A) indicating the unconstrained environment around them. An extra electron density with features of an acetate molecule was also observed in the proximity of active site (Fig. 3.18 B). However, the most striking observation pertained to detecting the extra electron density at the sulfur atom of residue, Met89. It clearly suggested that there could be two extra oxygen atoms which might be covalently attached to Sulfur atom of Met89 and the residue could be a modified methionine as Sulfone Met89 (SMet89) (Fig. 3.18 C). All the atoms of the side chain of SMet89 refined well with full occupancies. *Sp*ChiD is a single domain protein with 406 amino acid residues (Fig. 3.19). The structure was comprised of 14 β-strands and 10 α-helices out of which eight β-strands, β1 (residues Leu24 - Asn30), β2 (residues His53 - Tyr62), β4 (residues Lys106 - Val111), β5 (residues Ile148 - Asp151), β6 (residues Leu189 - Val194), β7 (residues Tyr216 - Met220), β8 (residues Leu269 - Gly274), and β14 (residues Gly390 - Glu396) and eight α-helices α1 (residues Pro86 - Gln101), α2 (residues Ala126 - Gln142), α3 (residues Pro167 - Ala183), α4 (residues Val198 -

PDB entry	4LGX
Data collection	
Space group	$P2_12_12$
Unit cell parameters (Å)	a = 75.3, b = 87.2, c = 59.5
Resolution (Å)	35.19 - 1.49 (1.52 - 1.49)
R_{sym} (%)	5.0 (25.0)
I/σ (I)	44.5 (6.1)
Completeness (%)	100 (100)
Multiplicity	8.1 (6.8)
Number of reflections measured	524810
Number of unique reflections	64748
Refinement	
R_{cryst}/R_{free}	0.162/0.176
Number of protein atoms	3164
Number of water oxygen atoms	593
Number of acetate ion	1
Number of glycerol molecules	2
R.M.S. deviations in	
Bond length (Å)	0.016
Bond angles (°)	1.6
Dihedral angles (°)	12.7
Mean B factor (Å)^2 for	
Main chain atoms	11.3
Side chain and water oxygen atoms	16.7
Overall	14.4
Ramachandran plot statistics	
Residues in the most favoured regions (%)	91.0
Residues in additionally allowed regions (%)	9.0

Table 3.4: Summary of X-ray crystallographic data collection and refinement
Values in the parentheses are for the highest resolution shell. Data were collected from one crystal.

NOTE: *Sp*ChiD was crystallized using hanging drop vapor diffusion method and the X-ray intensities were collected using a beamline, BM-14 at the European Synchrotron Radiation Facility (ESRF) in Grenoble (France). The structure was determined using molecular replacement method with program MOLREP from the CCP4 suite.

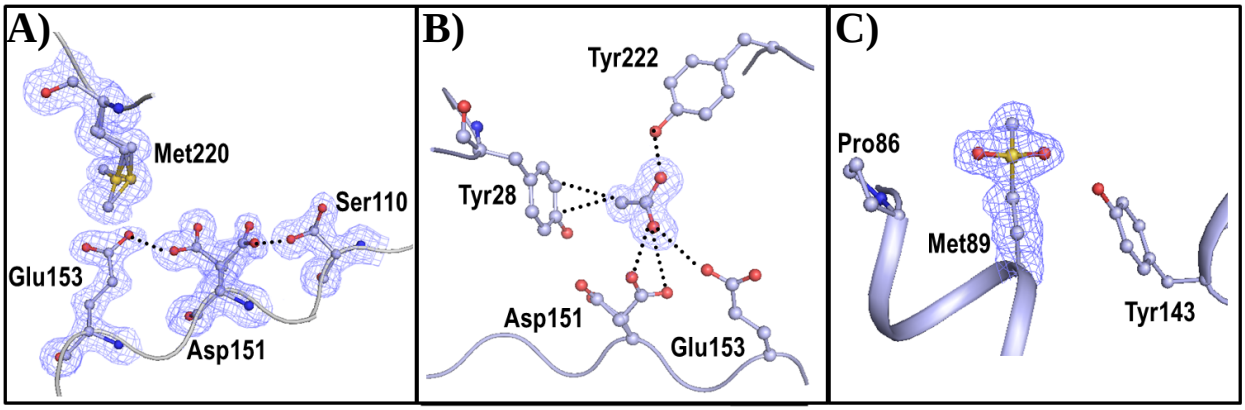

Figure 3.18: **The initial electron densities from ($2F_o - F_c$) map at 1.3 σ cutoffs** - for (A) residues Ser110, Asp151, Glu153 and Met220. The side chains of residues Ser110, Asp151 and Met220 adopt two distinct conformations (B) acetate ion and (C) sulfone Met89 (SMet89).

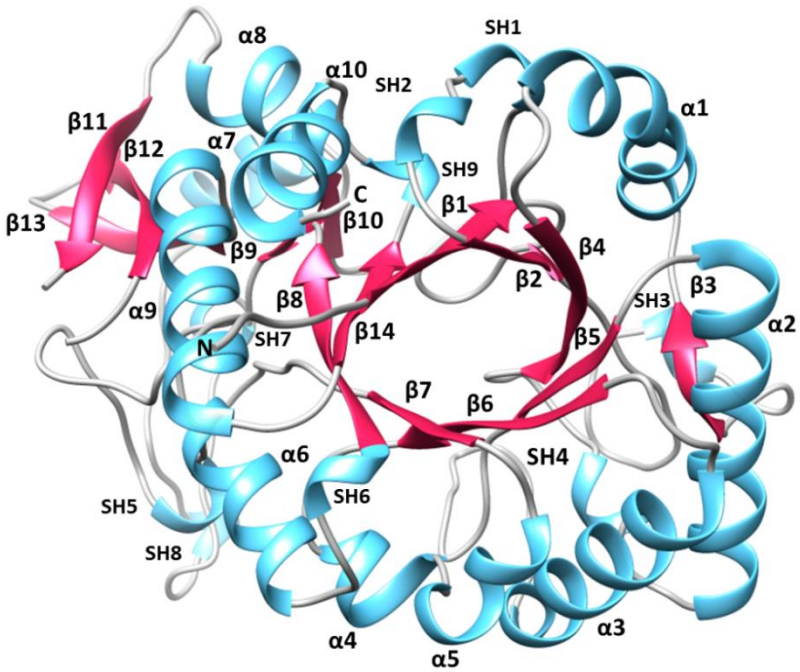

Figure 3.19: **Overall structure of *Sp*ChiD.** A view of the structure of *Sp*ChiD showing TIM barrel. The secondary structure elements α-helices, β-strands and short 3_{10}-helices have been labeled.

Trp204), α5 (residues Val207 - Tyr213), α6 (residues Ala252 - Ala261), α9 (residues Pro374 - Ser386) and α10 (residues Arg404 - Ser412) were part of the TIM barrel (Fig. 3.19) while β-strands β3 (residues Gln81 - Leu84), β9 (residues Tyr276 - Val279), β10 (residues Tyr325 - Lys327), β11 (residues Phe343 - Asp348), β12 (residues Val353 - Lys359) and β13 (residues Lys364 - Ile369) are outside the TIM barrel. Similarly, α-helices α7 (residues Ala307 - Ala315) and α8 (residues Tyr328 - Leu336) also deviated from TIM barrel. The structure also consisted of a 9 short 3_{10}-helices which are indicated as SH1, SH2, SH3, SH4, SH5, SH6, SH7, SH8 and SH9 (Fig. 3.19). The structure of *Sp*ChiD adopts a perfect $(\beta/\alpha)_8$ - TIM barrel fold, as observed in other family GH18 proteins.

3.3.3 Structure of the Substrate Binding Cleft

The polypeptide chain of *Sp*ChiD folds part-wise into two distinct parts between which the substrate binding cleft is formed. The lower N-terminal part consists of residues from Ala15 to Met220 while the upper part is made up of residues Thr221 to Gln420 (Fig. 3.20 A). However, the most striking feature of *Sp*ChiD pertains to the position of loop, Asn30 - Asp42 which intrudes into the substrate binding cleft and occupies nearly half of the space in substrate binding site (Fig. 3.20 B). The front face of the loop is equipped with residues, Val35 and Thr36 which may provide a favourable chemical interaction with the front residue of chitin oligomers in the cleft. The lower side of the wall consists of residues, Thr69, Trp114, Ala159, Trp160, and Leu162, while the upper wall has residues, Tyr226, Ala247, Arg278, Trp290, Asp291, Lys322 and Asp323 (Fig. 3.21 A). The lower side also contains three active site acidic residues, Asp149, Asp151 and Glu153 (Fig. 3.21 B). The side chain of Glu153 protrudes into the cleft. Its position with respect to the location of substrate is aligned in such a way that it could hydrolyze chitins to produce chitin monomers. At the entrance of the substrate binding cleft in *Sp*ChiD, the residues Trp160 and Trp290 are situated on the opposite sides. In case of *Sm*ChiA and *Sm*ChiB, the corresponding residues are Ile207 and Phe396, and Leu103 and Asp316, respectively (Fig. 3.22).

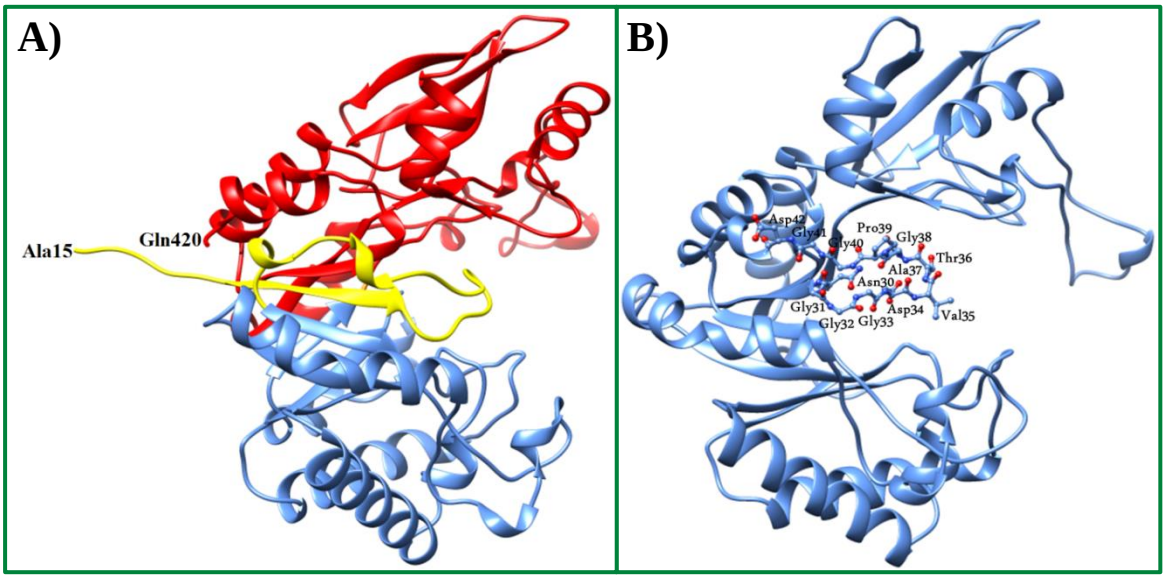

Figure 3.20: **Important structural features of *Sp*ChiD.** (A) Structure showing independent folding of lower N-terminal half and upper C-terminal regions. (B) The substrate binding cleft is hindered partially by the loop Asn30 - Asp42 and the residues comprising the loop region were shown in ball and stick.

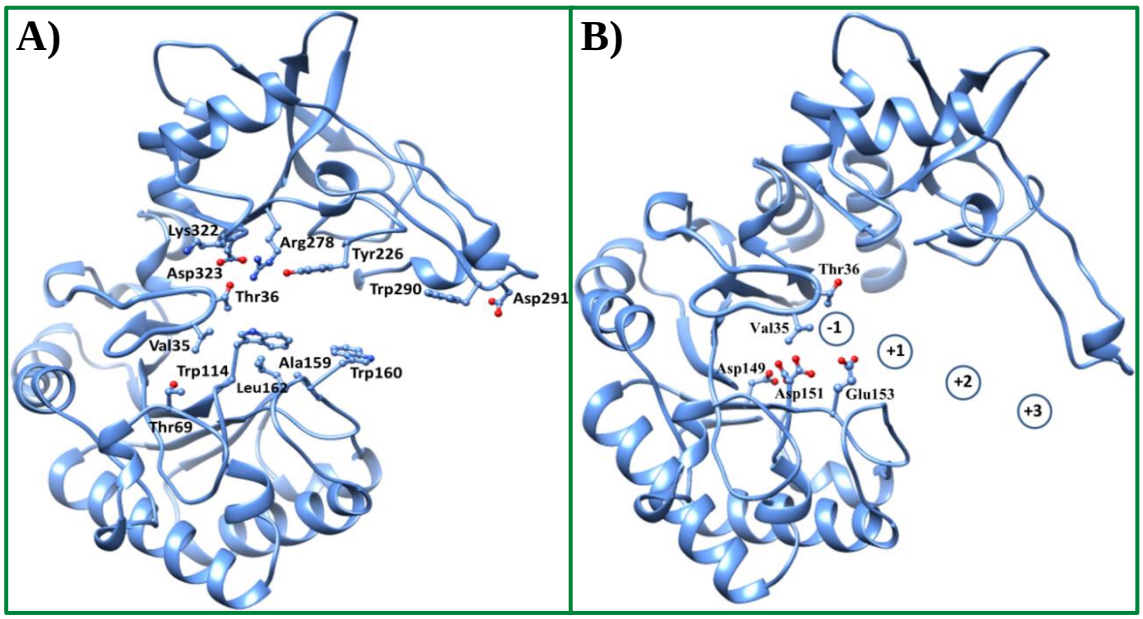

Figure 3.21: **Substrate binding cleft of *Sp*ChiD.** (A) Structure showing residues lining the substrate binding cleft. (B) Binding pocket showing residues crucial for catalysis (Asp149, Asp151 and Glu153) and residues at the front face of the loop (Val35 and Thr36) interacting with the -1 sugar of the incoming ligand.

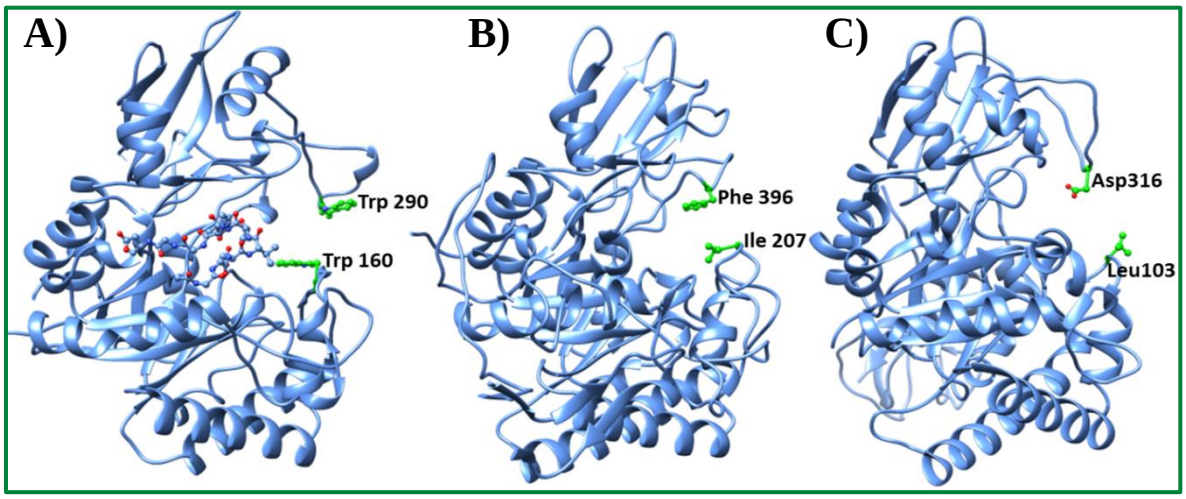

Figure 3.22: **Comparison of substrate binding clefts of three GH18 chitinases from *Serratia* sp.** 3D structures showing views of the substrate binding clefts in (A) *Sp*ChiD, (B) *Sm*ChiA and (C) *Sm*ChiB. A loop Asn30 - Asp42 in *Sp*ChiD located in the substrate binding site was indicated. The residues on either side of the entrance to the substrate binding clefts are also indicated.

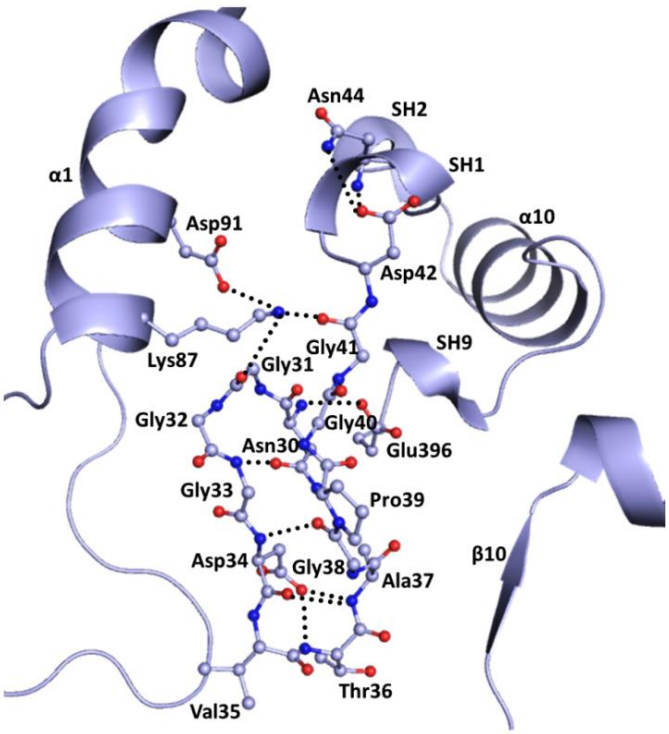

Figure 3.23: **Structure of novel loop in *Sp*ChiD.** The loop Asn30 - Asp42 was internally stabilized but poorly connected to rest of the protein.

3.3.4 Catalytic Site

The size of the substrate binding cleft in *Sp*ChiD decreased to less than half as compared to those in *Sm*ChiA and *Sm*ChiB due to the insertion of a loop, Asn30 - Asp42. The positions of catalytic residues Asp149, Asp151 and Glu153 are arranged in such a way that Glu153 is oriented appropriately to interact with the glycosidic linkage between residues at –1 and +1 subsites (Fig. 3.21 B). In the *Sp*ChiD structure, Asp151 exists in two conformations. In one state Asp151 is oriented towards Asp149 and forms hydrogen bonds with it. In this arrangement Ser110 also forms a hydrogen bond with one of the carboxyl oxygen atoms. However, in the other state, Asp151 turns towards Glu153. In this orientation, Asp151 forms a hydrogen bond with Glu153. This orientation of Glu153 is appropriate to interact with disaccharide at the glycosidic linkage leading to hydrolysis of chitin and generates monomers.

3.3.5 Structure of Loop (Asn30 - Asp42)

The substrate binding cleft in *Sp*ChiD has an additional feature where the groove is blocked partially by a loop Asn30 - Asp42 which is part of the N-terminal segment, Ser25 - Ile51 (Fig. 3.23). This segment consists of a β-strand, β1 (residues, 24 - 30) and two short 3_{10}-helices (SH1, residues 43 - 45 and SH2, residues 48 - 50). A part of this segment, Asn30 - Asp42 has been pushed into the substrate binding cleft. This is a unique feature of the structure of *Sp*ChiD and occurs due to specific amino acid sequence that induces a novel type1 β-turn that changes the path of the protein chain. The observed type1 β-turn at Asn30 - Gly31 - Gly32 - Gly33 with torsion angles of $\Phi_1 = -92.3°$, $\psi_1 = -36.7°$ and $\Phi_2 = -90°$, $\psi_2 = -10.3°$ is stabilized by a hydrogen bond Gly33NH - - - $O^{\delta 1}$Asn30 = 2.80 Å. The sequences of the corresponding segments in *Sm*ChiA and *Sm*ChiB (Fig. 3.17) seem to be unfavourable for forming such a tight type 1 β-turn and hence these segments remain parts of extended β-strands in other chitinases and hence do not move towards the cleft. The upper part of the N-terminal segment, Ser25 - Ile51 is sandwiched between α-helix, α1 (residues, 86 - 101) on one side and a β-strand, β14 (residues, 390 - 396), 3_{10}-helix SH9 (residues, 397 - 399) and α - helix, α10 (residues, 404 - 412) on the other side. This is firmly held at this position by several hydrogen bonds Lys87N^{z} - - - OGly31 = 2.78 Å, Asp91$O^{\delta 1}$ - - -

N^{z}Lys87 = 3.00 Å, Lys87N^{z} - - - OGly41 = 2.72 Å, Asn44$N^{\delta 2}$ - - - $O^{\delta 1}$Asp42 = 3.12 Å, Asn44$N^{\delta 2}$ - - - Asp42$O^{\delta 1}$ = 2.90 Å. As seen from Fig. 3.23, the loop Asn30 - Asp42 was internally well stabilized with the help of a number of intra-loop hydrogen bonds. This unique structure of *Sp*ChiD appears to be well designed to alter the nature of its hydrolytic action.

3.4 Analysis of the Loop Region through Mutational Approach

Residues Val35 and Thr36, occupying the front positions of the loop were mutated to Gly/Phe independently. The V35G/F and T36G/F variants were further analyzed. For HPLC studies each variant of *Sp*ChiD was incubated with 1 mM DP4 and fractions were collected at different time intervals. The results obtained were compared against *Sp*ChiD under the similar reaction conditions.

3.4.1 Kinetic Analysis

The kinetic parameters for the enzyme *Sp*ChiD and its loop variants were determined with colloidal chitin as the substrate using reducing end assay. Specific activity (nkatal/mg of protein) and substrate concentration (mg/mL) data were directly fitted to the Michaelis–Menten equation by nonlinear regression function (Fig. 3.24) of GraphPad Prism version 5.0 software. The kinetic values (K_m, V_{max}, K_{cat} and K_{cat}/K_m) were compared against *Sp*ChiD (Table 3.5). All the loop variants showed decreased K_m in the range 14-25 mg/mL (Table 3.5) when compared to *Sp*ChiD (35.1 mg/mL), indicating increased affinity towards the colloidal chitin substrate. Among the loop variants tested, the mutant T36F showed a very low K_m of 14.7 mg/mL with a very high overall catalytic efficiency of 63.5 sec^{-1} mg^{-1} mL. We could not determine kinetic parameters for the mutants Y28A and *Sp*ChiDΔ30-42 using colloidal chitin substrate, because of their feeble activity towards polymeric substrate.

3.4.2 'Val' Variants (V35G & V35F)

Both the variants displayed a similar trend in the activities, comparable to that of *Sp*ChiD with few exceptions. Though the initial DP4 concentration reduced very rapidly, the amount of DP1 and DP3 products formed by V35G at 30 min were low (4.6% & 20.2%) when compared to *Sp*ChiD (12.7% & 27.2%) (Fig. 3.25 A) and V35F (8.9% & 25.6%). Almost equal quantity of DP2 was produced by both the Val

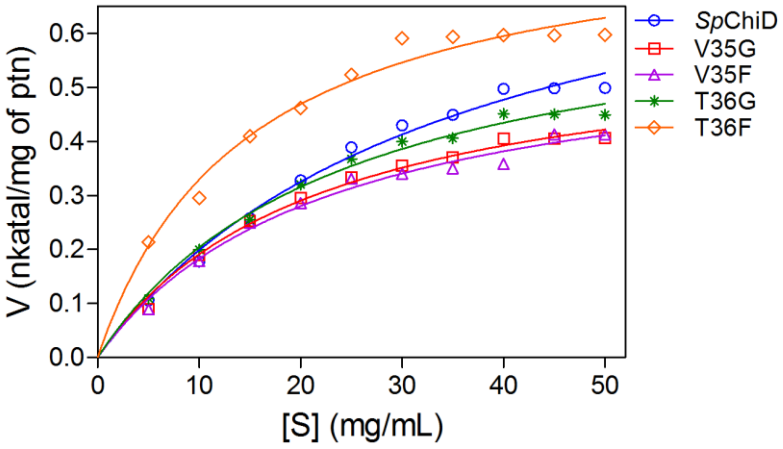

Figure 3.24: **Kinetic analysis for loop variants of *Sp*ChiD.** Different concentrations of colloidal chitin substrate (0-50 mg/mL) were incubated with *Sp*ChiD and its loop variants in 50 mM sodium phosphate buffer pH 8.0, with respective controls in triplicates at 40°C for 1 h at 200 rpm. Specific activity in nkatal/mg of protein was calculated and plotted against substrate concentration. The data was fitted to the Michaelis–Menten equation by nonlinear regression function using GraphPad Prism software version 5.0, to obtain the respective kinetic graphs and parameters.

Enzyme	K_m (mg/mL)	V_{max} (nkat/mg of protein)	K_{cat} (sec^{-1})	K_{cat}/K_m (sec^{-1} mg^{-1} mL)
*Sp*ChiD	35.12	0.896	10.3×10^2	29.33
V35G	21.7	0.605	6.95×10^2	32.06
V35F	22.73	0.598	6.88×10^2	30.26
T36G	24.19	0.697	8.01×10^2	33.13
T36F	14.75	0.815	9.36×10^2	63.47
Y28A*	ND	ND	ND	ND
Δ30-42*	ND	ND	ND	ND

Table 3.5: Kinetic parameters for loop variants of *Sp*ChiD

(*) Kinetic parameters not determined (ND) due to lack of activity on colloidal chitin.

variants (Fig. 3.25 B&C). The low concentration of DP1 and DP3 produced by V35G or V35F shifted the equilibrium towards increased quantities of DP5 and DP6 by the respective mutants. Both the mutants generated more of DP6 than DP5. V35G produced high amount of DP6 with 6.4% at 5 min, which was 6 times higher when compared to V35F (1.1%). The mutants V35G and V35F at 30 min, produced DP5 with a proportion of 4.3% and 3.4% whereas, DP6 with a proportion of 4.9% and 3.8%, respectively. TG was retained up to 75 and 105 min by V35G and V35F, respectively, when compared to *Sp*ChiD which displayed TG up to 90 min. The concentration of DP1 produced was lower for V35G and V35F with DP4 as the substrate, indicating possible effect of mutation on the chitobiase activity of *Sp*ChiD (Fig. 3.25 B&C).

3.4.3 'Thr' Variants (T36G & T36F)

Mutational effects of the residue Thr36 clearly translated into a major loss of chitobiase activity of *Sp*ChiD. Accumulation of more of DP2 and very low quantities of DP1 and DP3 strongly supports that the mutations have made a severe impact on the chitobiose degradation (Fig. 3.25 D&E). DP2 was accumulated to 89.2% and 81% at the end of 120 min (T36G) and 3 h (T36F), respectively. T36G produced more of DP6 right from the 0^{th} min with a high proportion at 5 min (6.8%), further a gradual decrease in the DP6 concentration was observed. DP5 formation started slowly at 0^{th} min with T36G, but, reached to of 3.8% at 30 min. In case of T36F, DP5 was detected from 5 min and reached to a maximum of 4.3% at 60 min. DP6 accumulated to 9% by 30^{th} min with T36F variant, which was 3 times higher compared to *Sp*ChiD (2.8%), and 2 times higher compared to T36G (4.2%). The TG activity was retained up to 75 and 120 min by T36G and T36F, respectively.

3.4.4 Effect of Loop Deletion (SpChiDΔ30-42)

The 13 residue loop Asn30 – Asp42, occupying half of the space in the substrate binding cleft was deleted using PCR based approach. HPLC analysis revealed that the deletion of loop had completely abolished the chitobiase activity of *Sp*ChiD on DP4 substrate, which was evident with the absence of DP1 in the fractions analyzed. A gradual decrease in the DP4 concentration through time was observed for the mutant

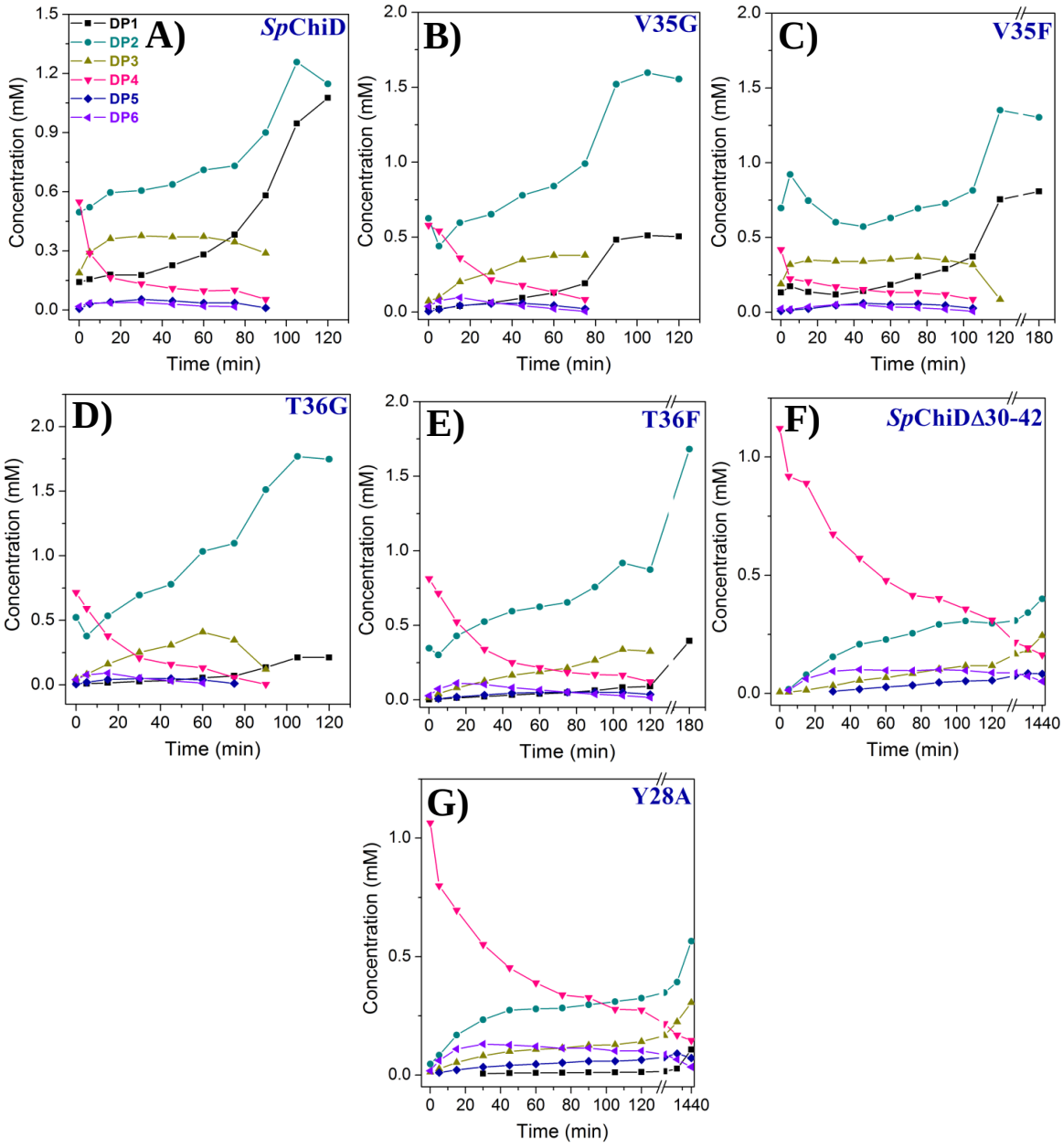

Figure 3.25: **Product profiles for the loop variants of *Sp*ChiD.** HPLC quantification profiles of *Sp*ChiD (A), 'Val' variants (B&C), 'Thr' variants (D&E), deletion mutant *Sp*ChiDΔ30-42 (F) and Y28A (G) obtained by a linear correlation between peak area and concentration of oligosaccharides in standard. Individual quantification graph represents all the hydrolytic (DP1-DP3) and TG (DP5, DP6) products accumulated during the course of reaction with 1 mM DP4 substrate.

*Sp*ChiDΔ30-42 (Fig. 3.25 F). Production of DP5 started at 30th min whereas, DP6 at 5th min. TG increased to a greater extent with more of DP6 accumulated rather than DP5 up to 180 min. At 30th min the proportion of DP5 and DP6 products was 0.9% and 9.8%, respectively. A slow increase in the DP5 product started from 60th min (3%) and reached to a maximum of 9.7% at 480 min. The proportion of DP6 produced at 30, 60, 120 and 480 min was 9.8, 10.9, 10.1 and 8.4%, respectively. The reaction was continued up to 24 h with the presence of products DP2-DP6 (Fig. 3.25 F) in proportions 42.4, 26, 17.3, 8.8 and 5.4%, respectively.

3.4.5 Tyr28 to Ala Exchange

The residue Tyr28 was present very close to the catalytic triad and was known to play a crucial role in the catalysis. Mutation of Tyr28→Ala also resulted in the decreased hydrolysis and concomitant increase in the TG activity. Formation of DP5 and DP6 products started from 5th and 0th min, respectively. Four times higher concentration of DP6 (12.6%) was detected compared to DP5 (3.2%) at 30th min. DP5 accumulated slowly at initial time points and reached to a proportion of 9.3% at the end of 480 min, whereas, DP6 quantity at 60, 120 and 480 min was 12.7, 11.2 and 6.8%, respectively. The 24 h fraction revealed the presence of products DP1-DP6 (Fig. 3.25 G) in proportions 8.7, 46, 24.8, 11.8, 5.8 and 2.8%, respectively. Though DP1 was detected in the fractions, DP2 remained as the major end product even after 24 h of reaction with DP4 as the substrate.

3.4.6 Degradation of DP2

All the loop variants and the mutant Y28A produced low quantities of DP1 from the substrate DP4, suggesting loss of chitobiase activity of *Sp*ChiD in these variants. To further understand the mutational effects on chitobiase activity, DP2 degradation studies were performed with the respective mutants. HPLC analysis revealed that the deletion mutant (*Sp*ChiDΔ30-42) and Y28A completely lost the chitobiase activity. In case of Val variants V35F displayed unaltered chitobiase activity, but the mutant V35G and both the Thr variants showed strong effect on DP2 degradation (Fig. 3.26). The proportion of DP1 produced after 72 h by *Sp*ChiD, V35G, V35F, T36G and

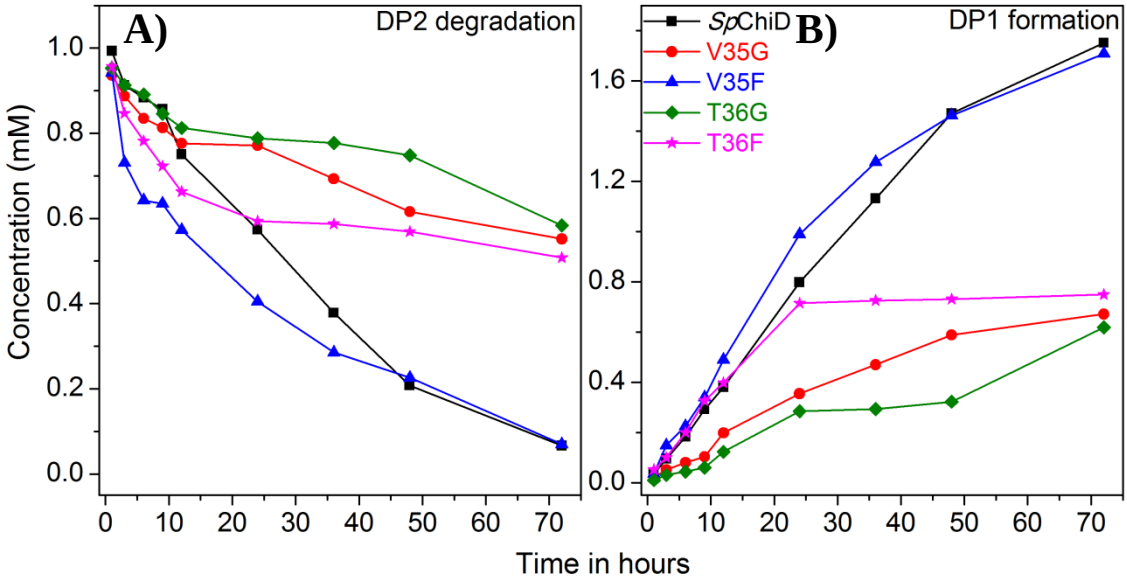

Figure 3.26: **Chitobiose (DP2) degradation by the loop variants compared against *Sp*ChiD.** HPLC quantification profiles of *Sp*ChiD and its loop variants showing the effect of mutations on chitobiase activity. Decrease in the DP2 quantity (A) and the concomitant increase in the DP1 quantity (B) were monitored by performing reactions in 50 mM sodium phosphate buffer pH 8.0, at 40°C. The fractions collected at regular time intervals were analyzed by measuring absorption at 210 nm following an isocratic HPLC separation of products on an Amino-P50 4E column. Product quantification was done by a linear correlation between peak area and concentration of oligosaccharides in standard samples.

T36F was 96.4, 54.8, 96, 51.4 and 59.5%, respectively. These data suggested the importance of residues Tyr28, Val35, Thr36 and the entire loop in DP2 degradation.

3.5 Thermal Stability & Binding Properties of SpChiD or the Mutant E153A

3.5.1 CD Spectroscopy

To investigate thermal stability of *Sp*ChiD, far and near-UV-CD spectra were recorded at different temperatures. Spectra recorded at 30, 40, 45 and 50°C were shown in the Fig. 3.27 A&B. The secondary structure of the protein did not alter at 30 and 40°C. The spectra recorded at 45°C showed lower signal intensity when compared to the spectra recorded up to 40°C, indicating perturbations in the secondary structural elements. Further increase in the temperature to 50°C resulted in the complete collapse of secondary structure for *Sp*ChiD. Near-UV-CD spectra at the identical temperatures showed a similar pattern in the loss of tertiary structure. Thus, the protein *Sp*ChiD was thermally stable up to 40°C. Far-UV-CD spectra of *Sp*ChiD, recorded in different pH conditions (pH 2, 4, 6, 7, 8, and 10) revealed that there were no major changes in the secondary structure (Fig. 3.27 C).

3.5.2 DSC Measurements

Thermal stability and the mechanism of unfolding of *Sp*ChiD were studied under different conditions by using high-sensitivity DSC measurements. Fig. 3.28 A, shows a typical DSC thermogram of *Sp*ChiD alone corrected for buffer base line at pH 8.0. The data shown in the thermograms was best fitted to a non-two-state model. Deconvolution analysis of the thermogram (shown in dotted lines) indicated the presence of two distinct transitions centred at 44.8 and 47.3°C, respectively, at pH 8.0. DSC scans for the native *Sp*ChiD as a function of pH revealed that the protein was thermally stable at pH 6.0 and showed regular two distinct transitions centred at 50.1 and 52.7°C, respectively (Fig. 3.28 B). Values of the calorimetric enthalpy (ΔHc), van't Hoff enthalpy (ΔHv) and their ratio (ΔHc/ΔHv) corresponding to these transitions at different pH were given in Table 3.6. Thermal denaturation of *Sp*ChiD was completely irreversible, as no transition could be seen when the sample was subjected to a second heating scan after it was cooled from the first run. In order to investigate the reversibility of each transition, DSC measurements were performed by

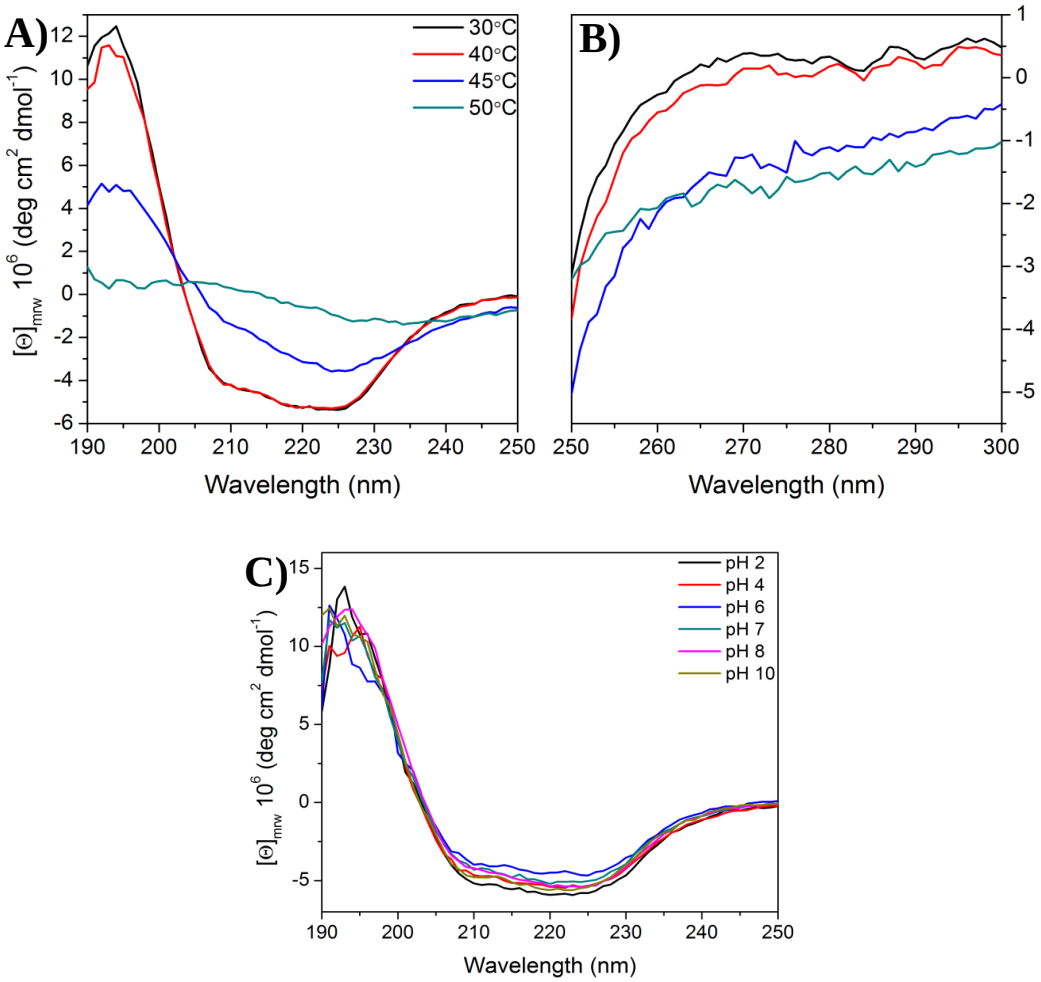

Figure 3.27: **CD spectral measurements of *Sp*ChiD.** Far (A) and near (B) UV-CD spectra were recorded at different temperatures. Structural stability of *Sp*ChiD was also investigated under different pH conditions (C) by recording far-UV-CD spectra.

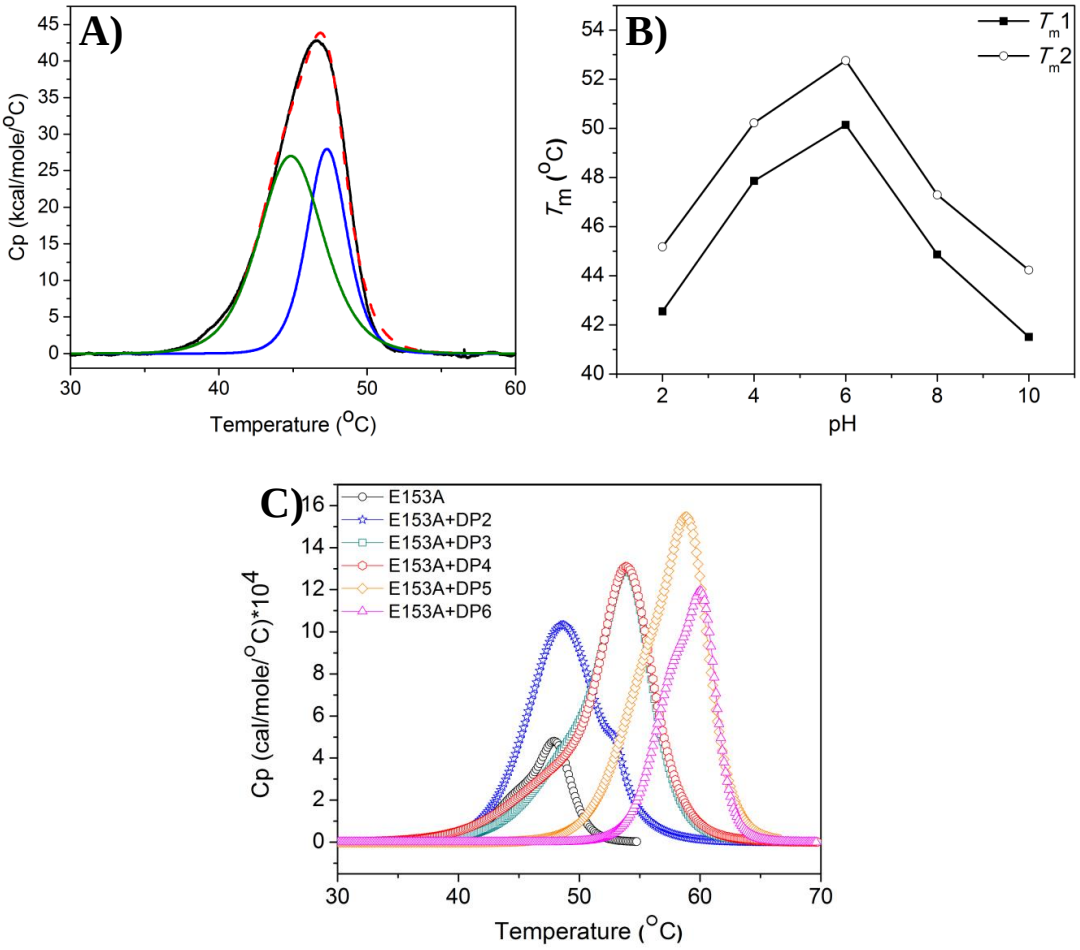

Figure 3.28: **DSC measurements of *Sp*ChiD and the mutant E153A.** DSC thermogram of *Sp*ChiD alone after buffer base line correction in 20 mM sodium phosphate, pH 8.0. Dotted line in red color indicates deconvolution analysis of the thermogram showing the presence of two distinct transitions (A). DSC scans for *Sp*ChiD as a function of pH, revealed that the protein was thermally stable at pH 6.0 and showed regular two distinct transitions (B). The effect of ligand binding on thermal stability of E153A was studied by pre-incubating the protein with CHOS of DP2-6 (C).

pH	Tm_1 (°C)	ΔHc_1 (kcal mol^{-1})	ΔHv_1 (kcal mol^{-1})	$\Delta Hc_1/\Delta Hv_1$	Tm_2 (°C)	ΔHc_2 (kcal mol^{-1})	ΔHv_2 (kcal mol^{-1})	$\Delta Hc_2/\Delta Hv_2$
2	42.55	81.14	126.9	0.639	45.18	64.83	204.1	0.317
4	47.86	134.0	143.0	0.937	50.22	118.0	238.8	0.494
6	50.14	101.5	132.4	0.766	52.76	65.80	234.4	0.280
8	44.87	157.1	138.2	1.13	47.29	100.5	227.3	0.442
10	41.51	108.9	138.6	0.785	44.23	76.14	207.0	0.367

Table 3.6: Values of the calorimetric enthalpy (ΔHc), van't Hoff enthalpy (ΔHv) and their ratio ($\Delta Hc/\Delta Hv$) corresponding to the transitions shown by *Sp*ChiD at different pH conditions obtained by DSC

	Tm (°C)		ΔH_C (kcal.mol^{-1})		ΔH_v (kcal.mol^{-1})		$\Delta H_C/\Delta H_v$	
	Transition-I	Transition-II	Transition-I	Transition-II	Transition-I	Transition-II	Transition-I	Transition-II
E153A	45.34±0.18	48.12±0.028	136.1±9.87	121±9.29	132.4±3.44	250.1±9.16	1.02	0.48
$(GlcNAc)_2$	48.78±0.03	53.16±0.096	798.5±7.14	22.03±4.1	106.5±1.07	499.5±92.1	7.49	0.04
$(GlcNAc)_3$	50.20±0.47	54.30±0.043	395.1±49.3	556.6±46.4	87.17±3.71	165.3±6.23	4.53	3.36
$(GlcNAc)_4$	48.88±0.52	54.10±0.032	361.6±38.7	643.0±35.0	70.95±3.63	153.2±4.33	5.09	4.19
$(GlcNAc)_5$	56.09±0.30	59.30±0.063	537.9±61.8	500.5±59.8	123.8±3.94	203.4±10.2	4.34	2.46
$(GlcNAc)_6$	58.15±0.19	60.49±0.055	379.6±36.7	234.5±35.2	176.8±4.67	306.9±22.1	2.14	0.76

Table 3.7: The transition temperatures (*T*m) of thermal unfolding and the thermodynamic parameters of CHOS binding to E153A using DSC

NOTE: All DSC measurements were carried out on a MicroCal VP-DSC apparatus (MicroCal LLC, Northampton, MA, USA). Absolute and excess heat capacities were analyzed using non-two-state fit of the thermogram using the Origin v 7.0 software provided with the instrument.

terminating the scans at the *T*m of transitions 1 and 2, the results obtained also indicated the irreversibility at the respective transitions for *Sp*ChiD (data not shown). When the DSC scans were performed using different concentrations of the protein (0.4–1 mg/mL), it was observed that the *T*m values and thermodynamic parameters associated with the unfolding transitions were independent of protein concentration (data not shown). To investigate ligand induced thermal stability of *Sp*ChiD, the mutant E153A, which lost complete activity but retained binding capacity was used. E153A also displayed similar two transitions whose *T*m values were centred at 45.3 and 48.1°C, respectively. The *T*m values for E153A were nearly identical with that of *Sp*ChiD, which allowed us to further proceed for ligand binding studies. The effect of ligand binding on thermal stability of E153A was studied by pre-incubating the protein with CHOS of DP2-6 (Fig. 3.28 C) and the thermodynamic parameters obtained were given in Table 3.7. Though, there was no much difference among the *T*m values at the respective transitions upon DP2-DP4 binding, the stability of the protein increased in presence of ligands. This observation was supported by HPLC analysis of *Sp*ChiD activities at different temperatures (Fig. 3.29). High *T*m values of 56, 59.3°C with DP5 and 58.2, 60.5°C with DP6 at the respective transitions were observed, compared to E153A alone. Increased thermal stability of E153A with increased chain length of CHOS was observed with DP5 and DP6.

3.5.3 'Trp' Exposure & Accessibility of E153A in Absence or Presence of CHOS

The exposure and accessibility of Trp residues of E153A in the presence and absence of CHOS was studied by fluorescence quenching experiments using the neutral quencher acrylamide. Fluorescence emission spectra of E153A corresponding to quenching experiments were obtained in the absence of ligand and in the presence of DP2-DP6 CHOS (Fig. 3.30). As a control, fluorescence quenching titrations with acrylamide were performed for *Sp*ChiD along with E153A in the absence of CHOS. Nearly, a similar percentage of quenching, in the absence of ligand was observed for both *Sp*ChiD (82.4%) and E153A (83.9%). This data strongly supported that there were no major perturbations due to mutation in the tertiary structure of the protein. The extent of quenching decreased with an increase in the chain length of CHOS

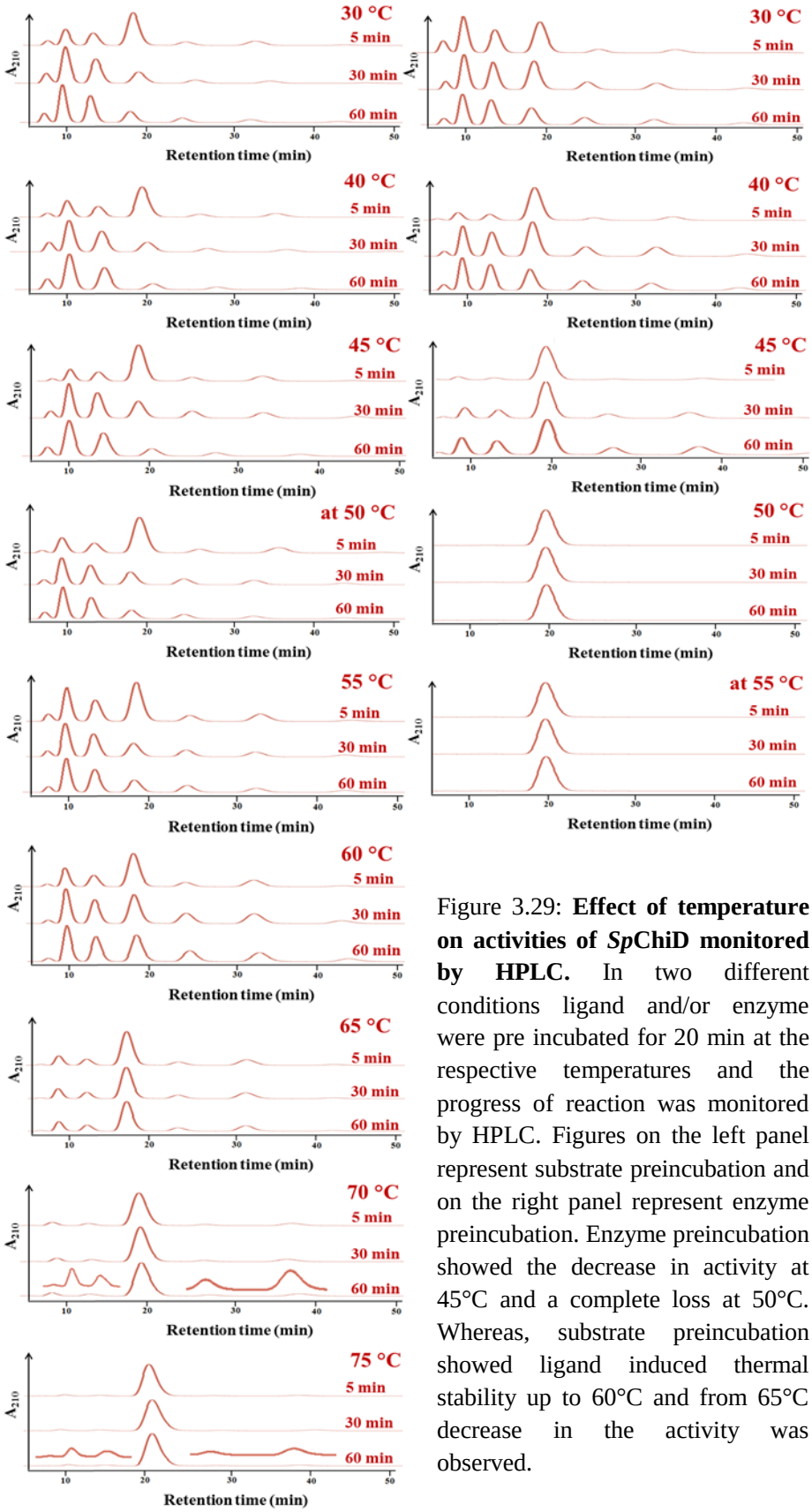

Figure 3.29: **Effect of temperature on activities of *Sp*ChiD monitored by HPLC.** In two different conditions ligand and/or enzyme were pre incubated for 20 min at the respective temperatures and the progress of reaction was monitored by HPLC. Figures on the left panel represent substrate preincubation and on the right panel represent enzyme preincubation. Enzyme preincubation showed the decrease in activity at 45°C and a complete loss at 50°C. Whereas, substrate preincubation showed ligand induced thermal stability up to 60°C and from 65°C decrease in the activity was observed.

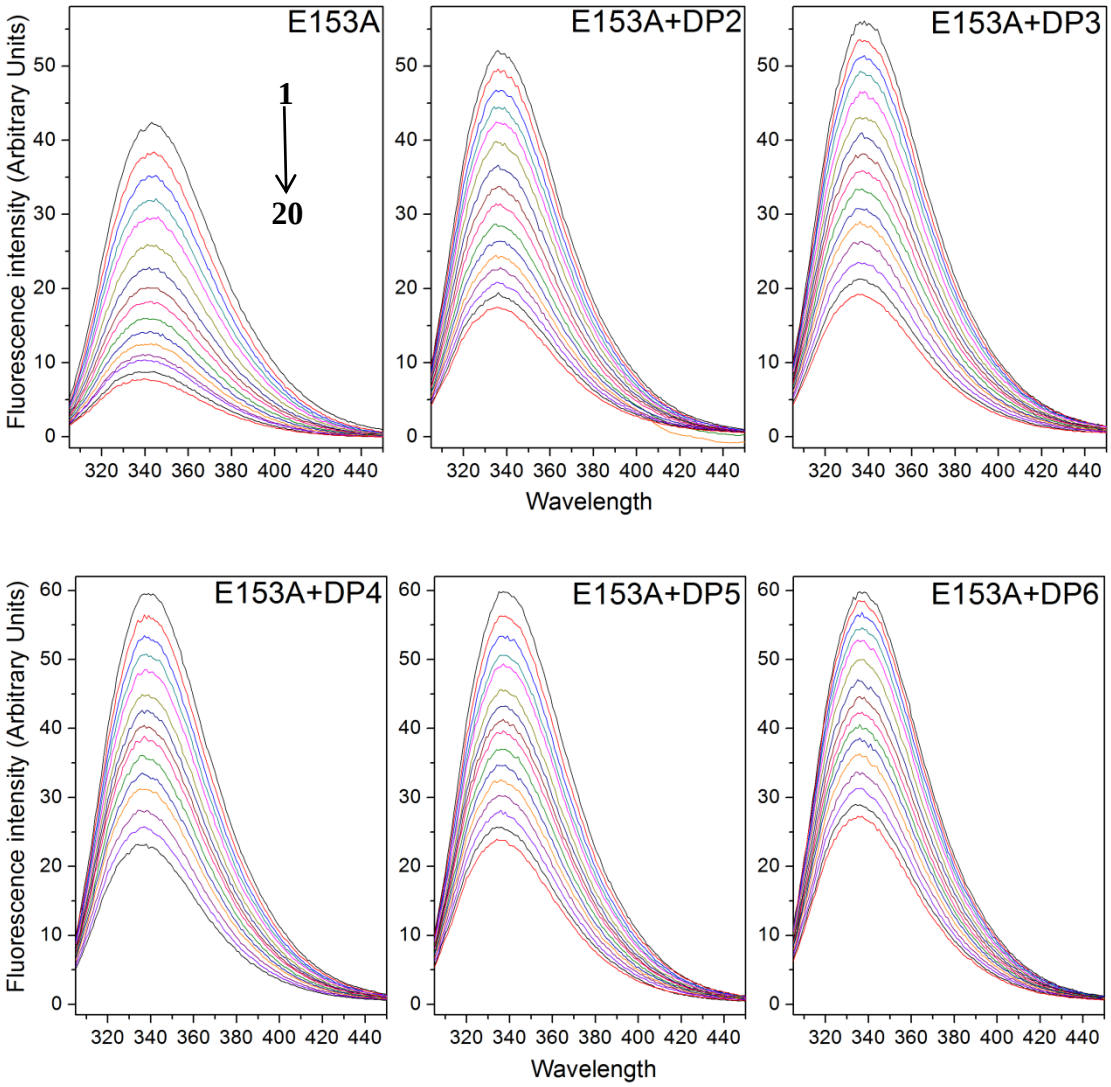

Figure 3.30: **Fluorescence quenching studies with E153A.** Fluorescence emission spectra corresponding to quenching experiments were carried out in the absence of any ligand and in the presence of CHOS with DP2-6. In the representation 1→20, 1-corresponds to the spectrum recorded for protein alone and the spectra 2-20 corresponds to increasing concentration of the quencher acrylamide. All the spectra were recorded under same conditions.

(from DP2-DP6) and the percentage quenching values were given in Table 3.8. The data was fitted to the linear curve fitting model, and the resultant slope provided the Stern-Volmer constant (K_{SV}) (Fig. 3.31). The K_{SV} values for *Sp*ChiD or E153A in the absence or presence of CHOS were given in the Table 3.8. The K_{SV} values decreased with the increase in chain length of CHOS, suggesting the reduced accessibility of Trp in the protein to the quencher.

3.5.4 ITC Analysis of CHOS Binding to E153A

The binding of CHOS to E153A was studied by ITC at 13 or 25°C and pH 8.0. Fig. 3.32 shows typical ITC thermograms and theoretical fits to the experimental data for CHOS with DP-2, 3, 5 and 6 binding to E153A. For DP2 the *n* value was 3, but for DP3 and DP5 it was 0.8 and 1, respectively, indicating a one to one stoichiometry, whereas, in case of DP6 binding the *n* value was 1.58. DP2 binds with a K_d of 0.24 μM (Table 3.9) and the binding was clearly entropically driven ($-T\Delta S$ = 5.89 kcal/mol and ΔS = 20.6 cal/mol/deg) with a small enthalpic penalty (ΔH = -0.15±0.026 kcal/mol). For DP3 binding, the K_d was 0.22 μM, which was similar to DP2 binding and this event was also entropically driven ($-T\Delta S$ = 4.26 kcal/mol and ΔS = 14.9 cal/mol/deg) with an enthalpic penalty (ΔH = -1.84±0.186 kcal/mol). Binding of lower chain CHOS *i.e.* DP2 and DP3 resulted in exothermic heat changes. In contrast, binding of longer chain CHOS *i.e.* DP5 and DP6 was accompanied by strong endothermic heat changes. DP5 binding was accompanied with a K_d of 0.013 μM and this reaction was largely entropically driven ($-T\Delta S$ = 11.53 kcal/mol and ΔS = 38.7 cal/mol/deg) with a small enthalpic contribution (ΔH = 3.53±0.047 kcal/mol). Though, DP6 binds very strongly to E153A, with a K_d of 0.005 μM, the reaction was quite similar to DP5 binding, which was entropically driven ($-T\Delta S$ = 10.81 kcal/mol and ΔS = 36.3 cal/mol/deg) with an enthalpic penalty (ΔH = 2.28±0.025 kcal/mol). Inspite of our best efforts we could not get a good thermogram for DP4 binding to E153A.

3.6 Mutational Analysis of 'Trp' at Substrate Binding Cleft of SpChiD

Observations from fluorescence quenching studies and ITC measurements prompted us to analyze, the possible involvement of Trp residues at the substrate binding cleft,

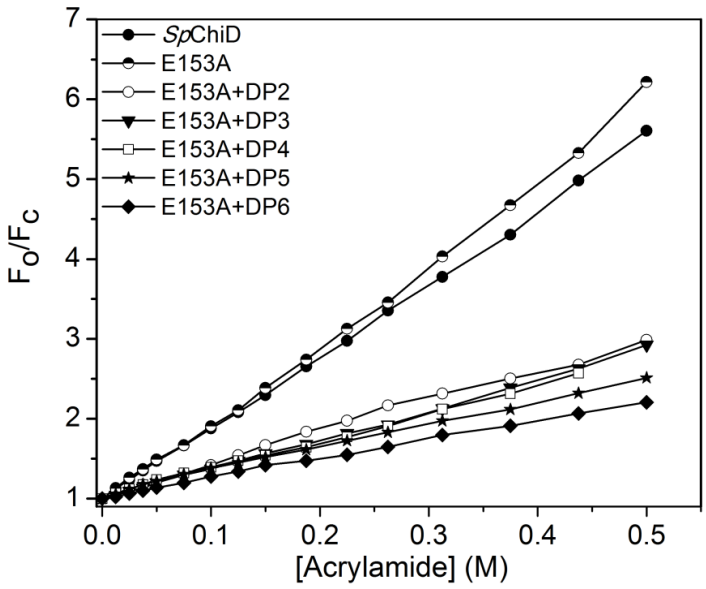

Figure 3.31: **Stern-Volmer plots of E153A.** The data obtained from the fluorescence emission spectra recorded in the absence and presence of ligands (DP2-6) was fitted to the linear curve fitting model, and the resulted slope was considered as the Stern-Volmer constant (K_{SV}). Stern-Volmer plot of *Sp*ChiD in the absence of ligands was also given to compare with the mutant E153A.

	% Quenching	*K*sv
*Sp*ChiD	82.4	9.17
E153A	83.9	10.09
$(GlcNAc)_2$	66.5	3.95
$(GlcNAc)_3$	65.8	3.73
$(GlcNAc)_4$	61.1	3.33
$(GlcNAc)_5$	60.2	2.91
$(GlcNAc)_6$	54.7	2.41

Table 3.8: Acrylamide quenching of E153A in the presence or absence of $(GlcNAc)_{2\text{-}6}$

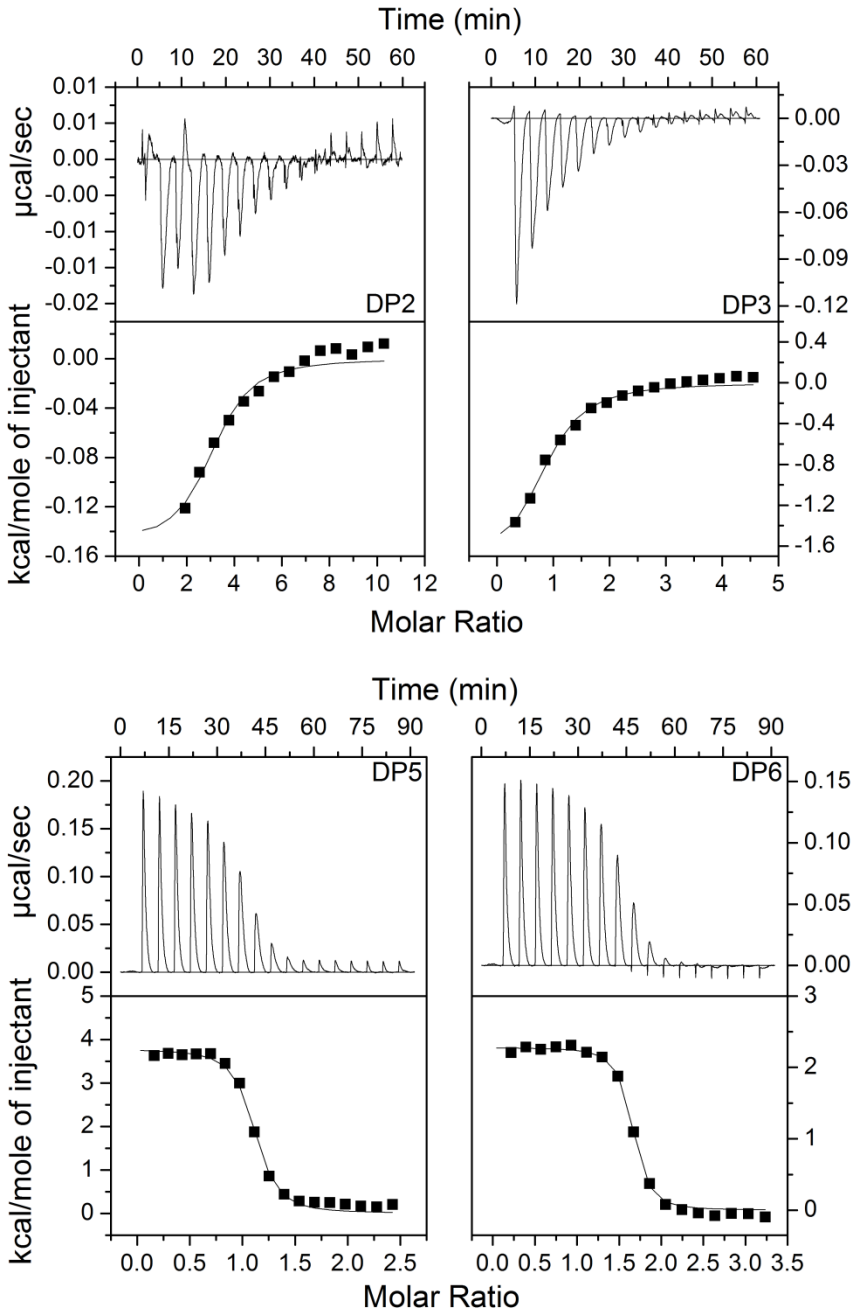

Figure 3.32: **ITC binding studies for the mutant E153A.** Thermograms (upper panels) and binding isotherms with theoretical fits (lower panels) obtained for the binding of CHOS with DP-2, 3, 5 and 6 to the mutant E153A. Titrations were performed at 13 or 25°C and pH 8.0.

Sugar	Temp	*n*	K_b $\times 10^5$ (M^{-1})	K_d($1/K_a$) μM	$-\Delta G°$ (kcal.mol^{-1})	$\Delta H°$ (kcal.mol^{-1})	$\Delta S°$ (cal.mol^{-1}.deg^{-1})	$-T\Delta S$ kcal.mol^{-1}
$(GlcNAc)_2$	13ºC	3.04±0.307	0.422±0.207	0.237	6.04	-0.1506±0.0261	20.6	5.89
$(GlcNAc)_3$	13ºC	0.839±0.0641	0.461±0.117	0.217	6.1	-1.837±0.186	14.9	4.26
$(GlcNAc)_5$	25ºC	1.09±0.00966	7.48±1.18	0.013	8	3.530±0.0468	38.7	11.53
$(GlcNAc)_6$	25ºC	1.58±0.00962	17.9±3.67	0.005	8.53	2.281±0.0249	36.3	10.81

Table 3.9: Thermodynamic parameters of CHOS binding to *Sp*ChiD-E153A derived from ITC.

NOTE: Calorimetric titrations were performed using a MicroCal iTC_{200} System (Microcal, Northampton, MA, USA). The obtained binding isotherms were analyzed by using MicroCal Origin v 7.0 software supplied with the ITC_{200} system.

in the unprecedented catalytic properties of *Sp*ChiD. The substrate binding cleft was occupied by four Trp residues, Trp114, Trp160, Trp290 and Trp395. Trp114 is the highly conserved residue in family GH18 chitinases and its mutational effects were explained in the section (3.1.4.2.2). The entrance of the substrate binding cleft in *Sp*ChiD was flanked on either side by the residues Trp160 and Trp290 (Fig. 3.22 A), whereas, Trp395 was situated with in the binding pocket. All the four Trp residues were subjected to point mutations and changed to respective Ala. Purified mutant proteins were used for kinetic and HPLC analysis.

3.6.1 Steady State Kinetic Analysis for 'Trp' Mutants

The kinetic parameters for the enzyme *Sp*ChiD and its Trp mutants were determined using colloidal chitin as the substrate and the Michaelis-Menten plots were shown in Fig. 3.33. The kinetic values (K_m, V_{max}, K_{cat} and K_{cat}/K_m) obtained were compared against *Sp*ChiD and given in the Table 3.10. The very high K_m values for the mutants W114A (105.1 mg/mL), W160A (208.9 mg/mL), W290A (133.6 mg/mL) and W160A/W290A (123.8 mg/mL) indicate decreased affinity towards colloidal chitin when compared to *Sp*ChiD (35.1 mg/mL). This clearly supported the involvement of Trp residues in binding to polymeric substrates like colloidal chitin. Mutational effects of these Trp residues also reflected in the overall catalytic efficiency, which decreased when compared to native *Sp*ChiD (Table 3.10). We were unable to obtain kinetic parameters for the mutant W395A using colloidal chitin substrate, because of its' feeble activity on polymeric substrate.

3.6.2 HPLC Analysis for the 'Trp' Mutants

Trp160 to Ala exchange resulted in the loss of TG activity to a greater extent and increased hydrolysis. The effect of mutation was comparable to that of mutation W114A. TG detected at 0^{th} min only, with a very less amount of quantifiable TG products DP5 (1.8%) and DP6 (0.8%) compared to native *Sp*ChiD (Fig. 3.34 A&B). At the end of 5 min there were only DP1 and DP2 with proportions 45.6 and 54.3%, respectively. After 60 min, DP1 was as the major end product with 54%. With the mutation W290A, TG was detectable up to 15 min (Fig. 3.34 C). The mutant W290A produced more of DP6 (5.5%) than DP5 (3.6%) at 5 min. But, hydrolysis was

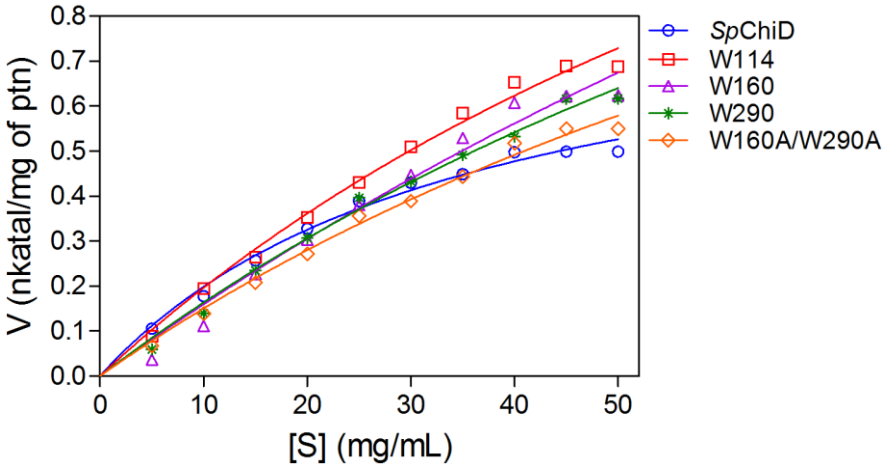

Figure 3.33: **Kinetic analysis for the Trp mutants of *Sp*ChiD.** Different concentrations of colloidal chitin substrate (0-50 mg/mL) were incubated with *Sp*ChiD and its Trp variants in 50 mM sodium phosphate buffer pH 8.0, with respective controls in triplicates at 40°C for 1 h at 200 rpm. Specific activity in nkatal/mg of protein was calculated and plotted against substrate concentration. The data was fitted to the Michaelis–Menten equation by nonlinear regression function using GraphPad Prism software version 5.0, to obtain the respective kinetic graphs and parameters.

Enzyme	K_m (mg/mL)	V_{max} (nkat/mg of protein)	K_{cat} (sec^{-1})	K_{cat}/K_m (sec^{-1} mg^{-1} mL)
*Sp*ChiD	35.12	0.896	10.3×10^2	29.33
W114A	105.1	2.262	25.99×10^2	24.73
W160A	208.9	3.494	40.14×10^2	19.22
W290A	133.6	2.352	27.02×10^2	20.23
W160A/W290A	123.8	2.014	23.14×10^2	18.69
W395A*	ND	ND	ND	ND

Table 3.10: Kinetic parameters of Trp variants of substrate binding cleft

(*) Kinetic parameters not determined (ND) due to lack of activity on colloidal chitin.

predominant throughout the reaction than TG, under equimolar enzyme concentrations tested. Only DP1 and DP2 were present at the end of 30 min with proportions 43.3 and 56.6%, respectively. As the residues Trp160 and Trp290 are flanking on either side of the substrate binding cleft, to see the combinatorial effect of these two residues, we have generated a double mutant of *Sp*ChiD *i.e.* W160A/W290A. Even the double mutant, W160A/W290A under standard reaction conditions was unable to display TG except at 0^{th} min (Fig. 3.34 D) with a very low yield of quantifiable TG products DP5 (0.8%) and DP6 (0.8%).

The mutation W395A showed a great impact on the rate of catalysis, which was evident from the very slow decrease in the initial DP4 substrate concentration (Fig. 3.34 E). W395A was able to display TG activity with DP5 produced at 15^{th} min (0.4%) and DP6 production started at 90^{th} min (0.3%). It was noticed that the mutant W395A was able to produce more of DP5 than DP6 throughout the reaction, analyzed up to 720 min. At 360 and 720 min, DP5 was present in 8.9 and 12.4%, whereas, DP6 was in the proportions 1.9 and 4.3%, respectively. An additive percentage of quantifiable TG products *i.e.* DP5+DP6 (16.7%) observed to be more than the amount of DP1+DP2 (7.2%), at the end of 720 min. Much of the DP4 substrate was left unaltered (52.5%) by W395A even after 720 min of reaction incubation. These data supported that the residue Trp395 has a crucial role in catalysis.

3.6.3 Mutational Effects at Low Enzyme Concentration

To confirm the observations pertaining to mutational effects of Trp residues at the substrate binding cleft, reactions were also performed by taking 5 times low concentration of each mutant W114A, W160A, W290A and the double mutant W160A/W290A. It was confirmed that the mutations W114A and W160A have severely hampered the TG activity of *Sp*ChiD, but, displayed increased hydrolysis (Fig. 3.35 A&B). Out of these two, only the mutant W160A showed TG up to 5 min, with very low levels of quantifiable TG products DP5 and DP6 detected with proportions 2.3 and 1.5%, respectively. Even though the mutant W290A displayed TG activity up to 120 min, hydrolysis was predominant under low enzyme conditions (Fig. 3.35 C). At 30^{th} min DP6 (6.3%) concentration was more than DP5 (4.3%),

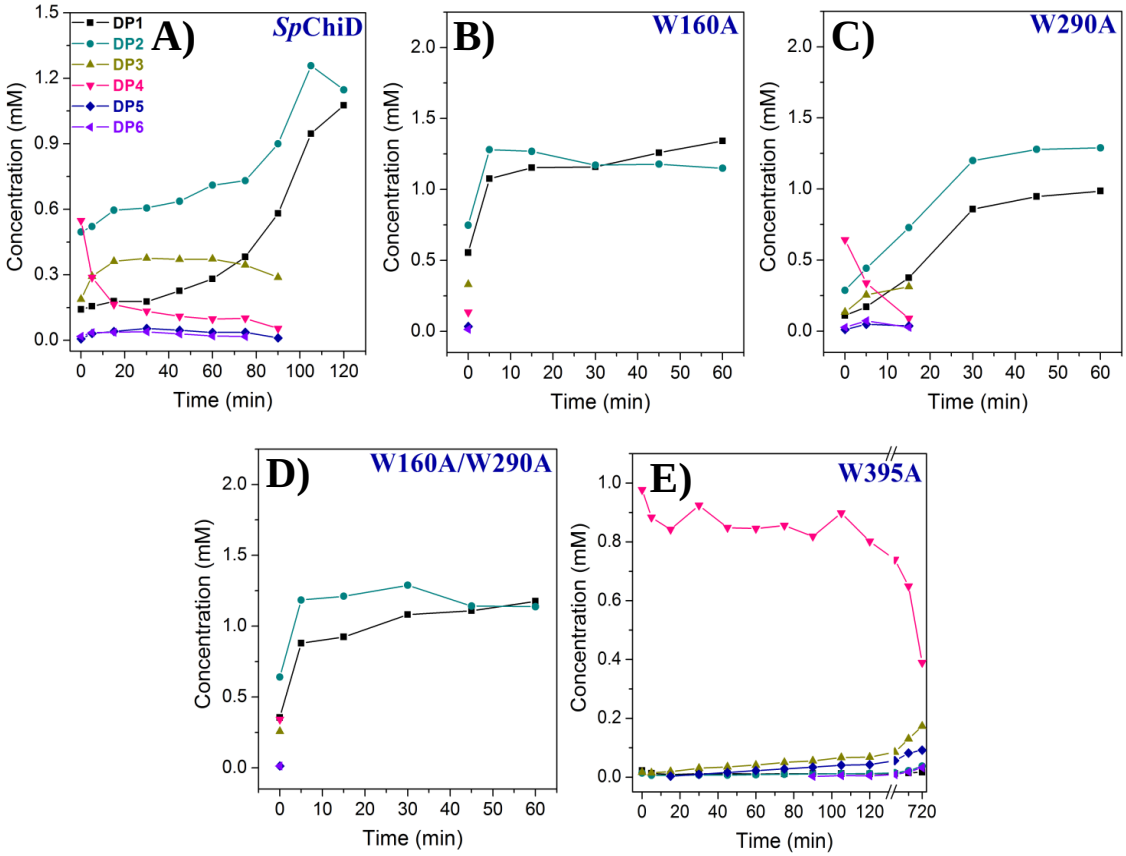

Figure 3.34: **Product profiles of the Trp mutants compared with native *Sp*ChiD.** HPLC quantification profiles of *Sp*ChiD (A) and the Trp targeted at the substrate binding cleft *i.e.* W160A (B) W290A (C), W160A/W290A (D) and W395A (E) obtained by a linear correlation between peak area and concentration of oligosaccharides in standard. Individual quantification graph represents all the hydrolytic (DP1-DP3) and TG (DP5, DP6) products accumulated during the course of reaction with 1 mM DP4 substrate.

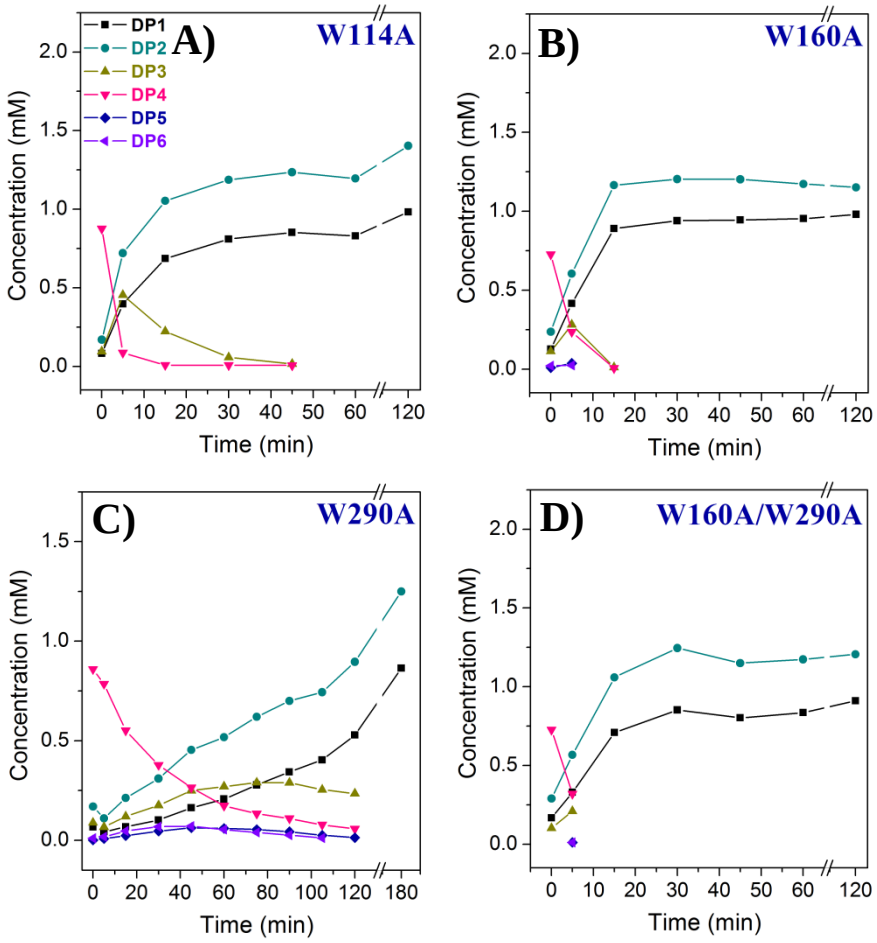

Figure 3.35: **Product profiles of the Trp mutants at low enzyme concentration.** HPLC quantification profiles obtained for the selected Trp variants of substrate binding cleft at low enzyme concentrations to further confirm the mutational effects. Analysis was performed for the mutants W114A (A) W160A (B) W290A (C) and W160A/W290A (D). Individual quantification graph represents all the hydrolytic (DP1-DP3) and TG (DP5, DP6) products accumulated during the course of reaction with 1 mM DP4 substrate.

whereas at 60 min both DP5 and DP6 were in equal proportions with 4.7 and 4.3%, respectively. Only DP1 and DP2 were detected at the end of 180 min with proportions 41 and 59%, respectively. In case of the double mutant, W160A/W290A, the effect of W160A was much severe, with which the double mutant was unable to display TG even at low enzyme conditions (Fig. 3.35 D). Traces of TG products DP5 (0.8%) and DP6 (0.7%) were detected only at 5 min. These results further support the crucial role of residues Trp114 and Trp160 in TG activity of *Sp*ChiD.

3.7 Elicitor Activity of CHOS Produced by SpChiD & the Mutant W114A

3.7.1 Generation & Characterization of CHOS from Chitosan Substrates

We have generated CHOS from chitosans with DA35% and 61% using *Sp*ChiD and the mutant W114A, which lost TG activity. Fractions collected at regular intervals were analyzed using HPTLC (Fig. 3.36) and 90 min for degradation of chitosan DA 35% with both *Sp*ChiD and W114A was selected. However, 90 and 30 min for degradation of chitosan DA 61% (Fig. 3.36) with *Sp*ChiD and W114A were selected, respectively. The prepared hydrolysates were lyophilized overnight and dissolved in sterile MilliQ water to a final concentration of 1 mg/mL. Further, these samples were characterized by MALDI-TOF-MS (Table 3.11) and tested for their elicitor activity in rice cell suspension culture systems.

3.7.2 Elicitor Activity of Crude CHOS Mixtures

Dose-dependent elicitation of oxidative burst in rice cell suspension cultures was carried out with 50, 100 and 150 µg/mL of each crude mixture generated by *Sp*ChiD or the mutant W114A as described in the section 2.7.5. The crude mixture from chitosan DA35% showed good elicitor activity only at doses 100 and 150 µg/mL, whereas, crude mixture from DA61% chitosan, showed elicitor activity at all the different concentrations tested. It proves that the production of H_2O_2 (µM) was dependent on the type of starting substrate used for elicitor preparation and on the elicitor concentration applied (50-150 µg/mL). It was also observed that the chitosan crude mixtures produced by the mutant W114A were more active than *Sp*ChiD (Fig. 3.37), though there were subtle differences seen in the MALDI-TOF-MS analysis (Table 3.11). The oxidative burst induced by DA35% crude mixtures of *Sp*ChiD and

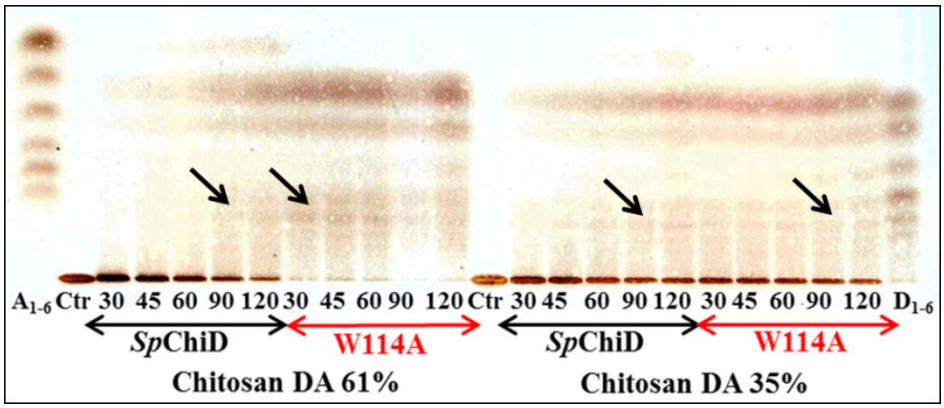

Figure 3.36: **HPTLC analysis of chitosan hydrolysates obtained with *Sp*ChiD and W114A.** Fractions collected at different time intervals during the course of chitosan (DA61% and 35%) hydrolysis by *Sp*ChiD and W114A were analyzed using HPTLC. A_{1-6}-was the standard mixture of $(GlcNAc)_1$-$(GlcNAc)_6$ and D_{1-6} represents the mixture of $(GlcN)_1$-$(GlcN)_6$. Ctr-indicates substrate control without enzyme addition. Arrow marks represent the selected time points of degradation by *Sp*ChiD and W114A for chitosans with DA61% and 35%.

	***Sp*ChiD with DA61%**	**W114A with DA61%**
DP2	AD, A2	AD, A2
DP3	AD2, A2D, A3	AD2, A2D
DP4	A2D2, A3D	AD3, A2D2, A3D
DP5	A2D3, A3D2	A2D3, A3D2
DP6	A2D4, A3D3, A4D2	A2D4, A3D3, A4D2
DP7	A2D5, A3D4, A4D3, A5D2	A2D5, A3D4, A4D3
DP8	A3D5, A4D4, A5D3	A2D6, A3D5, A4D4
DP9	A4D5, A5D4	A3D6, A4D5
DP10	A4D6, A5D5	A4D6, A5D5
DP11	A5D6	A5D6
DP12	A2D10	
	***Sp*ChiD with DA35%**	**W114A with DA35%**
DP2	AD, A2	AD, A2
DP3	AD2, A2D	D3, AD2, A2D
DP4	D4, AD3, A2D2, A3D	D4, AD3, A2D2, A3D, A4
DP5	A2D3, A3D2	AD4, A2D3, A3D2
DP6	A2D4, A3D3,	D6, AD5, A2D4, A3D3
DP7	A2D5, A3D4	AD6, A2D5, A3D4
DP8	A2D6, A3D5	A2D6, A3D5
DP9	A2D7, A3D6	A2D7, A3D6
DP10		A3D7

Table 3.11: MALDI-TOF-MS analysis of crude mixtures generated by *Sp*ChiD and W114A from chitosans with DA61% and 35%. Differences in the CHOS were shown in red.

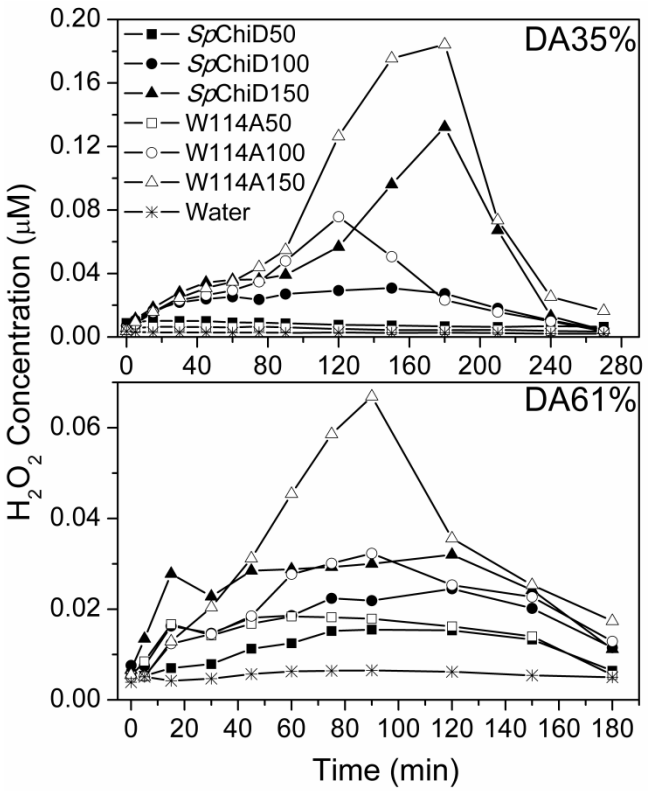

Figure 3.37: **Elicitor activity using crude CHOS mixtures generated by *Sp*ChiD and W114A.** Dose-dependent elicitation of oxidative burst experiments were performed in rice cell suspension cultures. CHOS crude mixtures obtained by degradation of chitosans (DA61% and 35%) with *Sp*ChiD and W114A were used as elicitors. 50, 100 and 150 μg of each crude mixture and sterilized MilliQ water as negative control were used for elicitor activity studies. Data shown are from one representative of three independent experiments with similar results.

W114A, showed maximum levels of H_2O_2 production between 120-180 min and then reached to their initial stage by 270 min. Crude mixtures generated by *Sp*ChiD and W114A with DA61% chitosan induced higher levels of H_2O_2 between 75-90 min and 90 min, respectively and reached to the initial stage by 180 min.

3.7.3 Elicitor Activity of Purified CHOS Produced from Chitosan DA61%

One hundred milligrams of chitosan DA61% substrate was incubated with *Sp*ChiD or W114A, followed by purification using SEC. Size distribution of oligomers after purification and the respective HPTLC confirmations were shown in Fig. 3.38. Fractions 12 to 17 generated by *Sp*ChiD and W114A were further analyzed using MALDI-TOF-MS (Fig. 3.39), to know the DP and differences in DA of oligomers produced (Table 3.12). Fractions with DP8, 9 and 10 produced by both *Sp*ChiD and W114A were used for oxidative burst experiments in rice cell suspension culture systems, in a dose dependent manner (30, 50 and 70 μg/mL). Though there was no clear dose dependency, it was observed that the purified oligomeric fractions from *Sp*ChiD were more active than W114A (Fig. 3.40). The oxidative burst induced by DP8 and DP9 reaches to its peak at 60 and 15 min, respectively, after elicitation and then decreased to the initial stage by120 min. In case of elicitation with DP10, induction of H_2O_2 was biphasic. An early response occurred between 5-15 min which was decreased and again reached to a maximum at 60 min.

3.7.4 TG between Fully Acetylated & Fully/Partially Deacetylated CHOS

The capability of enzyme *Sp*ChiD to generate CHOS with different PA was tested by performing TG reactions between DP4 and fully/partially deacetylated CHOS in equimolar ratios, as described in the section 2.7.6. Fractions collected at regular time intervals were analyzed by HPTLC and MALDI-TOF-MS. Results from HPTLC (Fig. 3.41) and MALDI-TOF-MS (Fig. 3.42 A-C) confirmed that the enzyme *Sp*ChiD showed only hydrolysis but no TG, with different combinations of CHOS tested. TG was not detected even with the substrate DP4 with pattern **DAAA.** These results suggested that *Sp*ChiD lost the TG activity in presence of oligomers having '**D**' units.

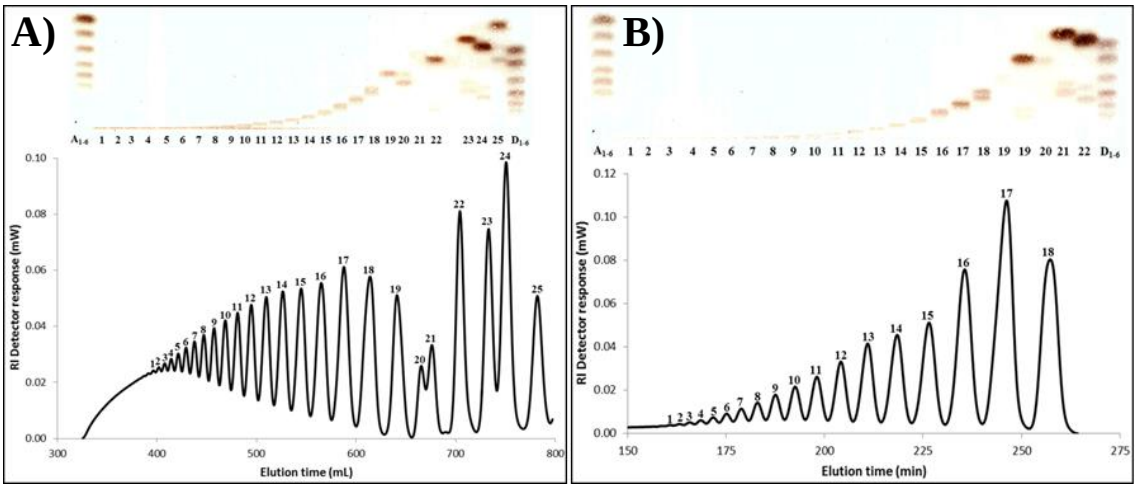

Figure 3.38: **Purification of CHOS produced by *Sp*ChiD and W114A.** One hundred milligrams of chitosan DA61% substrate was used for the degradation experiments with *Sp*ChiD (A) or W114A (B). The crude mixtures generated were purified using SECcurity GPC System equipped with a refractive index detector. Figures in the lower panel represent typical SEC purification profiles and upper panel includes the corresponding HPTLC images of CHOS produced by *Sp*ChiD and W114A. $A_{1\text{-}6}$-was the standard mixture of $(GlcNAc)_1$-$(GlcNAc)_6$ and $D_{1\text{-}6}$ represents the mixture of $(GlcN)_1$-$(GlcN)_6$.

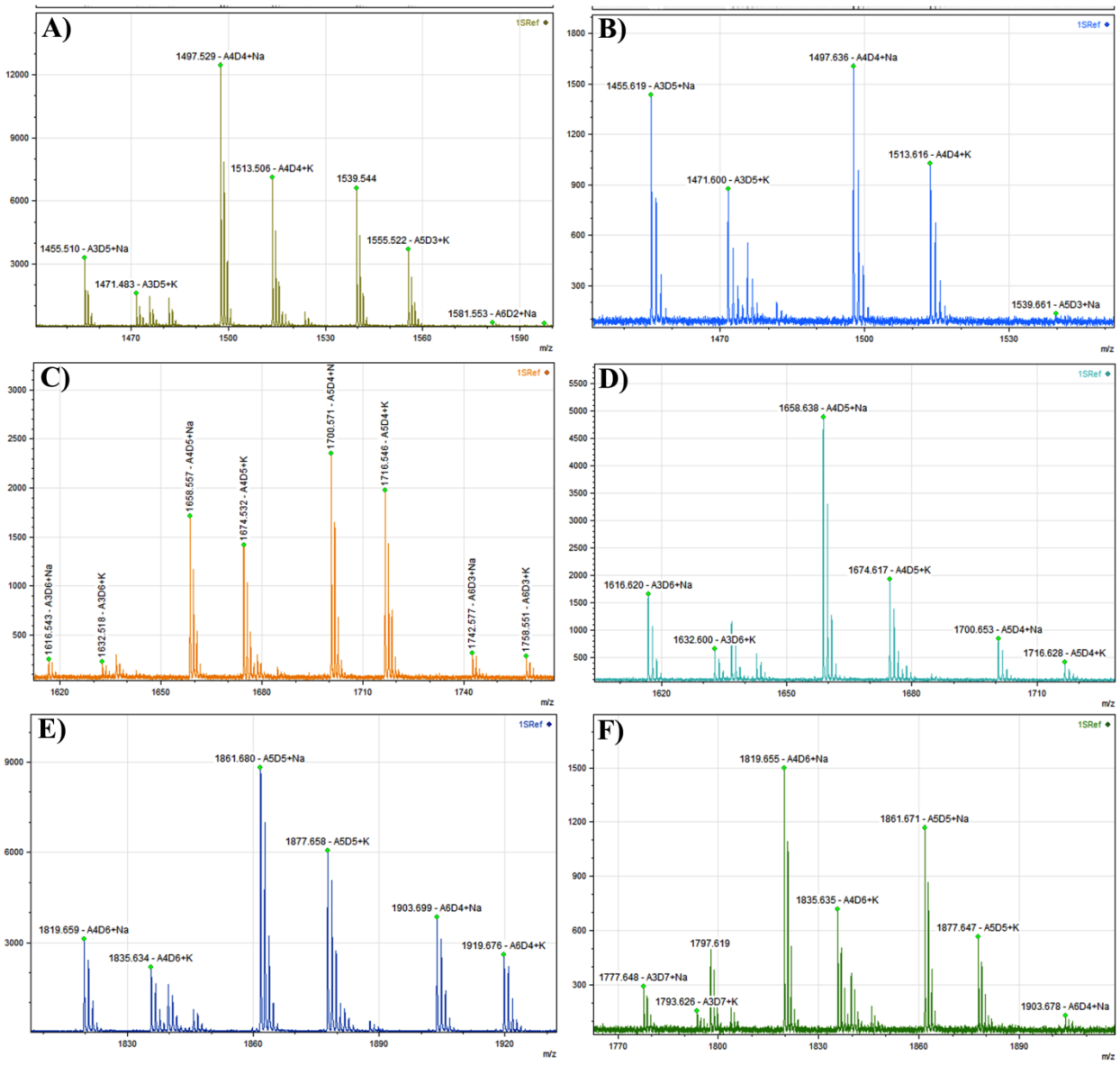

Figure 3.39: **MALDI-TOF-MS analysis of purified CHOS generated by *Sp*ChiD and W114A.** Fractions 12 to 17 were analyzed using MALDI-TOF-MS, to know the DP and differences in DA of oligomers produced. MALDI-TOF analysis for the fractions 15, 14 and 13 generated by *Sp*ChiD (A, C, E) and W114A (B, D, F) revealed that the DP of CHOS ranges from 8-10, respectively with varied DA.

Fraction Number	Type of oligosaccharides obtained from chitosan DA61%		Degree of polymerization
	*Sp*ChiD	W114A	
12	A4D7, A5D6, A6D5, A7D4	A3D8, A4D7, A5D6, A6D5	11
13	A4D6, A5D5, A6D4	A3D7, A4D6, A5D5, A6D4	10
14	A3D6, A4D5, A5D4, A6D3	A3D6, A4D5, A5D4	9
15	A3D5, A4D4, A5D3, A6D2	A3D5, A4D4, A5D3	8
16	A2D5, A3D4, A4D3, A5D2	A2D5, A3D4, A4D3	7
17	A2D4, A3D3, A4D2, A5D	A2D4, A3D3, A4D2	6

Table 3.12: MALDI-TOF-MS analysis of purified fractions generated by *Sp*ChiD and W114A from chitosan DA61%. Differences in the CHOS detected were shown in red

NOTE: Samples were analyzed with an Autoflex Speed MALDI-TOF mass spectrometer (Bruker Daltonics, Bremen, Germany) equipped with a SmartBeam™ NdYAG-laser (355 nm). Peak lists were generated from the MS spectra using Bruker FlexAnalysis software (Version 3.0).

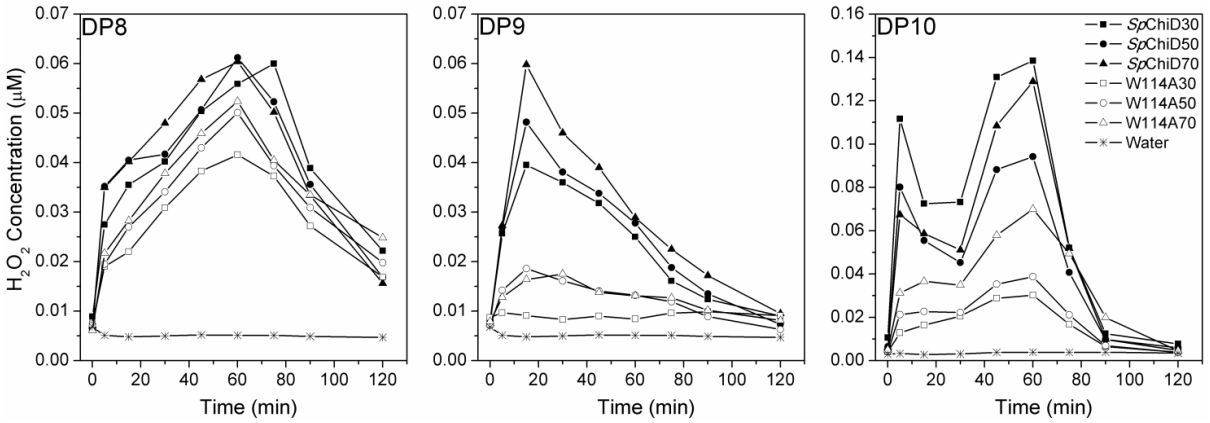

Figure 3.40: **Elicitor activity of purified CHOS with DP8-10 generated by SpChiD and W114A from DA61% chitosan.** Dose-dependent elicitation of oxidative burst experiments were performed in rice cell suspension cultures. Purified CHOS with DP8-10 were used as elicitors. 30, 50 and 70 µg of each purified CHOS and sterilized MilliQ water as negative control were used for elicitor activity studies. Data shown are from one representative of three independent experiments with similar results.

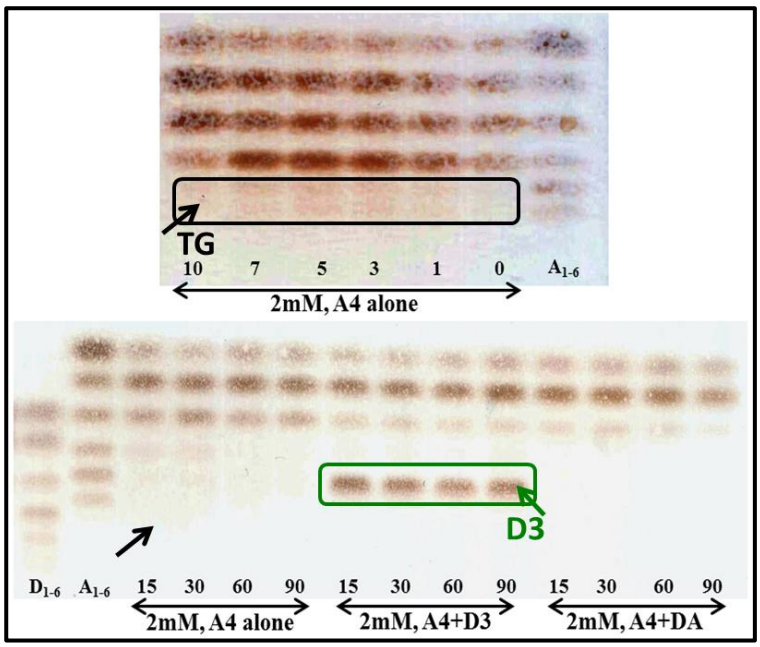

Figure 3.41: **TG between acetylated and deacetylated chitin oligomers by *Sp*ChiD.** The TG ability of enzyme *Sp*ChiD was tested between A4 $(GlcNAc)_4$ and fully/partially deacetylated CHOS (D3-$(GlcN)_3$ and DA-disaccharide with one acetyl group) in equimolar ratios. 20 µL of each fraction collected at different time points was analyzed on HPTLC. $A_{1\text{-}6}$-was the standard mixture of $(GlcNAc)_1$-$(GlcNAc)_6$ and $D_{1\text{-}6}$ represents the mixture of $(GlcN)_1$-$(GlcN)_6$.

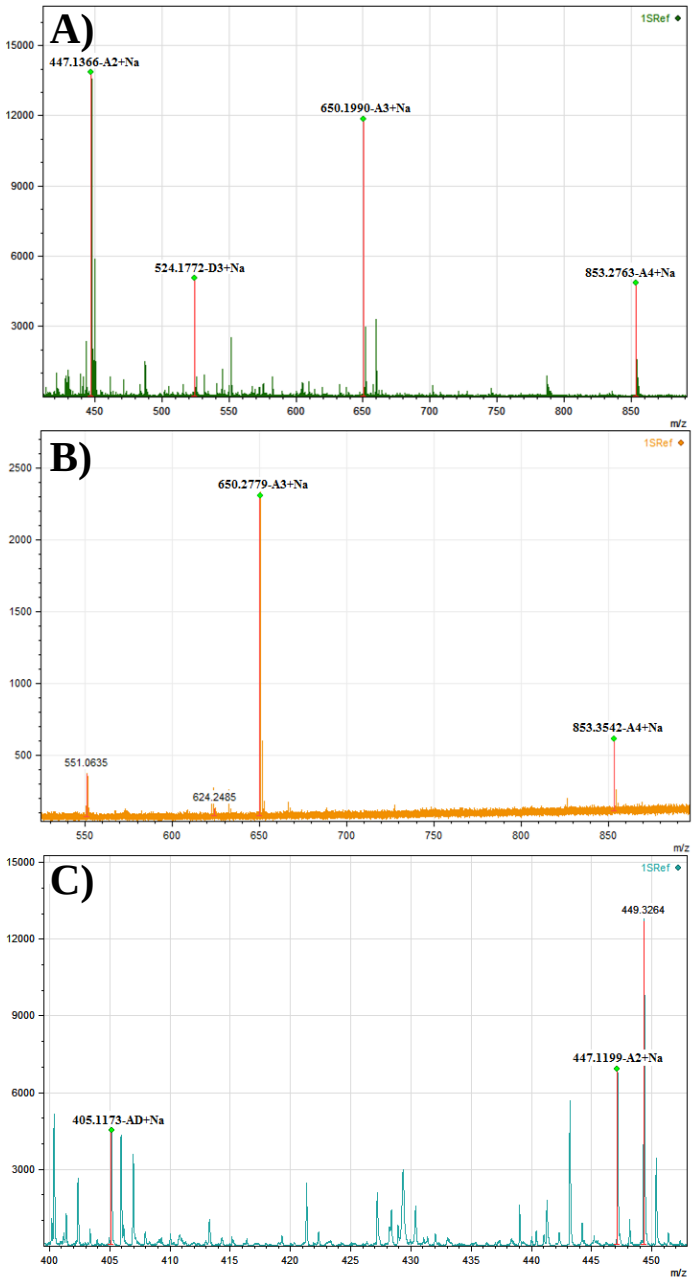

Figure 3.42: **MALDI-TOF-MS confirmation of CHOS by *Sp*ChiD.** TG between acetylated and fully/partially deacetylated CHOS was tested for *Sp*ChiD with different combinations 2 mM $(GlcNAc)_4$ + 2 mM $(GlcN)_3$ (A), 2 mM $(GlcNAc)_4$ + 2 mM dimer with pattern **DA** (B) and 2 mM tetramer alone with pattern **DAAA** (C). Fractions at 15 min were analyzed by MALDI-TOF-MS. All the reactions were performed in 50 mM sodium acetate pH 5.2 at 40°C.

3.8 Characterization of SpChiD Fusion Chimeras

3.8.1 Expression, Purification & Dot Blot Assay

E. coli Rosetta-gami II (DE3) cells harbouring the plasmids of *Sp*ChiD and the corresponding fusion chimeras were used for protein expression. Induced cells were harvested and processed for isolation of PF as described in the section 2.4.5.2. Soluble proteins of *Sp*ChiD and its fusions in the PFs were passed through Ni-NTA affinity matrix to obtain pure proteins (please see the section 2.4.5.3 for details). SDS-PAGE analysis confirmed the purity of collected protein fractions and also the expected molecular masses of *Sp*ChiD (~ 44.7 kDa) and its fusions CBP+ChiD & ChiD+CBP (~ 63.5 kDa), PKD+ChiD & ChiD+PKD (~ 58.7 kDa), PDC & CDP (~ 77.5 kDa) (Fig. 3.43 A). The dark blue spots in the in gel assay confirmed the activity of *Sp*ChiD and its fusions (Fig. 3.43 B).

3.8.2 Kinetic Analysis

The kinetic parameters for the enzyme *Sp*ChiD and its fusion chimeras were determined using colloidal chitin as the substrate (Fig. 3.44). The derived kinetic values (K_m, V_{max}, K_{cat} and K_{cat}/K_m) were compared against *Sp*ChiD and presented in the Table 3.13. Of all the six fusion chimeras analyzed, the C-terminal fusions ChiD+CBP and ChiD+PKD showed decreased K_m values of 17.6 and 15.2 mg/mL, indicating increased affinity towards colloidal chitin substrate when compared to *Sp*ChiD (35.1 mg/mL). The order of overall catalytic efficiency (sec^{-1} mg^{-1} mL) values of *Sp*ChiD and its fusion chimeras was as follows: ChiD+PKD (57.4) > ChiD+CBP (38.5) = CBP+ChiD (38.6) > *Sp*ChiD (29.3) > PKD+ChiD (25.1) ≈ CDP (24.8) > PDC (21.1).

3.8.3 Time Course of Colloidal Chitin Hydrolysis

The efficiency of *Sp*ChiD fusion chimeras in degrading insoluble polymeric substrate like colloidal chitin was tested in a time dependent manner. Equimolar amounts of all the fusion enzymes were used for performing degradation studies on colloidal chitin (25 mg/mL) and the activities were compared against *Sp*ChiD. CBP21 was known to act synergistically with the chitinases and helps in increasing the efficiency of enzymes toward crystalline chitin hydrolysis. In the present study, CBP21 was also

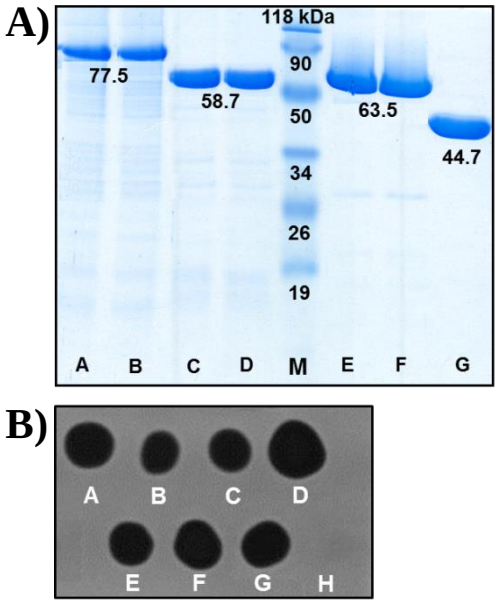

Figure 3.43: **Purification and activity analysis of *Sp*ChiD and the fusions.** (A) Recombinant *Sp*ChiD and its fusions were purified by Ni-NTA agarose affinity chromatography using elution buffer containing 50, 150 and 250 mM imidazole and loaded on 12% SDS-PAGE followed by staining with Coomassie brilliant blue G-250. The molecular weights of all the proteins and the standards are indicated in kDa. M: Pre-stained protein molecular weight marker. Lanes A-G: Purified proteins PDC, CDP, PKD+ChiD, ChiD+PKD, CBP+ChiD, ChiD+CBP and *Sp*ChiD, respectively.

(B) Purified *Sp*ChiD and its fusions were spotted (5 µg) on glycol chitin substrate containing polyacrylamide gel and incubated overnight at 37°C in humid chamber. After incubation, the gel was stained with 0.01% Calcofluor white M2R for 10 min at 4°C. The gel was placed on UV transilluminator to visualize lytic zone. Spots A-F were due to the activity of fusion enzymes PDC, CDP, PKD+ChiD, ChiD+PKD, CBP+ChiD and ChiD+CBP, respectively. *Sp*ChiD was the positive control (G); buffer as negative control (H).

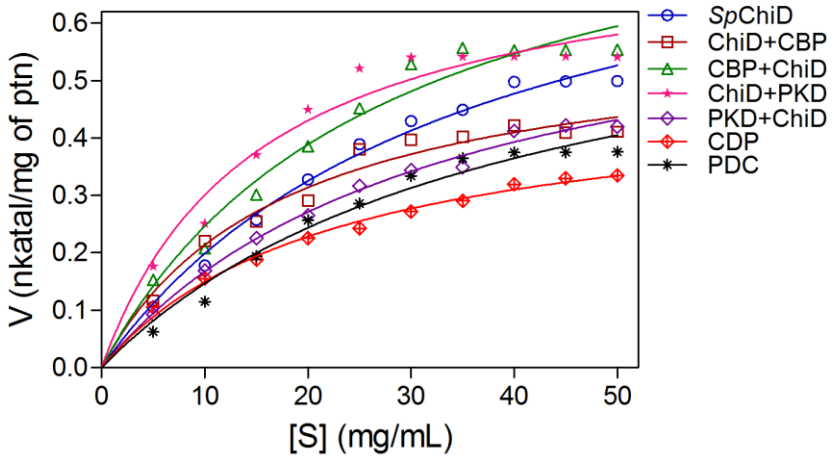

Figure 3.44: **Kinetic analysis for the *Sp*ChiD fusion chimeras.** Different concentrations of colloidal chitin substrate (0-50 mg/mL) were incubated with *Sp*ChiD and its fusions in 50 mM sodium phosphate buffer pH 8.0, with respective controls in triplicates at 40°C for 1 h at 200 rpm. Specific activity in nkatal/mg of protein was calculated and plotted against substrate concentration. The data was fitted to the Michaelis–Menten equation by nonlinear regression function using GraphPad Prism software version 5.0, to obtain the respective kinetic graphs and parameters.

Enzyme	K_m (mg/mL)	V_{max} (nkat/mg of protein)	K_{cat} (sec^{-1})	K_{cat}/K_m (sec^{-1} mg^{-1} mL)
*Sp*ChiD	35.12	0.8964	10.3×10^2	29.33
ChiD+CBP	17.6	0.5903	6.8×10^2	38.54
CBP+ChiD	27.4	0.9213	10.6×10^2	38.64
ChiD+PKD	15.15	0.7564	8.7×10^2	57.37
PKD+ChiD	32.67	0.7141	8.2×10^2	25.12
CDP	22.37	0.4838	5.6×10^2	24.86
PDC	39.48	0.7248	8.3×10^2	21.09

Table 3.13: Kinetic parameters of *Sp*ChiD fusion chimeras

fused with *Sp*ChiD, therefore, one reaction as a positive control was set up to check the synergism, by adding individual entities of CBP21 and *Sp*ChiD (CBP21 protein was kindly provided by Purushotham). Fractions collected at different intervals were analyzed by reducing end assay, as described in the section 2.4.7. CBP only fusions showed more activity compared to *Sp*ChiD (Fig. 3.45 A). The addition of CBP21 had only minor effect on the activity of *Sp*ChiD in colloidal chitin degradation, compared to the individual chimeras fused with CBP21 alone. Minor differences were observed between the fusions, ChiD+CBP and CBP+ChiD in the initial rates of degradation up to 90 min. From 120 min, the difference in the activities of these chimeras was high, with the C-terminal fusion (*i.e.* ChiD+CBP) showing more activity (Fig. 3.45 A). After an incubation of 720 min, the CBP only fusions had higher activity compared to *Sp*ChiD and *Sp*ChiD+CBP21 (synergy).

Unlike the chimeras fused with CBP alone, fusions of PKD and CDP showed good activity right from 30 min of reaction incubation. Though, the PKD fusions showed good initial rates, the differences between ChiD+PKD and PKD+ChiD were less up to 90 min, an observation quite similar to the CBP only fusion chimeras. The PKD fusions were more active right from 30 min, than any other *Sp*ChiD fusion chimeras (Fig. 3.45 B). But, at the end of 720 min, out of the six fusion chimeras analyzed, ChiD+CBP was more active. From the data obtained, the CDP appeared to be more active than PDC up to 210 min. In the later time points 360 and 720 min, there was no big difference in the activities of CDP and PDC (Fig. 3.45 B). Time dependent degradation studies on colloidal chitin also revealed, that the C-terminal *Sp*ChiD fusion chimeras *i.e.* ChiD+CBP and ChiD+PKD were more active than the other chimeras tested.

3.8.4 Hydrolyzing Activities of SpChiD Fusions on 'α' & 'β' Chitin

The effect of binding domains (CBP or PKD) fused to *Sp*ChiD was analyzed by performing hydrolyzing reactions with α- or β-chitin substrates as described in the section 2.4.10. Under the standard reaction conditions, all the enzymes showed higher activity on β-chitin compared to α-chitin. Among all the fusion chimeras, ChiD+PKD showed highest activity on α-chitin whereas, ChiD+CBP showed highest activity on

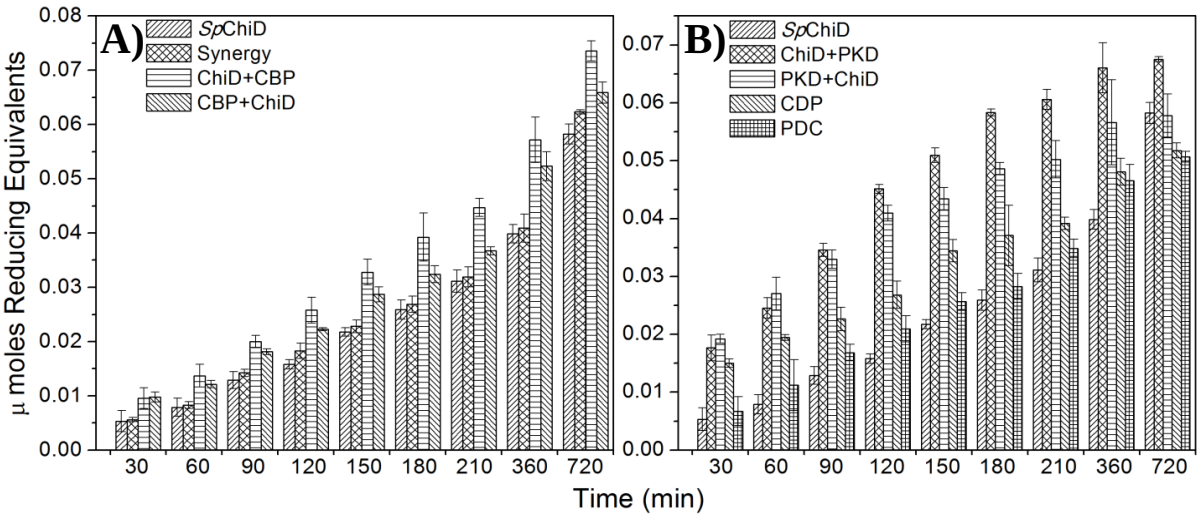

Figure 3.45: **Time course degradation of colloidal chitin by *Sp*ChiD fusion chimeras.** Time dependent degradation of colloidal chitin by native *Sp*ChiD and its fusion chimeras was performed by incubating 25 mg/mL of colloidal chitin with 38 µg of each fusion enzyme in 50 mM sodium phosphate, pH 8.0. Reaction mixtures were incubated at 40°C, 800 rpm in a thermomixer. Plots represent the average of three independent data sets obtained for each enzyme. (For clarity comparison of seven chimeras with native *Sp*ChiD, Figure 3.45 was presented in two parts A & B).

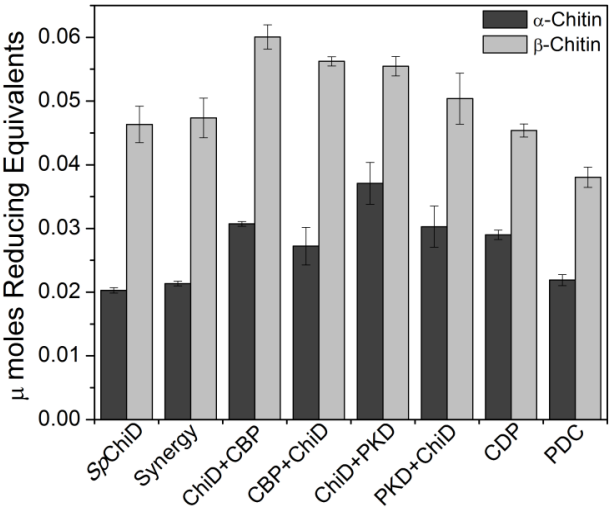

Figure 3.46: **Degradation of α- and β-chitin by *Sp*ChiD fusion chimeras.** 2.5% (wt/vol) α-chitin (or) β-chitin was used for the degradation studies by *Sp*ChiD and its fusion chimeras. All the reactions were performed at 40°C for 1 h, in 50 mM sodium acetate buffer, pH 5.2 with 1 µM each of *Sp*ChiD or its fusion chimeras. Plots represent the average of three independent data sets obtained for each enzyme.

β-chitin (Fig. 3.46). The order of activities on α-chitin was as follows: ChiD+PKD > ChiD+CBP = PKD+ChiD > CDP ≈ CBP+ChiD > PDC ≈ Synergy ≈ *Sp*ChiD. But, on β-chitin these enzymes followed a different order of priority as follows: ChiD+CBP > CBP+ChiD ≈ ChiD+PKD > PKD+ChiD > Synergy ≈ *Sp*ChiD ≈ CDP > PDC.

3.8.5 Effect of Fusions on TG Activity of SpChiD with DP4

3.8.5.1 ChiD+CBP & CBP+ChiD

The fusions ChiD+CBP and CBP+ChiD showed more of hydrolysis than TG activity compared to *Sp*ChiD (Fig. 3.47 A-C). A very rapid decrease in the initial DP4 substrate was observed when the substrate was completely converted to DP1 and DP2 by the end of 60 min (Fig. 3.47 B&C). Quantifiable TG products DP5 and DP6 were detected in very low quantities at all the time points, except at 5 min where, a minor increase in the TG products was observed. ChiD+CBP and CBP+ChiD produced DP5 in proportions 1.7 and 2.3%, whereas, DP6 in proportions 1.5 and 2.1%, respectively, at 5 min. After 5 min, the TG products decreased with time and only DP5 was detected at the end of 45 min for both the fusions. The fusion of only CBP21 either at N- or at C-terminus did not result in the increased TG activity, rather there was a decrease in the TG activity when compared to *Sp*ChiD.

3.8.5.2 ChiD+PKD & PKD+ChiD

The C-terminal PKD fusion *i.e.* ChiD+PKD displayed an improved TG, in terms of quantity of TG products produced and also the duration of TG, retained up to 105 min (Fig. 3.47 D). A good amount of TG products appeared right from the 0^{th} min, with more of DP6 (2.4%) than DP5 (0.8%). At 15 min, the quantities of DP5 and DP6 products generated by ChiD+PKD increased to 6.9 and 8.3%, respectively. But, these relative proportions got reversed by the end of 30 min, with DP5 and DP6 detected in quantities 8 and 6.3%, respectively. This was 2-fold higher compared to *Sp*ChiD, which displayed its maximum TG at 30 min (DP5-3.9% and DP6-2.8%). The fusion PKD+ChiD, showed nearly similar product profile as that of ChiD+CBP or CBP+ChiD, with more of hydrolysis than TG (Fig. 3.47 E). PKD+ChiD showed maximum TG at 15 min with DP5 and DP6 in proportions 2 and 1.7%, respectively.

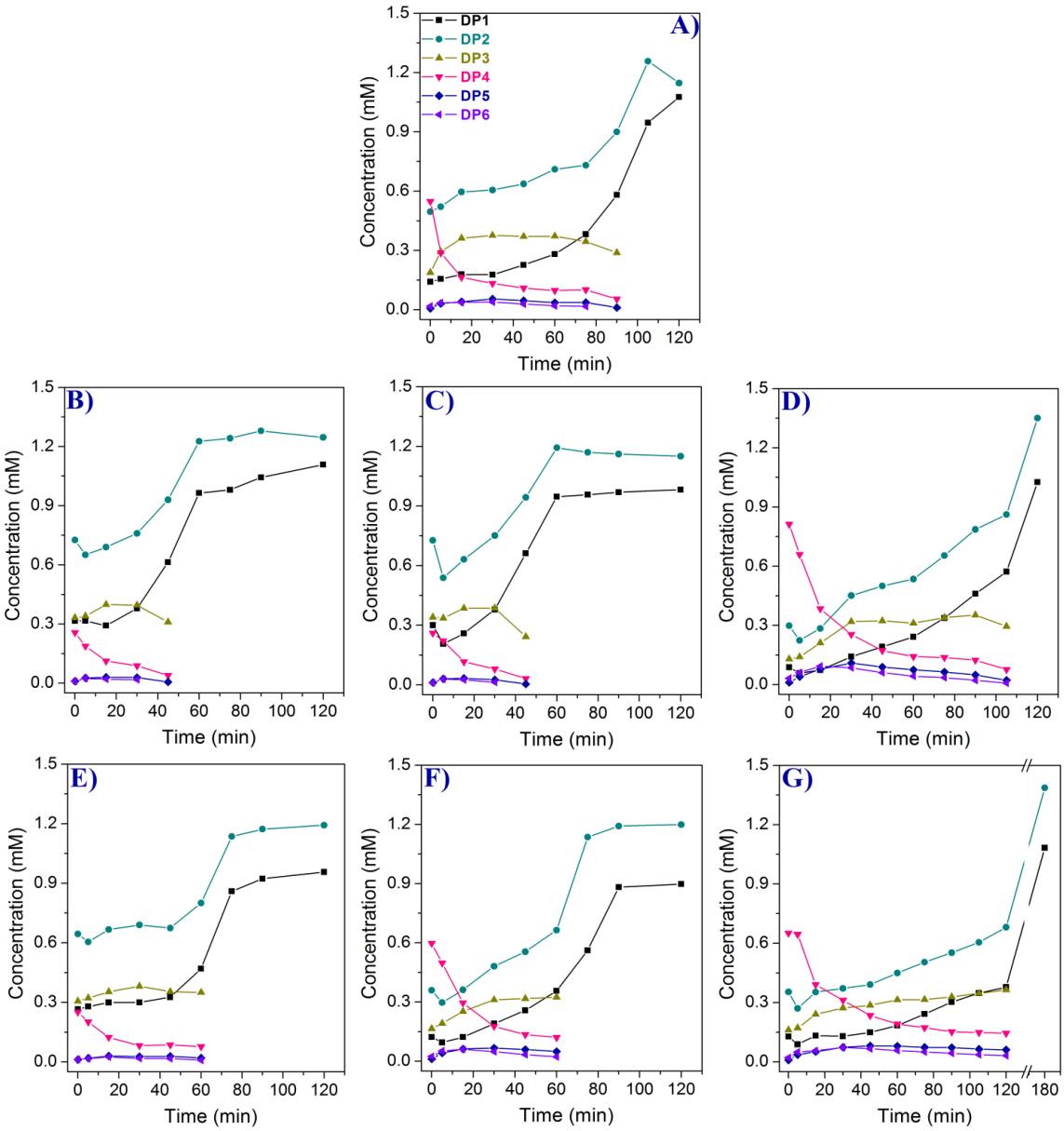

Figure 3.47: **Product profiles of the *Sp*ChiD fusion chimeras.** HPLC quantification profiles obtained for the *Sp*ChiD fusions. Individual quantification graphs represents all the hydrolytic (DP1-DP3) and TG (DP5, DP6) products accumulated during the course of reaction with 1 mM DP4 substrate. All the reactions were performed at 40°C, in 50 mM sodium phosphate buffer, pH 8.0.

Later TG decreased and was detectable up to 60 min only. At the end of 75 min, there were only DP1 (42%) and DP2 (58%) in the fraction analyzed.

3.8.5.3 CDP & PDC

Both CDP and PDC produced higher amounts of TG products compared to *Sp*ChiD. At 15 min CDP produced equal quantities of DP5 and DP6 with proportions 5.4 and 5.2%, respectively. The concentration of DP5 remained unaltered till the end of 30 min, but, a decrease in the quantity of DP6 (3.8%) was observed. TG products were detectable up to 60 min only for CDP with DP5 and DP6 in proportions 3.2 and 1.5%, respectively (Fig. 3.47 F). Similar to CDP, PDC also produced equal quantities of DP5 (4.2%) and DP6 (4.6%) at 15 min and these proportions increased to 6 and 5.8%, respectively by the end of 30 min. There was a decrease in the quantity of TG products from 90 min. The extent of TG activity showed by PDC at 120 min (Fig. 3.47 G) was equivalent to the maximum TG displayed by *Sp*ChiD at 30 min. Thus, the PDC displayed efficient TG than CDP and *Sp*ChiD both in terms of quantity of TG products produced and the extended duration of TG activity.

3.9 Phylogenetic Analysis

To know the relationship of *Sp*ChiD, phylogenetic analysis was performed with 131 bacterial family GH18 sequences. The unrooted phylogenetic tree revealed that except three chitinases (*Ye*Chi1, *Ye*Chi2 and *Ef*Chi), all the single domain GH18 sequences from the family Enterobacteriaceae related to *Sp*ChiD clustered into a separate group (highlighted in yellow) (Fig. 3.48). Thus *Sp*ChiD was falling into a distinctly divergent group. The novel loop identified in *Sp*ChiD, corresponding to the region Asn30-Asp42 was highly conserved throughout the Group-3 chitinases showing their divergence from other groups.

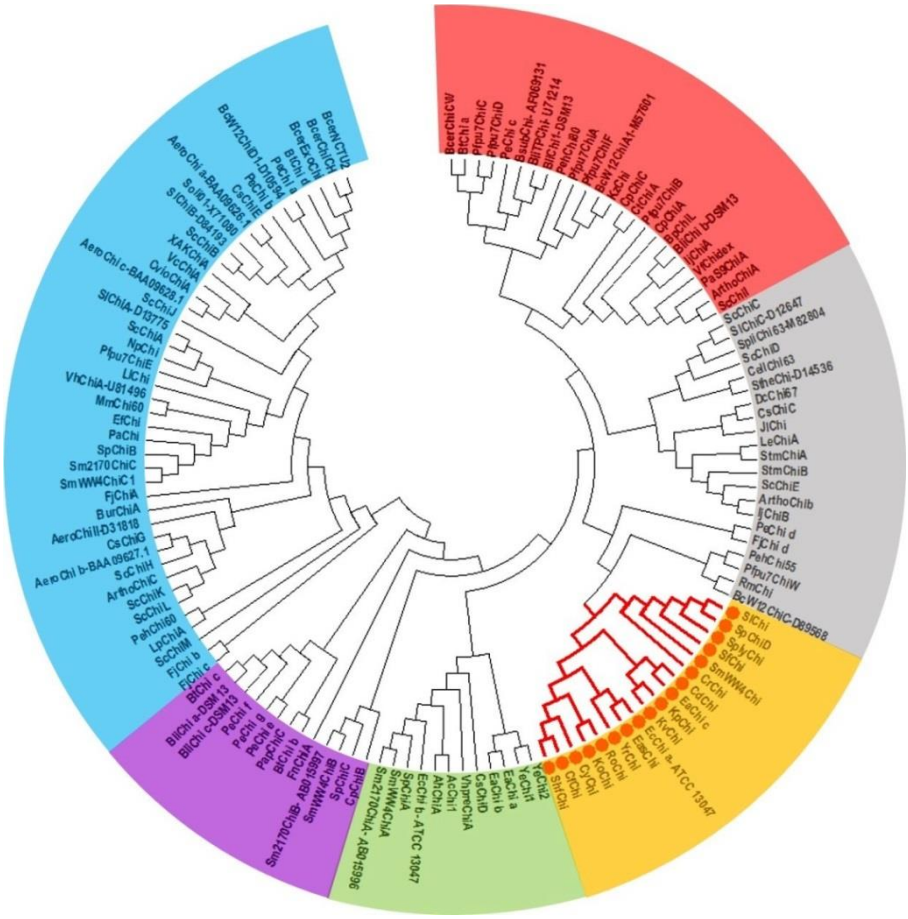

Figure 3.48: **Phylogenetic analysis of *Sp*ChiD.** The unrooted phylogenetic tree was constructed by analyzing 131 amino acid sequences of bacterial family GH18 chitinases. All positions containing gaps and missing data were eliminated. There were a total of 70 positions in the final dataset and the evolutionary analyses were conducted in MEGA6 (Tamura et al., 2013). Region highlighted in yellow represents a group of chitinases very close to *Sp*ChiD.

Discussion


His points are invalid
When will I get to speak
I am right, I know everything
I should change my view he could be right
I am not interested

4.1 SpChiD & its TG Activity

S. proteamaculans 568, a member of family Enterobacteriaceae, was isolated as a root endophyte from *Populus trichocarpa* (Taghavi *et al.*, 2009). The Carbohydrate Active enZYme data base (CAZyhttp:// www.cazy.org/) (Cantarel *et al.*, 2009) showed at least eight genes in the genome sequence of *S. proteamaculans* 568 could be potentially involved in chitin turnover. We have cloned and characterized *Sp*ChiA, *Sp*ChiB, *Sp*ChiC, and *Sp*ChiD from *S. proteamaculans* 568 (Purushotham *et al.*, 2012). *Sp*ChiD had very less sequence identity (<25% and only 23% identity with human chitotriosidase) with other well characterized chitinases, except with chitinase II from *Klebsiella pneumoniae* for which the enzyme characterization was not available. *Sp*ChiD was the first characterized bacterial, family 18 processive endo-chitinase with single catalytic domain. Among the characterized single-domain chitinases, *Sp*ChiD showed significant TG activity with a potential to synthesize CHOS with DP up to 13 (Purushotham & Podile, 2012). *Sp*ChiD, therefore, attained importance as a unique hyper TG chitinase produced by an endophytic bacterium. The enormous potential of *Sp*ChiD to modulate chitin substrates may have implication in the plant-microbe interaction. The chitinase-catalysed TG activity provides a potentially useful tool for synthesis of CHOS and also the neoglycoproteins (Fan *et al.*, 2012).

TG could be improved by reducing the effective concentration of water, performing the TG reactions at high concentrations of substrate and the addition of large excesses of the acceptor molecule (Williams & Withers, 2000). The product association or product release was the rate determining step for chitinase- catalyzed degradation of insoluble chitin or soluble chitosan, respectively. Moreover, deglycosylation step may be the rate determining step in hydrolysis/TG (Zakariassen *et al.*, 2010). Since the TG products are kinetically controlled, monitoring of the reaction is necessary to ensure maximum yields. But, in the present study there was no temporal difference between the hydrolytic and TG activities of *Sp*ChiD. As both hydrolytic and TG activities start simultaneously at 0^{th} min even at very low enzyme and substrate concentrations (Fig. 3.4), mutational approach for improving the TG

activity could be most appropriate. Very few mutational studies were carried to improve the TG activity in terms of extended time of TG reaction and the quantity of TG products produced by a chitinase (Aronson *et al*., 2006; Zakariassen *et al*., 2010; Taira *et al*., 2010). The present study provides deeper insight into the different possibilities of targeting *Sp*ChiD to improve TG activity.

4.2 Targeted Mutagenesis of SpChiD to Improve TG Activity

4.2.1 Residues at the Catalytic Center

Among the five different amino acid substitutions made at the catalytic center, three showed increased TG activity. Met220 and Tyr222, present on the β6 strand of the TIM barrel, with their side chains in proximity to the catalytic triad D*X*D*X*E, have the potential to interact with the sugar molecule during catalysis. The residue Met220 is not directly involved in catalysis, but is an important supporting residue for catalytic activity of *Sp*ChiD. Substitution of Met243 to Glu in family 18 chitinase from *Aspergillus fumigatus,* showed that the mutant M243E lost the TG activity towards *p*-nitrophenyl-(*N*-acetylglucosamine)$_2$ but not with DP4 substrate (Lü *et al*., 2009). Docking studies revealed that M243E forms hydrogen bond with backbone oxygen of −1 sugar instead of a hydrophobic stack between Met243 and +1 subsite sugar moiety. However, in the present study, substitution of Met220 with Ala decreased the hydrophobic interactions needed for usual pace of reaction, which probably gives a chance to oxazolinium intermediate to stay longer at the catalytic center. Moreover, it was evident that a chitin-chitosan hybrid polysaccharide could be synthesized *via* chitinase-catalyzed polymerization of an oxazoline derivative of a GlcN $\beta(1\rightarrow4)$ GlcNAc monomer. Monomer was designed as a transition-state analogue substrate for chitinase catalysis, which belongs to the GH18 (Makino *et al*., 2006). Therefore, we explain that the increased stay of substrate/intermediate resulted in increased TG activity both in terms of quantity of TG products formed, and the duration of TG activity of the mutant M220A. It was proposed that the Tyr214 in *Sm*ChiB is conserved and stabilizes the transition state (Synstad *et al*., 2004). In Y222A, where similar kind of interactions were possible with the phenolic hydroxyl group of Tyr222, also had improved the TG activity. The mutants M220A and Y222A

accommodate smaller side chains on the β6 strands and therefore possess larger cavity revealed the possibility of increasing TG activity possibly by decreasing the rate of reaction. Quantifiable TG products DP5 and DP6 were detected in proportions 12.0% and 5.8% by M220A, 13.6% and 6.8% by Y222A, while it was 6.3% and 4% only by *Sp*ChiD.

Arg278 located on the β7 strand of the TIM barrel, with its side chain protruding towards the active site forms ion pair interactions with Asp221 in its free state. It was observed from the crystal structure of chitinase in complex with sugar (PDB _ID 1D2K, 1E15, and 1EDQ), that Arg278 also forms ion pairs with the substrate at the catalytic center. Based on these two observations, we mutated Arg278 to Ala, and caused perturbations in the ion pair forming ability of *Sp*ChiD with the incoming DP4 substrate. Such subtle changes at the catalytic center resulted in a gradual increase in the proportion of TG products DP5 (6.4%) and DP6 (9.0%) up to 30 min. But, the proportion of DP5 and DP6 products was reversed by the end of 150 min with 9.8% and 6.2%, respectively, and continued till the end of 6 h (8.2% of DP5 and 4.0% of DP6). Shifting towards increased synthesis of DP5 product by Arg278 could be due to the dynamic ion pair interactions with the substrate or within the protein, a possibility that remains to be examined.

The catalytic residue Asp142 in *Sm*ChiB is in the ‘down’ position, interacting with Asp140 in the free state of GH18 chitinase-mediated catalysis. Upon substrate-binding, Asp142 moves to the ‘up’ position and interacts with the substrate and Glu144 (Synstad *et al.*, 2004). Such dynamic changes in all the three catalytic residues play a crucial role during chitin degradation. As the carboxyl group of Glu204 could not be substituted by Asp in chitinase A1 of *Bacillus circulans* W12, it was concluded that the relative disposition of the carboxyl group of Glu204 to substrate was critical for the catalytic activity (Watanabe *et al.*, 1993). In the present study, Glu153 located on the β4 strand of TIM barrel of *Sp*ChiD was mutated to Asp, which resulted in substantial loss of both hydrolytic and TG activities, suggesting that the length of the side chain in Glu153 was not only important for hydrolysis but also for TG activity. Due to a subtle change, with the removal of a single $–CH_2$ group, the

mutant E153D had a significant difference in the activity. The adjacent residue Tyr154 substituted with Ala, reduced the time of TG to 45 min, against 90 min with *Sp*ChiD. The DP4 substrate was utilized rapidly within 60 min as against 120 min with *Sp*ChiD. The results indicated that the phenolic hydroxyl group in the Tyr154 was important for an extended TG activity up to 90 min. The mutant Y154A acquired subtle changes at the catalytic center that favoured hydrolysis but not TG.

4.2.2 Residues at the Catalytic Groove

We have selected five different amino acid residues in the catalytic groove for point mutations. Phe58 was replaced with Trp, Gly113 was replaced with Ser, Ser110 was mutated to Gly, and Phe119 and Trp114 were replaced with Ala. Phe58 was located on the β2 strand of the TIM barrel and its substitution with Trp resulted in increased synthesis of TG products up to 60 min (12.9% of DP5 and 6.6% of DP6), later channelled in the gradual decrease up to 6 h (8.0% of DP5 and 4.2% of DP6). Though the Phe and Trp residues confer aromaticity, the bulky side chain (increased surface area) of Trp facilitates more number of interactions with the incoming substrate. The Trp also might assist in correct positioning and guiding of the sugar molecule into the active site (Zakariassen *et al*., 2010). The increased TG by F58W for 60 min and further gradual decrease may be because the sugar molecules with higher DP will have more of possible interactions with the Trp residue. F58W when coupled with E153D, the double mutant E153D/F58W regained the activity by 3 times in substrate utilization. The hydrolysis decreased to a greater extent for E153D/F58W, but produced DP5 product as efficient as *Sp*ChiD at 30 min (Fig. 3.7 B). In E153D, the relative positioning of the carboxylate group of Glu was perturbed by replacement with Asp. But, the increased aromatic surface area at the catalytic groove, in F58W conversion could overcome the loss of function of E153D to a greater extent, at least, on TG activity.

The residues Gly113 and Trp114 were present on the β3 strand of TIM barrel very close to the catalytic center. Both these residues were thought to maintain the architecture of the catalytic groove, to a major extent maintained by Trp114 with its bulky side chain. As these two residues are directly involved in threading of the chitin

molecules towards the catalytic center, point mutations were planned to identify the key residue for TG in chitin path and also to increase the TG. To achieve this Trp114 was mutated to Ala, and Gly113 was replaced with Ser. Exchange of Trp97 to Ala in *Sm*ChiB significantly increased the rate of hydrolysis (Krokeide *et al*., 2007), and removal of such a residue resulted in the loss of TG activity (Zakariassen *et al*., 2010). W114A had lost the ability of TG after 5 min, and almost completely degraded the DP4 substrate by 30 min. The very low TG activity at the early time points (0-5 min) could be due to the strong inherent TG activity of the *Sp*ChiD, but lost completely when the trafficking of water molecules along with CHOS increased through the groove, because of the lack of guiding aromatic residue at 114th position. This proved that the residue Trp114 was also involved in the direct interactions with the sugar molecules. However, increased TG activity was observed with the mutant G113S. There were pre-existing stacking interactions shown by Trp114 with the substrate which further increased with the adjacent Ser –OH group. Increased interactions at the positions 113 and 114 in turn increased the TG activity of G113S mutant.

For an efficient TG to occur, enzyme should have an active site architecture that disfavours correct positioning of the hydrolytic water molecule and/or favours binding of incoming carbohydrate molecules, through strong interactions in the aglycon subsites (Zakariassen *et al*., 2010). S93 in *Sm*ChiB stabilizes the first D (Asp140) in the D*X*D*X*E motif, when the second D (Asp142) turns away from Asp140 to Glu144 and the oxazoline intermediate (Synstad *et al*., 2004). The second D (Asp142) was shown to be important for catalysis and its mutation D142N yielded an enzyme with high TG activity (Zakariassen *et al*., 2010). The QM/MM calculations show that Asp142 is important in transition state and intermediate stabilization (Jitonnom *et al*., 2011). It was proposed that active site electrostatics may change by this mutation and that this may affect the catalyzing water. In line with these observations, we have mutated Ser110 → Gly. The residue Ser110 is present on the β3 strand of the TIM barrel with its side chain traversing the void between the two Asp residues of the catalytic triad. Mutant S110G resulted in the

decreased hydrolytic ability with concomitant increase in the TG activity. The residue Phe119 was present at the α3 helix of the TIM barrel with its side chain eclipsing the D*X*D*X*E region from the bottom-side of the active site. This was the conserved aromatic residue found in the family 18 chitinases, whose side chain forms π-π, CH-π interactions with Trp152 located between Asp151 and Glu153 of catalytic triad. The mutant F119A has shortage of the aromatic side chain because of which the ascribed interactions could be disturbed. These subtle changes in the interactions resulted in increased TG activity.

4.2.3 Residue at the Solvent Accessible Region

Trp241 is on the turn region next to the *β*6 strand of the TIM barrel. Soluble substrates like CHOS were assumed to enter the substrate binding cleft from various directions, while a chitin chain from crystalline chitin enters the binding site only from the edge of the cleft (Watanabe *et al*., 2003). There was no significant effect on hydrolysis of DP5 substrate with the mutants Y56A and W53A, but the hydrolysing activity against *β*-chitin microfibrils decreased in chitinase A1 from *B. circulans*. But, in the present study decreased rate of hydrolysis followed by increased TG activity was observed for the mutant W241A. This aromatic residue with the bulky side chain could stack against the pyranoside rings and its replacement to Ala altered the inherent activity of the *Sp*ChiD. This clearly indicates that the residue Trp241 has an important role in the activity of *Sp*ChiD towards soluble CHOS substrates like DP4. There is no correlation between the k_{cat} for hydrolysis and apparent TG activity. It is the other factors such as positioning and activation of the catalytic water and optimal aligning of the acceptor are likely to play a role (Zakariassen *et al*., 2010).

4.2.4 Partial Blocking of Product Exit Improved the TG Activity of SpChiD

To understand the biochemical properties of carbohydrate active enzymes, more detailed investigations are needed on the protein-carbohydrate interactions. A majority of these interactions are accomplished by the aromatic amino acids like tryptophan, tyrosine, and phenylalanine, wherein aromatic rings can stack against planar faces of carbohydrate rings *via* carbohydrate-π interactions (Payne *et al*., 2011). GHs are ubiquitous in nature and typically exhibit tunnels, clefts, or pockets

lined with aromatic residues for processing carbohydrates. Removal of aromatic residues at the entrance and exit of the *Trichoderma reesei* family 6 cellulase (Cel6A) tunnel dramatically impacted the binding affinity, suggesting that these residues play a role in chain acquisition and product stabilization, respectively (Payne *et al*., 2011). On the basis of structural characteristics (Perrakis *et al*., 1994; van Aalten *et al*., 2000) and enzymological work (Suzuki *et al*., 2002) it was suggested that *Sm*ChiA and *Sm*ChiB are exo-chitinases, which degrade chitin chains from opposite ends (Horn *et al*., 2006). In an alternative approach, the end specificity of *Sm*ChiA and *Sm*ChiB was experimentally demonstrated. Hult *et al*. (2005) used a combined analysis of tilt micro-diffraction method to determine the crystallographic axes and the BXH-SG (biotinamidocaproyl hydrazide–streptavidin–gold) labeling method specific to the reducing ends of the enzymatically degraded *β*-chitin microcrystals.

Interactions displayed by the aromatic amino acid side-chains with the planar faces of carbohydrates are typical signature motifs (Ling *et al*., 2009). In agreement with this, we mutated two glycine residues to corresponding tryptophans, on either side of the *Sp*ChiD tunnel. In the native *Sp*ChiD, glycine and tryptophan are present at positions '113' and '114', respectively. The residue region 113-114 was considered as the probable substrate entry point. Detailed analysis of the *β*-*α*3 loop in *Sm*ChiC, (residues 102-114) revealed the presence of a conserved sequence motif S*X*GG (from residues 102-105) in GH18 chitinases. This conserved motif is usually followed by a Trp in processive chitinases (in *Sm*ChiA and *Sm*ChiB: S*I*GGW), which is vital for processivity and the ability to efficiently degrade insoluble chitin (Zakariassen *et al*., 2009). In *Sp*ChiD, the S*X*GG motif corresponds to 110-113 region and the Gly113 targeted is from the motif itself, followed by Trp at 114th position which is a characteristic feature of processive chitinases. The residues Gly113 and Trp114 were present on the *β*3 strand of TIM barrel closer to the catalytic center. Both these residues were thought to maintain the architecture of the catalytic groove and to a major extent maintained by Trp114 with its bulky side chain. Mutation of Trp114 to Ala in *Sp*ChiD resulted in a substantial loss of TG activity and increased hydrolysis, whereas, change of Gly113 to Ser resulted in increased TG activity. The pre-existing

stacking interactions of Trp114 with the substrate, which further increased with the adjacent Ser-OH group, might contribute to increased TG activity (Madhuprakash *et al*., 2012).

Mutation of Gly113 to Trp, resulted in the loss of both hydrolytic and TG activities to a greater extent (Madhuprakash *et al*., 2014). The involvement of Trp113 in binding to the DP4 substrate was assessed through MD simulations and SIE studies. The very high and increased vdW and coulomb interaction energies (Table 3.3) indicate not only the side chain of Trp113 experienced closer interactions with the DP4 substrate but also retained the interactions with Trp114. From the trajectory of MD simulations, we also observed that the side chains of these two residues are blocking the tunnel entrance to a major extent. The RMSD of DP4 substrate was stabilized at 0.22 nm in the active site and showed better interactions with the Trp113 residue (Fig. 3.14), in turn, restricting the movement of the substrate within the active site.

The average number of hydrogen bonds also increased in comparison to the *Sp*ChiD-DP4 complex during MD simulations for mutant G113W. The loss of hydrolytic and TG activities to a greater extent may be due to the major hindrance caused by abutting bulky side chains of Trp (positions 113 and 114) at the tunnel entrance and allowed only a few substrate molecules to reach the active site. The soluble substrates like CHOS could enter the substrate binding cleft from various directions, possibly contributed to the feeble activity displayed by the mutant G113W. Commencement of TG activity at 20 min and its very little increase up to 6 h in terms of quantifiable TG products was plotted and compared against *Sp*ChiD and three other single mutants (Fig. 4.1). The concentration of quantifiable TG products, DP5 and DP6 remained similar till the end of 6 h. The major loss of both hydrolytic and TG activities for the mutant G113W supports the assumption that Gly113 is part of substrate entry site for *Sp*ChiD.

When the residue Gly113 was mutated to Ser instead of Trp, the mutant G113S displayed increased TG and decreased hydrolysis (Madhuprakash *et al*., 2012). The side chain of Ser113 had consistent electrostatic interactions with the

catalytic residues of D*X*D*X*E motif throughout the 50 ns MD simulations. SIE calculations revealed that Ser113 had very less vdW and coulomb energy contributions in comparison to *Sp*ChiD-DP4 complex, suggesting decreased interactions with DP4 substrate. The weak interactions of DP4 substrate with Ser113 and a minor increase in vdW and coulombic energies of the Gly195 suggested a favoured movement of DP4 substrate towards the tunnel exit. The void left unfilled at the tunnel entrance of mutant G113S was greater when compared to the mutant G113W, which will allow the substrate DP4 to enter the active site and expression of hydrolytic and TG activities. DP4 exhibited a decrease in the average number of hydrogen bonds with the mutant G113S when compared to G113W. The stable RMSD (~0.25 nm) of DP4 along the active site of G113S indicated a free movement of DP4 that helps in hydrolysis and TG activities. The mutant G113S also produced nearly similar quantities of TG products DP5 and DP6 up to 6 h (Fig. 4.1). But, the concentration of TG products produced in the early phase of reaction was less compared to *Sp*ChiD. DP5 concentration was low up to 60 min, whereas, DP6 concentration was low up to 30 min when compared to *Sp*ChiD. The concentration of TG products was increased slowly up to 120 min and a considerable hike was observed at 150 min.

The residue Trp114, adjacent to Gly113, is an important aromatic residue which maintains the architecture of the catalytic groove and also controls the threading of chitin molecules towards the catalytic center (Madhuprakash *et al*., 2012). The decreased vdW and coulomb energy for the Ala114 residue indicates that the Ala side chain showed decreased interactions with DP4. The less favorable interactions observed for the Ala114 and Gly113 with DP4 and minor increase in interactions for Gly195 suggest that the movement of DP4 is towards the tunnel exit. Tunnel entrance of the mutant W114A showed a lot of empty space available because of which the substrate molecules can enter freely and reach the active site. The trafficking of water molecules also increased through the entrance and this could be the main reason for increased hydrolysis with the concomitant loss of TG activity. The architecture of the tunnel exit remained undisturbed. The DP4 substrate RMSD

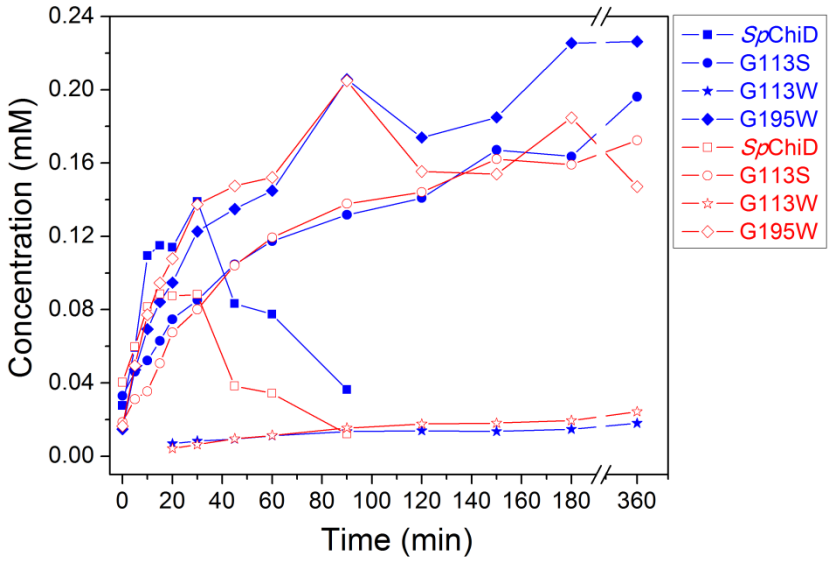

Figure 4.1: **Comparison of quantifiable TG products produced by Gly variants of *Sp*ChiD.** Profiles were generated by *Sp*ChiD or its variants with 2 mM DP4 substrate in 20 mM sodium acetate buffer pH-5.6 at 40°C. Quantifiable TG products *i.e.* DP5 represented in blue-filled symbols and DP6 with red-open symbols. Product quantification was done by a linear correlation between peak area and concentration of oligosaccharides in standard samples.

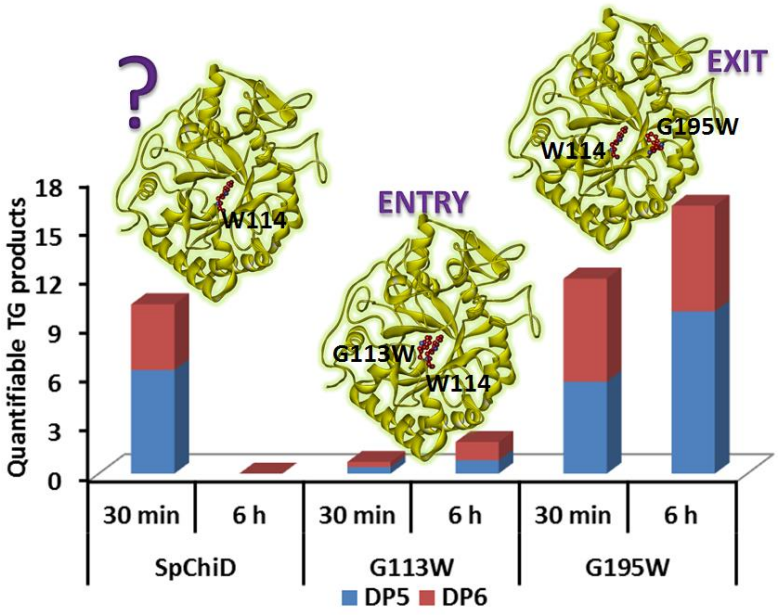

Figure 4.2: **Schematic representation showing the partial blocking of product exit in *Sp*ChiD improved the TG activity.**

(~0.12 nm) in the groove of the W114A mutant indicates that the stability of substrate is high compared to the overall protein RMSD (~0.4 nm). The relative average number of hydrogen bonds is similar for the DP4 as that of *Sp*ChiD.

The residue Gly195 corresponds to the +2 subsite of *Sp*ChiD and its mutation to Trp resulted in increased TG. The mutant residue Trp195 was observed in the region of tunnel exit and its side chain is partially closing the exit. Trp195 experienced increased vdW and coulomb interactions with DP4 and decreased interactions with the residues Gly113 and Trp114. The RMSD (~0.22 nm) of DP4 in the active site converged throughout the MD simulations and the increased average number of hydrogen bonds for G195W shows the affinity for the substrate. The increased TG could be, either due to the high affinity of substrate to the bulky side chain of Trp195, or may be the introduction of a hydrophobic patch (*i.e.* preventing the entry of a water molecule that would favor hydrolysis). This may further be translated into increased retention time of either the intermediate oxazoline or the substrate DP4 at the active site and favoring TG. The mutant G195W produced more of TG products from the early time of reaction with a sudden hike in the concentration of DP5 and DP6 at 90 min (Fig. 4.1). The TG products were more up to 6 h by G195W, when compared to *Sp*ChiD and the three single mutants (G113S, G113W and W114A). The mutant G195W thus displayed increased TG among all the three Gly variants reported in the present study. Increase of TG activity by partial blocking of the tunnel exit, for family 18 GHs like *Sp*ChiD is hitherto not reported. An overview of this approach and the mutational effects were shown in a graphic abstract (Fig. 4.2).

4.3 Structural Characteristics of SpChiD

*Sp*ChiD is a TIM barrel containing single domain protein which folds region-wise into two molecular halves, where the lower molecular half (residues, Ala15 - Met200) is designated as N - region and the upper half (residues, Tyr221 - Glu420) is termed as C - region. In comparison, *Sm*ChiA contains two domains, N - terminal domain (residues, Ala24 - Asp132) and the main $(\beta/\alpha)_8$ TIM barrel catalytic domain (residues, Thr133 - Gly561) whereas *Sm*ChiB also contains two domains having main catalytic

TIM barrel domain (residues, Thr3 - Gly442) and a C -terminal domain (residues, Val443 - Val498). The extra domains in both *Sm*ChiA and *Sm*ChiB with several aromatic residues provide additional binding support to polymeric substrates. In contrast, due to the absence of extra domain *Sp*ChiD, it binds weakly to the insoluble polymeric substrates. In the structure of *Sp*ChiD, sulfone methionine, SMet89 was observed at the site on the surface of protein which corresponds to the site in *Sm*ChiB structure where an extra domain was attached (van Aalten *et al*., 2000).

The deep substrate binding cleft in *Sp*ChiD is essentially formed at the interface of two molecular halves (Fig. 3.20 A). However, it is partially filled by its own loop, Asn30 - Asp42 allowing a relatively smaller space for the binding of chitin oligomers unlike well-organized grooves in other chitinases. At the entrance of the cleft in *Sp*ChiD, the residues Trp160 and Trp290 are situated on the opposite sides. However, in case of *Sm*ChiA and *Sm*ChiB, the corresponding residues are Ile207 and Phe396, and Leu103 and Asp316, respectively (Fig. 3.22). The approximate nearest distance between the pairs of above residues at the entrance of the clefts were found to be 9.4 Å in *Sp*ChiD, 17.0 Å in *Sm*ChiA and 10.1 Å in *Sm*ChiB. The estimated length of the cleft in *Sp*ChiD was 11.0 Å while the corresponding distances in *Sm*ChiA and *Sm*ChiB were 21.0 Å and 23.1 Å, respectively. The differences in the length and width of the cleft due to the presence or absence of extra domains could be responsible for the preferences in sizes of substrates as well as in the nature of products.

4.3.1 Catalytic Mechanism of SpChiD

The active site in *Sp*ChiD contains three acidic residues, Asp149, Asp151 and Glu153 as part of the D*X*D*X*E signature of GHs. In *Sp*ChiD structure, an acetate molecule is also observed at the active site in the proximity of Asp151. It is noteworthy that the side chains of Ser110 and the middle acidic residue, Asp151 adopt two conformations in the present structure (Fig. 4.3). The critical factor that seems to induce double conformation in Asp151 is the environment of Ser110 as the side chain of Ser110 is flanked by two aromatic residues Tyr28 and Phe58 on its two sides forming similar van der Waals contacts (Fig. 4.3). The conformation of Ser110 with its side chain

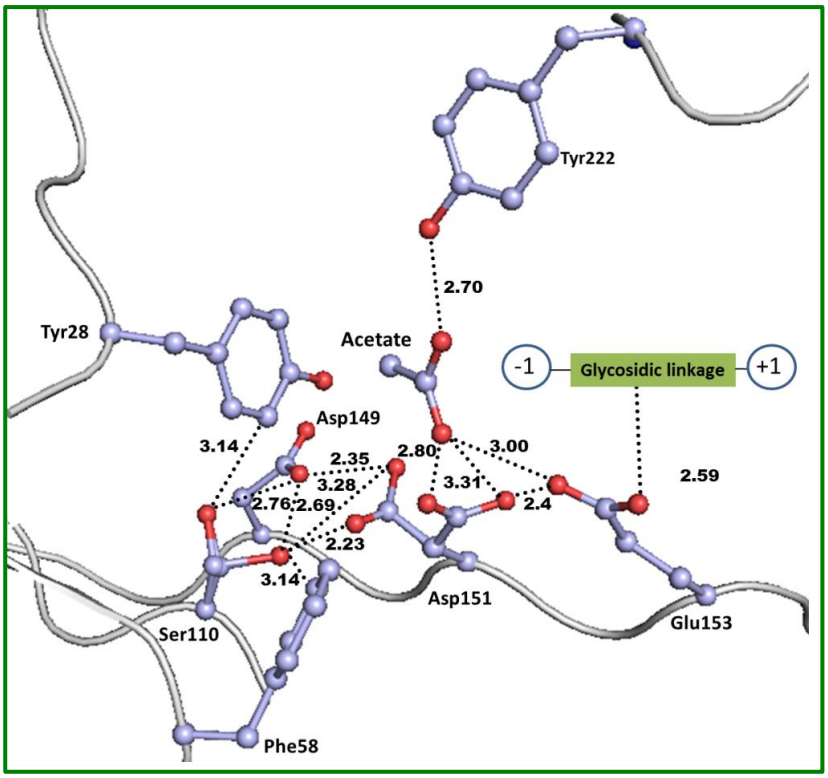

Figure 4.3: **Catalytic mechanism of *Sp*ChiD.** The side chains of Ser110 and the middle acidic residue, Asp151 adopt two conformations. But, the critical factor that seems to induce dual conformation in Asp151 is the environment of Ser110, as the side chain of Ser110 is flanked by two aromatic residues Tyr28 and Phe58 on its two sides forming similar van der Waals contacts. It is noteworthy, that the acetate molecule helps in orienting Glu153 to the correct orientation and occupies the position of chitin residue at (i+2) position.

towards Asp149 corresponds to resting state while the other conformation when its side chain is turned towards Asp151 is considered as the intermediate state. The conformation the side chain of Ser110 in the resting state corresponds to the side chain torsion angle, χ^1 = –84°, when the side chain of Ser110 forms van der Waals contacts with the side chain of Tyr28. The conformation in the intermediate state corresponds to side chain torsion angle, χ^1 = 180° where the side chain of Ser110 forms van der Waals contacts with Phe58 (Fig. 4.3). This indicates that the side chain of Ser110 can flip flop easily into opposite directions.

It may also be noted that Ser110 O^{γ} forms H-bonds with Asp149 at both positions, resting state, (Ser110 $O^{\gamma}H$ - - - $O^{\delta 2}$ Asp149 = 2.76 Å) and intermediate state, (Ser110 $O^{\gamma}H$ - - -$O^{\delta 2}$ Asp149 = 2.69 Å). However, when Ser110 is in the intermediate state, its O^{γ} atom causes in severe steric constraints with the side chain of Asp151 in the resting state (resting state, χ^1 = –65°) at a distance of Ser110 O^{γ} - - - $O^{\delta 2}$ Asp151 = 2.23 Å. As a result, the side chain of Asp151 flips to the position corresponding to the intermediate state (χ^1 = –180°) where the distance between Ser110 O^{γ} and $O^{\delta 2}$ of Asp151 is 4.11 Å. In the new position, the side chain of Asp151 forms two bifurcated hydrogen bonds with the acetate OH group at distances 2.80 Å and 3.31 Å (Figure 10). The $O^{\delta 1}$ atom of the side chain of Asp151 forms a strong hydrogen bond (2.40 Å) with Glu153 $O^{€2}$. The Glu153 $O^{€2}$ is also hydrogen bonded to acetate OH at a distance of 3.00 Å. As a result of these interactions, the $O^{€1}$ atom of Glu153 is appropriately placed to interact with the glycosidic bond between chitin residues at subsites +1 and –1. In this scheme, Ser110 protonates Asp151, which in turn protonates Glu153. The acetate molecule helps Glu153 to attain the correct orientation (Madhuprakash *et al*., 2013).

The presence of residues Trp160 and Trp290 in the substrate binding cleft, at +2 position makes *Sp*ChiD as a favourable molecule for the TG activity. Mutation of Phe396 to Trp in *Sm*ChiA increased the TG activity (Zakariassen *et al*., 2011) with increased binding effects. Another important factor was concerned with the position of Glu153, to avoid hydrolytic effect. It was shown that mutation of Ser110 which is

responsible for the cascade effect on attaining the correct orientation of Glu153 reduced hydrolytic activity and increased the TG activity of *Sp*ChiD (Madhuprakash *et al*., 2012). A similar effect can also be achieved by mutating Asp151. The structure determination has provided a deeper insight into the hydrolytic and TG activities of *Sp*ChiD. The novel structural features like the presence of a well stabilized Asn30 - Asp42 loop, sulfonation of Met89 and interactions of other residues with the loop region, provide an ideal platform for the activities of *Sp*ChiD.

4.4 Role of Loop Asn30 - Asp42

Complete chitin hydrolysis proceeds *via* a three-enzyme system: a chitinase first hydrolyzes chitin to DP2 and then a chitobiase hydrolyzes DP2 to DP1 which is further converted to GlcN by a deacetylase. The exo-acting enzymes of family GH18 usually release chitobiose (DP2) from either the reducing end, such as *Sm*ChiA, or the non-reducing end, such as *Sm*ChiB and ChiB of *Aspergillus fumigatus* (Horn *et al*., 2006; Jaques *et al*., 2003). The exclusive release of monomers (DP1) is a property usually found in the GH20 family, but there the reaction starts at the non-reducing end. The fungal family 18 exochitinase CfcI from *Aspergillus niger* released monomers with CHOS $(GlcNAc)_{(3–6)}$, as well as $(GlcNAc)_2$–pNP and $(GlcNAc)_3$–pNP. The shorter CHOS *i.e.* GlcNAc-*β*–pNP, GlcNAc-*α*–pNP and $(GlcNAc)_2$ were not hydrolyzed by CfcI (van Munster *et al*., 2012). *Sp*ChiD is the only bacterial family GH18 chitinase reported to degrade chitobiose (Purushotham & Podile, 2012). Thus, *Sp*ChiD being a GH18 chitinase had the ability to display chitobiase activity similar to that of GH20 enzymes. Crystal structure of *Sp*ChiD revealed that the residues Val35 and Thr36 from the loop (Asn30 - Asp42) may interact with the incoming substrate. Among all the Val and Thr variants analyzed, the mutant T36F displayed high affinity of binding (K_m values of *Sp*ChiD and T36F were 35.12 and 14.75 mg/mL, respectively) and overall catalytic efficiency compared to native *Sp*ChiD (K_{cat}/K_m values of *Sp*ChiD and T36F were 29.33 and 63.5 sec^{-1} mg^{-1} mL, respectively) on colloidal chitin. These results proved that Thr36 from the loop was making good interactions with the incoming substrate. The increased substrate affinity and the catalytic efficiency of T36F might be due to the improved

interactions by the aromatic residue Phe36 with the polymeric substrate. The other loop variants (V35G/F and T36G), though displayed little of increased affinities towards colloidal chitin, showed no change in the overall catalytic efficiency. The loop deletion mutant, *Sp*ChiDΔ30-42 and Tyr28 displayed no detectable activity on colloidal chitin, suggesting their crucial role in assisting catalysis.

Activities of these loop variants and the mutant Y28A with DP4 substrate revealed important observations. Though the Val and Thr variants displayed subtle differences in the activities with DP4 substrate, a clear effect on monomer production was observed. The monomer producing ability was much reduced for the mutants V35G, T36G and T36F which resulted in the accumulation of DP2 (Fig. 3.26). This lead to the accumulation of more of DP6 than DP5 by all the three mutants V35G, T36G and T36F (Fig. 4.4). This was further supported by the DP2 degradation studies where all the three mutants displayed decreased hydrolytic activity. These observations concluded that the residues Val35 and Thr36 are crucial for chitobiase activity. More importantly the polar nature of Thr36 could be required for making better interactions with DP2, rather than the aromaticity conferred by the mutant Phe36, to display chitobiase activity. The mutant V35F showed equal rates of DP2 degradation as *Sp*ChiD (Fig. 3.26) and displayed a marginal increase in the quantifiable TG products DP5 and DP6 (Fig. 4.4). Thus, the decreased chitobiase activity translated into the increased TG activity with the selective accumulation of more of even chain CHOS (at least the quantifiable TG product DP6). Though the loop occupies half of the space in the substrate binding cleft, it should be flexible for the enzyme to display activities on polymeric substrates. Crystal structure of *Sp*ChiD revealed that the loop was poorly connected with the rest of the protein (Madhuprakash *et al*., 2013). The native *Sp*ChiD can degrade different polymeric chitin substrates, which strongly supports the assumption of loop flexibility (Purushotham & Podile, 2012). Thus the flexible loop in *Sp*ChiD might be involved in threading the polymeric chitin chain into the substrate binding cleft. Therefore, the deletion mutant, *Sp*ChiDΔ30-42 lost not only the hydrolytic activity on polymeric chitin substrates but also the chitobiase activity.

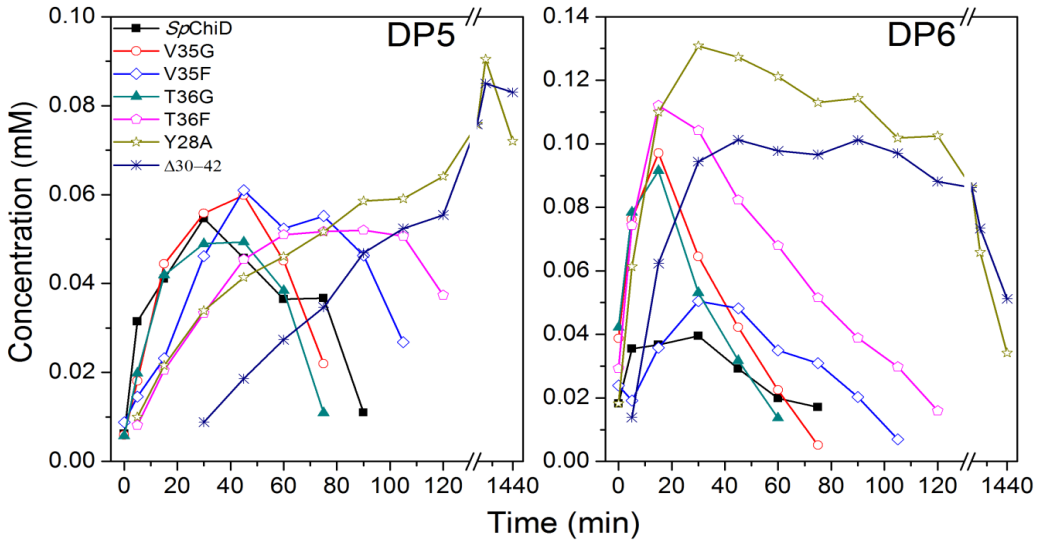

Figure 4.4: **Comparison of quantifiable TG products produced by loop variants of *Sp*ChiD.** Profiles were generated by *Sp*ChiD or its variants with 1 mM DP4 substrate in 20 mM sodium acetate buffer pH-5.6 at 40°C. Product quantification was done by a linear correlation between peak area and concentration of oligosaccharides in standard samples.

Structural studies of the exochitinase *Sm*ChiB revealed that the residues in the core of the catalytic TIM barrel, Tyr10, Ser93 and Asp140 (Tyr28, Ser110 and Asp149 are the corresponding residues in *Sp*ChiD) were conserved in most of the family 18 chitinases, because they participate in a system for dispersion of charge and displacement of protons during catalysis (van Aalten *et al*., 2001). The proposed roles of the residues Tyr10 and Ser93 of *Sm*ChiB in stabilizing the charge on Asp140 during catalysis were proved by mutational analysis. Both the mutants Y10F and S93A showed decreased the activity with 4- methylumbelliferyl-$(GlcNAc)_2$. In line with these observations, mutants of *Sp*ChiD (S110G and Y28A) also displayed decreased specific activity with the DP4 substrate and increased TG activity. The enhancement in the TG activity for Y28A was much higher compared to the mutant S110G and persisted up to 24 h. The mutation Y28A also resulted in the complete loss of chitobiase activity and in turn an increased quantity of even chain length quantifiable TG product *i.e.* DP6. A very slow decrease in the concentration of DP4 substrate by the mutant Y28A indicated the potential effect of mutation on the rate of catalysis. Perturbations in the charge stabilizing role played by the residue Tyr28 might have resulted in the increased retention time of intermediate oxazoline or the substrate and thus increasing the TG activity.

4.5 Thermal Unfolding using CD & DSC for SpChiD or the Mutant E153A

Though it was reported that the *Sp*ChiD was optimally active at 40°C (Purushotham & Podile, 2012) there was no structural evidence so far supporting the biochemical analysis. Temperature dependent CD spectroscopic studies revealed that the enzyme *Sp*ChiD was stable up to 40°C, without any perturbations in the secondary and tertiary structure. With an increase of temperature by 5°C the protein started unfolding and the structure got completely collapsed when the temperature reached 50°C. The effect of temperature on structural integrity and in turn the functional property of *Sp*ChiD was further analyzed by pre-incubating the enzyme for 20 min at the respective temperatures followed by monitoring the changes in activity using HPLC (Fig. 3.29). This data strongly supported the observations from temperature-dependent CD analysis.

Thermal stability of *Sp*ChiD was further investigated using high sensitivity DSC measurements. DSC based thermal stability studies for bacterial GH18 chitinases were very limited. The DSC thermal unfolding studies for chitinases *Ar*ChiA, *Ar*ChiB from *Arthrobacter* sp. strain TAD20 and *Mm*Chi60 from *Moritella marina* showed single peaks with apparent T_ms of 54.3, 54, and 56.4°C, respectively. The apparent T_m values of these psychrophilic chitinases were lower than the T_m of *Sm*ChiA (64.2°C) from mesophilic *S. marcescens* (Lonhienne *et al*., 2001a; Stefanidi & Vorgias, 2008). In contrast to these observations, *Sp*ChiD being produced by the mesophilic bacterium *S. proteamaculans* showed two distinct transitions centred at 44.8 and 47.3°C, respectively, at pH 8.0. But, the DSC scans for *Sp*ChiD as a function of pH revealed that the protein was thermally stable at pH 6.0 and showed regular two distinct transitions centred at 50.1 and 52.7°C, respectively. This is the first report, that a single domain GH18 TG chitinase showing two distinct transitions using DSC. This kind of two state transition was reported for a family GH20 chitobiase, from *Arthrobacter* sp. strain TAD20 (*Ar*Chb), but, transition 1 was assigned to catalytic domain and transition 2 to the galactose-binding domain (Lonhienne *et al*., 2001b). Despite the multi-modular architecture of *Ar*ChiA, *Ar*ChiB, *Mm*Chi60 and *Sm*ChiA, they displayed a single transition in DSC thermograms, whereas, *Sp*ChiD was unique with its two different transitions confined to the single catalytic domain. This indicates that the complete unfolding of *Sp*ChiD involves an intermediate state. Thus, it appears that the transition 1 corresponds to the intermediate state and transition 2 to the final unfolded state of *Sp*ChiD.

Ligand-induced thermal stability of *Sp*ChiD was also investigated by performing DSC with the catalytically inactive mutant E153A. The mutant E153A alone had a T_m value of 45.3°C and 48.1°C, for transitions 1 and 2, respectively. There was a considerable increment in the T_m of both the transitions in presence of ligands DP2-DP6. But, the difference of increased T_m values upon each ligand binding to the E153A protein alone (*i.e.* [T_m of E153A + $(DP)_n$] – T_m of E153A alone), revealed that the transition 2 was much stabilized than transition 1 with lower chain CHOS of DP2-DP4. Inspite of a high degree of stabilization upon DP5

(T_{m1}+10.5°C and T_{m2}+11.2°C) or DP6 (T_{m1}+12.8°C and T_{m2}+12.4°C) binding, no considerable difference was observed between the two transitions, after subtracting the respective T_m values of E153A alone. Increased thermal stability of *Sp*ChiD in the presence of ligand DP4 was further confirmed through HPLC analysis (Fig. 3.29).

It is well known, that increased flexibility is the most important factor to show good catalytic efficiency for the enzymes acting at low temperatures. Several structural factors govern the low thermal stability, which is related to increased flexibility. 'Arg' residues are important stabilizing elements in proteins, where they can form multiple hydrogen bonds with backbone carbonyl and side chain oxygens (Mrabet *et al*., 1992). On the other hand, 'Pro' residues are thought to modulate the entropy of protein unfolding by affecting backbone flexibility (Matthews *et al*., 1987). Most importantly the lack of side chain in 'Gly' residue, allows chain rotations and dihedral angles not available to other residues (Van den Burg *et al*., 1998). Thus the content of Arg, Pro and Gly is very crucial for modulating molecular flexibility, catalytic efficiency and in turn the thermal stability. A comparison between *Mm*Chi60 (optimum temperature 28°C) and *P. aeruginosa* ChiC (*Pa*ChiC) (optimum temperature 50°C) revealed that *Mm*Chi60 had lower Gly (8.5%) and nearly the same Pro (4%) content compared to *Pa*ChiC, where it was 9.9 and 4.6%, respectively. Thus, it could be the Arg content seems to contribute to the flexibility of the *Mm*Chi60 overall protein, which was 2.5% compared to 6.0% in *Pa*ChiC. In agreement with these observations, *Sp*ChiD also showed a lower Arg content (3.4%) and nearly similar Pro (4.9%) and Gly (8.8%) contents as that of *Mm*Chi60 and *Pa*ChiC. Another important feature was a high Ala content (11.3%) which may not be excluded, because, the substitution of Ala82 with Pro in bacteriophage T4 lysozyme increased the thermal stability (Matthews *et al*., 1987). On the whole it could be the very high Gly and Ala contents and low Arg content playing crucial role in the increased flexibility of *Sp*ChiD related to the increased heat lability, allowing conformational changes necessary to display an exceptional hyper TG activity.

4.6 Free Energy Changes during the Binding of CHOS to E153A

The binding of CHOS with DP-2, 3, 5 and 6 to E153A was investigated by ITC. We report for the first time the binding of DP2 to a family GH18 TG chitinase like *Sp*ChiD with a K_d value of 0.24 μM. Until now three chitinases, two belonging to family GH18 (*Sm*ChiB and an insect chitinase *Of*ChtI) and one belonging to family GH19 chitinase from moss species, *Bryum coronatum* (*Bc*ChiA) were studied in great detail for their binding properties using ITC (Norberg *et al*., 2010; Chen *et al*., 2014b & Ohnuma *et al*., 2011b). Among these three chitinases, *Sm*ChiB displayed higher binding affinities towards DP4-DP6. The K_d value of 0.24 μM for DP2 binding by E153A was nearly 3 times lower than the DP5 binding to *Sm*ChiB (K_d = 0.67 μM). Since, lower the K_d value higher the binding affinity, which, indicates the binding affinity for DP2 by *Sp*ChiD was nearly 3 times higher than DP5 binding to *Sm*ChiB. However, the binding affinity of E153A for DP3 was 1,515 fold higher when compared to *Sm*ChiB. There was no much difference observed in the K_d value of DP3 binding to E153A (0.22 μM), when the DP increased by a single GlcNAc residue. The obtained binding affinities of DP5 and DP6 to the mutant E153A were 52 and 26 times higher, respectively, than observed for *Sm*ChiB. These are the very high binding affinities compared to any other GH18 or GH19 chitinase reported so far. Increased binding affinity with an increase in the chain length of CHOS was observed for the mutant E153A. A similar trend was observed for the T_m values obtained upon DP2-DP6 binding to E153A using DSC. These high binding affinities for CHOS with DP-2, 3, 5 and 6 might be crucial for the enzyme *Sp*ChiD to display an unprecedented hyper TG.

The free-energies for binding DP2 and DP3 were similar with 6.04 and 6.1 kcal mol^{-1}, respectively and that of DP5 and DP6 were also same with 8 and 8.53 kcal mol^{-1}, respectively. An average free-energy gain of approximately -1.0 and -0.9 kcal mol^{-1} per GlcNAc residue was observed for *Of*ChtI and *Sm*ChiB, respectively (Chen *et al*., 2014b), whereas, such a gradual increase in the free-energy per GlcNAc residue was not observed in case of *Sp*ChiD. Binding of lower chain CHOS *i.e.* DP2 and DP3 resulted in exothermic heat changes, in contrast, longer chain CHOS *i.e.*

DP5 and DP6 was accompanied by strong endothermic heat changes. Electrostatic interactions form exothermically and are therefore stabilized at low temperatures in contrast, hydrophobic interactions form endothermically and are weakened by a decrease in temperature (Lonhienne *et al*., 2001b). In agreement with these observations, it can be explained that the ITC titrations for DP2 and DP3 worked well at lower temperature *i.e.* 13°C and driven by exothermic heat changes. Whereas, for DP5 and DP6 titrations worked at 25°C with a concomitant endothermic heat change. It could be the binding of smaller ligands is mediated by more of electrostatic interactions, but, the longer ligands are more flexible and can mediate more of hydrophobic stacking interactions with the aromatic residues in the binding pocket. All the reactions were entropically driven with small enthalpic penalties, the important factor for this could be the topology and the structure of binding site in *Sp*ChiD, designed for modulating both hydrolytic and TG activities.

4.7 'Trp' Fluorescence Quenching Studies

The results from ITC and DSC strongly suggested that, the longer the chain length of ligand, stronger the ligand binding to the enzyme *Sp*ChiD and thermal stability. In agreement with these observations, we examined the role of Trp residues in ligand (DP2-DP6) binding to E153A by fluorescence quenching experiments using the neutral quencher acrylamide. The accessibility of Trp residues in the binding site of the mutant E153A decreased with increased chain length of CHOS. The percentage decrease of quenching upon DP6 binding was much higher compared to CHOS with DP2-DP5. The same pattern was reflected with the K_{SV} values, which were decreased with the increased chain length of CHOS, suggesting the reduced accessibility of Trp residues in the protein to the quencher. This strongly supports that the longer chain CHOS can efficiently mediate hydrophobic stacking interactions with the Trp residues at the binding pocket. Thus, it can be concluded that the high binding affinities are mainly due to the Trp residues at the substrate binding cleft, which may influence the TG activity of *Sp*ChiD.

4.8 Probing the Role of Trp Residues at the Substrate Binding Cleft of SpChiD

The substrate binding cleft was occupied by four Trp residues, Trp114, Trp160, Trp290 and Trp395. Trp114 is the highly conserved residue in family GH18 chitinases and its mutation Ala resulted in loss of TG activity (Madhuprakash *et al*., 2012). Trp160 and Trp290 were flanking on either side of the substrate binding cleft and the mutation of these residues to Ala affected the TG activity and to a greater extent by the mutation W160A. The minimal TG activity showed by the mutant W290A was also lost when it was combined with the mutant W160A. Threading the chitin molecules towards the catalytic center could be mediated by the residues Trp114, Trp160 and to a lesser extent by the residue Trp290. Due to the lack of these guiding aromatic residues at the substrate binding cleft (or) the decreased hydrophobicity at the binding cleft might have increased the trafficking of water molecules along with CHOS and thus favoured more of hydrolysis than TG. Enzyme kinetic studies revealed very high K_m values for all the Trp mutants which mean the decreased affinity towards the substrate. Loss of activity on polymeric substrates and decreased rate of catalysis with DP4 substrate by the mutant W395A proved the supporting role of Trp395 in *Sp*ChiD mediated catalysis.

4.9 Elicitor Activity of CHOS Produced from Chitosans by SpChiD or W114A

CHOS from chitosans possess antimicrobial activity against bacteria and fungi (Raafat *et al*., 2008) and are well-documented plant defense elicitors (Shibuya & Minami, 2001). Addition of chitin or chitosan to plant cells elicits typical defense responses including ion fluxes, generation of reactive oxygen species (ROS), activation of mitogen-activated protein kinases (MAPKs), induction of defense gene expression, synthesis of phytoalexins, cell wall strengthening and in some cases, induction of cell death (Shibuya & Minami, 2001; Lin *et al*., 2005; Cabrera *et al*., 2006). In general, the biological activities of CHOS were greatly influenced by the DP, DA and the concentration in a given species (Cabrera *et al*., 2006). The biological activity of CHOS increases with the DP and the highest activity was reported for DP7 (or) DP8 and little or no activity for smaller CHOS with DP < 5 (Hamel & Beaudoin, 2010).

In the present study, the ability of *Sp*ChiD and its mutant W114A (lost TG activity) to generate CHOS elicitors with efficient biological activity was investigated. This study may clarify degradation of chitosans with a chitinase having both hydrolysis and TG activities, for obtaining bioactive CHOS, would be a better choice or not. To the best of our knowledge, this is the first report of the biological activities of well characterized CHOS, obtained by degradation of chitosans with different DA, using pure recombinant chitinases. Chitosans with DA35% and 61% were subjected to degradation using *Sp*ChiD or W114A. MALDI-TOF-MS analysis revealed minor differences in the oligomers produced by both the enzymes. One extra acetylated unit was detected in the oligomers produced by *Sp*ChiD with chitosan DA61%, but, the reverse was true for W114A with chitosan DA35%.

The rapid and transient release of H_2O_2 in an oxidative burst is generally used as a sensitive indicator of the induction of disease defense responses and common stress responses in plant cells as it has been assumed to 'orchestrate' the hypersensitive reaction (Levine *et al*., 1994). The well characterized crude mixtures generated by *Sp*ChiD and W114A were used for elicitor activity studies, as a measure of oxidative burst in rice cell suspension culture systems. The chitosan crude mixtures produced by the mutant W114A were more active than *Sp*ChiD, inspite of subtle differences in the DA of CHOS, confirmed by the MALDI-TOF-MS analysis. This might be due to the increased hydrolytic activity of W114A and thus transformed much of the polymeric fraction into highly active oligomeric fraction. Irrespective of the type of enzyme used for degradation, crude mixtures from chitosan DA35% showed elicitor activity only at doses 100 and 150 µg/mL, whereas, crude mixtures from DA61% chitosan, showed elicitor activity at all the different concentrations tested. This strongly supports that the higher DA in the oligomeric fractions generated from DA61% chitosan, might be responsible for the activity even at low concentration. On the other hand, the fully deacetylated CHOS were able to display elicitor activity in *Arabidopsis thaliana* cell suspension systems. The progressive reacetylation of these completely deacetylated CHOS impaired their ability to enhance H_2O_2 accumulation for both short and long exposures. Even the

CHOS with DA > 65%, elicited cells did not accumulate H_2O_2 and did not die, even in the presence of high elicitor concentrations (Cabrera *et al*., 2006).

CHOS produced by the mutant W114A were verified, whether they can still display higher elicitor activity even after size based purification, than the CHOS produced by *Sp*ChiD. It was observed that the crude mixtures obtained by the degradation of chitosan DA61% were active even at low concentration (50 µg/mL). Also, an assumption, that higher the DA of substrate, greater the chance for *Sp*ChiD to display a different mode of action with its TG activity. In view of these points, large scale preparation of CHOS and their purification was restricted to the chitosan with DA61%, using *Sp*ChiD and its mutant W114A. The purified CHOS fractions after detailed characterization by MALDI-TOF-MS were used for elicitor activity studies. Fractions with DP8, DP9 and DP10 from *Sp*ChiD were more active than from W114A. Though the DP of oligomers produced by both the enzymes was same it might be the DA (or) PA of CHOS influencing the elicitor activity. It is very difficult to conclude, whether the different mode of action of *Sp*ChiD with its TG activity is influencing the DA and PA of CHOS and thus differences in the activities. However, a receptor has been identified for *N*-acetylated-CHOS, (Okada *et al*., 2002), but, how the CHOS with differential DA (or) PA are perceived by the plant cells is still unknown. This was often considered as a non-specific interaction of a polycation with negatively charged plasma membrane phospholipids that mimics and activates a common MAP kinase-dependent defence response (Shibuya & Minami, 2001). Thus it is very hard to explain the differences in the activities shown by CHOS obtained from chitosans. But, from our study it can be concluded that an enzyme with moderate degradation ability can be used for chitosan hydrolysis to generate elicitor-active CHOS. The crude mixtures of chitosan hydrolysates, with active ingredients can be used for immunising plants, rather than going for cumbersome purification methods which are not cost effective.

4.10 TG between Fully Acetylated and Fully/Partially Deacetylated CHOS

The catalysis of GH18 chitinases proceeds *via* the substrate-assisted mechanism, which has a strong preference for a GlcNAc in the -1 subsite. If the partially

deacetylated CHOS bind in such a way that a GlcN ends up in the crucial -1 subsite, they will act as an inhibitors. Thus, the binding of a GlcN would be non-productive, but, perhaps stronger than binding of GlcNAc. This shows that the idea of developing partially deacetylated CHOS as inhibitors for family GH18 chitinases. Partially deacetylated CHOS, mainly the DP5 molecule with the sequence "**DADAA**", exhibited a very good inhibitory effect with an IC_{50} value of 16 μM against *Sm*ChiB (Cederkvist *et al*., 2008). Chen *et al*., (2014a) reported that fully deacetylated CHOS with DP2-DP7 act as efficient inhibitors against the insect chitinase, *Of*ChtI, human chitotriosidase and the bacterial chitinases *Sm*ChiA and *Sm*ChiB with IC_{50} values ranging from 10^1–10^3 μM. In contrast, fully/partially deacetylated CHOS selectively inhibited TG activity of *Sp*ChiD without affecting hydrolysis and thus it can be considered as an exceptional behavior of *Sp*ChiD in family GH18 chitinases. This further suggests that the TG activity of *Sp*ChiD may be inhibited to a greater extent with the CHOS generated during the hydrolysis of chitosan polymers with differential DA.

On the whole *Sp*ChiD was a unique bacterial GH18 TG chitinase with its unprecedented structural and functional properties. These include the presence of an extra loop Asn30-Asp42, governing the chitobiase activity, two different transitions detected from DSC studies, very high binding affinities to CHOS, revealed from ITC analysis and the loss of TG activity in presence of fully or partially deacetylated CHOS. Further, the enzyme *Sp*ChiD also displayed its divergent nature from other bacterial chitinases, which was evident from phylogenetic analysis. An unrooted phylogenetic tree, obtained by comparing 131 bacterial GH18 sequences, revealed that all the single domain GH18 sequences from the family Enterobacteriaceae related to *Sp*ChiD clustered into a separate group (highlighted in yellow) (Fig. 3.48). The residues targeted in the present study were conserved in the entire single domain GH18 chitinases with loop (Asn30-Asp42), from the family Enterobacteriaceae (Fig. 4.5). Thus, we expect that all the properties pertaining to *Sp*ChiD and the mutational effects could be similar in all other seventeen chitinases in the group highlighted yellow.

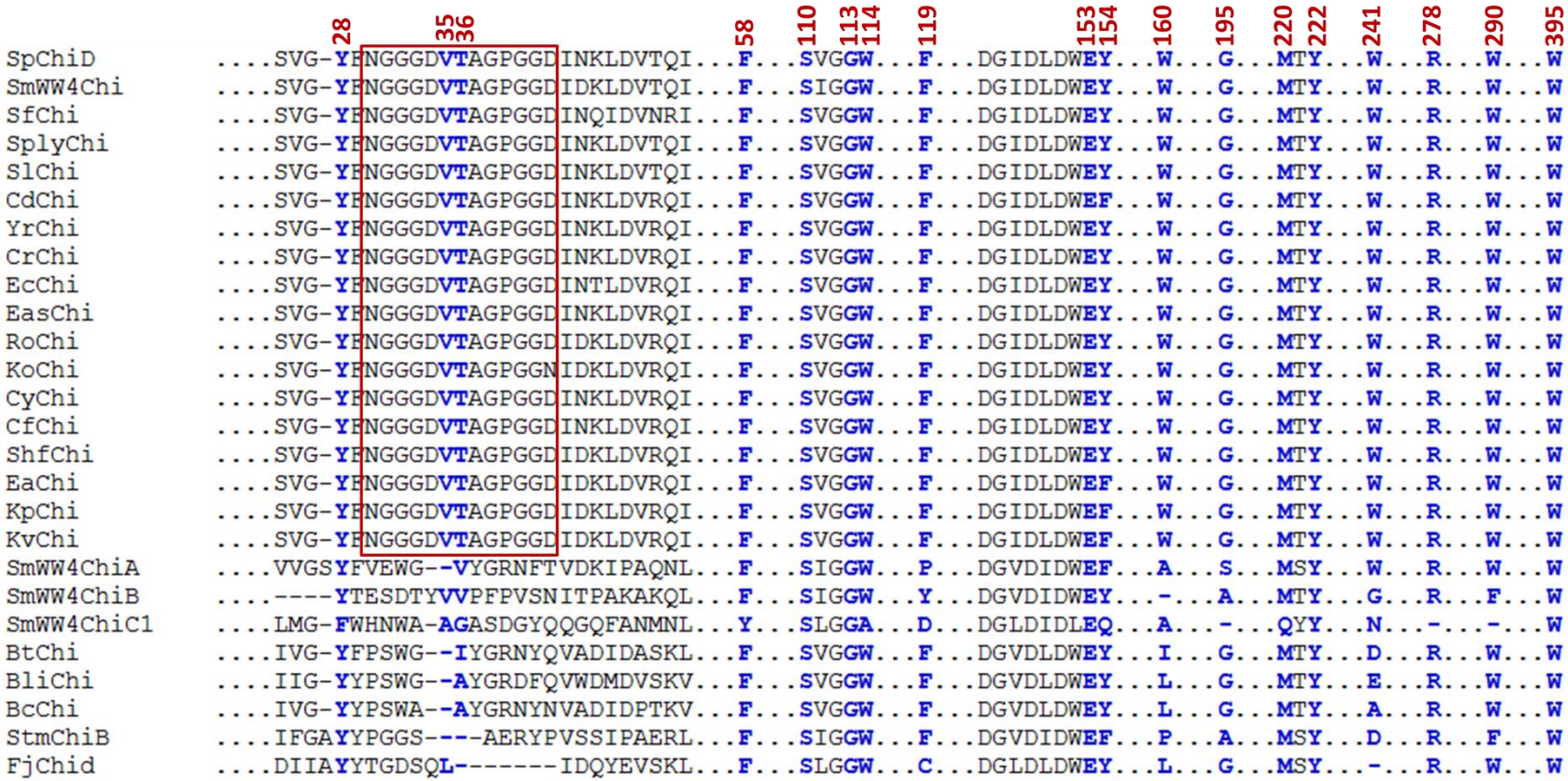

Figure 4.5: **Multiple sequence alignment of *Sp*ChiD**. The residues analyzed through mutational approach in the present study were highlighted in blue and were conserved in the entire single domain GH18 chitinases with loop (Asn30-Asp42), from the family Enterobacteriaceae. The loop region was shown in rectangular box.

4.11 Effect of Domain Fusions on Activities of SpChiD

GHs degrade crystalline polysaccharides in a relatively inefficient manner, as their target glycosidic bonds are often inaccessible to the active site of the appropriate enzymes. In order to overcome these problems, many of the GHs that utilize insoluble substrates evolved to be multimodular, comprising catalytic modules appended to one or more non-catalytic auxiliary domains (CBMs, PKD and Fn3). Despite the lack of hydrolytic activity, these auxiliary domains increase the binding affinity towards soluble and insoluble carbohydrate substrates. It has been reported that single-module polysaccharide hydrolases, such as cellobiohydrolase (Thongekkaew *et al*., 2013) and mannanase (Tang *et al*., 2013), exhibit higher catalytic activity as well as thermostability when attached to heterologous CBMs. These auxiliary domains usually bring the catalytic domains in close proximity to the substrates and in turn improve the enzyme activity.

Though, *Sp*ChiD was able to bind to polymeric substrates like colloidal, α- and β- chitin, it displayed lower hydrolytic activities, due to the lack of accessory domains (Purushotham & Podile, 2012). The difference in the hydrolyzing/binding activity of *Sp*ChiD may not be solely due to the difference in the binding activity or absence of accessory binding domains. The interactions from several aromatic residues located at the catalytic domains of chitinases probably are essential for substrate binding by *Sp*ChiD. This was well exemplified in case of *Sm*ChiA, where all the three residues, Trp69, Trp33, and Trp245 were crucial to express full binding activity. Of these three residues, Trp69 and Trp33 were located in the N-terminal domain, whereas, Trp245 was located in the catalytic domain, but, were proposed to act cooperatively in the chitin binding by *Sm*ChiA (Uchiyama *et al*., 2001). This N-terminal region corresponds to the PKD domain and whose role was well studied in crystalline α-chitin hydrolysis. Thus *Sm*ChiA and *Al*ChiA showed maximum activity on crystalline α-chitin compared to other chitinases produced by the respective bacterial species (Suzuki *et al*., 2002; Orikoshi *et al*., 2005).

Apart from these auxiliary domains associated with chitinases, few proteins were secreted by the chitinolytic bacteria in response to chitin. CBP21 was one such a

protein (now referred as CBM33 type protein), which showed a strong affinity to β-chitin (Vaaje-Kolstad *et al*., 2005). These proteins introduce chain breaks and generate oxidized chain ends, thus promoting further degradation by chitinases (Vaaje-Kolstad *et al*., 2010). Unlike the case with other CAZys', this is the first report to the best of our knowledge, where, an attempt was made to increase the insoluble polymer degradation capacity of a single modular GH18 chitinase with TG, by domain fusion with PKD or CBP21. Among all the six *Sp*ChiD fusion chimeras analyzed, two C-terminal fusions ChiD+CBP, ChiD+PKD and one N-terminal fusion CBP+ChiD showed decreased K_m values of 17.6, 15.2 and 27.4 mg/mL, indicating increased affinity towards colloidal chitin substrate when compared to *Sp*ChiD (35.1 mg/mL). The overall catalytic efficiency was also increased for these three fusions, but, to a greater extent for ChiD+PKD (57.4 sec^{-1} mg^{-1} mL) compared to *Sp*ChiD (29.33 sec^{-1} mg^{-1} mL). However, higher ligand-binding capacity/affinity does not guarantee an improved cellulase activity, as the ultra-tight binding could become a restriction for the dynamic motion of the enzymes (Boraston *et al*., 2004). In line with this argument, though the fusion CDP displayed decreased K_m value of 22.4 mg/mL, its overall catalytic efficiency was low (24.86 sec^{-1} mg^{-1} mL) compared to *Sp*ChiD (29.33 sec^{-1} mg^{-1} mL).

The effect of domain fusions on *Sp*ChiD activity was further investigated by performing time course degradation studies on colloidal chitin substrate. These studies also revealed that the C-terminal *Sp*ChiD fusion chimeras *i.e.* ChiD+CBP and ChiD+PKD were more active than the other chimeras tested (Fig. 3.45). Whereas, activities on crystalline chitin substrates revealed that out of the two C-terminal fusions, ChiD+PKD was more active on α-chitin, but, ChiD+CBP was more active on β-chitin (Fig. 3.46). The latter observation was consistent with the substrate preferences of the appended auxiliary domains. CBP21 was known to act synergistically with the chitinases on crystalline chitin substrates and helps in increasing the catalytic efficiency of these enzymes (Vaaje-Kolstad *et al*., 2005). But, the addition of CBP21 had only minor effect on the activity of *Sp*ChiD in colloidal, α- and β- chitin degradation, compared to individual CBP21 fusion chimeras. Among

all the CBP fusions ChiD+CBP displayed more activity in the time dependent degradation of colloidal chitin. This can be explained well in terms of a distinct intramolecular synergism, reported in endoglucanase A (CenA) from the bacterium *Cellulomonas fimi*. CenA composed of a catalytic domain and a non-hydrolytic cellulose-binding domain that can function independently. The individual domains interact synergistically in the disruption and hydrolysis of cellulose fibers (Din *et al*., 1994). Functional independence of CBP21 was reported recently with its enzymatic activity on β- chitin nanowhiskers and now referred as lytic polysaccharide monooxygenase (LPMO) (Vaaje-Kolstad *et al*., 2010). Thus, the addition of CBP21 for improving catalytic efficiency of chitinases can be considered as an example of intermolecular synergism, whereas, the CBP fusion chimeras as examples for intramolecular synergism. The probable reason could be there will be a competition for the binding sites in substrate between the two individual protein molecules, which may decrease the overall catalytic efficiency (Din *et al*., 1994). The increased activity of ChiD+PKD fusion chimera may be due to the linear arrangement of aromatic residues on the surface of the chimeric protein, both from the PKD domain and the catalytic domain of *Sp*ChiD. Such a linear arrangement of aromatic residues is crucial for CAZys' for tethering to the crystalline polysaccharides, guiding sugar chains towards the catalytic center and displaying increased catalytic efficiencies (Uchiyama *et al*., 2001).

HPLC analysis for *Sp*ChiD fusion chimeras using DP4 substrate revealed alterations in the hydrolysis and TG activities. The fusions ChiD+CBP, CBP+ChiD and PKD+ChiD produced very low amounts of quantifiable TG products (DP5 & DP6) compared to *Sp*ChiD (Fig. 4.6). The C-terminal PKD fusion *i.e*. ChiD+PKD displayed an improved TG, both in terms of quantity of TG products produced and also the duration of TG, retained up to 105 min (Fig. 4.6). The dual domain fusions (*i.e.* CDP & PDC), which displayed low catalytic efficiencies towards insoluble polysaccharides, produced higher amounts of TG products with DP4 compared to *Sp*ChiD. But, PDC displayed efficient TG than CDP and *Sp*ChiD both in terms of quantity of TG products produced and the extended duration of TG activity. The

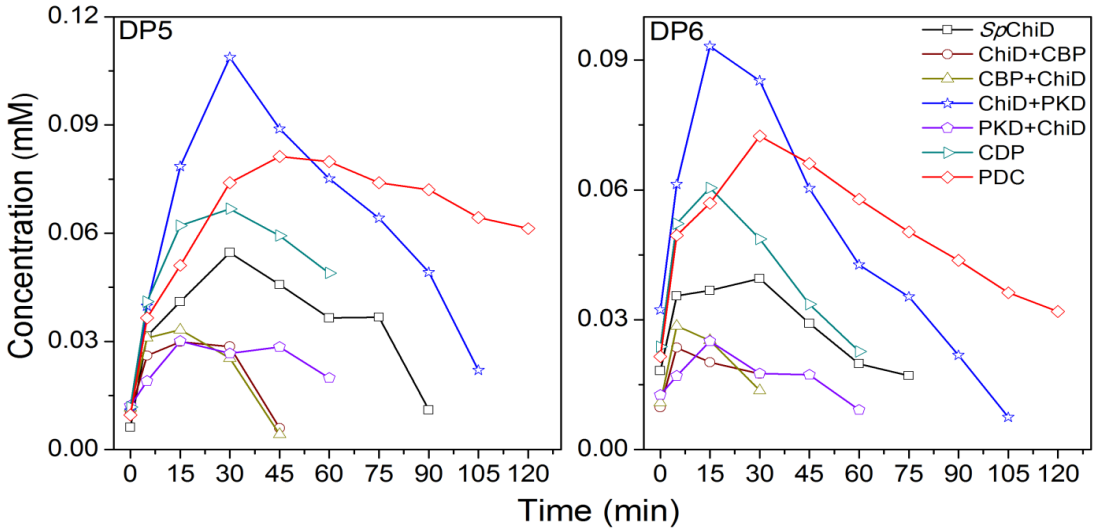

Figure 4.6: **Comparison of quantifiable TG products produced by *Sp*ChiD fusion chimeras.** Profiles were generated by *Sp*ChiD or its variants with 1 mM DP4 substrate in 20 mM sodium acetate buffer pH-5.6 at 40°C. Product quantification was done by a linear correlation between peak area and concentration of oligosaccharides in standard samples.

reasons behind enhanced or diminished TG activities of *Sp*ChiD fusion chimeras with soluble CHOS like DP4 are difficult to predict. It could be either the orientation of auxiliary domains or the final fold of chimeric proteins influencing the hydrolysis/TG activities, which yet to be confirmed through structural analysis.

Summary & conclusion

5.0 Back Ground & Objective

CHOS can be produced either by partial depolymerization of chitin/chitosan, or by oligomerization of the basic monosaccharide building blocks *i.e.* GlcNAc and GlcN. Production of CHOS is of interest not only to the agriculture but also to the food and medicine-related biotechnology industries due to their diverse applications. Enzymatic methods may provide an opportunity to produce CHOS with specific DP and PA and, thus, desired bio-activity, to develop an efficient and eco-friendly process. The specificity of chitin/chitosan-degrading enzymes has been studied by extensive enzymatic degradation of chitin/chitosan polymers, followed by isolation and characterization of the resulting oligomers. However, chitobiose is the major end product of chitinase mediated hydrolysis, due to their processive mode of action on chitin/chitosan substrates. But, higher DP CHOS are suitable for plant protection and other biological applications, which, can be produced by a nonprocessive endo-enzyme of known specificity or an enzyme having TG ability. *Sp*ChiD is one of the endo-acting enzymes with hyper TG ability, which can produce TG products like DP7, DP10, DP11-12 and DP11-DP13 from DP3, DP4, DP5 and DP6 substrates, respectively (Purushotham & Podile, 2012). But, the TG products produced during the initial stages of reaction become substrates for hydrolytic activity of *Sp*ChiD in a prolonged incubation. In the present study we made an attempt to further improve the TG activity and to understand the structural properties for better insights into the mode of action of *Sp*ChiD.

5.1 Mutagenesis to Improve TG activity of SpChiD

To improve the TG activity of *Sp*ChiD, the amino acid residues in the catalytic center, catalytic groove and in the surface exposed region were selected for mutagenesis. Among the five different amino acid substitutions made at the catalytic center, three showed increased TG activity (M220A, Y222A and R278A). The product profile of the mutants M220A and Y222A was similar except that the latter lost chitobiase activity and a gradual decrease in the initial DP4 substrate, through time was detected. It could be the increased stay of substrate/intermediate resulted in increased TG activity both in terms of quantity of TG products formed, and the

duration of TG activity of the mutants M220A and Y222A. The residue Arg278 also forms ion pairs with the substrate at the catalytic center and its mutation to Ala, caused perturbations in the ion pair forming ability of *Sp*ChiD with the incoming DP4 substrate. Such subtle changes at the catalytic center resulted in a gradual increase in the proportion of TG products DP5 and DP6 up to 30 min.

The residue Glu153 is crucial for chitinase-mediated catalysis and its mutation, E153D resulted in significant loss of both hydrolytic and TG activities leaving 92.5% of DP4 substrate at the end of 6 h. The very adjacent residue Tyr154 and the corresponding mutation Y154A, was unique from all other mutants, which retained TG activity even when hydrolytic activity increased. However, out of five different amino acid residues targeted at the catalytic groove, four mutations *i.e.* F58W, S110G, G113S and F119A displayed increased TG rather than hydrolysis whereas, the mutation W114A resulted in significant loss of TG activity with increased hydrolysis. Trp114 maintains the architecture of the catalytic groove, with its bulky side chain and also it was directly involved in threading of the chitin molecules towards the catalytic center. Thus, the mutation W114A showed a severe effect on TG activity of *Sp*ChiD. The pre-existing stacking interactions shown by Trp114 with the substrate were further increased with the mutation G113S. Increased interactions at the positions 113 and 114 in turn increased the TG activity of G113S.

Ser110 and Phe119 are the two important residues, known to involve in the catalysis but, a key role was played by Ser110. Thus, the mutations S110G and F119A had a severe effect on the rate of catalysis, which in turn helped in the increased TG. The substitution of Phe58 to Trp increased the hydrophobicity at the catalytic groove and also aromatic interactions with the incoming substrate molecule, which will favour more of TG activity compared to hydrolysis. The mutation W241A also resulted in the increased TG activity confirming the potential role of solvent accessible residue Trp241 in guiding the CHOS molecules to the catalytic center. We also showed that the partial blocking of the tunnel exit, by the mutation G195W, in *Sp*ChiD improved the TG activity, a new approach, hitherto not reported for any of family 18 or 19 GHs. This was further supported by MD simulations.

5.2 Structural Aspects of SpChiD

The *Sp*ChiD was crystallized with 2M sodium formate as the precipitating agent. The structure of the *Sp*ChiD was determined at 1.49 Å resolution and refined to an R-factor of 16.2%. The single catalytic domain of *Sp*ChiD is consisting of 406 amino acid residues. The structure determination showed that the polypeptide chain of *Sp*ChiD adopts a $(\beta/\alpha)_8$-TIM barrel conformation. It contains three acidic residues, Asp149, Asp151 and Glu153 as part of its catalytic scheme. While both Asp149 and Glu153 adopt well defined single conformations, Asp151 is observed in two conformations. In this structure, the substrate binding cleft is partially obstructed by a protruding loop Asn30-Asp42 causing the reduction in the number of available subsites in the substrate binding site. Apparently, the positioning of this loop in the cleft seems to have resulted in the TG activity. The structure determination of *Sp*ChiD also revealed an unusual feature, where, Met89 was found as sulfone Met89 (SMet89) with two oxygen atoms covalently attached to the sulfur atom of Met89. Mutational studies of the loop Asn30-Asp42, revealed its crucial role in the chitobiase activity of *Sp*ChiD. A complete deletion of the loop resulted in the loss of chitobiase activity with a concomitant enhancement in the TG activity of *Sp*ChiD.

5.3 Thermal Stability & Ligand Binding Energetics of SpChiD

Temperature dependent CD spectroscopic studies revealed that the enzyme *Sp*ChiD was stable up to 40°C, without any perturbations in the secondary and tertiary structure. Thermal stability of *Sp*ChiD was further investigated using high sensitivity DSC measurements, which revealed the presence of two distinct transitions centred at 44.8 and 47.3°C, respectively, at pH 8.0. But, the DSC scans for *Sp*ChiD as a function of pH revealed that the protein was thermally stable at pH 6.0 and showed regular two distinct transitions centred at 50.1 and 52.7°C, respectively. Ligand induced thermal stability of *Sp*ChiD was also investigated by performing DSC with the catalytically inactive mutant E153A. Free energy changes during the binding of CHOS with DP-2, 3, 5 and 6 to E153A were also investigated by ITC. The exposure and accessibility of Trp residues of E153A in the presence and absence of CHOS was studied by fluorescence quenching experiments using the neutral quencher

acrylamide. These studies proved that the increased chain length of CHOS increased the thermal stability, binding efficiency and in turn strongly suggested the role of Trp in ligand binding. We further analyzed the role of four Trp (Trp114, Trp160, Trp290 and Trp395) residues in the activities of *Sp*ChiD, at the substrate binding cleft through mutational studies.

5.4 Biological Activity Studies with CHOS Produced by SpChiD & W114A

In the present study the abilities of *Sp*ChiD and its mutant W114A (lost TG activity) to generate CHOS with efficient biological activity were investigated. The comparison was made between two enzymes, with and without TG ability. This is to clarify, whether an enzyme having TG would be a better choice for obtaining CHOS from chitosans or not. Chitosans with DA35% and 61% were subjected to degradation using *Sp*ChiD or W114A. The crude mixtures generated were characterized by MALDI-TOF-MS analysis. On the other hand CHOS were also prepared in large scale from chitosan DA61% and purified using SEC. The purified CHOS fractions were also subjected to detailed characterization by MALDI-TOF-MS. Both, the crude mixtures and the purified CHOS displayed elicitor activities with subtle differences, when tested for oxidative burst measurements in rice cell suspension culture systems. Further, the TG activity of *Sp*ChiD was also tested between fully acetylated and fully or partially deacetylated CHOS.

5.5 SpChiD Fusion Chimeras

Due to the lack of accessory domains *Sp*ChiD displayed very low bind affinities to the crystalline chitin substrates and thus low catalytic activity. We made an attempt to increase the insoluble polymer degradation capacity of this single modular GH18 chitinase with TG, by domain fusion with PKD or CBP21. Biochemical analysis revealed that the C-terminal *Sp*ChiD fusion chimeras *i.e.* ChiD+CBP and ChiD+PKD were more active than the other chimeras tested for their degradation abilities on colloidal, α- or β- chitin, with minor differences. The effect of domain fusions on the hydrolysis and TG activities of *Sp*ChiD with DP4 substrate were also investigated using HPLC. Improved TG activity, in terms of quantity of TG products produced and the duration of TG was observed for the fusions ChiD+PKD and PDC.

5.6 Conclusions & Future Scope

*Sp*ChiD was a unique bacterial GH18 TG chitinase with its unprecedented structural and functional properties. The divergent nature of *Sp*ChiD from other 131 bacterial GH18 chitinases was showed using phylogenetic analysis. However, from the past few years TG received a considerable attention for the production of CHOS with longer DP. In order to synthesize adequate quantities of longer chain CHOS with immense potential for various biological activities, there is a definite need for exploitation of TG activity. The present study provides insights into the structural and dynamic features of *Sp*ChiD, a family 18 chitinase with TG activity. The efficiency of TG by the wild-type enzyme is inevitably limited by enzyme-catalyzed hydrolysis of the product. So, there is a definite need for reducing/curtailing the hydrolytic activity for improving TG. The improved *Sp*ChiD variants are useful in developing a process for the production of longer chain CHOS.

5.7 Major Findings in the Present Study

- ✓ Three mutants from the catalytic center, (M220A, Y222A and R278A), four from the catalytic groove, (F58W, S110G, G113S and F119A) and one from the solvent accessible region (W241A) displayed increased TG with a concomitant decrease in the rate of hydrolysis.
- ✓ In a new approach, partial blocking of the tunnel exit, by the mutation G195W, in *Sp*ChiD improved the TG activity.
- ✓ Crystal structure of *Sp*ChiD was solved at a resolution of 1.49 Å which revealed the presence of dual conformations for the side chains of Ser110, Asp151 and Met220 and also an extra electron density for an acetate molecule at the proximity of active site and sulfone Met89 (SMet89) were observed.
- ✓ The presence of loop, Asn30-Asp42, reduced the length of substrate binding cleft to less than half and its deletion resulted in the loss of chitobiase activity with a concomitant enhancement in the TG activity of *Sp*ChiD.
- ✓ Thermal unfolding experiments using DSC revealed two different transitions for *Sp*ChiD and the thermal stability of its mutant E153A increased with increased chain length of CHOS.

- ✓ Accessibility of Trp residues in the binding site of E153A decreased with increased chain length of CHOS and the mutational analysis confirmed that the residues Trp114, Trp160 and Trp290 are crucial for TG activity of *Sp*ChiD.
- ✓ Binding of lower and higher chain CHOS to E153A resulted in exo and endothermic heat changes, respectively. CHOS with DP-2, 3, 5 and 6 displayed very high binding affinities to E153A, compared to any other GH18 or GH19 chitinase reported so far.
- ✓ Chitosan crude mixtures produced by the mutant W114A were more active than *Sp*ChiD, whereas, the reverse is true for the purified oligomeric fractions.
- ✓ Selective inhibition of TG activity was observed for *Sp*ChiD without any alterations in the hydrolytic activity.
- ✓ Among all the *Sp*ChiD fusion chimeras, two C-terminal (ChiD+CBP & ChiD+PKD) and one N-terminal fusions (CBP+ChiD) showed increased affinity and overall catalytic efficiency.
- ✓ The fusions ChiD+PKD and PDC displayed increased TG activity, both in terms of quantity of TG products produced and the duration of TG compared to *Sp*ChiD.
- ✓ Phylogenetic analysis revealed that *Sp*ChiD and other seventeen single domain bacterial GH18 chitinases, having the loop region Asn30-Asp42, from Enterobacteriaceae formed a separate group and showed their divergent nature from other bacterial GH18 chitinases.

References

Aam, B. B., Heggset, E. B., Norberg, A. L., Sørlie, M., Vårum, K. M., and Eijsink, V. G. (2010) Production of chitooligosaccharides and their potential applications in medicine. *Mar. Drugs*. 8, 1482-1517.

Aguilera, B., Ghauharali-van der Vlugt, K., Helmond, M. T., Out, J. M., Donker-Koopman, W. E., Groener, J. E., Boot, R. G., Renkema, G. H., van der Marel, G. A., van Boom, J. H., Overkleeft, H. S., and Aerts, J. M. (2003) Transglycosidase activity of chitotriosidase: improved enzymatic assay for the human macrophage chitinase. *J. Biol. Chem.* 278, 40911-40916.

Aqvist, J., Luzhkov, V. B., and Brandsdal, B. O. (2002) Ligand binding affinities from MD simulations. *Acc. Chem. Res*. 35, 358-365.

Arai, N., Shiomi, K., Yamaguchi, Y., Masuma, R., Iwai, Y., Turberg, A., Kolbl, H., and Omura, S. (2000) Argadin, a new chitinase inhibitor, produced by *Clonostachys* sp. FO-7314. *Chem. Pharm. Bull*. 48, 1442-1446.

Aronson, N. N. Jr., Halloran, B. A., Alexeyev, M. F., Zhou, X. E., Wang, Y., Meehan, E. J., and Chen, L. (2006) Mutation of a conserved tryptophan in the chitin-binding cleft of *Serratia marcescens* chitinase A enhances transglycosylation. *Biosci. Biotechnol. Biochem.* 70, 243-251.

Barber, M. S., Bertram, R. E., and Ride, J. P. (1989) Chitin oligosaccharides elicit lignification in wounded wheat leaves. *Physiol. Mol. Plant Pathol*. 34, 3-12.

Bhatnagar, A., and Sillanpää, M. (2009) Applications of chitin and chitosan derivatives for the detoxification of water and wastewater - A short review. *Adv. Colloid Interface Sci.* 152, 26-38.

Biarnes, X., Ardevol, A., Planas, A., Rovira, C., Laio, A., and Parrinello, M. (2007) The conformational free energy landscape of β-D-glucopyranose. Implications for substrate preactivation in β-glucoside hydrolases. *J. Am. Chem. Soc.* 129, 10686-10693.

Boraston, A. B., Bolam, D. N., Gilbert, H. J., and Davies, G. J. (2004) Carbohydrate-binding modules: fine-tuning polysaccharide recognition. *Biochem. J*. 382, 769-781.

Bortone, K., Monzingo, A. F., Ernst, S., and Robertus, J. D. (2002) The structure of an allosamidin complex with the *Coccidioides immitis* chitinase defines a role for a second acid residue in substrate-assisted mechanism. *J. Mol. Biol.* 320, 293-302.

Brameld, K. A., and Goddard, W. A. (1998) Substrate distortion to a boat conformation at subsite -1 is critical in the mechanism of family 18 chitinases. *J. Am. Chem. Soc.* 120, 3571-3580.

Bussi, G., Donadio, D., and Parrinello, M. (2007) Canonical sampling through velocity-rescaling. *J. Chem. Phys*. 126, 014101.

Cabrera, J. C., Messiaen, J., Cambier, P., and van Cutsem, P. (2006) Size, acetylation and concentration of chitooligosaccharide elicitors determine the switch from defense involving PAL activation to cell death and water peroxide production in *Arabidopsis* cell suspensions. *Physiol. Plant*. 127, 44-56.

Cantarel, B. L., Coutinho, P. M., Rancurel, C., Bernard, T., Lombard, V., and Henrissat, B. (2009) The Carbohydrate-Active enZYmes database (CAZy): an expert resource for Glycogenomics. *Nucleic. Acids. Res*. 37, D233-D238.

Cederkvist, F. H., Parmer, M. P. Vårum, K. M., Eijsink, V. G. H., and Sørlie, M. (2008) Inhibition of a family 18 chitinase by chitooligosaccharides. *Carbohydr. Polym.* 74, 41-49.

Cederkvist, F. H., Saua, S. F., Karlsen, V., Sakuda, S., Eijsink, V. G., and Sorlie, M. (2007) Thermodynamic analysis of allosamidin binding to a family 18 chitinase. *Biochemistry*. 46, 12347-12354.

Chen, L., Liu, T., Zhou, Y., Chen, Q., Shen, X., and Yang, Q. (2014b) Structural characteristics of an insect group I chitinase, an enzyme indispensable to moulting. *Acta Crystallogr. D Biol. Crystallogr*. 70, 932-942.

Chen, L., Zhou, Y., Qu, M., Zhao, Y., and Yang, Q. (2014a) Fully deacetylated chitooligosaccharides act as efficient glycoside hydrolase family18 chitinase inhibitors. *J. Biol. Chem.* 289, 17932-17940.

Cote, G. L., and Tao, B. Y. (1990). Oligosaccharide synthesis by enzymatic transglycosylation. *Glycoconj. J.* 7, 145-162.

Coutino Ramirez, L., Marin-Cervantes, M. C., Huerta, S., Revah, S., and Shirai, K. (2006) Enzymatic hydrolysis of chitin in the production of oligosaccharides using *Lecanicillium fungicola* chitinases. *Process Biochem*. 41, 1106-1110.

Das, S. N., Madhuprakash, J., Sarma, P. V. S. R. N., Purushotham, P., Suma, K., Manjeet, K., Rambabu, S., El Gueddari, N. E., Moerschbacher, B. M., and Podile, A. R. (2013) Biotechnological approaches for field applications of chitooligosaccharides (COS) to induce immunity in plants. *Cri. Rev. in Biotechnol*. doi: 10.3109/ 07388551. 2013.798255.

Davies, G., and Henrissat, B. (1995) Structures and mechanisms of glycosyl hydrolases. *Structure.* 3, 853-859.

Defaye, J., Gadelle, A., and Pedersen, C. (1994) A convenient access to β-(1,4)-linked 2-amino-2-deoxy-D-glucopyranosyl fluoride oligosaccharides and β-(1,4)-linked 2-amino-2-deoxy-D-glucopyranosyl oligosaccharides by fluorolysis and fluorohydrolysis of chitosan. *Carbohydr. Res.* 261, 267-277.

Din, N., Damude, H. G., Gilkes, N. R., Miller, R. C. Jr., Warren, R. A., Kilburn, D. G. (1994) C1-Cx revisited: intramolecular synergism in a cellulase. *Proc. Natl. Acad. Sci. U.S.A.* 91, 11383-11387.

Eijsink, V. G., Vaaje-Kolstad, G., Varum, K. M., and Horn, S. J. (2008) Towards new enzymes for biofuels: lessons from chitinase research. *Trends. Biotechnol.* 26, 228-235.

Elias, J. A., Homer, R. J., Hamid, Q., and Lee, C. G. (2005) Chitinases and chitinase-like proteins in Th2 inflammation and asthma. *J. Allergy. Clin. Immunol.* 116, 497-500.

Emsley, P., and Cowtan, K. (2004) Coot: model-building tools for molecular graphics. *Acta Crystallogr. D Biol. Crystallogr.* 60, 2126-2132.

Essmann, U., Perera, L., Berkowitz, M. L., Darden, T., Lee, H., and Pedersen, L. G. (1995) A smooth Particle Mesh Ewald method. *J. Chem. Phys.* 103, 8577-8593.

Eweis, M., Elkholy, S. S., and Elsabee, M. Z. (2006) Antifungal efficacy of chitosan and its thiourea derivatives upon the growth of some sugar-beet pathogens. *Int. J. Biol. Macromol.* 38, 1-8.

Fan, Q., Huang, W., and Wang, L. X. (2012) Remarkable transglycosylation activity of glycosynthase mutants of endo-D, an endo-β-*N*-acetylglucosaminidase from *Streptococcus pneumoniae. J. Biol. Chem.* 287**,** 11272-11281.

Faoro, F., Maffi, D., Cantu, D., and Iriti, M. (2008) Chemical-induced resistance against powdery mildew in barley: the effects of chitosan and benzothiadiazole. *Biocontrol.* 53, 387-401.

Felsenstein, J. (1985) Confidence limits on phylogenies: An approach using the bootstrap. *Evolution.* 39, 783-791.

Forsberg, Z., Vaaje-Kolstad, G., Westereng, B., Bunaes, A. C., Stenstrom, Y., MacKenzie, A., Sørlie, M., Horn, S. J., and Eijsink, V. G. H. (2011) Cleavage of cellulose by a CBM33 protein. *Protein. Sci.* 20, 1479-1483.

Fukamizo, T., Goto, S., Torikata, T., and Araki, T. (1989) Enhancement of transglycosylation activity of lysozyme by chemical modification. *Agric. Biol. Chem.* 53, 2641-2651.

Fukamizo, T., Sasaki, C., Schelp, E., Bortone, K., and Robertus, J. D. (2001) Kinetic properties of chitinase-1 from the fungal pathogen *Coccidioides immitis*. *Biochemistry*. 40, 2448-2454.

Gardner, K. H., and Blackwell, J. (1975) Refinement of structure of β-chitin. *Biopolymers.*14, 1581-1595.

Gotthardt, U., and Grambow, H. J. (1992) Near-isogenic wheat suspension cultures. Establishment, elicitor induced peroxidase activity, and potential use in the study of host/pathogen interactions. *J. Plant. Physiol*. 139, 659-665.

Hamel, L. P., and Beaudoin, N. (2010) Chitooligosaccharide sensing and downstream signaling: contrasted outcomes in pathogenic and beneficial plant-microbe interactions. *Planta*. 232, 787-806.

Hashimoto, M., Ikegami, T., Seino, S., Ohuchi, N., Fukada, H., Sugiyama, J., Shirakawa, M., and Watanabe, T. (2000) Expression and characterization of the chitin-binding domain of chitinase A1 from *Bacillus circulans*WL-12. *J. Bacteriol*. 182, 3045-3054.

Hess, B., Bekker, H., Berendsen, H. J. C., and Fraaije, J. G. E. M. (1997) LINCS. A linear constraint solver for molecular simulations. *J. Comput. Chem*. 18, 1463-1472.

Horn, S. J., Sørbotten, A., Synstad, B., Sikorski, P., Sørlie, M., Vårum, K. M., and Eijsink, V. G. (2006) Endo/exo mechanism and processivity of family 18 chitinases produced by *Serratia marcescens*. *FEBS J*. 273, 491-503.

Houston, D. R., Eggleston, I., Synstad, B., Eijsink, V. G. H., and van Aalten, D. M. (2002) The cyclic dipeptide CI-4 [cyclo-(l-Arg-d-Pro)] inhibits family 18 chitinases by structural mimicry of a reaction intermediate. *Biochem. J*. 368, 23-27.

Hult, E. L., Katouno, F., Uchiyama, T., Watanabe, T., and Sugiyama, J. (2005) Molecular directionality in crystalline-chitin: Hydrolysis by chitinases A and B from *Serratia marcescens* 2170. *Biochem. J*. 388, 851-856.

Imoto, T., and Yagishita, K. (1971) A simple activity measurement of lysozyme. *Agricu. and Biolo. Chemi.* 35, 1154-1156.

Iriti, M., Sironi, M., Gomarasca, S., Casazza, A. P., Soave, C., and Faoro, F. (2006) Cell death-mediated antiviral effect of chitosan in tobacco. *Plant Physiol. Biochem.* 44, 893-900.

Jaques, A. K., Fukamizo, T., Hall, D., Barton, R. C., Escott, G. M., Parkinson, T., Hitchcock, C. A., and Adams. D. J. (2003) Disruption of the gene encoding the

ChiB1 chitinase of *Aspergillus fumigatus* and characterization of a recombinant gene product. *Microbiology*. 149, 2931-2939.

Jitonnom, J., Lee, V. S., Nimmanpipug, P., Rowlands, H. A., and Mulholland, A. J. (2011) Quantum mechanics/molecular mechanics modeling of substrate-assisted catalysis in family 18 chitinases: conformational changes and the role of Asp142 in catalysis in ChiB. *Biochemistry*. 50, 4697-4711.

Jones, D. T., Taylor, W. R., and Thornton, J. M. (1992) The rapid generation of mutation data matrices from protein sequences. *Computer Applications in the Biosciences.* 8, 275-282.

Jones, T. A., Zou, J. Y., Cowan, S. W., and Kjeldgaard, M. (1991) Improved methods for building protein models in electron density maps and the location of errors in these models. *Acta Crystallogr. A.* 47, 110-119.

Ke, S. H., and Madison, E. L. (1997) Rapid and efficient site-directed mutagenesis by single-tube 'megaprimer' PCR method. *Nucleic Acids Res.* 25, 3371-3372.

Kim, H. M., Hong, S. H., Yoo, S. J., Baek, K. S., Jeon, Y. J., and Choung, S. Y. (2006) Differential effects of chitooligosaccharides on serum cytokine levels in aged subjects. *J. Med. Food*. 9, 427-430.

Kim, S. K., and Rajapakse, N. (2005) Enzymatic production and biological activities of chitosan oligosaccharides (COS): A review. *Carbohydr. Polym.* 62, 357-368.

Kim, T. J., Park, C. S., Cho, H. Y., Cha, S. S., Kim, J. S., Lee, S. B., Moon, T. W., Kim, J. W., Oh, B. H., and Park, K. H. (2000) Role of the glutamate 332 residue in the transglycosylation activity of *Thermus maltogenic* amylase. *Biochemistry.* 39, 6773-6780.

Kohlhoff, M., El Gueddari, N. E., Gorzelanny, C., Haebel, S., Alonso, M. J., Franco, T. T., and Moerschbacher, B. M. (2009) Bioengineering of chitosans with non-random patterns of acetylation - a novel sequence-specific chitosan hydrolase generating oligomers with block-PA. *Adv. Chitin Sci.* 11, 463-468.

Koping-Hoggard, M., Tubulekas, I., Guan, H., Edwards, K., Nilsson, M., Vårum, K. M., and Artursson, P. (2001) Chitosan as a nonviral gene delivery system: structure–property relationships and characteristics compared with polyethylenimine *in vitro* and after lung administration *in vivo*. *Gene Ther.* 8, 1108-1121.

Köping-Höggård, M., Vårum, K. M., Issa, M., Danielsen, S., Christensen, B. E., Stokke, B. T., and Artursson, P. (2004) Improved chitosan-mediated gene delivery based on easily dissociated chitosan polyplexes of highly defined chitosan oligomers. *Gene Ther.* 11, 1441-1452.

Kristiansen A, Vårum, K. M., and Grasdalen, H. (1998) The interactions between highly de-*N*-acetylated chitosans and lysozyme from chicken egg white studied by ^{1}H-NMR spectroscopy. *Eur. J. Biochem.* 251, 335-342.

Krokeide, I. M., Synstad, B., Gåseidnes, S., Horn, S. J., Eijsink, V. G. H., Sørlie, M. (2007) Natural substrate assay for chitinases using high-performance liquid chromatography: a comparison with existing assays. *Anal. Biochem.* 363, 128-134.

Lakowicz, J. R. (1999) Principles of Fluorescence Spectroscopy, 2nd Edition, Kluwer Academic Publishers, New York, 698 pp.

Laskowski, R. A., MacArthur, M. W., Moss, D. S, and Thornton, J. M. (1993) PROCHECK: a program to check the stereochemical quality of protein structures. *J. Appl. Cryst.* 26, 283-291.

Lee, D. X., Xia, W. S., and Zhang, J. L. (2008) Enzymatic preparation of chitooligosaccharides by commercial lipase. *Food Chem.* 111, 291-295.

Lee, H. W., Park, Y. S., Choi, J. W., Yi, S. Y., and Shin, W. S. (2003) Antidiabetic effects of chitosan oligosaccharides in neonatal streptozotocin-induced noninsulin-dependent diabetes mellitus in rats. *Biol. Pharm. Bull.* 26, 1100-1103.

Levine, A., Tenhaken, R., Dixon, R., and Lamb, C. (1994) H_2O_2 from the oxidative burst orchestrates the plant hypersensitive disease resistance response. *Cell.* 79, 583-593.

Lin, W., Hu, X., Zhang, W., Rogers, W. J., and Cai, W. (2005) Hydrogen peroxide mediates defence responses induced by chitosans of different molecular weights in rice. *J. Plant Physiol.* 162, 937-944.

Ling, Z., Suits, M. D., Bingham, R. J., Bruce, N. C., Davies, G. J., Fairbanks, A. J., Moir, J. W., and Taylor, E. J. (2009) The X-ray Crystal structure of an *Arthrobacter protophormiae* endo-β-*N*-acetylglucosaminidase reveals a $(\beta/\alpha)_8$ catalytic domain, two ancillary domains and active site residues key for transglycosylation activity. *J. Mol. Biol.* 389, 1-9.

Lonhienne, T., Mavromatis, K., Vorgias, C. E., Buchon, L., Gerday, C., and Bouriotis, V. (2001a) Cloning, sequences, and characterization of two chitinase genes from the Antarctic *Arthrobacter* sp. strain TAD20: isolation and partial characterization of the enzymes. *J. Bacteriol.* 183, 1773-1779.

Lonhienne, T., Zoidakis, J., Vorgias, C. E., Feller, G., Gerday, C., and Bouriotis, V. (2001b) Modular structure, local flexibility and cold-activity of a novel chitobiase from a psychrophilic Antarctic bacterium. *J. Mol. Biol.* 310, 291-297.

Lü, Y., Yang, H., Hu, H., Wang, Y., Rao, Z., and Jin, C. (2009) Mutation of Trp137 to glutamate completely removes transglycosyl activity associated with the *Aspergillus fumigatus* AfChiB1. *Glycoconj. J.* 26, 525-534.

Lüthy, R., Bowie, J. U., and Eisenberg, D. (1992) Assessment of protein models with three-dimensional profiles. *Nature*. 356, 83-85.

Ly, H. D., and Withers, S. G. (1999) Mutagenesis of glycosidases. *Annu. Rev. Biochem*. 68, 487-522.

Macdonald, J. M., Tarling, C. A., Taylor, E. J., Dennis, R. J., Myers, D. S., Knapp, S., Davies, G. J., and Withers, S. G. (2010) Chitinase inhibition by chitobiose and chitotriose thiazolines. *Angew. Chem. Int. Ed. Engl*. 49, 2599-2602.

Madhuprakash, J., Singh, A., Kumar, S., Sinha, M., Kaur, P., Sharma, S., Podile, A. R., and Singh, T. P. (2013) Structure of chitinase D from *Serratia proteamaculans* reveals the structural basis of its dual action of hydrolysis and transglycosylation. *Int. J. Biochem. Mol. Biol*. 4, 166-178.

Madhuprakash, J., Tanneeru, K., Karlapudi, B., Guruprasad, L., and Podile, A. R. (2014) Mutagenesis and molecular dynamics simulations revealed the chitooligosaccharide entry and exit points for chitinase D from *Serratia proteamaculans*. *Biochim. Biophys. Acta. General Sub*. doi: 10.1016/j.bbagen. 2014. 06.014.

Madhuprakash, J., Tanneeru, K., Purushotham, P., Guru Prasad, L., and Podile, A. R. (2012) Transglycosylation by chitinase D from *Serratia proteamaculans* improved through altered substrate interactions. *J. Biol. Chem*. 287, 44619-44627.

Makino, A., Kurosaki, K., Ohmae, M., and Kobayashi, S. (2006) Chitinase-catalyzed synthesis of alternatingly *N*-deacetylated chitin: A chitin-chitosan hybrid polysaccharide. *Biomacromolecules*. **7**, 950-957.

Martinez, E. A., Boer, H., Koivula, A., Samaina, E., Driguez, H., Armand, S., and Cottaz, S. (2012) Engineering chitinases for the synthesis of chitin oligosaccharides: catalytic amino acid mutations convert the GH-18 family glycoside hydrolases into transglycosylases. *J. Mol. Catal. B: Enz.* 74, 89-96.

Matthews, B. W., Nicholson, H., and Bectel, W. J. (1987) Enhanced protein thermostability from site-directed mutations that decrease the entropy of unfolding. *Proc. Natl. Acad. Sci. U.S.A.* 84, 6663-6667.

Minke, R., and Blackwell, J. (1978) The structure of α-chitin. *J. Mol. Biol.* 120, 167-181.

Moerschbacher, B. M., Kogel, K. H., Noll, U., and Reisener, H. J. (1986) An elicitor of the hypersensitive lignification response in wheat leaves isolated from the rust fungus *Puccinia graminis* f. sp. *tritici*. I. Partial purification and characterization. *Z. Naturforsch*. 41, 830-838.

Mori, T., Okumura, M., Matsuura, M., Ueno, K., Tokura, S., Okamoto, Y., Minami, S., and Fujinaga, T. (1997) Effects of chitin and its derivatives on the proliferation and cytokine production of fibroblasts in vitro. *Biomaterials.* 18, 947-951.

Mrabet, N. T., Van den Broeck, A., Van den brande, I., Stanssens, P., Laroche, Y., Lambeir, A. M., Matthijssens, G., Jenkins, J., Chiadmi, M., and van Tilbeurgh, H. (1992) Arginine residues as stabilizing elements in proteins. *Biochemistry*. 8, 2239-2253.

Murshudov, G. N., Skubak, P., Lebedev, A. A., Pannu, N. S., Steiner, R. A., Nicholls, R. A., Winn, M. D., Long, F., and Vagin, A. A. (2011) REFMAC5 for the refinement of macromolecular crystal structures. *Acta. Crystallogr. D Biol. Crystallogr*. 67, 355-367.

Muzard, M., Aubry, N., Plantier-Royon, R., O'Donohue, M., and Rémond, C. (2009) Evaluation of the transglycosylation activities of a GH39 β-xylosidase for the synthesis of xylose-based glycosides. *J. Mol. Catal. B Enzym.* 58, 1–5.

Naïm, M., Bhat, S., Rankin, K. N., Dennis, S., Chowdhury, S. F., Siddiqi, I., Drabik, P., Sulea, T., Bayly, C. I., Jakalian, A., and Purisima, E. O. (2007) Solvated interaction energy (SIE) for scoring protein-ligand binding affinities. 1. Exploring the parameter space. *J. Chem. Inf. Model* 47, 122-133.

Nam, K. S., Kim, M. K., and Shon, Y. H. (2007) Inhibition of pro-inflammatory cytokine-induced invasiveness of HT-29 cells by chitosan oligosaccharide. *J. Microbiol. Biotechnol*. 17, 2042-2045.

Norberg, A. L., Karlsen, V., Hoell, I. A., Bakke, I., Eijsink, V. G. H., and Sørlie, M. (2010) Determination of substrate binding energies in individual subsites of a family 18 chitinase. *FEBS Lett*. 584, 4581-4585.

Nordtveit, R. J., Vårum, K. M., and Smidsrød, O. (1994) Degradation of fully water-soluble, partially *N*-acetylated chitosans with lysozyme. *Carbohydr. Polym.* 23, 253-260.

Ohnuma, T., Numata, T., Osawa, T., Mizuhara, M., Vårum, K. M., and Fukamizo, T. (2011a) Crystal structure and mode of action of a class V chitinase from *Nicotiana tabacum*. *Plant. Mol. Biol.* 75, 291–304.

Ohnuma, T., Sørlie, M., Fukuda, T., Kawamoto, N., Taira, T., and Fukamizo, T. (2011b) Chitin oligosaccharide binding to a family GH19 chitinase from the moss *Bryum coronatum*. *FEBS J.* 278, 3991-4001.

Okada, M., Matsumura, M., Ito, Y., and Shibuya, N. (2002) High-affinity binding proteins for *N*-acetyl chitooligosaccharide elicitor in the plasma membranes from wheat, barley and carrot cells: conserved presence and correlation with the responsiveness to the elicitor. *Plant Cell Physiol.* 43, 505-512.

Omura, S., Arai, N., Yamaguchi, Y., Masuma, R., Iwai, Y., Namikoshi, M., Turberg, A., Kolbl, H., and Shiomi, K. (2000) Argifin, a new chitinase inhibitor, produced by *Gliocladium* sp. FTD-0668. I. Taxonomy, fermentation, and biological activities. *J. Antibiot*. 53, 603-608.

Orikoshi, H., Nakayama, S., Miyamoto, K., and Tsujibo, H. (2005) Role of the N-terminal polycystic kidney disease domain in chitin degradation by chitinase A from a marine bacterium, *Alteromonas* sp. strain O-7. *J. Appl. Microbiol*. 99, 551-557.

Otwinowski, Z., and Minor, W. (1997) Processing of X-ray diffraction data collected in oscillation mode. *Methods Enzymol*. 276, 307-326.

Palma-Guerrero, J., Huang, I. C., Jansson, H. B., Salinas, J., Lopez-Llorca, L. V., and Read, N. D. (2009) Chitosan permeabilizes the plasma membrane and kills cells of *Neurospora crassa* in an energy dependent manner. *Fungal Genet. Biol*. 46, 585-594.

Park, Y., Kim, M. H., Park, S. C., Cheong, H., Jang, M. K., Nah, J. W., and Hahm, K. S. (2008) Investigation of the antifungal activity and mechanism of action of LMWS-chitosan. *J. Microbiol. Biotechnol*. 18, 1729-1734.

Parrinello, M., and Rahman, A. (1981) Polymorphic transitions in single crystals. A new molecular dynamics method. *J. Appl. Phys*. 52, 7182-7190.

Payne, C. M., Bomble, Y. J., Taylor, C. B., McCabe, C., Himmel, M. E., Crowley, M. F., and Beckham, G. T. (2011) Multiple functions of aromatic carbohydrate interactions in a processive cellulase examined with molecular simulation. *J. Biol. Chem*. 286, 41028-41035.

Perrakis, A., Tews, I., Dauter, Z., Oppenheim, A. B., Chet, I., Wilson, K. S., and Vorgias, C. E. (1994) Crystal-structure of a bacterial chitinase at 2.3 Å resolution. *Structure. 2*, 1169-1180.

Purushotham, P., and Podile, A. R. (2012) Synthesis of long-chain chitooligosaccharides by a hyper transglycosylating processive endo-chitinase of *Serratia proteamaculans* 568. *J. Bacteriol.* 194, 4260-4271.

Purushotham, P., Sarma, P. V. S. R. N., and Podile, A. R. (2012) Multiple chitinases of an endophytic *Serratia proteamaculans* 568 generate chitin oligomers. *Bioresour. Technol.* 112 261-269.

Raafat, D., von Bargen, K., Haas, A., and Sahl, H. G. (2008) Insights into the mode of action of chitosan as an antibacterial compound. *Appl. Environ. Microbiol.* 74, 3764-3773.

Ramachandran, G. N., Ramakrishnan, C., and Sasisekharan, V. (1963) Stereochemistry of polypeptide chain configurations. *Mol. Biol.* 7**,** 95-99.

Rao, F. V., Houston, D. R., Boot, R. G., Aerts, J. M., Sakuda, S., and van Aalten, D. M. (2003) Crystal structures of allosamidin derivatives in complex with human macrophage chitinase. *J. Biol. Chem.* 278, 20110-20116.

Ratanavaraporn, J., Kanokpanont, S., Tabata, Y., and Damrongsakkul, S. (2009) Growth and osteogenic differentiation of adipose-derived and bone marrow-derived stem cells on chitosan and chitooligosaccharide films. *Carbohydr. Polym.* 78, 873-878.

Rhoades, J., Gibson, G., Formentin, K., Beer, M., and Rastall, R. (2006) Inhibition of the adhesion of enteropathogenic *Escherichia coli* strains to HT-29 cells in culture by chito-oligosaccharides. *Carbohydr. Polym*. 64, 57-59.

Sakuda, S., Isogai, A., Matsumoto, S., Suzuki, A., and Koseki, K. (1986) The structure of allosamidin, a novel insect chitinase inhibitor, produced by *Streptomyces* sp. *Tetrahedron Lett.* 27, 2475-2478.

Sali, A., and Blundell, T. L. (1993) Comparative protein modelling by satisfaction of spatial restraints. *J. Mol. Biol.* 234, 779-815.

Sashidhar, B., Inampudi, K. K., Guruprasad, L., Kondreddy, A., Gopinath, K., and Podile, A. R. (2010) Highly conserved Asp-204 and Gly-776 are important for activity of the quinoprotein glucose dehydrogenase of *Escherichia coli* and for mineral phosphate solubilization. *J. Mol. Microbiol. Biotechnol.* 18, 109-119.

Schipper, N. G. M., Vårum, K. M., and Artursson, P. (1996) Chitosans as absorption enhancers for poorly absorbable drugs.1. Influence of molecular weight and degree of acetylation on drug transport across human intestinal epithelial (Caco-2) cells. *Pharmaceut Res.* 13, 1686-1692.

Schuttelkopf, A. W., Andersen, O. A., Rao, F. V., Allwood, M., Lloyd, C., Eggleston, I. M., and van Aalten, D. M. (2006) Screening-based discovery and structural dissection of a novel family 18 chitinase inhibitor. *J. Biol. Chem.* 281, 27278-27285.

Shahabuddin, M., Toyoshima, T., Aikawa, M., and Kaslow, D. C. (1993) Transmission-blocking activity of a chitinase inhibitor and activation of malarial parasite chitinase by mosquito protease. *Proc. Natl. Acad. Sci. USA.* 90, 4266-4270.

Shi, J., Blundell, T. L., and Mizuguchi, K. (2001) FUGUE: sequence-structure homology recognition using environment-specific substitution tables and structure-dependent gap penalties. *J. Mol. Biol.* 310, 243-257.

Shibuya, N., and Minami, E. (2001) Oligosaccharide signalling for defense responses in plant. *Physiol. Mol. Plant Pathol*. 59, 223-233.

Sinnott, M. L. (1990) Catalytic mechanisms of enzymatic glycosyl transfer. *Chem. Rev.* 90, 1171-1202.

Sousa da Silva, A. W., and Vranken, W. F. (2012) ACPYPE – AnteChamber PYthon Parser interfacE. *BMC Res. Notes.* 5, 367.

Stefanidi, E., and Vorgias, C. E. (2008) Molecular analysis of the gene encoding a new chitinase from the marine psychrophilic bacterium *Moritella marina* and biochemical characterization of the recombinant enzyme. *Extremophiles.* 12, 541-552.

Suzuki, K., Sugawara, N., Suzuki, M., Uchiyama, T., Katouno, F., Nikaidou, N., and Watanabe, T. (2002) Chitinases A, B, and C1 of *Serratia marcescens* 2170 produced by recombinant *Escherichia coli:* Enzymatic properties and synergism on chitin degradation. *Biosci. Biotechnol. Biochem.* 66, 1075-1083.

Synstad, B., Gaseidnes, S., van Aalten, D. M. F., Vriend, G., Nielsen, J. E., and Eijsink, V. G. H. (2004) Mutational and computational analysis of the role of conserved residues in the active site of a family 18 chitinase. *Eur. J. Biochem.* 271, 253-262.

Taghavi, S., Garafola, C., Monchy, S., Newman, L., Hoffman, A., Weyens, N., Barac, T., Vangronsveld, J., and van der Lelie, D. (2009) Genome survey and characterization of endophytic bacteria exhibiting a beneficial effect on growth and development of poplar trees. *Appl. Environ. Microbiol.* 75, 748-757.

Taira, T., Fujiwara, M., Dennhart, N., Hayashi, H., Onaga, S., Ohnuma, T., Letzel, T., Sakuda, S., and Fukamizo, T. (2010) Transglycosylation reaction catalyzed by a class V chitinase from cycad, *Cycas revoluta*. A study involving site-directed mutagenesis, HPLC, and real time ESI-MS. *Biochim. Bio-phys. Acta.* 1804, 668-675.

Takahashi, Y., Miki, F., and Nagase, K. (1995) Effect of sonolysis on acid degradation of chitin to form oligosaccharides. *Bull. Chem. Soc. Jpn.* 68, 851-857.

Takaya, N., Yamazaki, D., Horiuchi, H., Ohta, A., and Takagi, M. (1998) Intracellular chitinase gene from *Rhizopus oligosporus*: molecular cloning and characterization. *Microbiology*. 144, 2647-2654.

Tamura, K., Stecher, G., Peterson, D., Filipski, A., and Kumar, S. (2013) MEGA6: Molecular Evolutionary Genetics Analysis version 6.0. *Molecular Biology and Evolution.* 30, 2725-2729.

Tang, C. D., Li, J. F., Wei, X. H., Min, R., Gao, S. J., Wang, J. Q., Yin, X., and Wu, M. C. (2013) Fusing a carbohydrate-binding module into the *Aspergillus usamii* β-mannanase to improve its thermostability and cellulose-binding capacity by *in silico* design. *PLoS One*. 8, e64766.

Tanneeru, K., and Guruprasad, L. (2013) Ponatinib is a pan-BCR-ABL kinase inhibitor: MD simulations and SIE study. *PLoS One.* 8, e78556.

Terwisscha van Scheltinga, A. C., Hennig, M., and Dijkstra, B. W. (1996) The 1.8 Å resolution structure of hevamine, a plant chitinase/lysozyme, and analysis of the conserved sequence and structure motifs of glycosyl hydrolase family 18. *J. Mol. Biol*. 262, 243-257.

Tews, I., Terwisscha van Scheltinga, A. C., Perrakis, A., Wilson, K. S., and Dijkstra, B. W. (1997) Substrate assisted catalysis unifies two families of chitinolytic enzymes. *J. Am. Chem. Soc.* 119, 7954-7959.

Thongekkaew, J., Ikeda, H., Masaki, K., and Iefuji, H. (2013) Fusion of cellulose binding domain from *Trichoderma reesei* CBHI to *Cryptococcus* sp S-2 cellulase enhances its binding affinity and its cellulolytic activity to insoluble cellulosic substrates. *Enzyme. Microb. Technol.* 52, 241-246.

Tikhonov, V. E., Stepnova, E. A., Babak, V. G., Yamskov, I. A., Palma-Guerrero, J., Jansson, H. B., Lopez-Llorca, L. V., Salinas, J., Gerasimenko, D.V., Avdienko, I. D., and Varlamov, V. P. (2006) Bactericidal and antifungal activities of a low molecular weight chitosan and its N-/2(3)-(dodec-2-enyl) succinoyl/-derivatives. *Carbohydr. Polym*. 64, 66-72.

Trombotto, S., Ladavie`re, C., Delolme, F., and Domard, A. (2008) Chemical preparation and structural characterization of a homogeneous series of chitin/chitosan oligomers. *Biomacromolecules*. 9, 1731–1738.

Uchida, Y., Izume, M., and Ohtakara, A. (1989) Preparation of chitosan oligomers with purified chitosanase and its application. In: Skjak-Braek, G., Anthonsen, T., Sandford, P., (eds.) Chitin and Chitosan. Amsterdam, The Netherlands: Elsevier, pp. 373-382.

Uchiyama, T., Kaneko, R., Yamaguchi, J., Inoue, A., Yanagida, T., Nikaidou, N., Regue, M., and Watanabe, T. (2003) Uptake of *N*, *N'*-diacetylchitobiose [$(GlcNAc)_2$] *via* the phosphotransferase system is essential for chitinase production by *Serratia marcescens* 2170. *J. Bacteriol*. 185, 1776-1782.

Uchiyama, T., Katouno, F., Nikaidou, N., Nonaka, T., Sugiyama, J., and Watanabe, T. (2001) Roles of the exposed aromatic residues in crystalline chitin hydrolysis by chitinase A from *Serratia marcescens* 2170. *J. Biol. Chem.* 276, 41343-41349.

Umemoto, N., Ohnuma, T., Mizuhara, M., Sato, H., Skriver, K., and Fukamizo, T. (2013). Introduction of a tryptophan side chain into subsite +1 enhances transglycosylation activity of a GH-18 chitinase from *Arabidopsis thaliana*, AtChiC. *Glycobiology*. 23, 81-90.

Uni, F., Lee, S., Yatsunami, R., Fukui, T., and Nakamura, S. (2012) Mutational analysis of a CBM family 5 chitin binding domain of an alkaline chitinase from *Bacillus* sp J813. *Biosci. Biotechnol. Biochem.* 76, 530-535.

Usami, Y., Minami, S., Okamoto, Y., Matsuhashi, A., and Shigemasa, Y. (1997) Influence of chain length of *N*-acetyl-D-glucosamine and D-glucosamine residues on direct and complement-mediated chemotactic activities for canine polymorphonuclear cells. *Carbohydr. Polym*. 32, 115-122.

Usui, T., Matsui, H., and Isobe, K. (1990) Enzymic synthesis of useful chitooligosaccharides utilizing transglycosylation by chitinolytic enzymes in a buffer containing ammonium sulfate. *Carbohydr. Res.* 203, 65-77.

Vaaje-Kolstad, G., Horn, S. J., Sørlie, M., and Eijsink, V. G. (2013) The chitinolytic machinery of *Serratia marcescens* -a model system for enzymatic degradation of recalcitrant polysaccharides. *FEBS J.* 280, 3028-3049.

Vaaje-Kolstad, G., Horn, S. J., van Aalten, D. M., Synstad, B., and Eijsink, V. G. (2005) The non-catalytic chitin-binding protein CBP21 from *Serratia marcescens* is essential for chitin degradation. *J. Biol. Chem.* 280, 28492-28497.

Vaaje-Kolstad, G., Westereng, B., Horn, S. J., Liu, Z. L., Zhai, H., Sørlie, M., and Eijsink, V. G. H. (2010) An oxidative enzyme boosting the enzymatic conversion of recalcitrant polysaccharides. *Science*. 330, 219-222.

Vagin, A., and Teplyakov, A. (2010) Molecular replacement with MOLREP. *Acta Crystallogr. D Biol. Crystallogr*. 66, 22-25.

van Aalten, D. M. F., Komander, D., Synstad, B., Gåseidnes, S., Peter, M. G., and Eijsink, V. G. H. (2001) Structural insights into the catalytic mechanism of a family 18 exo-Chitinase. *Proc. Natl. Acad. Sci. U.S.A.* 98, 8979-8984.

van Aalten, D. M., Synstad, B., Brurberg, M. B., Hough, E., Riise, B. W., Eijsink, V. G. H., and Wierenga, R. K. (2000) Structure of a two-domain chitotriosidase from *Serratia marcescens* at 1.9 Å resolution. *Proc. Natl. Acad. Sci. U.S.A.* 97, 5842-5847.

Van den Burg, B., Vriend, G., Veltman, O. R., Venema, G., and Eijsink, V. G. H. (1998) Engineering an enzyme to resist boiling. *Proc. Natl. Acad. Sci. U.S.A.* 95, 2056-2060.

van Munster, J. M., van der Kaaij, R. M., Dijkhuizen, L., and van der Maarel, M. J. (2012) Biochemical characterization of *Aspergillus niger* CfcI, a glycoside hydrolase family 18 chitinase that releases monomers during substrate hydrolysis. *Microbiology*. 158, 2168-2179.

Vander, P., Varum, K. M., Domard, A., Eddine El Gueddari, N., and Moerschbacher, B. M. (1998) Comparison of the ability of partially *N*-acetylated chitosans and chitooligosaccharides to elicit resistance reactions in wheat leaves. *Plant Physiol*. 118, 1353-1359.

Vårum, K. M., Ottøy, M. H., and Smidsrød, O. (1994) Water solubility of partially *N*-acetylated chitosans as a function of pH – effect of chemical composition and depolymerization. *Carbohydr. Polym.* 25, 65-70.

Vishukumar, A. B., Varadaraj, M. C., Gowda, L. R., and Tharanathan, R. N. (2005) Characterization of chitooligosaccharides prepared by chitosanolysis with the aid of papain and pronase, and their bactericidal action against *Bacillus cereus* and *Escherichia coli*. *Biochem. J*. 391, 167-175.

Vocadlo, D. J., Davies, G. J., Laine, R., and Withers, S. G. (2001) Catalysis by hen egg-white lysozyme proceeds *via* a covalent intermediate. *Nature*. 412, 835-838.

Wang, J., Wang, W., Kollman P. A., and Case, D. A. (2006) Automatic atom type and bond type perception in molecular mechanical calculations. *J. Mol. Graph. Model*. 25, 247-260.

Warm, E., and Laties, G. G. (1982) Quantification of hydrogen peroxide in plant extracts by the chemiluminiscence reaction with luminol. *Phytochemistry*. 21, 827-831.

Watanabe, T., Ariga, Y., Sato, U., Toratani, T., Hashimoto, M., Nikaidou, N., Kezuka, Y., Nonaka, T., and Sugiyama, J. (2003) Aromatic residues within the substrate-binding cleft of *Bacillus circulans* chitinase A1 are essential for hydrolysis of crystalline chitin. *Biochem. J*. 376, 237-244.

Watanabe, T., Kobori, K., Miyashita, K., Fujii, T., Sakai, H., Uchida, M., and Tanaka, H. (1993) Identification of glutamic acid 204 and aspartic acid 200 in

chitinase A1 of *Bacillus circulans* WL-12 as essential residues for chitinase activity. *J. Biol. Chem.* 268, 18567-18572.

Williams, S. J., and Withers, S. G. (2000) Glycosyl fluorides in enzymatic reactions. *Carbohydr. Res*. 327, 27-46.

Winn, M. D., Ballard, C. C., Cowtan, K. D., Dodson, E. J., Emsley, P., Evans, P. R., Keegan, R. M., Krissinel, E. B., Leslie, A. G., McCoy, A., McNicholas, S. J., Murshudov, G. N., Pannu, N. S., Potterton, E. A., Powell, H. R., Read, R. J., Vagin, A., and Wilson, K. S. (2011) Overview of the CCP4 suite and current developments. *Acta Crystallogr. D Biol. Crystallogr.* 67, 235-242.

Xu, J. G., Zhao, X. M., Han, X. W., and Du, Y. G. (2007) Antifungal activity of oligochitosan against *Phytophthora capsici* and other plant pathogenic fungi *in vitro* Pestic. *Biochem. Physiol*. 87, 220-228.

Yin, H., Zhao, X., and Du, Y. (2010) Oligochitosan: a plant diseases vaccine, a review. *Carbohydr. Polym*. 82, 1–8.

Yoon, J. H. (2005) Enzymatic synthesis of chitooligosaccharides in organic co-solvents. *Enzyme. Microb. Technol.* 37, 663-668.

Yu, C., Lee, A. M., Bassler, B. L., and Roseman, S. (1991) Chitin utilization by marine bacteria. A physiological function for bacterial adhesion to immobilized carbohydrates. *J. Biol. Chem*. 266, 24260-24267.

Zakariassen, H., Aam, B. B., Horn, S. J., Vårum, K. M., Sørlie, M., and Eijsink, V. G. (2009) Aromatic residues in the catalytic center of chitinase A from *Serratia marcescens* affect processivity, enzyme activity, and biomass converting efficiency. *J. Biol. Chem*. 284, 10610-10617.

Zakariassen, H., Eijsink, V. G. H., and Sørlie, M. (2010) Signatures of activation parameters reveal substrate-dependent rate determining steps in polysaccharide turnover by a family 18 chitinase. *Carbohydr. Polym*. 81, 14-20.

Zakariassen, H., Hansen, M. C., Jøranli, M., Eijsink, V. G. H., and Sørlie, M. (2011) Mutational effects on transglycosylating activity of family 18 chitinases and construction of a hyper transglycosylating mutant. *Biochemistry.* 50, 5693-5703.

Zhu, Z., Zheng, T., Homer, R. J., Kim, Y. K., Chen, N. Y., Cohn, L., Hamid, Q., and Elias, J. A. (2004) Acidic mammalian chitinase in asthmatic Th2 inflammation and IL-13 pathway activation. *Science*. 304, 1678-1682.